DISSERTATION

SUSTAINABLE POLYMER SYNTHESIS THROUGH THE DESIGN OF ORGANIC PHOTOREDOX CATALYSTS AND DEVELOPMENT OF POLY(NORBORNANE TRITHIOLANES)

Submitted by

Mariel Jene Price

Department of Chemistry

In partial fulfillment of the requirements

For the Degree of Doctor of Philosophy

Colorado State University

Fort Collins, Colorado

Fall 2023

Doctoral Committee:

Advisor: Garret Miyake

Robert Paton
Joseph Zadrozny
Margarita Herrera-Alonzo

ABSTRACT

SUSTAINABLE POLYMER SYNTHESIS THROUGH THE DESIGN OF ORGANIC PHOTOREDOX CATALYSTS AND DEVELOPMENT OF POLY(NORBORNANE TRITHIOLANES)

There are many avenues through which the sustainability synthesis, use, and disposal of polymeric materials can be approached. One of the two approaches explored in this work is the sustainable design and use of polymerization catalysts. Proper employment of catalysis can greatly decrease the energy input required to synthesize polymers and intentional design of those catalysts can enable their use in small quantities without compromising their effectiveness or the sustainability with which they are made and used. Herein, the development of a new class of metal-free photoredox catalysts (made from abundant elements) which can use visible wavelengths of light (a readily available, replenishable, and mild source of energy) to control the polymerization acrylate monomers is reported. Through this work we provide insight into how catalyst structure can be tuned to achieve desired properties and what properties might render certain catalysts more effective at lower loadings. The second approach explored herein towards improving the sustainability of polymer synthesis, use, and disposal is related to the recyclability of the polymeric materials. In addition to sustainable synthesis through catalysis, one way to improve the sustainability of polymeric materials is to increase their viable economic lifetime. Polymeric materials that are readily recyclable prevent the loss of materials through disposal. In the work reported herein methods for the synthesis and polymerization of sulfur-containing monomers to generate polymeric materials with intrinsic recyclability are investigated, approaches for efficient depolymerization of such polymers improved, and the scope of these materials expanded.

ACKNOWLEGEMENTS

Over the last five years I had the privilege to live through what was the opportunity of a lifetime. Pursuing a degree in any higher-education institution is a luxury that many cannot afford. As such, I would like to first acknowledge and thank all those whom, in the past, made sacrifices or took risks so that this opportunity could be available to me.

Throughout my life, I have been fortunate to have many great mentors including my parents, my grandparents, aunts and uncles, teachers, coaches, and family friends and thank them for believing in me, pushing me, giving me second chances, and for giving me safe places to learn, speak, ask questions, and grow.

I must, of course, acknowledge Professor Garret Miyake and the entire Miyake group, past and present. Garret constantly encouraged me, not only in my research endeavors, but in pursuing many professional development opportunities outside of the lab. Garret was an extremely patient mentor and never left me in doubt about how much he cared about my success, the success of the group, and about our general happiness and well-being. He always made sure that there were means for me to explore my research interests and put a lot of effort into cultivating a positive group culture that would be conducive to our professional growth. Several Miyake group alumni including Blaine, Max, and Daniel have continued to serve as mentors for me even after leaving the group—the enormity of their positive influence on the group set up a cascade of strong mentorship that has benefited many, including myself.

Though it was Dr. Benton Cartledge and Professor Brian Majestic who gave me my first opportunity to work in a lab as an undergraduate student at the University of Denver, my first research projects really took place in my parents' kitchen. As a child I was allowed to make "potions" and pursue self-invented cooking endeavors which, unfortunately, usually culminated in me using a wire wheel brush attachment on a drill to clean out my Mom's pots. When something broke on our family car my parents always tried to fix it themselves first and were happy to involve

us in the process. When my sister and I needed to make an amendment to a bike so that we could tow our dog around in a cart, my parents were there with tools in hand ready to guide us in designing and building some crazy rig that to realize our dreams. Growing up in a household where I was allowed creative freedom, allowed to ask questions, encouraged to explore despite inherent risks, and where my ideas were given value laid the groundwork I needed to be interested in and to achieve in the sciences. Mom and Dad, thank you.

During my undergraduate studies at the University of Denver I was fortunate to be welcomed into the lab of Professor Brian Majestic where I was mentored by Dr. Benton Cartledge. While in the Majestic lab I was provided many opportunities to do research that coincided with my interest in environmental health, trusted to speak at conferences, and encouraged to apply for funding to pursue my own research interests. My experience working in the Majestic was a great foundation for my future career because of the trust, patience, respect, and encouragement that was afforded to me. Thank you, Brian and Benton for jumpstarting my research career.

After earning my bachelor's degree at the University of Denver, I was lucky enough to work as an intern and then as a technician at the National Renewable Energy Laboratory (NREL). It was there that my eyes were truly opened to the endless opportunities that exist to use chemistry to positively shape the way that humans experience life on earth and how we interact with the planet and its resources. At NREL I was mentored by Dr. Nolan Wilson, Dr. Nick Rorrer, and Dr. Greg Beckham—all incredible scientists and leaders. I would like to thank them for the continued support and guidance I have received from them through my Ph.D. work and as I continue my career in research. During my time at NREL I was also fortunate enough to forge several lifelong friendships with people who all share a passion for the outdoors and for science. My gratitude for the culture at NREL and the experiences, friendships, and lessons that I gained and learned while there is everlasting. I hope that I will find my way back to NREL in some capacity in the years to come.

To my sister and all of my friends: you all have spent so much time listening, checking in, reading papers to me in the car while I drive up rocky mountain passes, chatting with me on the phone while I speculate over every aspect of my career, and, importantly, building me up both when my cup is full and when I have been beyond empty. I love you all dearly and am eternally grateful for each of you, all you have given me, especially over the last five years, and for all we have shared. Having friends who are passionate about science and sustainability and are willing to dive into discussions about these things while taking long car trips into remote mountains, walking through knee deep water in slot canyons, and climbing peaks in wind, snow, and scorching heat—this is what makes life worth living and has kept my engine running over the last five years. My friends, thank you.

Finally, I would also like to acknowledge my partner, Curtis, and his family. Despite the strain that resulted from my graduate studies combined with our living in different cities, Curtis was a constant source of support throughout my entire doctorate program. Daily phone calls and weekend visits added so much to my life over the last five years. Having someone that I trusted and who understood me better than many was an irreplaceable part of my ability to finish the program. Curtis, you and your family put so many smiles on my face, have been unendingly understanding and supportive, and have given me a loving environment to escape into both when things were going well and when they were not. Thank you.

To my aunts, uncles, and grandparents: your involvement in my life and interest in my career has positively shaped my experiences and influenced my decisions from the start of elementary school through now and will continue to in the years to come. Growing up in a family where education is valued, science is respected, and where voicing an opinion is encouraged was paramount to my ability to be where I am and who I am today. Thank you for everything that you have given to me and shared with me.

Acknowledgements by Dissertation Chapter

Chapter 1 contains work reproduced from the journal article “Structure-property relationships of core-substituted diaryl dihydrophenazine organic photoredox catalysts and their application in O-ATRP” by Mariel J. Price, Katherine O. Puffer, Max Kudisch, Declan Knies, and Garret M. Miyake (*Polym. Chem.* **2021**, 12, 6110-6122). Katherine O. Puffer performed transient absorption spectroscopy experiments and helped with the synthesis and characterization of *N,N*-diaryl dihydrophenazine catalysts with 1-naphthyl *N*-aryl substituents. Declan Knies, a high school student from Rocky Mountain High School, assisted with catalyst synthesis and purification. This work was performed with the support of Colorado State University (CSU). The research reported was also supported by the National Science Foundation (NSF) (2055742) as well as Graduate Women in Science (Nell Mondy and Monique Braude Fellowships). Nuclear magnetic resonance experiments and mass spectrometry were performed at the CSU Analytical Resources Center with help from the incredible staff.

Chapter 2 contains unpublished work from a manuscript in preparation titled “Approaches for synthesis, polymerization, and depolymerization of norbornane trithiolanes and their polymers” by Mariel J. Price, Katherine L. Harry, Analiese J. Wiedenbeck, Cameron H. Chrisman, and Garret M. Miyake. In this work, Katherine L. Harry contributed to the investigation of reaction conditions for the synthesis of the monomers as well as in the synthesis of the monomers at scale. Cameron H. Chrisman synthesized several monomers that informed the direction of the work described in the manuscript and helped with method development for monomer synthesis. Analiese J. Wiedenbeck contributed to the depolymerization section of this manuscript as well as in the synthesis and purification of the monomers. This work was performed with the support of Colorado State University (CSU), and in part by Colorado Office of Economic Development and International Trade and American Chemical Society Petroleum Research Fund. Nuclear magnetic resonance experiments, mass spectrometry, and thermal analyses were performed at the CSU Analytical Resources Center.

DEDICATION

To my family, friends, and Curtis.

TABLE OF CONTENTS

CHAPTER 1 – Structure-Property Relationships of Core-Substituted Diaryl Dihydrophenazine Organic Photoredox Catalysts and their Application in O-ATRP

1.1 Overview

Photoinduced organocatalyzed atom-transfer radical polymerization (O-ATRP) is a controlled radical polymerization technique that can be driven using low-energy, visible light and makes use of organic photocatalysts. Limitations of O-ATRP have traditionally included the need for high catalyst loadings (1000 ppm) and the narrow scope of monomers that can be controllably polymerized. Recent advances have shown that *N,N*-diaryl dihydrophenazine (DHP) organic photoredox catalysts (PCs) are capable of controlling O-ATRP at PC loadings as low as 10 ppm, a significant advancement in the field. In this work we synthesized five new DHP PCs and examined their efficacy in controlling O-ATRP at low ppm catalyst loadings. We found that we were able to polymerize methyl methacrylate at PC loadings as low as 10 ppm (relative to monomer) while producing polymers with dispersities as low as $Đ$ = 1.33 and achieving initiator efficiencies (I^*) near unity (102%). In addition to applying these PCs in O-ATRP, we carried out a thorough investigation into the structure-property relationships of the new DHP PCs reported herein and report new photophysical characterization data for previously reported DHPs. The insight into the DHP structure–property relationships that we discuss herein will aid in the elucidation of their ability to catalyze O-ATRP at low catalyst loadings. Additionally, this work sheds light on how structural modifications affect certain PC properties with the goal of bolstering our understanding of how to tune PC structures to overcome current limitations of O-ATRP such as the controlled polymerization of challenging monomers.

1.2 Introduction

The development of organic photoredox catalysts (PCs) has revolutionized the way that chemists can approach both small molecule and macromolecular syntheses.[1,2,3,4,5] Establishing

structure-property relationships of organic PCs is essential for guiding the development of new PCs with targeted properties and to increase their use and application in new chemical transformations. One specific application that knowledge of structure-property relationships in PCs has been leveraged for is organocatalyzed-atom transfer radical polymerization (O-ATRP). O-ATRP is a reversible-deactivation radical polymerization (RDRP) technique that employs the energy of visible light to synthesize polymers with controlled molecular weights and architectures (Figure 1.1). In RDRPs, successful control over the polymerization is typically assessed by the

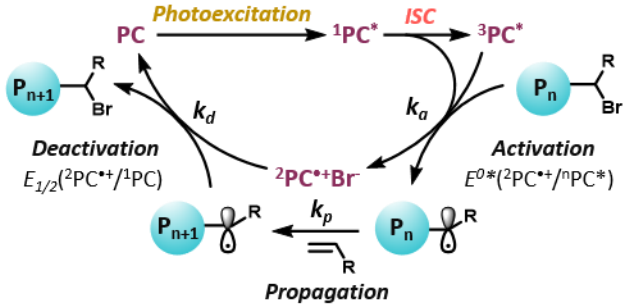

Figure 1.1: Proposed mechanism for O-ATRP.

ability to produce polymers with low dispersity (*Đ*) (*Đ* < 1.5), targeted molecular weights, and retention of the polymer chain end group. O-ATRP was developed as an alternative to traditional metal catalyzed atom transfer radical polymerization (ATRP), one of the most widely used RDRP techniques. O-ATRP offers certain advantages over traditional metal catalyzed ATRP in that it enables the synthesis of polymers free of metal contaminants. Without metal contamination, polymers synthesized via O-ATRP can more readily be used for metal sensitive applications such as in electronics or biomedical technologies. From a sustainability perspective, O-ATRP utilizes a readily abundant source of energy (light) to drive a useful chemical reaction. Although non-organic catalysts have also been developed for visible light-driven ATRP,[4,6,7] they necessitate the use metals such as copper, ruthenium, or iridium which limits the potential applications of the polymers, as highlighted above. Furthermore, concerns about the sustainability of using precious metals such as iridium motivate use of organic PCs.[8]

Our research group has worked in the development of different families of highly reducing PCs originally tailored for O-ATRP, including *N*-aryl phenoxazines,[9,10,11] *N,N*-diaryl dihydrophenazines (DHPs),[12,13,14,15,16,17] *N*-aryl phenothiazines,[18] and *N*-aryl dimethyl dihydroacridines[19] all of which are comprised solely of atoms with high natural abundance, further bolstering their prowess as sustainable catalysts.

Significant advances have been made toward increasing our understanding of the impact of certain PC properties on specific steps of the proposed O-ATRP mechanism.[20,21,22,23,24] Simultaneous with the advancements in our understanding of relevant PC properties has been growth in our understanding of the intricacies of the proposed O-ATRP mechanism.[24] Here, we discuss a distilled version of the proposed mechanism for O-ATRP (Figure 1.1). In the first step of O-ATRP, a PC is photoexcited via irradiation. The excited state PC ($^{n}PC^{*}$) reduces either the alkyl halide initiator via a single electron transfer reaction to initiate polymerization or, once the polymerization has been initiated, reduces the halide-capped polymer chain end to re-activate polymerization. The rate of activation is defined as k_a. Reduction of the initiator/halide-capped polymer chain end yields a carbon-centered radical on the initiator/polymer chain end which can propagate through a reaction with monomer leading to polymerization. The rate of polymerization is defined as k_p. Reduction of the alkyl halide initiator or halide-capped polymer chain end also generates the oxidized PC species ($^{2}PC^{\bullet+}$) and a halide anion (X^{-}) which we propose to form an ion pair.[25] This ion pair ($PC^{\bullet+}X^{-}$) is proposed to deactivate the carbon centered radical on the chain end group of the growing polymer through reinstallation of the halide; the rate of deactivation is described as k_d. Deactivation yields both the halide-capped polymer and ground state PC. Key to the success of ATRP and O-ATRP is that k_d is faster than k_a. Rapid deactivation of the radical on the end group of the growing polymer chain helps minimize side reactions such as bimolecular radical termination and disproportionation, which are counterproductive to the synthesis of polymers with controlled molecular weights.

There are several thermodynamic requirements that PCs used to catalyze O-ATRP through an oxidative quenching cycle (Figure 1.1) must meet. The reduction potential of the excited state PC ($E°^*(\ ^2PC^{\bullet+}\ /\ ^nPC^*)$) must be reducing enough (~−0.6 to −0.8 V vs. SCE) to reduce both the alkyl halide bond of the initiator and the polymer chain end alkyl halide bond.[12] Additionally, the ion pair of $^2PC^{\bullet+}$ and X^- must be sufficiently oxidizing to deactivate the growing polymer chain (~ -0.8 V) to reinstall the halide. There are also several photophysical PC properties that are relevant to the O-ATRP mechanism (Figure 1.2). The absorption of visible light (400 nm–

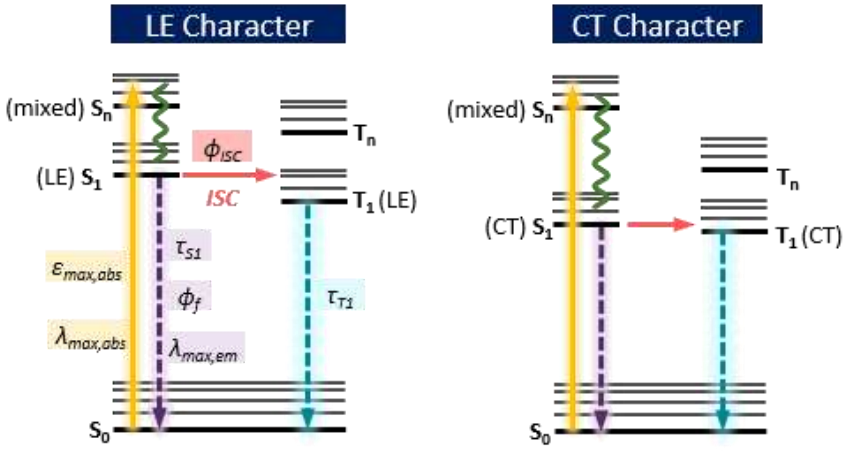

Figure 1.2: Jablonski diagrams representing PCs that form excited states with either local excitation (LE) character (left) or charge transfer (CT) character (right) in their lowest photoexcited states. Solid yellow arrow indicates photoexcitation from S_0 to S_n to form photocatalyst in the singlet excited state ($^1PC^*$). Purple and blue dashed arrows represent radiative decay from the lowest energy singlet excited state (S_1) and the lowest energy triplet excited state (T_1), or fluorescence and phosphorescence, respectively. Pink arrow represents inner system crossing (ISC) from S_1 to T_1 to form photocatalyst in the triplet excited state ($^3PC^*$). Green waved line represents internal conversion (IC). PC properties associated with each type of aforementioned transition are labeled adjacent to those transitions in the Jablonski diagram on the left.

700 nm), and therefore a PC wavelength of maximum absorption ($\lambda_{max,abs}$) > 400 nm, enables the use of visible light to, selectively, stimulate photoexcitation of the PC. This attribute is desirable as use of ultraviolet (UV) light can cause unwanted side reactions due to the ability of many organic molecules, including those used in O-ATRP, to absorb UV light. PCs that possess a high

molar extinction coefficient ($\varepsilon_{max,abs}$) at the wavelength used for photoexcitation are preferred as having ^{n}PC* in higher concentrations can lead to more efficient and uniform activation in O-ATRP and as the system is likely to be more resilient to differences in irradiation intensity. Upon photoexcitation, the PC is promoted to some singlet excited state (S_n) (Figure 1.2) from which it relaxes to the lowest S_1 energy state. From S_1 the PC, considered to be in the lowest energy singlet excited state (^{1}PC*) can relax back to the ground state either *via* a radiative pathway (fluorescence) or non-radiative pathway (Fig. 2), can react with a substrate via electron-transfer or energy transfer, or can undergo intersystem crossing to access the triplet excited state (T_1). The PC in the triplet excited state (^{3}PC*) most commonly reacts with some substrate or via a radiative pathway (phosphorescence) or via non-radiative decay back to the ground state (S_0) (Fig. 2). Both ^{1}PC* and ^{3}PC* are highly reducing for the PCs discussed in this work and are likely responsible for activation in O-ATRP, though their individual contributions to activation has been speculated to be dependent on reactant concentrations.[20] As triplet excited state lifetimes (τ_{T1}) are longer than singlet excited states lifetimes (τ_{S1}) and are therefore more likely to engage in a bimolecular interaction, ^{3}PC* is commonly attributed as the species responsible for activation. However, recent studies have shown that there are several factors that can influence the ratios of ^{1}PC* and ^{3}PC* responsible for activation in O-ATRP such as the concentration of initiator used,[20] the solvent that the polymerization is conducted in,[22] and electron transfer rates influenced by the PC structure.[21] As ^{n}PC* is responsible for activation, it is important to understand how the structure of the PC influences the nature of ^{n}PC*. DHP PCs that access charge-transfer (CT) type excited states have been shown to be more effective PCs in controlling O-ATRP.[13] In CT PCs, photoexcitation triggers a shift in electron density from one part of the molecule (the donor) to another part (the acceptor) generally resulting in a more-polar and stabilized excited state (Figure 1.2). The specific role of CT in improving PC control in O-ATRP is still debated.[11,23,26,27]

In previous work, core-extension of *N*-aryl phenoxazines, DHPs, and *N*-aryl dimethyl dihydroacridines has been shown to significantly impact PC properties and improve control in O-

ATRP.[11,14,15,16,17,19] Prior work on aryl core-extended DHPs explored how core-extension of a particular DHP (which possessed an electron withdrawing 4-trifluoromethylphenyl N-aryl group)

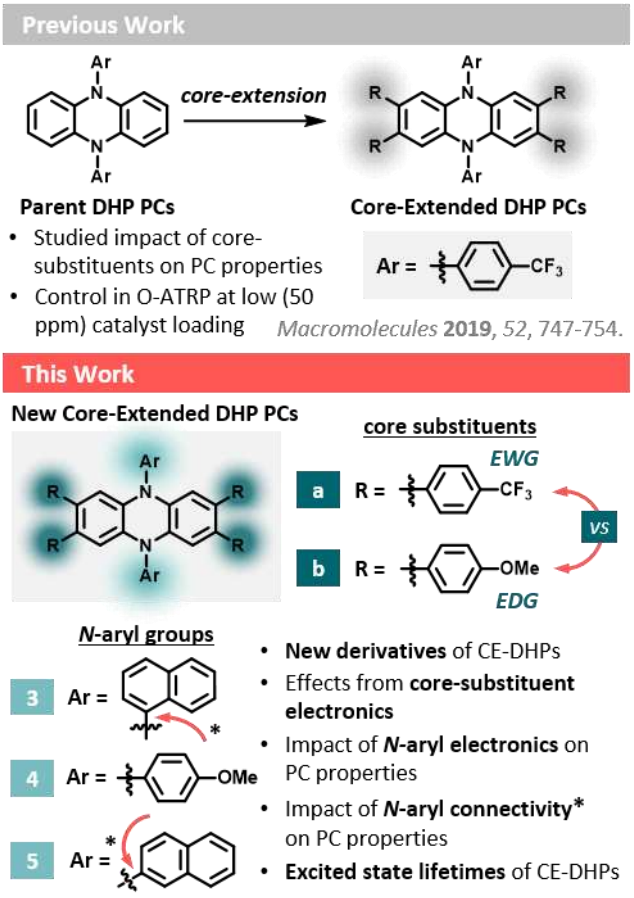

Figure 1.3: Previously reported work on core-extended DHPs (top). Focus of this work and structures for new core-extended DHPs developed in this work (bottom). *Different points of connectivity for naphthalene N-aryl group to DHP PC are indicated by red arrows.

impacted PCs properties and control in O-ATRP (Figure 1.3).[14] Importantly, the aryl-core extended DHPs were shown to control O-ATRP at catalyst loadings as low as 10 ppm, producing polymers with controlled molecular weights ($Đ$ < 1.42) while achieving I^* > 90%.[14] The application of PCs at low ppm (<1000 ppm) was a significant advancement in the field of O-ATRP. The ability to control polymerizations at low PC loadings is beneficial both from a sustainability perspective and from a practical standpoint as low ppm PC loadings limits contamination of the polymers by the PC. In this work, we sought to further investigate structure-property relationships in core-extended

DHPs first, to gain insight into the properties that enable them to control O-ATRP at low ppm PC loadings and second, because deeper understanding of structure-property relationships in PCs can help direct the development of new PCs with properties that can help overcome current limitations in O-ATRP (Figure 1.3). Herein, we demonstrate the synthesis and characterization of five new core-extended DHP PCs, examine the structure-property relationships in those PCs, and investigate their ability to control the polymerization of acrylate and methacrylate monomers in O-ATRP. Furthermore, we provide new photophysical characterization data for previously reported DHPs and test their ability to control O-ATRP at low ppm PC loadings for the first time.

1.3 Results and Discussion

1.3.1 Synthesis of PCs. The synthesis of core-extended DHPs involves several steps beginning with the reduction of phenazine (**1**) to dihydrophenazine (**2**) (Figure A1.3).[28] Following the synthesis of dihydrophenazine (**2**), Buchwald-Hartwig C-N cross coupling conditions are used to access the parent (non-core extended) DHP PCs **3**, **4**, and **5**. PC **5** was synthesized using C-N coupling conditions employed by our group for the synthesis of PCs **3**, **4**, and **5**, when we first reported the use of these PCs for O-ATRP in 2016.[12] Unfortunately, under these previous conditions the yield reported for PC **3** was only 3%.[12] In this work, we explored other C-N cross coupling conditions for the synthesis of PC **3** that were previously reported for the synthesis of 2-naphthyl-10-phenoxazine.[11] Using bis(dibenzylideneacetone) palladium(0) ($Pd(dba)_2$)and tri-tertbutyl phosphine ($P(tBu)_3$) for the C-N cross coupling of dihydrophenazine (**2**) and 1-bromonaphthalene (instead of RuPhos and RuPhos precatalyst), we observed improved yields of PC **3** (57%). PC **4** was also synthesized using $Pd(dba)_2$ and $P(tBu)_3$. Core-extension of PCs **3**, **4**, and **5** was accomplished by first brominating the DHP core (utilizing previously reported methods for the synthesis of core-extended DHPs)[14] then through a Suzuki-Miyaura C-C cross-coupling reaction with the brominated DHP and the boronic acid of a phenyl substituent with either an electron withdrawing group (**a**) or an electron donating group (**b**) (Figure 1.3). Non-core-extended

DHPs (or "parent DHPs") discussed in this work include PCs **3**, **4**, and **5** which have *N*-aryl group **3**, **4**, or **5**, respectively (Figure 1.3). Core-extended DHPs discussed in this work include PCs **3a**, **4a**, and **5a** (which have electron withdrawing core substituent **a** and *N*-aryl group **3**, **4**, **or 5**, respectively, as well as PCs **3b** and **5b** which have electron donating core substituent **b** and either *N*-aryl group **3** or **5**, respectively.

1.3.2 Photophysical characterization. To study the photophysical properties of the core-extended DHPs, we employed a combination of spectroscopic techniques and computational approaches. First, we sought to probe how the *N*-aryl group and core substituents in core-extended DHPs impact photophysical PC properties (specifically the $\lambda_{max,abs}$, $\varepsilon_{max,abs}$), the ability to access CT states, the excited state energies (E_{S1} & $E_{T1,comp}$), quantum yield of fluorescence (ϕ_f), and the excited state lifetimes (τ_{S1} & τ_{T1}).

1.3.2a Absorption. We hypothesized that core-extension would generally lead to a red-shift in the $\lambda_{max,abs}$ through stabilization of the π* orbitals involved in photoexcitation, but were uncertain how the electron withdrawing or donating character of the core substituents might influence $\lambda_{max,abs}$. In previous studies where structure-property relationships of PCs with donor-acceptor structures similar to core-extended DHPs reported herein were examined (i.e., *N*-aryl phenoxazines[11], *N,N*-diaryl dihydrophenazines[14], and *N*-aryl dimethyl dihydroacridines[19]), core-extension was shown to red-shift $\lambda_{max,abs}$. We observed that core-extension does lead to a red-shifted $\lambda_{max,abs}$ for these PCs (Table 1.1), however there appeared to be little to no notable effect on $\lambda_{max,abs}$ imparted by the electron withdrawing or electron donating character of the core-substituent. The $\lambda_{max,abs}$ for **3a** ($\lambda_{max,abs}$ = 385 nm) and **3b** ($\lambda_{max,abs}$ = 385 nm) were experimentally determined to be identical and that the $\lambda_{max,abs}$ of **5a** ($\lambda_{max,abs}$ = 373 nm) and **5b** ($\lambda_{max,abs}$ = 371 nm) are separated by only 2 nm. In contrast to the core substituents, the identity of the *N*-aryl group has a notable impact on $\lambda_{max,abs}$. The $\lambda_{max,abs}$ red-shifts by ~12 nm when the *N*-aryl group on CE-DHPs is changed from 2-naphthylene (PCs **5a** and **5b**) to 1-napthalene (PCs **3a** and **3b**). Additionally, exchanging a naphthalene *N*-aryl group for an electron donating *N*-aryl group (4-

methoxyphenol) results in a red-shift from 7 to 19 nm (PC **4a**: $\lambda_{max,abs}$ = 392 nm). Of the core-extended DHPs that have been reported, **4a** has the highest measured $\lambda_{max,abs}$ (392 nm).[14]

Table 1.1 Photophysical properties of PCs investigated in this study. [a]Maximum wavelength of absorption was measured using UV-Vis in DMAc. [b]Molar absorptivity calculated at λ_{max} in DMAc. [c] Maximum wavelength of emission was measured using steady-state fluorescence spectroscopy in DMAc. [d]Singlet energies were calculated using the maximum wavelength of emission (E(eV)=1239.8 / λ (nm)). [e]DFT calculations were performed at the uM06/6-311+G(d,p)//uM06/6-31+G(d,p) level of theory with CPCM-described solvation in DMAc. [f]Quantum yield of fluorescence was measured in DMAc using absolute methods. [g]Singlet excited state lifetime was determined by kinetic emission. [h] Triplet excited state lifetime was determined by kinetic absorption. [i]No triplet signal detected. [k]Singlet excited state lifetime was too short to measure as it was below the detection limit of the instrument.

PC	$\lambda_{max,abs}$ (nm)[a]	$\varepsilon_{max,abs}$ ($M^{-1}cm^{-1}$)[b]	$\lambda_{max,em}$ (nm)[c]	Stokes Shift (nm)	$E_{S1,exp}$ (eV)[d]	$E_{T1,comp}$ (eV)[e]	Φ_f (%)[f]	τ_{S1} (ns)[g]	τ_{T1} (μs)[h]
3	362	6,100	663	297	1.87	2.23	1.32	9	0.63
3a	385	22,200	586	201	2.12	1.91	9.00	17	144
3b	385	13,100	636	251	1.95	2.07	4.31	11	42
4	373	5,200	467	94	2.66	2.29	23.0	37	88
4a	392	20,900	599	207	2.07	1.82	36.0	13	--[i]
5	343	5,900	654	311	1.90	2.19	0.72	--[k]	3.5
5a	373	27,600	587	214	2.11	1.89	35.0	17	--[i]
5b	371	15,900	621	250	2.00	1.99	4.00	11	108

Though the identity of the core substituents has little measurable effect on $\lambda_{max,abs}$, the molar absorptivity at $\lambda_{max,abs}$ ($\varepsilon_{max,abs}$) is significantly impacted by the electronics of the core substituent (Figure 1.4). We hypothesized that, in accordance with previous work, $\varepsilon_{max,abs}$ would increase with core-extension as a result of extended conjugation of the PC core. Indeed, the measured $\varepsilon_{max,abs}$ values are between 7,000 and 21,700 $M^{-1}cm^{-1}$ larger for core-extended PCs than non-core-extended parent PCs. The measured increase in efficiency of photon absorption in core-extended PCs is corroborated by oscillator strength (f) values predicted using time-dependent density functional theory calculations (TD-DFT) (Figure 1.4B & Figures A1.61-A1.69). The predicted f values shown in Figures 3 and Figures A1.61-A1.69 approximate the strength of a certain electronic transition, in this case a π-π* transition. Furthermore, we found that the $\varepsilon_{max,abs}$ of PCs core-extended with the EWG **a** are significantly higher than the $\varepsilon_{max,abs}$ for PCs core-extended with EDG **b**. Specifically, the $\varepsilon_{max,abs}$ measured for **3a** ($\varepsilon_{max,abs}$ = 22,200) is 8,800 $M^{-1}cm^{-}$

[1] greater than the $\varepsilon_{max,abs}$ of **3b** ($\varepsilon_{max,abs}$ = 13,100) and the measured $\varepsilon_{max,abs}$ of **5a** ($\varepsilon_{max,abs}$ =27,600) is 11,400 $M^{-1}cm^{-1}$ higher than for **5b** ($\varepsilon_{max,abs}$ = 15,900). To explore potential factors that contribute

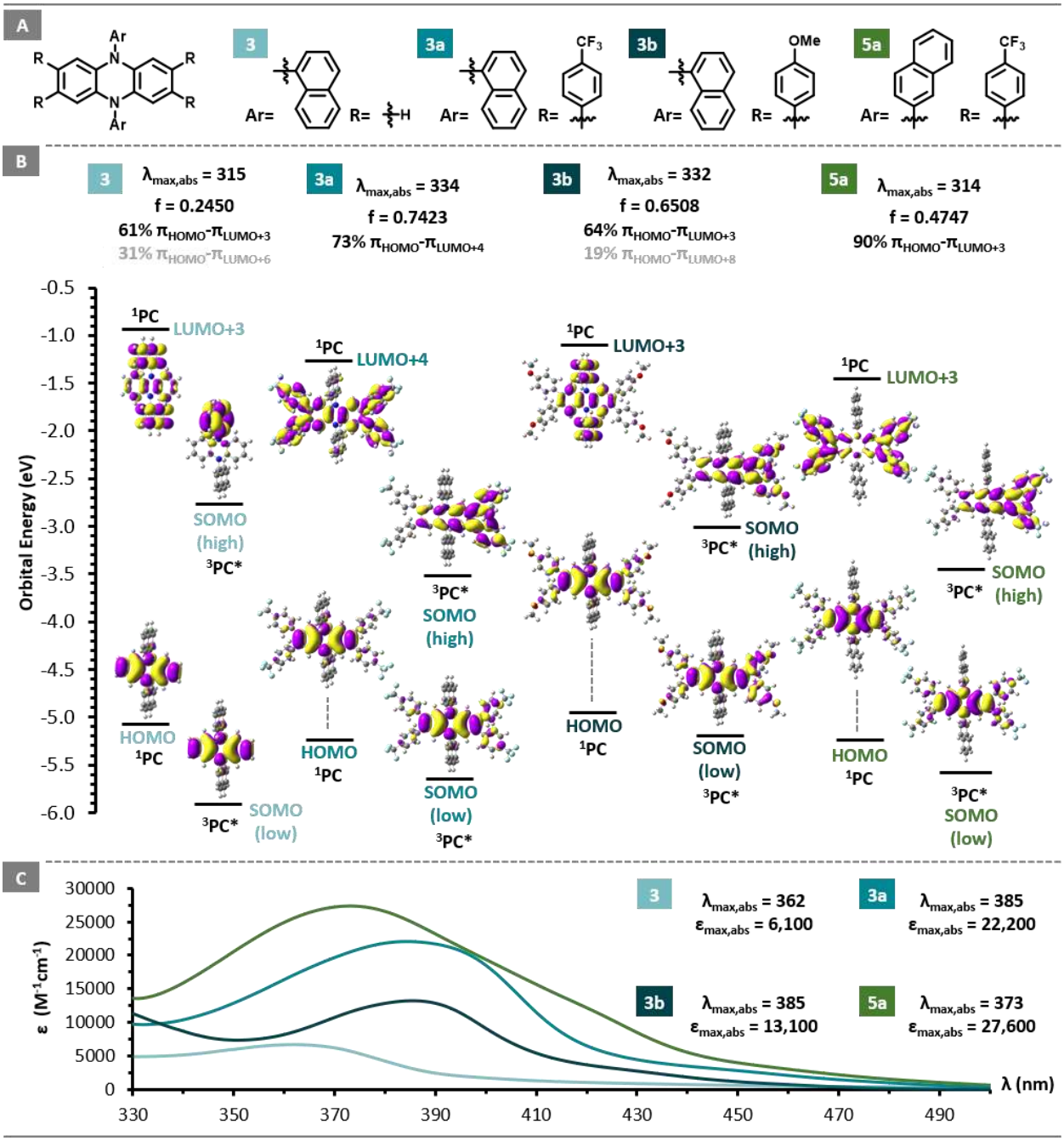

Figure 1.4: (A) Structures of PCs discussed in this figure. (B) Results from time-dependent density functional theory (TD-DFT) calculations of orbitals involved in excitation of PCs **3**, **3a**, **3b**, and **5a** at the predicted $\lambda_{max,abs}$ (top) and visualized molecular orbitals predicted to be involved in photoexcitation (bottom). (C) UV−vis spectra of PC **3**, **3a**, **3b**, and **5a** acquired in *N,N*-dimethylacetamide (DMAc) with observed maximum wavelength of absorption ($\lambda_{max,abs}$) in units of nm and molar extinction coefficient ($\varepsilon_{max,abs}$) in units of $M^{-1}cm^{-1}$ shown.

to the significant difference in $\varepsilon_{max,abs}$ between PCs **3a**, **4a**, and **5a** vs. PCs **3b** and **5b**, we used TD-DFT. The electronic transitions with the highest predicted oscillator strengths in PCs **3a**, **4a**, and **5a**, are predicted to occur between a π_{HOMO} centered on the PC core and a π_{LUMO+n} spread across the PC core and all four core-substituents (Figure 1.4B & Figure A1.65-1.66). In contrast to PCs **3a**, **4a**, and **3b**, the electronic transitions with the highest predicted oscillator strengths for PCs **3b** and **5b** are forecasted to occur between a π_{HOMO} centered on the PC core and a π_{LUMO+n} spread across the core and both *N*-aryl substituents (Figure 1.4B and Figure A1.69). Interestingly, the π_{LUMO+n} is mixed excited state upon initial photoexcitation where charge transfer (CT) is not fully delocalized to the *N*-aryl group or the core-substituents, but nor is the nature of the excited state purely of predicted to have greater involvement in absorption resides more heavily on the core of **3b** than it does for **5b**. Our understanding is that all the core-extended DHPs are predicted to access a locally excited (LE) character. Considering the differences in where π_{LUMO+n} is predicted the PC could influence the efficiency of photon absorption accounting for the difference in $\varepsilon_{max,abs}$ reside for PCs **3a**, **4a**, and **5a** vs. for **3b** and **5b**, we postulate that the location of π* orbitals on that we observed for core-extended DHPs with different core-substituents but the same *N*-aryl to group, although further investigations are necessary to further support this hypothesis.

Though there is a measurable change in the $\varepsilon_{max,abs}$ for CE-DHPs with different *N*-aryl groups, the shifts are of a lesser magnitude than for those observed from changing electron donating core substituents to electron withdrawing core substituents on PCs with the same *N*-aryl group. **4a** has the lowest $\varepsilon_{max,abs}$ of **3a**, **4a**, and **5a**, but only ~1,300 $M^{-1}cm^{-1}$ lower than **3a**. Of all the CE-DHPs investigated here, **5a** has the highest molar extinction coefficient at $\varepsilon_{max,abs}$ ~27,600 $M^{-1}cm^{-1}$.[14] Despite the measured $\varepsilon_{max,abs}$ of **5a** being ~5,400 $M^{-1}cm^{-1}$ higher than **3a**, TD-DFT calculations predicted the $\varepsilon_{max,abs}$ to be highest for **3a** and lowest for **5a** (Figure 1.4C).

1.3.2b Charge Transfer. A combination of DFT and experimental approaches were used to examine the nature of PC*. Studies of non-core extended DHPs support access to a CT excited state located primarily on the naphthalene *N*-aryl substituent for PCs **3** and **5**[25] and that the

connectivity of the *N*-naphthalene group, specifically in *N*-aryl phenoxazines, does have an impact on CT.[26] In this work, we sought to investigate how core-extension and the *N*-aryl group impact CT in core-extended DHP PCs. First, we used fluorescence spectroscopy to measure the maximum emission wavelength ($\lambda_{max,em}$) and emission profile of parent and core-extended PCs (Table 1.1). For all the PCs, except PC **4**, we observed broad and featureless emission profiles suggesting that these PCs access a CT state for ^{1}PC*. We then used the measured $\lambda_{max,em}$ to calculate the Stokes shift ($\Delta\lambda$) for each PC [$\Delta\lambda = \lambda_{max,em}$ (nm) - $\lambda_{max,abs}$ (nm)]. We observed that $\Delta\lambda$ for PCs **3** and **5** decreases as a result of core-extension (Table 1.1). Interestingly, core-extension of PC **4** ($\Delta\lambda$ = 94 nm) to PC **4a** ($\Delta\lambda$ = 207 nm) results in a 113 nm increase in $\Delta\lambda$, suggesting that through specific core-modifications, parent DHPs that do not possess CT character can be modified to enable access to a CT state. As there is previous work supporting that core-extended *N*-aryl phenoxazines and core-extended DHPs can access a CT state located on the core substituents,[11,14] we hypothesized that core-extension with EWG **a** would increase the $\Delta\lambda$ of PCs **3a** and **5a** relative to PCs with EDG **b** (**3b** and **5b**). To the contrary, we observed that the $\Delta\lambda$ of PCs **3a** ($\Delta\lambda$ = 201 nm) and **5a** ($\Delta\lambda$ = 214 nm) was significantly less than for PCs **3b** ($\Delta\lambda$ = 251 nm) and **5b** ($\Delta\lambda$ = 250 nm). In addition to examining the Stokes shift, CT character can be assessed for ^{n}PC* by investigating solvatochromism, where the PC is dissolved in solvents of increasing polarity then photoexcitation via irradiation reveals how the energy of emission from polarized ^{n}PC* is stabilized by solvents of increasing polarity resulting in a lower energy (red-shifted) emission (Figure 1.5B and Figures A1.46-A1.53). Solvatochromism of **3b** and **5b** appear more extensive than solvatochromism of **3a** and **5a** supporting our observation that the former have a larger $\Delta\lambda$.

DFT calculations were also used to probe the CT character of PCs in the ground state and of ^{3}PC*. Generation and visualization of singly occupied molecular orbitals (SOMOs) of the parent and core-extended ^{3}PC* species show some degree of spatial separation between the low-lying SOMOs and high-lying SOMOs (Figure 1.5B & Figures A1.70-A1.72). For core-extended PCs,

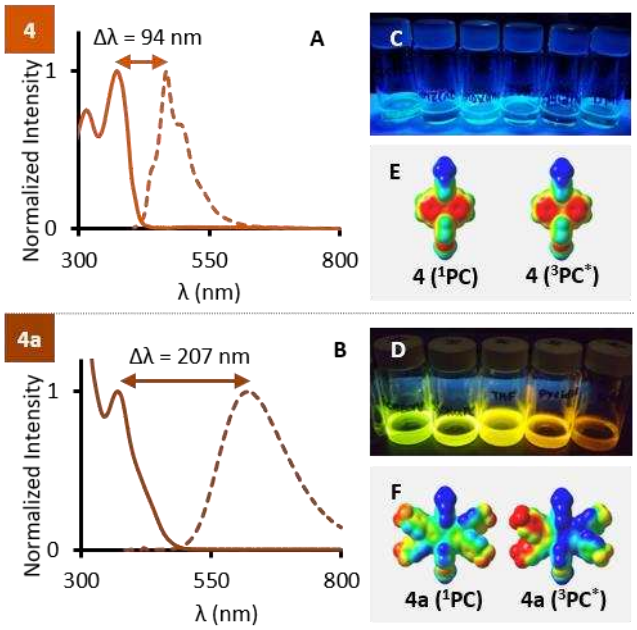

Figure 1.5: (A&B) Normalized absorption (solid) and emission (dashed) spectra of PCs **4** and **4a**, respectively, with Stokes shift shown in nm. (C&D) Photographs of PCs 4 and **4a** in solvents of increasing polarity from left to right while being irradiated with 365 nm light. (E&F) Electrostatic potential (ESP) maps (generated using DFT) showing areas of high electrostatic potential (red) and low electrostatic potential (blue) for the PC in the singlet ground state (left) and in the triplet excited state (right).

the high-lying SOMO of ^{3}PC* is predicted to be distributed across the core and two of the core substituents whereas the low-lying SOMO is predicted to reside centered primarily on the core of ^{3}PC* (Figure 1.5B and Figures A1.70-A1.72). Interestingly, there is minimal observable difference between the nature of the high lying SOMOs for **3b** and **3a** or between **5b** and **5a**.

Excited state absorption spectra of ^{3}PC* for core-extended DHPs was measured using time-resolved absorption (TA) spectroscopy. The spectral signals were followed at a single wavelength over time to obtain kinetic data which was then used to determine triplet excited state lifetimes for the PCs. When comparing spectral absorption traces (Figure 1.6) of PCs with the same core substituent (i.e., **3b** and **5b**) and PCs with the same *N*-aryl group (i.e., **3**, **3a**, and **3b**) we observed similar features that support the SOMOs computationally predicted by DFT (Figure 1.4). For **3**, **3a**, and **3b**, a similar absorption feature of ^{3}PC* is observed at ~333 nm. We propose that this absorption feature is representative of a high energy absorption from the low lying SOMO

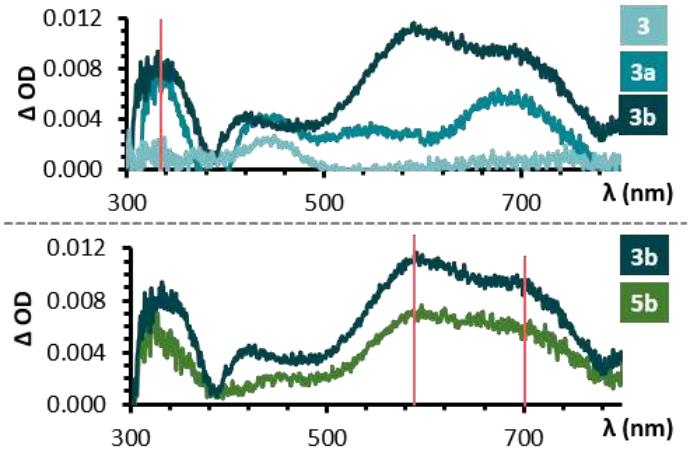

Figure 1.6: Overlapping spectral absorption traces of ^{3}PC* for **3**, **3a**, and **3b** (top) as well as PCs **3b** and **5b** (bottom).

of ^{3}PC* to some higher energy unoccupied molecular orbital ($LUMO_{+n}$). As the low lying SOMO of PCs **3**, **3a**, and **3b** are predicted to reside primarily on the core of the PC (Figure A1.70), it makes sense that the absorption features they have at ~333 nm would look similar. Furthermore, when comparing the spectral absorption traces of ^{3}PC* for **3b** and **5b**, we note two similar features at ~590 nm and ~698 nm. We propose that these lower energy transitions are representative of excitation from the higher lying SOMO on the PC core substituent to some $LUMO_{+n}$. As these PCs share the same core substituent, it seems logical that these spectral absorption features at ~590 nm and ~698 nm would be similar.

Interestingly, ESP maps of ^{3}PC* generated using DFT suggest that the electrostatic potential of **3a**, **4a**, and **5a** is, largely, shifted away from the *N*-aryl group to one side of the molecule where for **3b**, **4b**, and **5b** electron density, though also shifted away from the *N*-aryl group, is shared between all four core substituents (Figures A1.73-A1.75). For PC **4**, a small Δλ is observed (Figure 1.5A) as well as a lack of solvatochromism (Figure 1.5C) and there is no observable shift in electrostatic potential between the ground state singlet PC (^{1}PC) and ^{3}PC* (Figure 1.5E). Interestingly, when PC **4** is core-extended with EWG **a,** there is a measurable increase in Δλ (Figure 1.5B), in the extent of solvatochromism (Figure 1.5D), and electrostatic potential in ^{3}PC* appears to shift from ^{1}PC* so that electron density is heavily centered across

two of the core substituents rather than on the PC core (Figure 1.5F). These observations suggest that core-extension can be used to modulate CT in PCs with a primary structure that does not possess CT character in the excited state.

1.3.2c Excited State Energies. Energies of PC singlet excited states ($E_{S1,exp}$) were experimentally determined from the $\lambda_{max,em}$ measured using fluorescence spectroscopy. $E_{S1,exp}$ for core-extended DHPs ranged from 1.95 eV to 2.12 eV and was determined to be higher for all core-extended DHPs than for non-core-extended DHPs (with PC **4** vs. **4a** as an exception). Transitioning from EWG **a** to EDG **b** resulted in a decrease in E_{S1} by 0.17 eV for **3a** (2.12 eV) to **3b** (1.95 eV) and by 0.11 eV for **5a** (2.11 eV) to **5b** (2.00 eV). For core-extended DHPs the *N*-aryl group seems to have a smaller impact on E_{S1} than the electronics of the core substituent. $E_{S1,exp}$ for **3a** and **5a** are nearly isoenergetic and are higher than **4a** by <0.05 eV. Additionally, $E_{S1,exp}$ for **3b** and **5b** are only separated by 0.05 eV. Interestingly, core-extension of DHPs is predicted to lower the energy of the lowest energy triplet excited state ($E_{T1,comp}$) relative to the parent non-core-extended PCs. PCs **3a** ($E_{T1,comp}$ = 1.91 eV) and **3b** ($E_{T1,comp}$ = 2.07 eV) $E_{T1,comp}$ is predicted to be lower than that of the parent DHP PC (PC **3:** $E_{T1,comp}$ = 2.23 eV). The same trend is observed between PCs **5** ($E_{T1,comp}$ = 2.19 eV), **5a** ($E_{T1,comp}$ = 1.89 eV) and **5b** ($E_{T1,comp}$ = 1.99 eV) as well as for PCs **4** ($E_{T1,comp}$ = 2.29 eV) and **4a** ($E_{T1,comp}$ = 1.82 eV). For core-extended DHPs with the same core substituents, $E_{T1,comp}$ does not change by more than 0.08 eV which is within the margin of error for these calculations observed for a similar series of PCs.[19] The same is true for the parent DHPs, where no more than a 0.10 eV shift in $E_{T1,comp}$ is predicted. Interestingly, the largest changes in $E_{T1,comp}$ are between core-extended DHPs with the same *N*-aryl group, but different core substituents. For example, for PC **3b** ($E_{T1,comp}$ = 2.07 eV) core-extended with EDG **b** $E_{T1,comp}$ is predicted to be 0.16 eV higher in energy than $E_{T1,comp}$ for **3a** ($E_{T1,comp}$ = 1.91 eV), the latter of which is core-extended with EWG **a.** Our observations suggest that the electronics of the core-substituent could have more impact on $E_{T1,comp}$ than the identity of the *N*-aryl group, however an expanded study of core-extended DHPs is necessary to confirm this.

1.3.2d Excited State Lifetimes. The excited state lifetimes (τ) of PCs are posited to have a significant role in PC reactivity as the lowest energy excited state must persist long enough to engage in a bimolecular reaction. Though there are exceptions, an excited state lifetime of >1 ns is typically considered sufficient time for the excited state molecule to engage in a bimolecular reaction. Unfortunately, without measuring quantum yield of intersystem crossing (ϕ_{ISC}), we can currently only speculate on the relative concentrations of ^{1}PC* and ^{3}PC* in our system through measuring the quantum yield of fluorescence (ϕ_f ; *vide infra*), however we are able to investigate the impact of structural changes on the excited state lifetimes of core-extended and non-core-extended DHPs. Of the PCs for which we were able to measure excited state lifetimes, the singlet excited state lifetimes (τ_{S1}) ranged from 9 ns – 37 ns and triplet excited state lifetimes (τ_{T1}) ranged from 0.63 µs – 144 µs. For PC **3** (τ_{S1}= 9 ns; τ_{T1}= 0.63 µs), both τ_{S1} and τ_{T1} are shorter than for core-extended derivatives **3a** (τ_{S1}= 17 ns; τ_{T1}= 144 µs) and **3b** (τ_{S1}= 11 ns; τ_{T1}= 42 µs). This trend could not be verified for PCs **5** due to insufficient data. In contrast to PC **3**, a decrease in τ_{S1} is observed after core-extension of PC **4** (τ_{S1}=37 ns) to **4a** (τ_{S1}=13 ns). When examining the effect of core substituent electronics on excited state lifetimes, we found that for PCs **3** and **5**, τ_{S1} is longer for derivatives that are core-extended with EWG **a** (PCs **3a** & **5a**: τ_{S1}=17 ns) than with EDG **b** (PCs **3b** & **5b**: τ_{S1}=11 ns). For PCs **3a** and **3b** the same trend is observed for ^{3}PC* where for PC **3a** τ_{T1}=144 ns and for **3b** τ_{T1}=42 ns. The effect of the *N*-aryl group on the excited state lifetimes of core-extended DHPs is unclear. The experimentally determined τ_{S1} of **3a** (τ_{S1}= 17 ns) and **5a** (τ_{S1}= 17 ns) are equal as well as the τ_{S1} of **3b** (τ_{S1}= 11 ns) and **5b** (τ_{S1}= 11 ns), however there is a disparity in the triplet excited state lifetimes of core-extended PCs with different *N*-aryl groups (**3b**: τ_{T1}=42 ns; **5b**: τ_{T1}=108 ns). Interestingly, for non-core extended DHPs, PC **4** has a significantly longer τ_{S1} than PC **3**, and a longer τ_{T1} than PC **3** and PC **5,** suggesting that the *N*-aryl group does have a significant impact on the excited state lifetimes of non-core extended DHPs. We were unable to confidently measure and report the singlet excited state lifetime (τ_{S1})

of PC **5** as it was below the detection limit of our instrument. Furthermore, we were unable to detect a triplet signal for PCs **4a** and **5a**, therefore a triplet excited state lifetime (τ_{T1}) is not reported for those PCs.

1.3.2e Quantum Yield of Fluorescence. There are several pathways known to compete with relaxation of a singlet excited state molecule via fluorescence including non-radiative decay pathways, quenching through energy transfer or electron transfer, and phosphorescence from T1. Though ϕ_f does not lend complete information regarding the contribution of the aforementioned pathways in relaxation of ^{n}PC* to ^{0}PC, a low measured ϕ_f suggests that high quantum yield of intersystem crossing is possible for that PC.[11] We used fluorescence spectroscopy to experimentally determine the ϕ_f for both the core-extended and non-core extended PCs discussed in this study. On the whole, core-extension of DHPs appears to increase ϕ_f. The experimentally determined ϕ_f of PCs **3** (ϕ_f = 1.32%) and **5** (ϕ_f = 0.72%) were both lower than ϕ_f measured for the core-extended derivatives **3a** (ϕ_f = 9.00%) and **3b** (ϕ_f = 4.31%) as well as **5a** (ϕ_f = 35.0%) and **5b** (ϕ_f = 4.00%), respectively. We found that this trend also holds true for PCs **4** (ϕ_f = 23.0%) and **4a** (ϕ_f = 36.0%) which we noted have the highest ϕ_f out of the non-core-extended and core-extended DHPs, respectively. Though we did observe that ϕ_f for core-extended DHPs with EWG **a** is higher than that for core-extended PCs with EDG **b** (i.e., **3a** vs **3b**), the ϕ_f of PC **3a** is 26% lower than **5a**, so it seem there is significant variability between PCs that, though possessing the same core substituents, have different N-aryl groups.

1.3.3 Redox Properties: After assessing the photophysical properties of new core-extended DHPs, we sought to examine their electrochemical properties (Table 1.2). The experimental singlet excited state reduction potentials ($E^{0*}_{S1,exp}(^{2}PC^{\bullet+}/^{1}PC^{*})$) for core-extended DHPs in this study range from -1.62 to -1.78 V vs SCE. The $E^{0*}_{S1,exp}(^{2}PC^{\bullet+}/^{1}PC^{*})$ we measured for **3a**, **3b**, **5a**, and **5b** suggest that they are slightly more reducing than the parent non-core extended analogues; however $E^{0*}_{S1,exp}(^{2}PC^{\bullet+}/^{1}PC^{*})$ does not vary by more than 0.14 V vs SCE. Contrary to this trend, $E^{0*}_{S1,exp}(^{2}PC^{\bullet+}/^{1}PC^{*})$ of PC **4a** ($E^{0*}_{S1,exp}(^{2}PC^{\bullet+}/^{1}PC^{*})$ = -1.73 V vs SCE) is lower (more

positive) than that of PC **4** ($E^{0*}_{S1,exp}$(^{2}PC$^{\bullet+}$/^{1}PC*) = -2.5 V vs SCE, respectively). The experimental oxidation potentials of ^{2}PC$^{\bullet+}$ were estimated from the $E_{1/2}$ (^{2}PC$^{\bullet+}$/^{1}PC) which was determined using

Table 1.2 Measured and predicted electrochemical properties of PCs investigated in this study. [a]All measurements were performed in a 3-compartment electrochemical cell with an Ag/AgNO$_3$ reference electrode in MeCN (0.01 M) and 0.1 M NBu$_4$PF$_6$ electrolyte solution. DMAc was used to solvate the PCs and in the working electrode compartment, while platinum was used as both the working and counter electrodes. *E* (V vs SCE) = *E* (V vs Ag/AgNO$_3$ [0.01 M]) + 0.298 V). [b]DFT calculations were performed at the uM06/6-311+G(d,p)//uM06/6-31+G(d,p) level of theory with CPCM-described solvation in DMAc. [c]Singlet excited state reduction potentials were calculated using the singlet energies (estimated from the maximum wavelength of emission) and the $E_{1/2}$. [d]Values were taken from ref. 11.

PC	$\lambda_{max,abs}$ (nm)[a]	$\varepsilon_{max,abs}$ ($M^{-1}cm^{-1}$)[b]	$\lambda_{max,em}$ (nm)[c]	Stokes Shift (nm)	$E_{S1,exp}$ (eV)[d]	$E_{T1,comp}$ (eV)[e]	ϕ_f (%)[f]	τ_{S1} (ns)[g]	τ_{T1} (µs)[h]
3	362	6,100	663	297	1.87	2.23	1.32	9	0.63
3a	385	22,200	586	201	2.12	1.91	9.00	17	144
3b	385	13,100	636	251	1.95	2.07	4.31	11	42
4	373	5,200	467	94	2.66	2.29	23.0	37	88
4a	392	20,900	599	207	2.07	1.82	36.0	13	--[i]
5	343	5,900	654	311	1.90	2.19	0.72	--[k]	3.5
5a	373	27,600	587	214	2.11	1.89	35.0	17	--[i]
5b	371	15,900	621	250	2.00	1.99	4.00	11	108

CV. $E_{1/2}$ (^{2}PC$^{\bullet+}$/^{1}PC) for core-extended DHPs reported in this study range from 0.23 to 0.38 V vs SCE. Core-extension of PCs **3** and **5** resulted in no more than a 0.17 V vs SCE increase in $E_{1/2}$ (^{2}PC$^{\bullet+}$/^{1}PC), however core-extension of **4** ($E_{1/2}$ (^{2}PC$^{\bullet+}$/^{1}PC) = 0.16 V vs SCE) with EWG **a** significantly decreased the stability of ^{2}PC$^{\bullet+}$ (PC **4a**: $E_{1/2}$ (^{2}PC$^{\bullet+}$/^{1}PC) = 0.34 V vs SCE). On the whole, core-extension of DHPs appears to destabilize ^{2}PC$^{\bullet+}$, rendering the core-extended derivatives more oxidizing than the parent DHPs while also destabilizing E_{S1} rendering **3a**, **3b**, **5a**, and **5b** more reducing from ^{1}PC* than the parent derivatives.

Taking a closer look at the effects of the core substituent electronics on the redox properties, we found that $E^{0*}_{S1,exp}$(^{2}PC$^{\bullet+}$/^{1}PC*) is slightly more negative for **3a** and **5a** than for **3b** and **5b**, though only by 0.06 to 0.11 V vs S CE (Figure 1.7). Changing the *N*-aryl group on core extended DHPs appears to have even less impact than core-electronics on $E^{0*}_{S1,exp}$(^{2}PC$^{\bullet+}$/^{1}PC*). Interestingly, computationally predicted triplet excited state reduction potentials

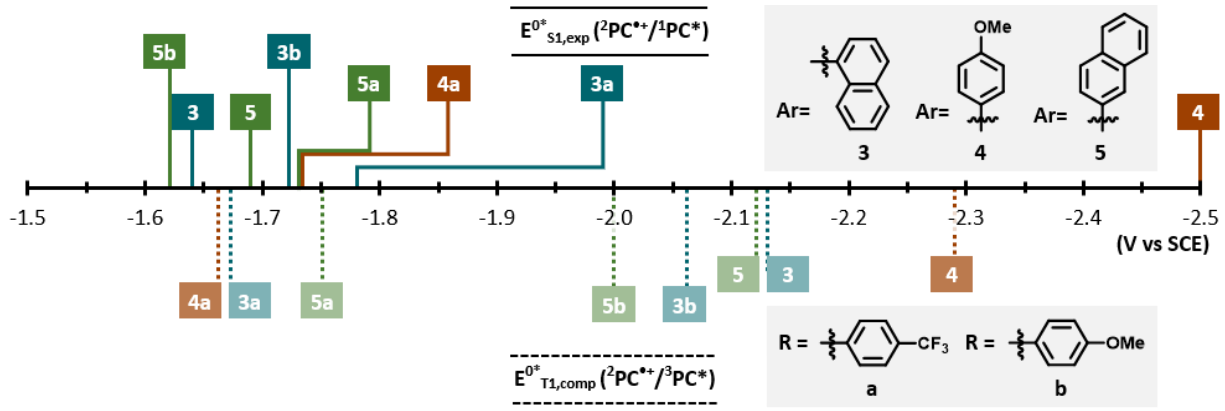

Figure 1.7: (Top) Electrochemical series of experimentally measured singlet excited state redox potentials (top) and computationally predicted triplet excited state reduction potentials (bottom) of PCs investigated in this study.

($E^{0*}_{T1,comp}$(^{2}PC$^{\bullet+}$/^{3}PC*)) have an opposite trend to what was observed for $E^{0*}_{S1,exp}$(^{2}PC$^{\bullet+}$/^{1}PC*) excluding PCs **4** and **4a**. $E^{0*}_{T1,comp}$(^{2}PC$^{\bullet+}$/^{3}PC*) is predicted to be lower for core-extended PCs (i.e., for **3** $E^{0*}_{T1,comp}$(^{2}PC$^{\bullet+}$/^{3}PC*) = -2.13 V vs SCE and for PC **3a** $E^{0*}_{T1,comp}$(^{2}PC$^{\bullet+}$/^{3}PC*) = -1.67 V vs SCE). When analyzing the effects of the core substituent electronics on $E^{0*}_{T1,comp}$(^{2}PC$^{\bullet+}$/^{3}PC*), we found that $E^{0*}_{T1,comp}$(^{2}PC$^{\bullet+}$/^{3}PC*) is slightly more negative for **3b** ($E^{0*}_{T1,comp}$(^{2}PC$^{\bullet+}$/^{3}PC*) = -2.06 V vs SCE)) and **5b** ($E^{0*}_{T1,comp}$(^{2}PC$^{\bullet+}$/^{3}PC*) = -2.00 V vs SCE)) than for **3a** ($E^{0*}_{T1,comp}$(^{2}PC$^{\bullet+}$/^{3}PC*) = -1.67 V vs SCE)) and **5a** ($E^{0*}_{T1,comp}$(^{2}PC$^{\bullet+}$/^{3}PC*) = -1.75 V vs SCE)). As was observed for $E^{0*}_{S1,exp}$(^{2}PC$^{\bullet+}$/^{1}PC*) values, changing the *N*-aryl group in core-extended DHPs is predicted to have a smaller effect on ($E^{0*}_{T1,comp}$(^{2}PC$^{\bullet+}$/^{3}PC*) than the changing the electronics of the core-substituent. Redox reversibility was observed for all core-extended DHPs to varying degrees suggesting that they can perform as catalysts in reactions dependent on repeated reduction and oxidation reactions such as O-ATRP (Figures A1.54-A1.60).

***1.3.4 O-ATRP*:** After investigating the structure-property relationships for the core-extended DHPs presented in this work, we sought to understand how those properties ultimately impact PC performance in O-ATRP. First, PCs were applied in the O-ATRP of methyl methacrylate (MMA) using diethyl 2-bromo-2methylmalonate (DBMM) as the polymerization initiator and *N,N*-dimethylacetamide (DMAc) as the solvent (unless otherwise noted) so that [MMA]:[DMAc]:[DBMM] = [1000]:[1000]:[10] (Figure 1.8 & Table 1.3). PC loadings were varied

between 500 ppm and 10 ppm with the ppm of PC being relative to mols of monomer. All polymerizations were irradiated in a white light LED beaker and carried out under N_2. PC

Figure 1.8: General reaction scheme for the light driven polymerization of methyl methacrylate (MMA) using a photocatalyst (PC) and diethyl 2-bromo-2-methylmalonate (DBMM) as the initiator.

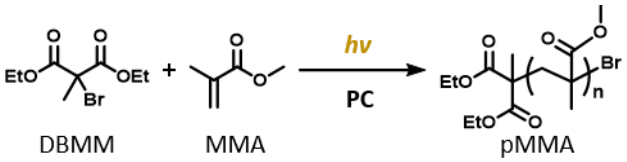

performance was assessed based on the degree of control with which the polymerization proceeded. Polymerization control was evaluated by first analyzing initiator efficiency (*I**) and dispersity (*Đ*). *I** is representative of the theoretical number average molecular weight ($M_{n,theo}$)

Table 1.3. O-ATRP Results from Employing PCs for the Polymerization of MMA at Varied Catalyst Loadings. [a]All polymerizations were conducted using MMA (9.35 mmol at 4.63 M) as the monomer and DBMM (0.093 mmol) as the initiator in a ratio of [1000]:[100] with DMAc as the solvent. [b]PC loading is relative to mols of monomer. [c] Determined by ^{1}H-NMR spectroscopy. [d]Measured using GPC. [e]Initiator efficiency (I*) calculated by ((theoretical M_n / observed M_n)*100). [g]Data obtained from ref. 12.; polymerization was conducted using ethyl α-bromophenylacetate as the initiator rather than DBMM.

Run	PC	[PC] (ppm)[b]	Conv.[c]	M_n (kDa)[d]	$Đ$ (M_w/M_n)[d]	I*[e]
2	3	100	68%	8.97	1.07	78%
3	3	50	85%	8.26	1.19	105%
5	3a	100	65%	7.71	1.10	87%
6	3a	50	86%	8.80	1.07	92%
7	3a	10	67%	7.17	1.49	97%
8	3b	100	51%	5.32	1.57	101%
9	4[g]	1000	70%	24.7	1.57	29%
10	4a	100	65%	7.57	1.15	90%
11	4a	50	76%	7.53	1.27	104%
12	4a	10	67%	7.17	1.49	97%
14	5	100	77%	8.74	1.18	91%
15	5	50	87%	12.8	1.20	70%
16	5	10	62%	7.43	1.79	88%
18	5a	100	73%	8.08	1.09	93%
19	5a	50	80%	7.34	1.28	112%
20	5a	10	70%	7.54	1.42	96%
22	5b	100	73%	8.25	1.54	92%

divided by the observed number average molecular weight (M_n). If *I** > 100%, this suggests that initiation was over efficient and that some of the polymer chains in the polymerization were

initiated by means other than through reaction with the initiator (autoinitiation is one example). If I^* < 100, this suggests that initiation was inefficient due to undesirable side reactions or other processes that interfered with the polymerization of one polymer chain from one molecule of initiator. Herein, an I^* > 90% after 8h is considered good. PC control over polymer dispersity is considered moderate if 1.3 < $Đ$ < 1.5, good if 1.1 < $Đ$ < 1.3, and excellent if $Đ$ < 1.1. Additionally, PC control over the polymerization was evaluated based on the linearity of M_n growth with respect to monomer conversion throughout the polymerization and by the proximity of M_n to $M_{n,theo}$) at the same percent conversions. Polymerizations that proceeded with linear M_n growth and with M_n closer to $M_{n,theo}$ were considered to have been more controlled than polymerization lacking those characteristics.

Previous work has demonstrated that DBMM can add to the core of parent DHP PC resulting in a decrease in I^*.[15,16] Based on the results of previous work, we hypothesized core-extension of PCs **3**, **4**, and **5** would yield polymers with initiator efficiencies closer to unity due to the presence of core-extending substituents blocking sites on the PC core known to undergo radical addition of the initiator.[14] Indeed, the I^* of polymers synthesized using core-extended DHPs was typically higher than for parent DHPs, however that increase varied largely (between 1% and 42% increase in I^*). Exceptions to this trend include PC **3a** employed at 50 ppm in DMAc (Table 1.3, Runs 6) and PC **5a** employed at 500 ppm (Table 1.3, Run 17) where polymers produced with the core-extended DHP did not have a higher I^* under the aforementioned conditions.

We also hypothesized that PCs **3a**, **3b**, **5a**, and **5b** would show increased control over the polymerization of MMA, in comparison to PCs **3** and **5**. Our reasoning stemmed from the fact that PCs **3a**, **3b**, **5a**, and **5b** have higher $\varepsilon_{max,abs}$ at a $\lambda_{max,abs}$ closer to the emission of the LEDs than PCs **3** and **5** and are equally if not more oxidizing from $^2PC^{\bullet+}$, have higher experimentally determined $E^{0*}_{S1,exp}$ ($^2PC^{\bullet+}/^1PC^*$), and possess CT character. To the contrary, we observed no trends suggesting that core-extended PCs consistently produce polymer with lower $Đ$ or closer to

unity I^* than their analogous non-core-extended DHP. In fact, we observed that between PCs **3** and **3a** and between PCs **5** and **5a,** at the same PC loadings (50ppm and higher), $Đ$ varied by less than 0.09, except for in run 6 (Table 1.3) where **3a** employed at 50 ppm loading yields polymer with $Đ$ lower by 0.12 than polymer produced with **3** at 50 ppm PC loading. Overall, PCs core-extended with EDG **b** (PCs **3b** and **5b**) did not perform well in O-ATRP of MMA. For PCs **3b** and **5b**, M_n growth was not linear with respect to monomer conversion and $Đ$ stayed above 1.5 at all conversions, indicating poor control throughout the duration of the polymerization (Figures A1.83, A1.95, & A1.96). As the properties of PCs **3b** and **5b** are comparable to other core-extended DHPs that performed well, we hypothesize that the relatively lower solubility of **3b** and **5b** may hinder their efficacy in controlling the polymerization. Neither **3b** nor **5b** dissolve completely during the polymerization, thus the catalyst loading is uncertain. Furthermore, the insolubility could cause scattering of light, compromising maximum irradiation of the dissolved polymerization mixture and lowering the efficiency and uniformity of activation.

One of the most notable results we observed as a result of core-extension was that for PC **4**. Core-extension of PC **4** with EWG **a** to make PC **4a** enabled good control over the synthesis of poly(methyl methacrylate) (PMMA) ($Đ$ = 1.27, I^* = 104%) at 50 ppm PC loading. In comparison, the parent PC to PC **4a** (PC **4**) has shown poor control over the O-ATRP of MMA at a PC loadings as high as 1000 ppm ($Đ$ = 1.57, I^* = 29%).[13] To explain this observation, we reviewed three notable differences in the photophysical and electrochemical properties of PCs **4** and **4a**. First, we have shown new data to support that **4a** can access a CT excited state due to core-extension whereas PC **4** is not predicted to access a CT excited state, the former of which has been attributed as an important PC property for success in O-ATRP.[13] Second, the oxidation potential of PC **4a** ($E_{1/2}$ ($^2PC^{\bullet+}/^1PC$) = 0.34 V vs SCE) provides more overpotential than PC **4** ($E_{1/2}$ ($^2PC^{\bullet+}/^1PC$) = 0.16 V vs SCE) for driving deactivation in O-ATRP, the latter being essential to minimizing termination reactions during the polymerization which compromise control. Last, the $\varepsilon_{max,abs}$ of PC **4a** ($\varepsilon_{max,abs}$=20,900 $M^{-1}cm^{-1}$) is significantly higher than for PC **4** ($\varepsilon_{max,abs}$=5,200 M^{-}

$^{1}cm^{-1}$). As noted earlier, a high $\varepsilon_{max,abs}$ is posited to increase the population of $^{n}PC^{*}$ enabling uniform activation,[29] however results observed from the application of PCs **3** ($\varepsilon_{max,abs}$=5,500 $M^{-1}cm^{-1}$) and **5** ($\varepsilon_{max,abs}$=5,900 $M^{-1}cm^{-1}$) show that polymerization control was achieved at PC loadings as low as 50 ppm despite their comparable $\varepsilon_{max,abs}$ values to PC **4**.

For PCs that yielded polymer with $Đ$ <1.5 after 8h of irradiation at 100 ppm PC loading (PCs **3**, **3a**, **4a**, **5**, **5a**), we proceeded to test their efficacy at even lower PC loadings (50 ppm and 10 ppm). Initially, we hypothesized that core-extended DHPs would give superior control at lower PC loadings in comparison to parent DHPs due to their high molar extinction coefficients and the blockage of sites on the PC core noted to undergo side reaction with the initiator. At 100 ppm PC **5a** outperforms PCs **3**, **3a, 4a**, and **5**; $Đ$ remained below 1.5 at all conversions, M_n growth was linear with respect to conversion, at 8h the initiator efficiency was closest to unity (I^* = 93%), and $Đ$ = 1.09 (Table 1.3, Run 18) (Figure A1.92). At 50 ppm, PC **3a** outperforms PCs **3**, **4a**, **5**, and **5a** (Table 1.3, Run 6). Although at 8 h, I^* is lower when using PC **3a** at 50 ppm (I^* = 92%) than for runs with PC **3**, **4a**, and **5a**, the run using PC **3a** is unique in that $Đ$ remained below 1.5 at all conversions and M_n growth remained linear with respect to conversion (Figure A1.81). Interestingly, for polymerizations shown in Table 1.3 that were run at 10 ppm PC loading, $Đ$ > 1.5 at all conversions, indicating poor control throughout the polymerization (Figures A1.82, A1.86, A1.90, & A1.94). Additionally, for the 10 ppm PC loading runs employing PCs **3a**, **4a**, and **5a**, pMMA only approaches the targeted M_n at high conversions—an indicator that initiation is slow. Initially, we posited that, the lack of control at 10 ppm PC loading was due to the concentration of PC being too low to afford a sufficient concentration of $^{n}PC^{*}$ upon photoexcitation. Interestingly, after doing a solvent screening using PC **3a** (see discussion below) we tried applying **4a** at 10 ppm in the same polymerization conditions noted above but using benzene as the solvent instead of DMAc (Table A1.4, run 33) and observed improved results in polymerization control ($Đ$ = 1.33 and I^* = 102%) compared to the run using **4a** at 10 ppm in DMAc ($Đ$ = 1.49 and I^* = 97%).

After determining that PC **3a** performed best at the lowest successful tested PC loading (50 ppm) for the polymerization of MMA in DMAc using DBMM as the initiator, we sought to assess the effect of solvent polarity on the polymerization results. Previously, several reports have shown that solvent can have a significant impact on polymerization control, especially for DHP PCs.[13,15,25] PC **3a** was used to polymerize MMA at 50 ppm PC loading in tetrahydrofuran (THF), ethyl acetate (EtOAc), benzene, and dichloromethane (DCM), in turn. Interestingly, we found that the performance of PC **3a** in the most polar solvent we tested (DMAc) ($Đ$ = 1.07, I^* = 92%) yielded nearly identical results at 8h as the polymerization conducted in the least polar solvent we tested (benzene) ($Đ$ = 1.06, I^* = 92%). For both of the aforementioned polymerizations (Table 1.4, Runs 6 & 25), M_n growth was linear with respect to monomer conversion and $Đ$ < 1.5 throughout the polymerization (Figures A1.81 & A1.99). As observed in previous studies,[13] monomer conversion was slower in solvents of increasing polarity.

Table 1.4. Solvent screening with PC **3a** for O-ATRP of MMA. [a]All polymerizations were conducted using MMA as the monomer, DBMM as the initiator, and PC **3a** as the catalyst in a ratio of [1000]:[100]:[0.05]. [b]Determined by ^{1}H-NMR spectroscopy. [d]Measured using GPC. [d]Initiator efficiency (I^*) calculated by ((theoretical M_n/observed M_n)*100).

Run	PC	Solvent	Conv.[b]	M_n (kDa)[c]	$Đ$ (M_w/M_n)[c]	I^*[d]
6	**3a**	DMAc	86%	8.80	1.07	92%
23	**3a**	THF	78%	9.88	1.17	81%
24	**3a**	EtOAc	87%	8.79	1.23	102%
25	**3a**	Benz	89%	10.0	1.06	92%
26	**3a**	DCM	94%	8.88	1.24	109%

Overall, the photophysical and electrochemical properties of core-extended PCs reported in Table 1.1 and Table 1.2 did not appear to significantly impact control over the polymerization of MMA through O-ATRP or their ability to control the polymerization at low ppm PC loadings > 50 ppm except for comparing results obtained using PC **4**[13] vs PC **4a**.

To further probe the activity of core-extended DHPs, we investigated their ability to control the polymerization of an acrylate monomer: n-butyl acrylate (nBA). The polymerization of nBA by O-ATRP has been a persistent challenge in the field for several reasons. First, the high rate of propagation of acrylates necessitates highly efficient deactivation to achieve a controlled

polymerization ($Đ$ < 1.5). Additionally, the increased bond strength of the carbon-bromine bond at the polymer chain end of poly(n-butyl acrylate) (pBA) relative to pMMA[30] necessitates a greater driving force for activation relative to methacrylates. In combination, these properties of acrylate monomers and polymers require increased driving force for both activation and deactivation from PCs. Though the conditions and PCs applied for O-ATRP of nBA in this work did not yield polymer with $Đ$ < 1.5 (Table A1.4), recent work by McCarthy *et al.* and Buss *et al.* demonstrated controlled polymerization of nBA via O-ATRP using alkyl core-substituted DHPs and *N*-aryl dimethyl dihydroacridines, respectively.[15,19] We hypothesize that under the conditions investigated in this study core-extended DHPs do not have sufficient driving force for enabling efficient deactivation, and thus controlled polymerization, of acrylates and other monomers with high rates of propagation.

One of the more well-studied PCs for O-ATRP is 3,7-di(4-biphenyl) 1-naphthalene-10-phenoxazine (**PhenO**). However, to the best of our knowledge, **PhenO** has not been applied in O-ATRP at PC loadings lower than 1000 ppm. **PhenO** has a comparable $\varepsilon_{max,abs}$ ($\varepsilon_{max,abs}$ = 26,600) to the PCs reported herein, absorbs at a comparable $\lambda_{max,abs}$ ($\lambda_{max,abs}$ = 388 nm), has a higher oxidation potential ($E_{1/2}$ ($^2PC^{\bullet+}/^1PC$) = 0.65V vs SCE), possesses CT character, has a longer triplet excited state lifetime (τ_{T1} = 480 µs), has a high ϕ_{T1} (ϕ_{T1} = 90%), and is sufficiently reducing ($E^{0*}_{S1,exp}$ ($^2PC^{\bullet+}/^1PC^*$) = -1.80 V vs SCE; $E^{0*}_{T1,comp}$ ($^2PC^{\bullet+}/^3PC^*$) = -1.70 V vs SCE) compared to core-extended DHPs.[31] To gain a better understanding of what properties might enable core-extended DHPs to work well at low ppm PC loadings, we decided to investigate **PhenO** in the O-ATRP of MMA at 50 ppm using DBMM as the initiator and DMAc as the solvent. As **PhenO** has comparable properties to core-extended DHPs, except for a higher oxidation potential (which could provide more driving force for efficient deactivation and improved polymerization control), we hypothesized that it would perform equally, if not better, in O-ATRP at a low PC loading. Interestingly, after 8 hours of polymerization, the dispersity reached using 50 ppm of **PhenO** ($Đ$ = 1.81) was higher than the dispersity of any polymer sample at 8 hours synthesized with any of

the core-extended or non core-extended DHP PCs that we investigated using the same polymerization conditions ([DMAc]:[MMA]:[DBMM] = [1000]:[1000]:[10]) (Table A1.4, run 34). Additionally, over the course of the polymerization M_n growth was not linear nor equivalent to $M_{n,theo}$. These data suggest that **PhenO** does not control O-ATRP of MMA under the aforementioned conditions (Fig. S105). We also investigated the activity of **PhenO** for O-ATRP of MMA at 100 ppm and 500 ppm PC loadings. After 8 hours of polymerization using 100 ppm of **PhenO**, the observed dispersity of the polymerization mixture was $Đ$ = 1.78 and the initiator efficiency was I^* = 67% (Table A1.4, run 35). After 8 hours of polymerization using 500 ppm of **PhenO**, the observed dispersity of the polymerization mixture was $Đ$ = 1.39 and the initiator efficiency was I^* = 107% (Table A1.4, run 36). Despite dispersity being less than 1.5 after 8 hours of polymerization using 500 ppm of **PhenO**, throughout the polymerization M_n growth is not linear with respect to conversion and M_n is consistently > 4kDa higher than $M_{n,theo}$ The results obtained using **PhenO** at 50, 100, and 500 ppm PC loadings for the polymerization of MMA demonstrate that **PhenO** is an inferior PC relative to DHPs for controlling the polymerization of MMA in O-ATRP at low ppm PC loadings under the conditions used in this work. One potential explanation for the inferior performance of **PhenO** relative to DHPs is that the overall yield of ^{1}PC* vs ^{3}PC* contributing to activation varies for different PCs at certain initiator concentrations.[20] If, at the concentration of DBMM used in our polymerizations, the concentration of the ^{n}PC* species with a greater driving force for activation is higher for DHPs than it is for **PhenO**, activation with DHPs would be, comparatively, more efficient.

When considering the dispersity observed after 8 hours of polymerization and the linearity of M_n growth throughout the polymerization, PC **3a** performed the best out of the seven PCs studied herein. At 50 ppm in DMAc PC **3a** produced pMMA with $Đ$ = 1.07 after 8 hours. PC **3** performed second best at 50 ppm in DMAc yielding PMMA with $Đ$ = 1.19 after 8 hours, followed by PC **5** ($Đ$ = 1.19 at 8 hours), then by PC **4a** ($Đ$ = 1.27 at 8 hours), then PC **5a** ($Đ$ = 1.28 at 8 hours). Importantly, after 8 hours I^* > 90% for all of these runs except the one using PC **5** (I^* =

70% after 8 hours). PCs **3b** and **5b** did not produce polymer with $Đ < 1.5$ at 100 ppm PC loading and were, for that reason, not investigated in O-ATRP of MMA at 50 ppm. On the whole, further investigation into the PC properties and polymerization conditions that allow for polymerization control with PCs **3**, **5**, **3a**, **4a**, and, **5a** at low ppm PC loadings is needed.

1.4 Conclusions

In this work, we were able to successfully synthesize five new highly reducing PCs, three of which proved to be excellent PCs for controlling the polymerization of MMA at PC loadings as low as 50 ppm and 10 ppm (under certain conditions). Furthermore, we demonstrated that non-core extended DHPs can achieve satisfactory polymerization results at PC loadings as low as 50ppm. The photophysical and electrochemical properties of the five new PCs reported here were investigated and the effect of core-extension, the electronics of the core substituents, as well as the identity and connectivity of the *N*-aryl group on PC properties were examined. We found that changing the *N*-aryl group in core-extended DHPs is predicted to have a smaller effect on predicted ($E^{0*}_{T1,comp}(^2PC^{\bullet+}/^3PC^*)$) vales and experimentally determined $E^{0*}_{S1,exp}(^2PC^{\bullet+}/^1PC^*)$ than the changing the electronics of the core-substituent. Additionally, core-extension of DHPs appears to destabilize $^2PC^{\bullet+}$, rendering the core-extended derivatives more oxidizing than the parent DHPs, but that overall neither changing the *N*-aryl group nor the core substituents has a significant impact on $E_{1/2}(^2PC^{\bullet+}/^1PC)$. For PC properties relevant to photoexcitation, we found that core extension red-shifts $\lambda_{max,abs}$, and significantly increases $\varepsilon_{max,abs}$. For $\lambda_{max,abs}$, the identity of the *N*-aryl group has a greater impact on $\lambda_{max,abs}$ than the electronics of core-substituents. To the contrary, we observed that though there is a measurable change in the $\varepsilon_{max,abs}$ for CE-DHPs with different *N*-aryl groups, the shifts are of a lesser magnitude than those observed when the core substituent is switched between EWG **a** and EDG **b** within PC families that have the same *N*-aryl group.-In our analysis of the measured Stokes shifts for core-extended PCs, the identity of the *N*-aryl group was determined to smaller effect on $\Delta\lambda$ (and therefore an influence on CT) than altering the electronics of the core-substituent. We also reported experimentally determined excited state

lifetimes for core-extended DHPs for the first time and found that core-extension appears to increase both τ_{S1} and τ_{T1}, that the electronics of the core have little effect on τ_{S1}, but do impact τ_{T1} for **3a** and **3b** and, additionally, we found that changing the connectivity of the *N*-aryl naphthalene group has no effect on τ_{S1} for core-extended DHPs **3a-b** and **5a-b**, but does impact τ_{S1} for the parent DHPs and τ_{T1} for both core-extended and non-core extended DHPs. Upon investigation ϕ_f for the PCs reported herein, we found that ϕ_f is relatively low (<9%) for all DHPs discussed in this work except for **4, 4a,** and **5a** for which ϕ_f was still less than 40%.

After probing the ability of DHP PCs and **PhenO** to control O-ATRP at low PC loadings, we are still uncertain as to the PC properties and polymerization conditions that facilitate control at low ppm PC loadings for DHP PCs. Further investigation into PC properties such as ϕ_{ISC} and k_a at relevant concentrations of monomer and initiator may shed light on this.

References

[1]N. A. Romero and D. A. Nicewicz, *Chem. Rev.*, 2016, **116**, 10075–10166.

[2] Y. Lee, M. S. Kwon, *Eur. J. Org. Chem.*, 2020, 6028–6043.

[3] M. Chen, M. Zhong, and J. A. Johnson, *Chem. Rev.*, 2016, **116**, 10167–10211.

[4] N. Zivic, M. Bouzrati-zerelli, A. Kermagoret, F. Dumur, J. Fouassier, D. Gigmes, J. Lalevee, *Chem. Cat. Chem.*, 2016, **8**,1617–1631.

[5] N. Corrigan, S. Shanmugam, J. Xu, C. Boyer, *Chem. Soc. Rev.,* 2016, **45**, 6165-6212.

[6] B. P. Fors and C. J. Hawker, *Angew. Chemie Int. Ed.*, 2012, **51**, 8850–8853.

[7] D. Konkolewicz, K. Schroder, J. Buback, S. Bernhard and K. Matyjaszewski, *ACS Macro Lett.*, 2012, **1**, 1219–1223.

[8] D. Volz, M. Wallesch, C. Fléchon, M. Danz, A. Verma, J. M. Navarro, D. M. Zink, S. Bräse and T. Baumann, *Green Chem.* 2015, **17**, 1988–2011.

[9] R. M. Pearson, C. H. Lim, B. G. McCarthy, C. B. Musgrave and G. M. Miyake, *J. Am. Chem. Soc.*, 2016, **138**, 11399–11407.

[10] B. G. McCarthy and G. M. Miyake, *ACS Macro Lett.*, 2018, **7**, 1016–1021.

[11] B. G. McCarthy, R. M. Pearson, C. H. Lim, S. M. Sartor, N. H. Damrauer and G. M. Miyake, *J. Am. Chem. Soc.*, 2018, **140**, 5088–5101.

[12] J. C. Theriot, C. H. Lim, H. Yang, M. D. Ryan, C. B. Musgrave and G. M. Miyake, *Science*, 2016, **352**, 1082–1086.

[13] M. D. Ryan, J. C. Theriot, C. H. Lim, H. Yang, A. G. Lockwood, N. G. Garrison, S. R. Lincoln, C. B. Musgrave and G. M. Miyake, *J. Polym. Sci. Part A Polym. Chem.*, 2017, **55**, 3017–3027.

[14] J. P. Cole, C. R. Federico, C. H. Lim, and G. M. Miyake, *Macromolecules*, 2019, **52**, 747–754.

[15] B. G. McCarthy, S. Sartor, J. Cole, N. Damrauer and G. M. Miyake, *Macromolecules*, 2020, **53**, 9208–9219.

[16] D. A. Corbin, K. O. Puffer, K. A. Chism, J. P. Cole, J. C. Theriot, B. G. McCarthy, B. L. Buss, C. H. Lim, S. R. Lincoln, B. S. Newell and G. M. Miyake, *Macromolecules*, 2021, **54**, 4507–4516.

[17] N. A. Swisher, D. A. Corbin and G. M. Miyake, *ACS Macro Lett.*, 2021, **10**, 453–459.

[18] S. M. Sartor, C. H. Chrisman, R. M. Pearson, G. M. Miyake and N. H. Damrauer, *J. Phys. Chem. A*, 2020, **124**, 817–823.

[19] B. L. Buss, C. H. Lim and G. M. Miyake, *Angew. Chemie - Int. Ed.*, 2020, **59**, 3209–3217.

[20] Y. M. Lattke, D. A. Corbin, S. M. Sartor, B. G. McCarthy, G. M. Miyake and N. H. Damrauer, *J. Phys. Chem. A*, 2021, **125**, 3109–3121.

[21] M. Sneha, A. Bhattacherjee, L. Lewis-Borrell, I. P. Clark and A. J. Orr-Ewing, *J. Phys. Chem. B*, 2021, **125**, 7840–7854.

[22] A. Bhattacherjee, M. Sneha, L. Lewis-Borrell, G. Amoruso, T. A.A. Oliver, J. Tyler, I. P. Clark, and A. J. Orr-Ewing, *J. Am. Chem. Soc.*, 2021, **143**, 3613–3627.

[23] D. Koyama, H. J. A. Dale and A. J. Orr-Ewing, *J. Am. Chem. Soc.*, 2018, **140**, 1285–1293.

[24] D. A. Corbin, B. G. McCarthy, Z. van de Lindt, and G. M. Miyake, *Macromolecules*, 2021, **54**, 4726–4738.

[25] C. H. Lim, M. D. Ryan, B. G. McCarthy, J. C. Theriot, S. M. Sartor, N. H. Damrauer, C. B. Musgrave and G. M. Miyake, *J. Am. Chem. Soc.*, 2017, **139**, 348–355.

[26] S. M. Sartor, Y. M. Lattke, B. G. McCarthy, G. M. Miyake and N. H. Damrauer, *J. Phys. Chem. A*, 2019, **123**, 4727–4736.

[27] L. Lewis-borrell, M. Sneha, A. Bhattacherjee, I. P. Clark, and A. J. Orr-Ewing, *Chem. Sci.*, 2020, **11**, 4475–4481.

[28] Z. Huang, S. Xiang, Q. Zhang, X. Lv, S. Ye, R. Guo and L. Wang, *J. Mater. Chem. C*, 2018, **6**, 2379.

[29] J. C. Theriot, B. G. McCarthy, C. H. Lim and G. M. Miyake, *Macromol. Rapid Commun.*, 2017, **38**, 1700040.

[30] M.B. Gillies, K. Matyjaszewski, P.O. Norrby, T. Pintauer, R. Poli, P. Richard, *Macromolecules* 2003, **36**, 8551–8559.

[31] Y. Du, R. M. Pearson, C. H. Lim, S. M. Sartor, M. D. Ryan, H. Yang, N. H. Damrauer, and G. M. Miyake, *Chem. Eur. J.*, 2017, **23**, 10962–10968.

CHAPTER 2 — Approaches for synthesis, polymerization, and depolymerization of norbornane trithiolanes and their polymers

2.1 Overview

Strong interest in the application of high sulfur-content materials and the increasing urgency for polymeric materials to be constructed with intrinsic recyclability necessitates the design of chemically-recyclable, high sulfur content polymers. Herein, we report new conditions and approaches for the synthesis and polymerization of norbornane trithiolanes as well as for the depolymerization of their respective polymers (poly(norbornane trithiolanes)). We found that a diverse scope of amines can be used in the synthesis of norbornane trithiolanes and that the polymerizability of different derivatives varies when ring opening polymerization (ROP) or photopolymerization conditions are employed. We report improved conditions for the chemically assisted depolymerization of poly(norbornane trithiolanes) and compare these approaches to thermal depolymerization techniques. Importantly, the depolymerization conditions we identified are amenable to significantly lower loadings of depolymerization initiator/catalyst than previously reported and achieve similar conversions in shorter times. The work presented herein demonstrates the amenability of norbornane trithiolanes as a platform for chemically recyclable sulfur-containing polymers. We envision that the versatility of methods for their polymerization and depolymerization will inspire future investigation into this class of monomers for the synthesis of novel chemically recyclable high sulfur-content materials.

2.2 Introduction

The use of elemental sulfur as a renewable chemical feedstock for the development of novel polymers and materials has been gaining popularity due to its abundance and cost effectiveness.[1,2,3] Elemental sulfur, S_8, is a byproduct of the petroleum and natural gas refining industry, which produces over 70 million metric tons of S_8 annually.[4,5] With increasing demand for

oil and natural gas, already exceedingly large stockpiles are expected to grow. As such, incorporation of sulfur into polymeric materials is advantageous first, from the perspective of resource utilization. Second, polymers that are sulfur rich and contain disulfide bonds are of particular interest and importance due to their diverse and useful properties including, but not limited to, high refractive indexes,[6,7] affinity for heavy metals,[8,9,10] and redox activity.[11,12] These properties are applied in technologies such as optics for infrared thermal imaging ,[7,13] heavy metal remediation,[14,15] and lithium sulfide batteries.[11,12] Of particular importance is the reversibility of disulfide (S-S) bonds. Disulfide bonds are weak covalent bonds that are common in proteins and have been extensively exploited in self-healing materials.[16,17,18,19] The innate reversibility of S-S bonds and the vast applications for high sulfur content materials makes norbornane trithiolanes an interesting class of monomers that we posit will see utilization as a platform for the synthesis of depolymerizable and/or chemically recyclable sulfur-containing polymers.

The first report of the sulfurization of the norbornene alkene to synthesize a norbornane trithiolane (**1**) (Figure 2.1) was by Kurtz and Shields in 1969.[20] In 1978, Inoue and colleagues expanded on the work by Kurtz and Sheilds through the demonstration of the photochemical synthesis of **1** using 360 nm irradiation.[21] In 1987, Bartlett and Ghosh published the first paper

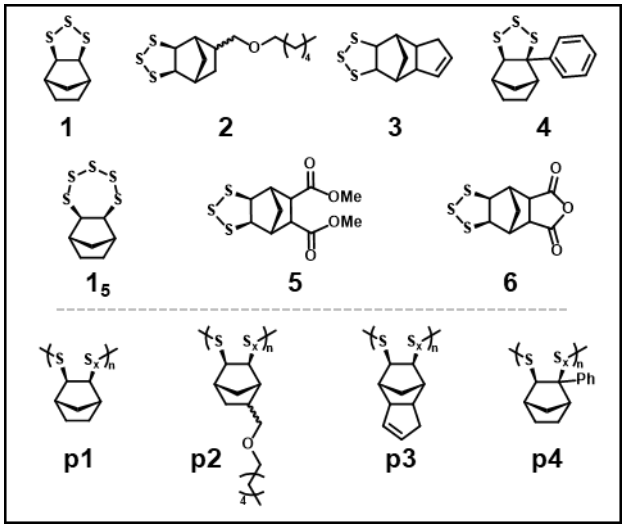

Figure 2.1: Chemical structures of norbornane trithiolane monomers (top) and polymers (bottom) discussed herein.

containing a comprehensive scope of norbornene trithiolanes in which they discussed the synthesis of several derivatives including **1**, $\mathbf{1_5}$, **3**, **4** (Figure 2.1).[22]

To the best of our knowledge, the first reports of the polymerization of norbornane trithiolanes were published in the early 1980's by Baran et al. and Emsley and Griffiths.[23,24] In these works Baran et al. reported the polymerization of **1** to **p1** using sodium thiophenolate to initiate an anionic ring opening polymerization (ROP) of **1** and Emsley and Griffiths reported both a thermal polymerization approach to the synthesis of **p3** from **3** as well as a light driven approach wherein a broad spectrum UV lamp was used to irradiate a solution of **3** to synthesize **p3** (Figure 2.1).[23,24] Notably, Emsley and Griffiths demonstrated the depolymerization of **p3** to **3** to 96% over five hours using a large excess of trithylamine[23] and Baran et al. reported 99% recovery of **1** through depolymerization of **p1**[24] which we posit was accomplished through a thermal depolymerization as the authors did extensive work to measure the ceiling temperature (T_c) of **p1**, however the method for depolymerization was not explicitly discussed. Recently, a report was published highlighting electrochemical methods for the polymerization of **1** and **3** as well as thermal depolymerization of **p1**.[25] In this work, the authors were able to recover 72% of **1** by heating **p1** to150 °C under reduced pressure (750 mTorr). Though an isolated depolymerization yield of 72% is notable, many norbornane trithiolane derivatives (other than **1**) are not volatile below their degredation temperatures therefore the thermal depolymerization is not broadly applicable.

Inspired by previous works described above in combination with the broad and impactful applications of sulfur-containing polymers and the intrinsic recyclability of poly(norbornane trithiolanes), we sought to expand the scope of known norbornane trithiolane monomers and methods for their synthesis, probe different methods and approaches to their polymerization, and attempt to identify a universal chemical depolymerization method that proceeds rapidly, gives high yields of the monomer, and requires minimal loading of initiator/catalyst.

2.3 Results and Discussion

2.3.1 Monomer Synthesis In this section we explore several approaches, both previously reported and novel, towards the synthesis of norbornane trithiolanes (Figure 2.2). In the first study of the reaction between norbornene and S_8 a catalytic amount of amine was used to activate S_8

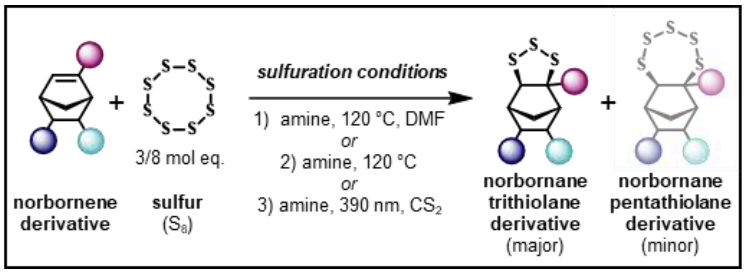

Figure 2.2: General schematic highlighting approaches toward norbornane trithiolane monomers.

yielding exo-norobornane trithiolane **1**.20 In this seminal report, bubbling ammonia gas was used as the amine source. Unfortunately, the use of gaseous ammonia complicates experimental setup especially at scale. As such, the use of non-gaseous reagents for S_8 activation are desirable. In 2005 a study reported the use of hexaamminenickel (II) chloride $[Ni(NH_3)_6]Cl_2$ for S_8 activation and, excitingly, observed high yields and no loss in selectivity for **1** over a known norbornane pentathiolane side product ($\mathbf{1}_5$) (Figure 2.1).[26] Using the methods reported by Poulain et al. (with $[Ni(NH_3)_6]Cl_2$ as a S_8 activating agent) we successfully reproduced the synthesis of **1** in addition to derivatives **2**-**6** several of which (**2**, **5**, & **8**) have never been reported to the best of our knowledge (Figure 2.1). Despite the robustness of this method several disadvantages exist including high reaction temperature (120 °C), the use of high boiling point solvents (*N,N*-dimethyl formamide (DMF) or dimethyl sulfoxide (DMSO)) which are difficult to remove from the product at scale, and the oxidation of $[Ni(NH_3)_6]Cl_2$ to byproducts. We hypothesized that nickel does not have any significant role in the sulfurization reaction and, as such, alternative non-gaseous amines might be able to activate S_8 for the synthesis of norbornane trithiolanes at a lower cost with less propensity for undesirable side products. Using primary amines (aniline and 1-naphthylamine), secondary amines (diphenyl amine), and tertiary amines (1,4-diazabicyclo[2.2.2]octane

(DABCO), triethylamine, *t*-butylamine) at a 2.00 mol% loading (relative to norbornene), we observed comparable selectivity for **1** over $\mathbf{1_5}$ (0.73-0.78 : 0.22-0.27, respectively) to the selectivity observed using $[Ni(NH_3)_6]Cl_2$ (0.75 : 0.25) (Table 2.1). In the absence of an amine, the ratio of **1**

Table 2.1: Relevant data from amine screening for synthesis of **1**.

Entry	Amine	Time (h)	Conv. (%)	1 : $\mathbf{1_5}$
1	none	18	>99	0.65 : 0.35
2	$[Ni(NH_3)_6]Cl_2$	18	>99	0.75 : 0.25
3	1-naphthylamine	18	>99	0.75 : 0.25
5	aniline	18	>99	0.77 : 0.23
6	diphenylamine	18	>99	0.76 : 0.24
7	DABCO	18	>99	0.78 : 0.22
8	triethylamine	18	>99	0.77 : 0.23
9	*t*-butylamine	18	>99	0.73 : 0.27

to $\mathbf{1_5}$ is 0.65 : 0.45, a notably lower selectivity than in the presence of amine (Table 2.1). In addition to each amine showing similar selectivity for the trithiolane vs. pentathiolane, the conversion of norbornene reached >99% by 18 hours for all runs (no norbornene peak in the alkene region is observed in the ^{1}H NMR spectra). To the best of our knowledge, these results demonstrate the most diverse scope of amines applied for the sulfurization of norbornenes to date. S_8 is a powder of a deep yellow color that can be activated at near visible wavelengths as first demonstrated by Inuoe et al. in 1978 wherein the synthesis of **1** (yield: 77%) through irradiation of norbornene and sulfur in carbon disulfide (CS_2) with UV light.21 We were curious if the addition of an amine would impact the photochemical sulfurization of norbornene, if this photosynthetic approach could be applied to other norbornene derivatives, and if lower energy irradiation could be used. We found that norbornene does undergo sulfurization to **1** at room temperature when S_8 (3/8 mol eq.), norbornene (1 mol eq.), and DABCO (0.02 mol eq.) are dissolved in CS_2 and irradiated at 390 nm. Interestingly, under photosynthetic conditions the selectivity for **1** (**1**:$\mathbf{1_5}$ = 0.84:0.16) is higher than what was observed using $[Ni(NH_3)_6Cl_2]$ as an activator at 120 °C in *N,N*-dimethylformamide (DMF) for sulfurization of **1** (Table 2.1). For five norbornene derivatives that were subjected to the

above photochemical sulfurization conditions, conversion to their respective trithiolanes was observed at between 11% and 40% (**1**: 40%, **3**: 34%, **4**: 11%, **5**: 40%, **6**: 32%).

In inverse vulcanization, molten S_8 is not only a reactant, but is the reaction medium in which the other reactant is dissolved. We posited that the use of solvent in the synthesis of norbornane trithiolanes could be circumvented by carrying out the sulfurization in the bulk using S_8 in the molten state as the "solvent." Norbornene (1.00 mol eq.), S_8 (3/8 mol eq.), and DABCO (0.02 mol eq.) were heated to 120 °C and stirred for 11 hours at which time the measured conversion of norbornene was >99%. Excitingly, in addition to a high conversion of starting material, the crude reaction mixture was able to be distilled without any preliminary workup to give pure **1** at an isolated yield of 60%. Under the neat reaction conditions, the selectivity for formation of **1** over $\mathbf{1_5}$ (0.62:0.38) was lower than for the same conditions wherein the reactants are dissolved in DMF. Possibly the reaction concentration plays a significant role in selectivity and/or the presence of DMF has an impact on selectivity. To the best of our knowledge, this work is the first example of a solvent-free synthesis of a norbornane trithiolane.

The six norbornane trithiolane monomers that were synthesized were then carried forward to investigate their polymerizability under various conditions. The monomers used in the polymerization portion of this work were all synthesized using the condition in DMF at 120 °C employing $[Ni(NH_3)_6]Cl_2$ as the S_8 activating agent.

2.3.2 Polymerization Ring opening polymerization (ROP) conditions were optimized using monomer **1** (Table A2.3). We first investigated the use of 1,3-di-*t*burylimidazol-2-ylidine (NHC*t*Bu)), a good nucleophile and strong base (pKa = ~23). Conversion of **1** to **p1** reached 43.4% using NHC*t*Bu as an initiator at a 0.01 mol eq. loading (relative to mols of **1**) and yielded **1** at a high molecular weight (M_n = 283 kDa) (Table 2.1, Entry 1). The calculated initiator efficiency (I^*) achieved under these conditions was extremely low at I^*=2.94%. Note that for a polymerization with controlled initiation I^* should be 100%. We hypothesize that a side reaction between NHC*t*Bu and a small impurity in the monomer could be hindering initiation or that the polymerization

conditions support catenation resulting in high molecular wight polymers with no chain end groups. Catenation has been observed when similar disulfides are polymerized. We next investigated the use of different initiators for the polymerization of **1** that are both strong bases and poor nucleophiles (DBU and P_4tBu).

It is known that strained and linear sulfur-sulfur bonds can be cleaved using bases and this approach has been used for the ROP of disulfides and depolymerization of the resulting polymers. Interestingly, in our work we found that DBU (pKa = 24) and P_4tBu (pKa = 42.1) performed similarly in the polymerization of **1** in regard to the observed conversion, molecular weights, and initiator efficiencies, however they performed very differently than NHC*t*Bu (Table 2.2). Both DBU and P_4tBu gave higher conversions than NHC*t*Bu (50.7% and 51.5% vs 43.7%, respectively) and had significantly higher initiator efficiencies (52.2% and 54.6% vs 2.94%, respectively).

Table 2.2: Initiator screening for polymerization of **1**.

Entry	Initiator	Conv. (%)	M_w (kDa)	M_n (kDa)	$Đ$ (M_w/M_n)	I^* (%)
1	NHC*t*Bu	43.7	509	283	1.80	2.94
2	DBU	50.7	38.5	18.5	2.08	52.2
3	P_4tBu	51.5	52.3	17.9	2.92	54.6
5	NHC*t*Bu/BnOH	45.7	29.7	13.4	2.22	66.0
6	DBU/BnOH	45.2	42.6	26.3	1.62	33.2
7	P_4tBu/BnOH	45.4	25.7	14.7	1.75	59.9

Next, we sought to test the impact of using benzyl alkoxide (BnO^-) as an initiator. For polymerizations initiated with BnO^- (Table 2.2, Entry 5-7) the base (NHC*t*Bu, DBU, or P_4tBu) was stirred with benzyl alcohol (BnOH) for 20 minutes prior to initiation to allow sufficient tome for complete deprotonation before being added to the monomer for polymerization. Each initiation system (Table 2.2, Entry 5-7) resulted in polymerization conversions of around 45%, however the calculated I^* varied wherein the DBU/BnOH system had a significantly lower I^* (I^* = 33.2%) compared to the NHC*t*Bu/BnOH and P_4tBu/BnOH initiator systems (I^* = 66.0% and 59.9%, respectively). We hypothesize that if measured, the rate of polymerization would be faster using

P_4*t*Bu/BnOH as an initiation system than for DBU/BnOH and NHC*t*Bu/BnOH due to the size of the counter cation being significantly larger. A larger counter cation associating at the active polymer chain end suggests that the interaction between the counter cation and polymer chain end will be weaker, thus the propagating anion will be more nucleophilic and propagation will proceed more rapidly. Note that the data shown in Table 2.2 was collected after 4h at which time we posit the conversion has reached it maximum and the relative concentrations of monomer and polymer have reached equilibrium.

With the aim to increase conversion above ~45%, we sought to perturb the equilibrium monomer concentration through lowering the polymerization temperature and increasing the starting concentration of monomer (Table 2.3, Entry 10-17). No conversion was observed for **1** at an initial monomer concentration ($[\mathbf{1}]_0$) of $[\mathbf{1}]_0$ = 2.49 M, however an increase from 24.5% conversion to 67.6% conversion was observed as $[\mathbf{1}]_0$ was increased from 4.02 M (Entry 11) to 6.52 M (Entry 14). Though the desired increase in conversion was observed as a result of increasing the initial monomer concentration, this came at the cost of a significant increase in the dispersity of the polymer (*Đ*) wherein at $[\mathbf{1}]_0$ = 4.02 M, *Đ* = 1.34 and at $[\mathbf{1}]_0$ = 6.52 M, *Đ* = 9.03. We hypothesized that at lower temperatures higher conversion would be observed, however (for the polymerization conditions tested) this was only true for Entry 15 ($[\mathbf{1}]_0$ = 4.02 M, conv. = 41.2%) (Table 2.3). For Entry 16 and 17, ($[\mathbf{1}]_0$ = 5.02 M and 6.00 M, respectively) the observed conversions

Table 2.3: Initial monomer concentration and temperature screening results for polymerization of **1**.

Entry	$[\mathbf{1}]_0$ (M)	Temp. (°C)	Conv. (%)	M_w (kDa)	M_n (kDa)	*Đ* (M_w/M_n)	*I** (%)
10	2.49	22	7.80	--	--	--	--
11	4.02	22	24.5	11.1	8.27	1.34	58.2
12	5.02	22	42.5	30.6	17.6	1.74	46.7
13	6.00	22	56.7	116	23.2	4.99	47.2
14	6.52	22	67.6	242	26.8	9.03	48.6
15	4.02	-34	41.5	26.3	15.2	1.73	52.6
16	5.02	-34	50.2	116	22.1	5.26	43.9
17	6.00	-34	55.2	153	23.9	6.39	44.6

were not significantly higher. We posit that at these higher concentrations, the majority of monomer freezes out of the polymerization mixture wherein at lower concentrations **1** remains dissolved. Using DSC, we found that the pure **1** monomer exhibits a distinct endotherm at 4 °C and a distinct exotherm at -30 °C supporting that at the lowered polymerization temperature (-34 °C), undissolved **1** could freeze (Figure A2.17). The last conditions examined for optimizing **1** polymerization through ROP was lowering the initiator loading (Table 2.4). Excitingly, with $[\mathbf{1}]_0$ = 6.00 M and an initiator loading of 0.1%, the polymerization conversion remained around 55% and the measured *I** reached 86.9% within 1 hour at room temperature.

Table 2.4: Initiator loading screening results for polymerization of **1**.

Entry	$[1]_0$ (M)	Temp. (°C)	Conv. (%)	M_w (kDa)	M_n (kDa)	$Đ$ (M_w/M_n)	*I** (%)
10	2.49	22	7.80	--	--	--	--
11	4.02	22	24.5	11.1	8.27	1.34	58.2
12	5.02	22	42.5	30.6	17.6	1.74	46.7
13	6.00	22	56.7	116	23.2	4.99	47.2
14	6.52	22	67.6	242	26.8	9.03	48.6
15	4.02	-34	41.5	26.3	15.2	1.73	52.6
16	5.02	-34	50.2	116	22.1	5.26	43.9
17	6.00	-34	55.2	153	23.9	6.39	44.6

Using NHC*t*Bu/BnOH as the initiator system at a 0.1% loading, we next investigated the polymerization of **2**, **3**, **4,** (Table 2.5) **5**, and **6**. The polymerization of **5** and **6** yielded insoluble solids at ~50% yield by mass which we hypothesized was a crosslinked version of what would

Table 2.5: Results from polymerization of **1**-**4** under anionic ROP conditions.

Entry	Monomer	$[M]_0$ (M)	Conv. (%)	M_w (kDa)	M_n (kDa)	$Đ$ (M_w/M_n)	*I** (%)
1	**1**	6.00	59.3	296	164	1.81	68.9
2	**3**	4.82	60.0	201	135	1.50	68.9
3	**2**	3.47	25.0	49.5	29.9	1.65	255
4	**4**	4.20	10.0	6.05	3.92	1.54	680

have been the trithiolane polymer. Crosslinking could happen through the ester or anhydride groups on monomers **5** and **6** as they are reactive towards transesterification under anionic polymerization conditions. For the other monomer derivatives, we hypothesized that the polymerization of **2** would proceed similarly to **1** as the MHE substituent likely has little to no

impact on the ring strain energy of the trithiolane and is distal enough not to interfere sterically with ring opening. Interestingly, low conversion was observed for the polymerization of **2** (Table 2.5, Entry 3, conv. = ~25%) as well as significantly low molecular weight (M_n = 49.5 kDa) and a high I^* (I^* = ~255%). We posited that polymerization of **4** through ROP could be challenging due to the steric bulk of the phenyl group adjacent to the proposed site of ring opening. Indeed, low conversion (<10%) and extremely low molecular weights (M_n = 3.92 kDa) were observed (Table 2.5, Entry 4). Excitingly, we observed similar results for the polymerization of **3** (Table 2.5, Entry 2) as compared to the polymerization of **1**. The conversion measured for ROP of **3** was ~60%, measured molecular weights were M_w = 201 kDa, M_n = 135 kDa, and I^* = 68.9%.

We next sought to investigate the polymerizability of **1**, **2**, **3**, and **4** using light. All four monomers are a deep yellow color and UV-Vis spectroscopy revealed that they absorb in the near visible region of the electromagnetic spectrum (Figure 2.3). Though the molar extinction

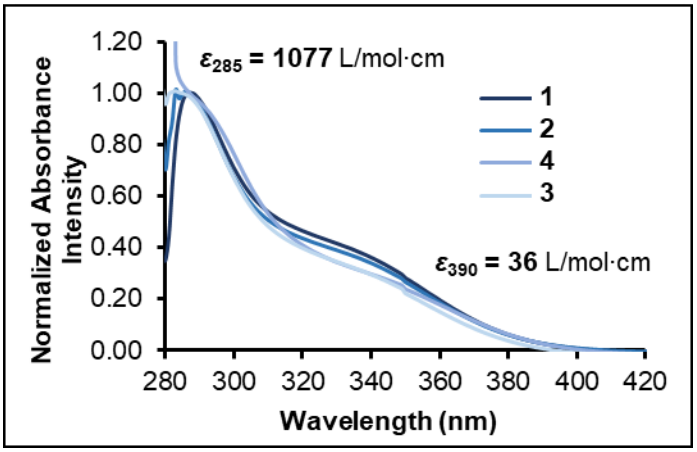

Figure 2.3: Absorption traces of **1**-**4** and molar extinction coefficient values for **1** at 285 nm and 390

coefficient (ε) measured for **1** at 390 nm is low (ε_{390} = 36 L·mol^{-1}cm^{-1}), we posited that the use of lower energy wavelengths (e.g. 390 nm) should be employed to avoid unwanted side reactions that might be caused by irradiation at higher energy wavelengths (e.g. 285 nm, the maximum wavelength of absorption for **1**). Excitingly, polymerization at 390 nm was observed for all four

monomers (Table 2.6). For **2** and **4** the measured conversions (conv. = 84% and 30%, respectively) were significantly improved compared to the conversions achieved through ROP.

Table 2.6: Relevant data for photopolymerization of **1** – **4**.

Entry	Monomer	$[M]_0$ (M)	Conv. (%)	M_w (kDa)	M_n (kDa)	$Đ$ (M_w/M_n)	T_d (°C)
1	**1**	6.00	46.2	43.1	28.5	1.52	175
2	**3**	4.82	47.0	106	69.1	1.54	147
3	**2**	3.47	84.0	19.9	16.5	1.21	160
4	**4**	4.20	30.0	28.4	12.8	2.21	189

2.3.3 Depolymerization We assessed the thermal stability of **1** and **3** as well as **p1-p4** using dynamic scanning calorimetry (DSC). The degredation temperatures (T_d) of **1** and **3** (Figure A2.15 and S16) are T_d = 114 °C and 159 °C, respectively and for **p1**-**p4** (synthesized through photopolymerization) T_d ranges from 147 °C to 189 °C (Figure A2.19) (Table 2.6). A recent report highlighting the thermal depolymerization of **p1** ran the depolymerization at 150 °C and were only able to recover 72% of **1**.[25] We posited that the less than quantitative recovery of **1** reported may be due to (a) competing decomposition process(es) and that at temperatures below the T_d of the **1** (T_d = 111 °C) , higher yields of the monomer could be recovered. Using an adaptation of a traditional distillation setup (Figure A2.21), **p1** (T_d = 175 °C) (synthesized through ROP) was heated to 105 °C and stirred under reduced pressure (100 mTorr) for 12 hours. The recovered monomer is pure by ^{1}H-NMR, however only 52.7% (by mass) was recovered. We posit that the low recovery of **1** in our thermal depolymerization approach was partly due to the small scale at which the experiment was run (190 mg of **p1**). Though distillation of **1** is a good approach for purification after monomer synthesis, the low volatility of **1** renders the distillation time intensive and an unfavorable approach for driving depolymerization. Unlike for **1**, attempts to melt and distill **2**, **3**, and **4** post-synthesis were unsuccessful at or near their degradation temperatures and under reduced pressure. As such, we posited that complete thermal depolymerization of **p2**, **p3**, and **p4** as well as many other poly(norbornane trithiolane) derivatives is unlikely to be successful due to the low volatility of their respective monomers.

Inspired by the work of Kurtz and Sheilds[27] which demonstrated the depolymerization of **p3** using excess triethylamine to realize >96 % depolymerization of **p3** back to **3** within 5 hours, we next investigated the chemical depolymerization of **p1**-**p4**. We hypothesized that a stronger base could yield depolymerization at a faster rate than reported by Kurtz and Sheilds and that the loading of the depolymerization initiator/catalyst could be lowered. Using **p1** as a model polymer for optimizing chemical depolymerization conditions, we first tested triethylamine (pKa = 10.8), pyrrolidine (pKa = 11.3), and DBU (pKa = 24.3) at a loading approximately equivalent to the number of monomer repeat units in the **p1** backbone (1 mol eq., determined by dividing the mass of polymer used by molecular weight of the monomer). Within 1 hour, >99% conversion to **1** was observed by ^{1}H NMR employing DBU and pyrrolidine as the base (Table 2.7, Entries 3 and 5). We posited that NHC*t*Bu (pKa = 48) could also be used to depolymerize **p1** and subsequently

Table 2.7: Results from chemical depolymerization conditions screening and scope.

Entry	Polymer	Solvent	Base	[Base] (mol eq.)	Depolymerization Conv. (%)	Rxn Time (h)
1	**p1**	Benz.	triethylamine	1	33.4	1
2	**p1**	Benz.	triethylamine	0.01	5.23	1
3	**p1**	Benz.	pyrrolidine	1	>99	1
4	**p1**	Benz.	Pyrrolidine	0.01	13.7	1
5	**p1**	Benz.	DBU	1	>99	1
6	**p1**	Benz.	DBU	0.01	74.0	1
7	**p1**	Benz.	NHCtBu	0.01	>99	1
8	**p2**	Benz.	NHCtBu	0.01	88.0	1
9	**p3**	Benz.	NHCtBu	0.01	87.0	1
10	**p4**	Benz.	NHCtBu	0.01	82.0	1

tested NHC*t*Bu, triethylamine, pyrrolidine, and DBU at (0.01 mol eq. relative to repeat units) (Table 2.7, Entries 2, 4, 6, 7).The conversion of **p1** to **1** after 1 hour correlated with the strength of the base wherein for DBU and NHC*t*Bu >99% depolymerization was achieved and for triethylamine and pyrrolidine only 5.23% and 13.7% conversion was observed, respectively. We sought to gain insight into the depolymerization mechanism by examining the kinetics of depolymerization with DBU and NHC*t*Bu through measuring the change in concentration of **1** over time (Figure 2.4-A) as well as the change in molecular weight of **p1** over time (Figure 2.4-B). It is apparent that

NHC*t*Bu results in a much faster rate of depolymerization than DBU, reaching 92.6% conversion to **1** within 1 minute wherein only 19.7% conversion to **1** was observed after 1 minute using DBU (Figure 2.4) (Table A2.7).

At the onset of this work, one of our goals was to identify a universal depolymerization method for moving toward chemical recycling of norbornane trithiolanes. Though demonstrating an effective depolymerization technique on four different poly(norbornane trithiolanes) can by no

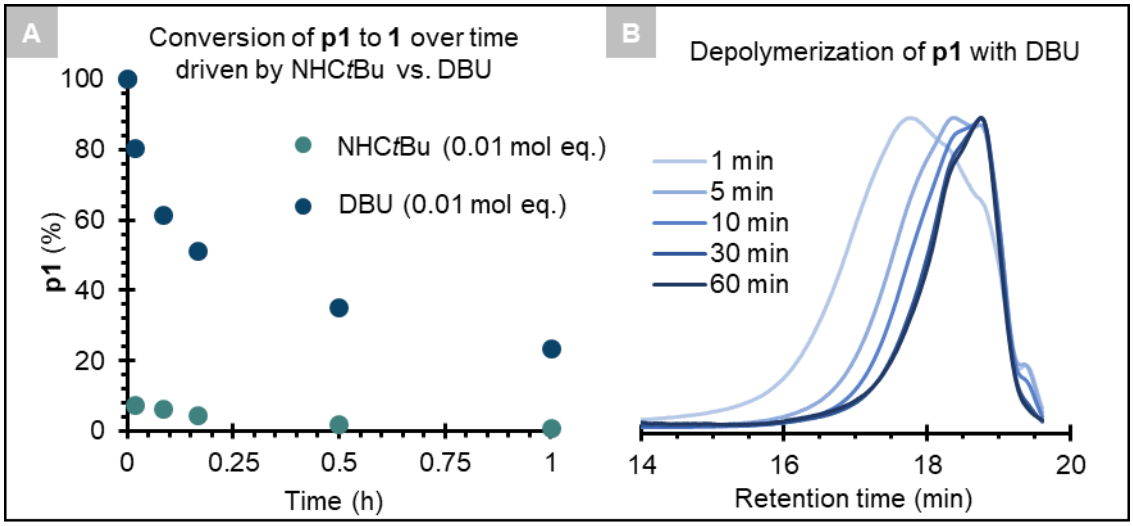

Figure 2.4: (A) Graph showing the change in concentration of p1 as a function of time when depolymerization is done in the presence of NHCtBu or DBU (Table A2.7). (B) Change in molecular weight of p1 over time when depolymerization is done in the presence of DBU (Table A2.7).

means be claimed as a "universal" approach, we were never the less excited that with a 1% loading of NHC*t*Bu, other poly(norbornane trithiolane) derivatives **p2**, **p3**, and **p4** were successfully depolymerized such that within 1 hour 88.0%, 87.0%, and 82.0% of their respective monomers were detected using ^{1}H NMR (Table 2.7).

2.4 Conclusions

Herein, we demonstrate the synthesis of several novel norbornane trithiolane monomers (**2**, **5**, and **6**), report several new approaches for the sulfurization of norbornene derivatives, show that these monomers can be readily polymerized through ROP and photopolymerization (the seminal example of the polymerization of **2** and **4**, to the best of our knowledge), and report

improved conditions for the depolymerization of several poly(norbornane trithiolanes) back to their respective monomers.

While the light-driven method for trithiolane synthesis showed promising results and was successfully used for the synthesis of five trithiolane derivatives, there are still significant drawbacks. CS_2 is a highly toxic and flammable solvent but, unfortunately, is one of the only solvents able to solubilize S_8 at ambient temperatures. Furthermore, under the light-driven conditions the conversion of the starting norbornene alkene was, in all cases, lower than with the thermal methods, only reaching up to 40%. Excitingly, we demonstrated that **1** could be synthesized under solvent-free conditions. Additionally, the polymerization of several new poly(norbornane trithiolanes) was achieved through the exploration of ROP and photopolymerization techniques. We highlighted the impact of the initiator, monomer concentration, temperature, and initiator loading on the polymerization of **1**. Lastly, we have demonstrated a significant improvement to the chemical depolymerization approach reported by Kutz and Sheilds. A chemical method that utilizes catalytic quantities (0.01 mol eq.) of base and realizes 82% to 99% depolymerization of 4 different poly(norbornane trithiolanes) within 1 hour was demonstrated. In this work, investigated the impact of varied combinations of thermal, chemical, and light driven techniques for the synthesis and polymerization of norbornane trithiolanes and depolymerization of their respective polymers and hope that the research performed herein will contribute to the further exploration and application of molecular and polymeric trithiolanes.

References

[1] Griebel, J. J.; Glass, R. S.; Char, K.; Pyun, J. *Prog. Poly. Sci*. **2016**, *58*, 90–125.

[2] Abbasi, A.; Yahya, W. Z. N.; Nasef, M. M. *Green Mater.* **2020**, *8*, 172–180.

[3] Chung, W. J.; Griebel, J. J.; Kim, E. T.; Yoon, H.; Simmonds, A. G.; Ji, H. J.; Dirlam, P. T.; Glass, R. S.; Wie, J. J.; Nguyen, N. A.; Guralnick, B. W.; Park, J.; Somogyi, Á.; Theato, P.; Mackay, M. E.; Sung, Y. E.; Char, K.; Pyun, J. *Nat. Chem.* **2013**, *5*, 518–524.

[4] Kutney, G. *Sulfur: History, Technology, Applications & Industry*, 2nd ed.; ChemTec Publishing: Toronto, **2013**, 1−260.

[5] Apodaca, L. E. *Sulfur. U.S. Geological Survey, Mineral Commodity Summaries*, January **2022**.

[6] Griebel, J. J.; Namnabat, S.; Kim, E. T.; Himmelhuber, R.; Moronta, D. H.; Chung, W. J.; Simmonds, A. G.; Kim, K.-J.; van der Laan, J.; Nguyen, N. A.; Dereniak, E. L.; MacKay, M. E.; Char, K.; Glass, R. S.; Norwood, R. A.; Pyun, J. *Adv. Mater.* 2014, *26*, 3014−3018.

[7] Kleine, T. S.; Glass, R. S.; Lichtenberger, D. L.; Mackay, M. E.; Char, K.; Norwood, R. A.; Pyun, J. *ACS Macro Lett.* **2020**, *9*, 245−259.

[8] Crockett, M. P.; Evans, A. M.; Worthington, M. J. H.; Albuquerque, I. S.; Slattery, A. D.; Gibson, C. T.; Campbell, J. A.; Lewis, D. A.; Bernardes, G. J. L.; Chalker, J. M. *Angew. Chem., Int. Ed.* **2016**, *55*, 1714−1718.

[9] Worthington, M. J. H.; Kucera, R. L.; Albuquerque, I. S.; Gibson,C. T.; Sibley, A.; Slattery, A. D.; Campbell, J. A.; Alboaiji, S. F. K.; Muller, K. A.; Young, J.; Adamson, N.; Gascooke, J. R.; Jampaiah, D.; Sabri, Y. M.; Bhargava, S. K.; Ippolito, S. J.; Lewis, D. A.; Quinton, J.S.; Ellis, A. V.; Johs, A.; Bernardes, G. J. L.; Chalker, J. M. *Chem.Eur. J.* **2017**, *23*, 16219−16230.

[10] Wu, X.; Smith, J. A.; Petcher, S.; Zhang, B.; Parker, D. J.; Griffin, J. M.; Hasell, T. *Nat. Commun.* **2019**, *10*, 647.

[11] Chung, W. J.; Griebel, J. J.; Kim, E. T.; Yoon, H.; Simmonds, A. G.; Ji, H. J.; Dirlam, P. T.; Glass, R. S.; Wie, J. J.; Nguyen, N. A.; Guralnick, B. W.; Park, J.; Somogyi, A.; Theato, P.; Mackay, M. E.; Sung, Y.-E.; Char, K.; Pyun, J. *Nat. Chem.* **2013**, *5*, 518−524.

[12] Zhao, F.; Li, Y.; Feng, W. *Small Methods* **2018**, *2*, 1800156.

[13] Tonkin, S. J.; Pham, L. N.; Gascooke, J. R.; Johnston, M. R.; Coote, M. L.; Gibson, C. T.; Chalker, J. M. *Adv. Optical Mater.* **2023**, 2300058.

[14] Sheard, W.; Park, K. W.; Leitao, E. M. *ACS Sustainable Chem. Eng.* **2023**, *11*, 3557−3567.

[15] Chalker, J. M.; Mann, M.; Worthington, M. J. H.; Esdaile, L. J. *Org. Mater.* **2021**, *3*, 362−373.

[16] Griebel, J. J.; Nguyen, N. A.; Namnabat, S.; Anderson, L. E.; Glass, R. S.; Norwood, R. A.; MacKay, M. E.; Char, K.; Pyun, J. *ACS Macro Lett.* **2015**, *4*, 862−866.

[17] Xin, Y.; Peng, H.; Xu, J.; Zhang, J. *Adv. Funct. Mater.* **2019**, *29*, 1808989.

[18] Tonkin, S. J.; Gibson, C. T.; Campbell, J. A.; Lewis, D. A.; Karton, A.; Hasell, T.; Chalker, J. M. *Chem. Sci.* **2020**, *11*, 5537−5546.

[19] Rekondo, A.; Martin, R.; Ruiz de Luzuriaga, A.; Cabanero, G.; Grande, H.J., Odriozola, I. *Mater. Horiz.* **2014**, *1*, 237-240.

[20] Shields, T. C.; Kurtz, A. N. *J. Am. Chem. Soc.* **1969**, *91*, 5415-5416.

[21] Inoue, S.; Tezuka, T.; Oae, S. *Phos. Sulf. Rel. Elem.* **1978**, *4*, 219–221.

[22] Bartlett, P. D. and Ghosh T. *J. Org. Chem.*, **1987**, *52*, 22, 4937-4943.

[23] Emsley, J.; Griffiths, D. *Phosphorous and sulfur and the related elements* **1980**, *9*, 227–230.

[24] Baran, T.; Duda, A.; Penczek, S. *Journal of Polymer Science* **1984**, *22*, 1085–1095.

[25] Pople, J. M. M.; Nicholls, T. P.; Le Nhan Pham; Bloch, W. M.; Lisboa, L. S.; Perkins, M.V.; Gibson, C.T.; Coote, M. L.; Jia, Z.; Chalker, J.M. *J. Am. Chem. Soc.* **2023**, *145*, 11798-11810.

[26] Poulain, S.; Julien, S.; Dunach, E. *Tetrahedron Letters* **2005**, *46*, 7077-7079.

[27] Shields, T.C. and Kurtz, A. N. *J. Am. Chem. Soc.* **1969**, *91*, 19, 5415-5416.

APPENDIX 1 – Supporting Information for Chapter 1

MATERIALS AND METHODS

Purchased Chemicals and Materials

Phenazine Reduction (Figure A1.3-a): Phenazine was purchased from Sigma Aldrich, sodium dithionite was purchased from VWR, reagent alcohol was purchased from Sigma Aldrich. All chemicals were used as received.

Buchwald-Hartwig Coupling (Figure A1.3-b): (This method was used for the synthesis of PC **5**): 2-bromonaphthalene, sodium t-butoxide, anhydrous Sure/Seal dioxane, dicyclohexylphospino-2,6-diisopropoxybiphennyl (RuPhos), and RuPhos Pd G4, were purchased from Sigma Aldrich and used as received unless noted otherwise in "Chemical preparation and Storage."

Buchwald-Hartwig Coupling (Figure A1.3-b): (This method was used for the synthesis of PCs **3** and **4**): 4-bromoanisole, 2-bromonaphthalene, sodium t-butoxide, anhydrous Sure/Seal toluene, bis(dibenzylideneacetone) palladium(0) ($Pd(dba)_2$), and tritertbutylphosphine were purchased from Sigma Aldrich and used as received unless noted otherwise in "Chemical preparation and Storage."

Bromination Method I (Figure A1.3-c&e): Molecular bromine, benzene, and methanol purchased from Sigma Aldrich and used as received. Copper wire was purchased from Fisher and used as received.

Bromination Method II (Figure A1.3-c&d)**:** Molecular bromine, benzene, and methanol purchased from Sigma Aldrich and used as received. Reagent grade Acetone was purchased form Fischer Scientific ad used as received.

Suzuki Coupling (Figure A1.3-f): Tetrakis(triphenyl phosphine) palladium (0) ($Pd(PPh_3)_4$), 4-(trifluoromethyl)phenylboronic acid, 2-naphthylboronic acid, 4-methoxyphenylboronic acid, and Sure/Seal tetrahydrafuran (THF) were purchased from Sigma Aldrich. Potassium carbonate was

purchased from VWR. All chemicals were used as received unless noted otherwise in “Chemical preparation and Storage.”

Polymerizations: Monomers: methyl methacrylate (MMA), styrene, n-butyl acrylate (nBA), vinyl acetate (VA), and *N,N*-dimethylacrylamide (DMA), as well as solvents: anhydrous Sure/seal *N,N*-dimethylacetamide (DMAc), ethyl acetate (EtOAc), benzene, dichloromethane (DCM) and tetrahydrofuran (THF) and diethyl 2-bromo-2-methyl malonate (DBMM) were purchased from Sigma Aldrich.

Deuterated solvents for NMR: All deuterated solvents were purchased from Cambridge Isotope Laboratories Inc. and used without further purification.

Chemical Preparation and Storage

Cross coupling reactions: $Pd(dba)_2$ and $Pd(PPh_3)_4$ were used as received, but were transferred to a nitrogen-filled glovebox before use. Tetrakis(triphenyl phosphine) palladium(0) was stored in the dark at -10 °C. 4-bromoanisole was sparged with nitrogen while stirring for 20 minutes before use.

Monomers and initiators for polymerizations (add other monomers): MMA, styrene, nBA, VA, DMA, and DBMM, were dried by stirring over calcium hydride for 12-16 hours, distilled under vacuum, then degassed via three freeze-pump-thaw cycles before being transferred to amber vials in a nitrogen filled glovebox. Monomers and initiators were stored under nitrogen, in the dark, at -10 °C, but were allowed to warm to room temperature before use.

Solvents for polymerizations: Dimethylacetamide (DMAc), tetrahydrofuran (THF), dichloromethane (DCM), and ethyl acetate (EtOAc) were obtained from Sigma Aldrich in Sure/Seal bottles, then used without further purification. Benzene was obtained and purified using an mBraun MB-SPS-800 solvent purification system, kept under nitrogen atmosphere, and stored over 3Å molecular sieves.

Solvents for characterization: DMAc (99.8% anhydrous) was purchased form sigma Aldrich in Sure/Seal bottles and used without further purification. HPLC grade acetonitrile (MeCN) for cyclic voltammetry was purchased form Fischer Scientific and used without further purification.

Instrumentation for Characterization

Nuclear magnetic resonance (NMR) spectroscopy: NMR spectra were obtained using a Bruker 400 MHz NMR Spectrometer. All ^{1}H NMR experiments are reported in parts per million (ppm) and were measured relative to the signals for residual dimethyl sulfoxide (2.5 ppm), benzene (7.16 ppm), or chloroform (7.26) in deuterated dimethyl sulfoxide, deuterated benzene, or deuterated chloroform, respectively.

Mass Spectroscopy of Photocatalysts: Electrospray Ionization Mass Spectroscopy (ESI-MS) was performed at the Colorado State University Central Instrumentation Facility.

Ultraviolet-visible (UV-Vis) spectroscopy: UV-Vis spectroscopy was performed on a Cary 5000 spectrophotometer. DMAc was used as the solvent for all data presented in this work. All samples were analyzed in 1 cm pathlength quartz cuvettes.

Fluorescence spectroscopy: Emission Spectra: Emission spectra were obtained using an Edinburgh Instruments FS5 spectrofluorometer. DMAc was used as the solvent for all sample data presented in this work and all samples were measured in quartz cuvettes with a 1 cm pathlength.

Absolute fluorescence quantum yields: Absolute fluorescence quantum yields (AFQY) were measured using an FS5 Spectrofluorometer from Edinburg Instruments with an SC-30 Integrating Sphere accessory using a direct excitation method. All samples were dissolved in DMAc at a concentration where the absorption intensity (A) was between A=0.09 and A=0.1, those samples were sparged with argon gas for 20 minutes, then transferred to 1 cm pathlength quartz cuvettes in a nitrogen filled glovebox before quantum yield analysis. Measurement was made over the

photocatalyst samples (S) and reference solvents (R) scattering (R_s and S_s) and emission (R_e and S_e). The equation for the calculation of AFQY using the direct excitation method is:

$$AFQY = \frac{S_e - R_e}{R_s - S_s} \, x \, 100$$

The scattering and emission spectral regions were measured separately. The AFQY values were calculated using the Fluoracle software via the equation above.

AFQY values were measured at the maximum wavelength of emission.

Cyclic voltammetry: Cyclic voltammograms were obtained using a Gamry electrochemical analyzer with an Ag/AgNO3 (0.01 M in acetonitrile (MeCN)) reference electrode and tetrabutylalammonium hexafluorophosphate ($TBAPF_6$) (0.1 M in DMAc) as the electrolyte for the working electrode. All samples were analyzed in DMAc at a concentration between 0.06 mM and 1 mM (depending on solubility) at a total volume of 25.0 mL and were sparged with nitrogen for 15 minutes before data collection. Platinum was used for the working and counter electrodes. Analysis was conducted at scan rates of 100 mV/s, 80 mV/s, 50 mV/s, and 20 mV/s with 7 cycles each. Data from the 6^{th} cycle was analyzed unless otherwise noted. All voltammograms were corrected using the $E_{1/2}$ of ferrocene as a reference.

Transient Absorption Spectroscopy: Transient absorption (TA) spectroscopy for determination of phenazine photocatalyst (PC) singlet and triplet excited state lifetimes was performed on an Edinburgh Instruments LP980KS spectrometer with a Minilite Nd:YAG Q-switched laser (Continuum Lasers) configured to deliver a 355 excitation pulse. Spectral absorption data was acquired from 300-800 nm with time delays as indicated in the spectra shown below with an iStar ICCD camera (Andor) as the detector. Kinetic data was recorded utilizing a photomultiplier tube (included in the LP980) interfaced with an MD03022 mixed domain oscilloscope (Tektronix) as the detector. Time zero was set on the instrument using the emission of $[Ru(bpy)_3]Cl_2$ to locate

the pump pulse with a resolution of 1 ns. All kinetic traces shown were acquired with 50-75 averages and laser power between 3-15 mW/cm^2 at 1 Hz repetition rate. Time constants (excited state lifetimes) were calculated in the L900 software using an exponential tail fit. Spectral absorption data was offset corrected at all wavelengths using kinetic absorption data at the indicated wavelength to adjust ΔOD. Emission subtraction was done for spectra acquired at t = 0, while spectra acquired at t = 200 ns or t = 400 ns included a time delay to avoid emission signals and the emission subtraction step was omitted.

For each PC solution, the Beer-Lambert Law was used to calculate the concentration of PC needed for an absorbance intensity of 0.2 at the lambda max of absorbance. This resulted in solutions with an absorbance intensity of less than 0.2 at 355 nm (wavelength of the excitation pulse). To prepare the solutions, solid PC was weighed into a scintillation vial which was then brought into a N_2 filled glovebox. The appropriate amount of N,N-dimethylacetamide (DMAc) stored under N_2 was added to each vial, and 3 mL of the resulting solution was transferred to a quartz screw cap cuvette equipped with a Kontes valve and sidearm with a 1 cm path length. After completely sealing the cuvettes with caps, they were brought out of the glovebox. Each PC solution was analyzed by UV-vis on the instrument described herein both before and after TA spectroscopy to monitor if PC degradation occurred. None of the PC solutions analyzed in this work showed evidence of degradation after TA, indicated by no observable change in the UV-vis spectra before and after TA spectroscopy was performed (Figure A1.45).

Polymer Characterization: Sample Prep for Analysis of Polymerization Kinetics and Molecular Weight Growth: To evaluate the kinetics and growth of molecular weight relative to the conversion of monomer (into polymer), an 0.1 mL aliquot of reaction mixture was taken after 1 hour, 2 hours, 4 hours, 6 hours, and 8 hours then immediately injected into a GC vial containing 0.5 mL of a solution of deuterated chloroform containing 250 ppm of a radical inhibitor (butylated hydroxyl toluene (BHT)). The aliquot was then analyzed using ^{1}H NMR spectroscopy. Through ^{1}H NMR

spectroscopy the ratio of polymer to monomer (% conversion) was determined. After ^{1}H NMR NMR analysis, the solvent was evaporated under air, then the sample was re-dissolved in HPCL-grade THF, filtered into a GPC vial using a 0.45 μm nylon filter, and finally analyzed by GPC with MALS. Characterization Instrumentation: Monomer conversion was determined using a Varian 400 MHz NMR Spectrometer. Molecular weights were determined by Gel Permeation Chromatography (GPC) coupled with multi-angle light scattering (MALS) using an Agilent HPLC fitted with one guard column, three PL-gel 5 μm MIXED-C gel permeation columns, a Wyatt Technology TrEX differential refractometer, and a Wyatt Technology miniDAWN TREOS light scattering detector (MALS). The dn/dc value used for MMA in THF was 0.084, A dn/dc value of 0.063 in THF was used for poly(n-butyl) acrylate analysis.

Polymerization Batch Reactor Supplies and Design

Light Beakers for Polymerizations (Materials): One sixteen-inch strip of double-density white LEDs was purchased from Creative Lighting Solutions (item no. CL-FRS1210-5M-12V-WH). Emission spectra of LEDs used is shown in Figure A1.2.

Light Beakers for Polymerizations (Setup): White light LED strip from Creative Lighting Solutions was wrapped inside a 400 mL beaker and used as the visible light source for the polymerizations described in this paper. The sides and bottom of the beaker were completely

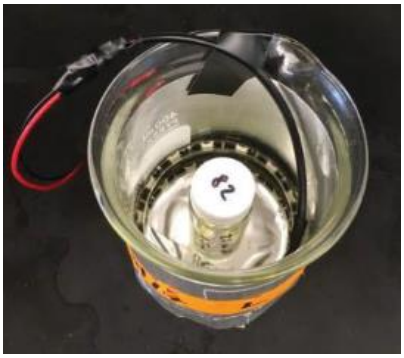

Figure A1.1. 400 mL white light LED beaker photoreactor for polymerizations.

wrapped with tin foil and the led strips were coiled inside the bottommost portion of the beaker walls (Figure A1.1).

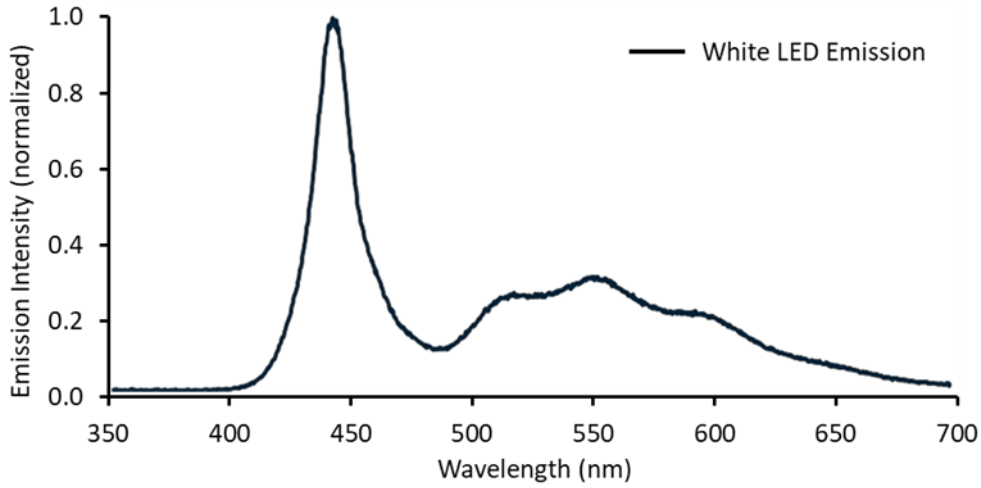

Figure A1.2. Normalized emission spectra of white light LEDs from creative lighting solutions.

PROCEDURES

Catalyst Synthesis

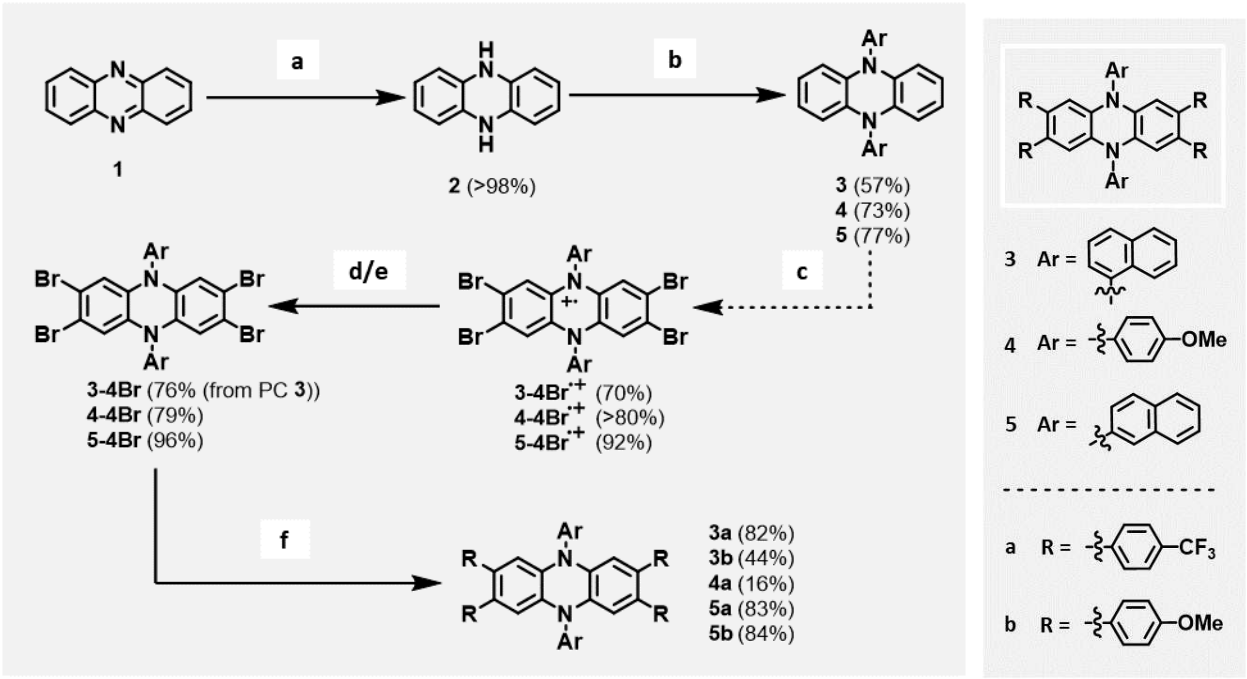

Figure A1.3. Synthetic scheme for synthesis of core-extended N,N-diaryl dihydrophenazines and structures. The mol percent yield from each step is noted adjacent to the labels of the final catalysts and catalyst intermediates.

Synthesis of *N,N*-diaryl dihydrophenazines (DHPs):

Synthesis of **2** (5,10-dihydrophenazine) (a)[1]: Phenazine (27.6 mmol) was dissolved in reagent alcohol (EtOH) (150 mL) that had been sparged with N_2 for 30 min. This mixture was brought to reflux under N_2 and a solution of sodium dithionite ($Na_2S_2O_4$) (555 mmol) dissolved in degassed water (~700 mL) was added to the solution of phenazine under N_2 via a canula transfer. The reaction was solution was refluxed for 3.5 hours and subsequently cooled to room temperature. The solid was collected using a swivel frit under N_2 and washed with sparged H_2O (3 x 100 mL). The solid was then dried overnight under vacuum before being brought into an N_2 filled glovebox. (yield: 94%)

Synthesis of **3** (b)[2,3]: 5,10-dihydrophenazine (1.098 mmol), NaOtBu (3.29 mmol), $P(tBu)_3$ (0.066 mmol), a stir bar, and 1-bromonaphthalene (4.39 mmol) were added to an oven dried Schlenk flask which was then cycled under reduced pressure and backfilled with N_2 three times. The Schlenk flask was then brought into in an N_2 filled glovebox and anhydrous 10 mL of Sure/Seal anhydrous toluene and $Pd(dba)_2$ (0.022 mmol) were added. The flask was then brought back out of the glovebox and the mixture was refluxed for 48 hours at 110°C then subsequently cooled to room temperature. The reaction mixture was then transferred to a separatory funnel and shaken in 100 mL of DI H_2O and 100 mL of DCM. The organic layer was recovered, washed with 100 mL of brine three times, then dried over Mg_2SO_4. After filtering off the Mg_2SO_4, the DCM was removed via rotary evaporation. The solids extracted from the crude reaction mixture were then dissolved in a minimal amount of DCM and recrystallized in the freezer after layering x3 volume of methanol on top of the DCM. Dark yellow solids were recovered. (Yield: 57%). ^{1}H NMR (400 MHz, C_6D_6) δ 8.68 – 8.54 (m, 2H), 7.75 – 7.66 (m, 2H), 7.64 (d, *J* = 8.5 Hz, 2H), 7.46 (dd, *J* = 17.4, 7.1 Hz, 2H), 7.27 (dd, *J* = 15.5, 7.9 Hz, 7H), 6.07 (dd, *J* = 5.9, 3.4 Hz, 4H), 5.73 – 5.58 (m, 4H).

Synthesis of **4** (b) [2,3]: 5,10-dihydrophenazine (12.6 mmol), NaOtBu (37.9 mmol), $P(tBu)_3$ (0.756 mmol), and a stir bar were added to an oven dried Schlenk flask which was then cycled under reduced pressure and backfilled with N_2 three times. The Schlenk tube was then brought into in an N_2 filled glovebox and anhydrous Sure/Seal toluene, $Pd(dba)_2$ (0.025 mmol), and 4-bromoanisole (21.1 mmol) (which was sparged under N_2 for 40 minutes) were added. The flask was then brought back out of the glovebox and the mixture was refluxed for 31 hours at 110°C then subsequently cooled to room temperature. The reaction mixture was dissolved in DCM (~100 mL) then washed twice with 400 mL of water, then with 100 mL of brine three times. The organic layer was dried using Mg_2SO_4 then filtered. Next, the solvent was removed via rotary evaporation. The solids obtained were dissolved in hot DCM, then x3 volume of warm hexanes was layered onto of the DCM. Bright yellow crystals were recovered. (Yield: 73 %) ^{1}H NMR (400 MHz, DMSO)

δ 7.34 – 7.27 (m, 4H), 7.24 – 7.17 (m, 4H), 6.24 (dd, *J* = 5.9, 3.4 Hz, 4H), 5.49 (dd, *J* = 5.8, 3.4 Hz, 4H), 3.84 (s, 6H).

Synthesis of **5** (b)[2,3]: 5,10-dihydrophenazine (27.4 mmol), NaOtBu (10.97 mmol), a stir bar, and 2-bromonaphthalene were added to an oven dried 250 mL Schlenk tube which was then cycled under reduced pressure and backfilled with N_2 three times. The Schlenk tube was then brought into in an N_2 filled glovebox and 50 mL of anhydrous Sure/Seal, RuPhos (1.09 mmol), and RuPhos Pd G4 (0.110 mmol) were added. The Schlenk tube was then brought back out of the glovebox and the mixture was refluxed for 48 hours at 110°C then subsequently cooled to room temperature. 600 mL of DCM and 300 mL of water were added to the crude reaction mixture. The product crashed out of solution over several minutes. Both aqueous and organic layers were filtered and the solid was collected. The product was then recrystallized from boiling DCM/MeOH in a 1:3 ratio to yield yellow crystals. (Yield: 77%) ^{1}H NMR (400 MHz, C_6D_6) δ 7.68 (dd, *J* = 5.3, 3.3 Hz, 4H), 7.64 – 7.57 (m, 2H), 7.57 – 7.49 (m, 2H), 7.32 (dd, *J* = 8.6, 2.0 Hz, 2H), 7.24 (dddd, *J* = 19.0, 8.2, 6.9, 1.4 Hz, 4H), 6.28 (dt, *J* = 7.5, 3.7 Hz, 4H), 5.86 (dd, *J* = 5.9, 3.4 Hz, 4H).

Synthesis of **3-4Br$^{\bullet+}$** (c)[4]: PC **3** (0.460 mmol), benzene (200 mL), and bromine (9.20 mmol) were added to a round bottom flask containing a stir bar. The solution was refluxed at 60°C for 38.5 hours with a tube bubbling vapors from the reaction into a saturated aqueous solution of sodium dithionite. After 38.5 hours the reaction was cooled to room temperature and filtered. The reaction yielded 267 mg of dark blue solids. The filtrate (containing unreacted bromine) was neutralized using a solution of DI H_2O saturated with sodium thiosulfate. (Yield ~70%) (Not characterized by ^{1}H-NMR).

Synthesis of **4-4Br$^{\bullet+}$** (c)[4]: PC **4** (0.761 mmol), benzene (500 mL), and bromine (15.2 mmol) were added to a round bottom flask containing a stir bar. The solution was refluxed at 60°C for 24.5 hours with a tube bubbling vapors from the reaction into a saturated aqueous solution of sodium dithionite. After 24.5 hours the reaction was cooled to room temperature and filtered. The reaction yielded 267 mg of dark purple solids. The filtrate (containing unreacted bromine) was neutralized using a solution of DI H_2O saturated with sodium thiosulfate. (Yield >80%) (Not characterized by ^{1}H-NMR).

Synthesis of **5-4Br$^{\bullet+}$** (c)[4]: PC **5** (11.5 mmol), benzene (200 mL), and bromine (23.0 mmol) were added to a round bottom flask containing a stir bar. The solution was refluxed at 60°C for 12 hours hours with a tube bubbling vapors from the reaction into a saturated aqueous solution of sodium dithionite. After 12 hours the reaction was cooled to room temperature and filtered. The reaction yielded 882 mg of dark purple solids. The filtrate (containing unreacted bromine) was neutralized using a solution of DI H_2O saturated with sodium thiosulfate. (Yield ~92%) (Not characterized by ^{1}H-NMR).

Synthesis of **3-4Br** (d) (Method I)[4]: 160 mg of the solids obtained from the synthesis of **3-4Br$^{\bullet+}$** (~0.193 mmol) were added to a 1L round bottom flask. 500 mL of methanol was added along with a stir bar and 8g of copper wire cut into 1 inch pieces. The reaction mixture (a deep magenta color) was then stirred at ~60 °C for 30 minutes. After 30 minutes the reaction mixture had turned a creamy-orange color. The reaction mixture was subsequently cooled to room temperature and 86.4 mg of orange/yellow solids were collected via vacuum filtration and used without further purification. (Yield ~60%) (This sample was not used in synthesis, only the sample synthesized using Method II (see below) was used.

Synthesis of **3-4Br** (Method II) (c&e): Step 1): PC **3** (0.587 mmol), benzene (300 mL), and bromine (11.7 mmol) were added to a round bottom flask containing a stir bar. The solution was refluxed for 48.5 hours with a tube bubbling vapors from the reaction vessel into a saturated aqueous solution of sodium dithionite. After 48.5 hours the reaction was cooled to room temperature and filtered yielding shiny dark blue solids. The filtrate (containing unreacted bromine) was neutralized using a solution of DI H_2O saturated with sodium thiosulfate. Step 2): The recovered solids were dissolved in acetone (~500 mL) and allowed to stir for five hours at room temperature. The reaction mixture slowly changed from a deep magenta color to an opaque pale-yellow color. The reaction mixture was filtered and ~333 mg of solids were recovered. (Yield from **3** → **3-4Br**: ~76%) ^{1}H NMR (400 MHz, C_6D_6) δ 8.36 (dd, *J* = 17.1, 8.4 Hz, 2H), 7.51 (dd, *J* = 8.3, 5.4 Hz, 2H), 7.45 (dd, *J* = 8.2, 4.5 Hz, 2H), 7.31 – 7.23 (m, 3H), 5.90 (d, *J* = 2.1 Hz, 4H).

Synthesis of **4-4Br** (d)[4]: 200 mg of the solids obtained from the synthesis of **4-4Br$^{\bullet+}$** (~0.253 mmol) were added to a 1L round bottom flask. 500 mL of methanol was added along with a stir bar and 10g of copper wire cut into 1 inch pieces. The reaction mixture (a deep magenta color) was then stirred at ~80 °C for 3 hours. After 3 hours the reaction mixture had turned a light tan color. The reaction mixture was subsequently cooled to room temperature and 142 mg of light tan/yellow solids were collected via vacuum filtration. These solids were used without further purification. (Yield: 79%). ^{1}H NMR (400 MHz, C_6D_6) δ 6.78 (d, *J* = 8.5 Hz, 4H), 6.59 (d, *J* = 8.6 Hz, 4H), 6.06 (s, 4H), 3.15 (s, 6H).

Synthesis of **5-4Br** (d)[4]: 500 mL of methanol was added to **5-4Br$^{\bullet+}$** solids in a round bottom flask with a stir bar. The solution was stirred at ~60 °C for 30 minutes. Then 7 ft of copper wire, cut into 1 inch pieces, was added to the round bottom flask. The solution was stirred at 60° C for 26 hours. The solution turned from a deep fusia color to a light orange color with a yellow solid precipitated. After 26 hours, the reaction mixture was cooled to room temperature and the solid was collected

via vacuum filtration. (Yield: ~96%). ^{1}H NMR (400 MHz, C_6D_6) δ 7.57 – 7.41 (m, 9H), 7.01 (dd, *J* = 8.6, 2.1 Hz, 2H), 6.08 (s, 4H).

Synthesis of **3a** (e)[4]: **3-4Br** (0.173 mmol), 4-trifluoromethylphenyl boronic acid (1.39 mmol) n and a stir bar were added to a 100mL Schlenk tube. The Schlenk tube was then put under vacuum then backfilled with N_2 (three cycles) before transferring it to an N_2 filled glovebox. $Pd(PPh_3)_4$ (0.026 mmol) and 25.0 mL of anhydrous sure/seal THF was added. The storage tube was then taken out of the glove box and 4.50 mL of 2.00 M aqueous K_2CO_3 (that had been sparged with N_2 for >30 min) was added to the storage tube under N_2. The mixture was heated to 110 °C and stirred for 45 hours. After allowing the reaction mixture to cool, the reaction mixture was transferred to a round bottom flask using THF, then 100 mL of water was added. The THF was removed via rotary evaporation and yellow/green solids crashed out into the water. The solution was then filtered to recover the solids. The recovered solids were then dissolved in DCM, and the solution was washed with eqivolume of water three times then the organic layer was washed with brine. The solution was then dried with using Na_2SO_4 then filtered and concentrated via rotary evaporation. The recovered yellow solids were then dissolved in a minimal amount of warm toluene and any undissolved solids were filtered off. Small amounts of silver/grey solids were recovered from the solution during this step. Next, the toluene was removed by rotary evaporation then the recovered solids were redissolved in a minimal volume of DCM. Methanol (in three time the volume of DCM) was then layered on top of the DCM and the solution was put into the freezer to recrystallize. Bright yellow solids were recovered (Yield: 82%). ^{1}H NMR (400 MHz, C_6D_6) δ 8.85 (dd, *J* = 8.4, 4.5 Hz, 2H), 7.70 – 7.53 (m, 6H), 7.45 – 7.19 (m, 7H), 6.69 (dd, *J* = 8.5, 2.3 Hz, 9H), 6.57 (dd, *J* = 8.1, 5.9 Hz, 8H), 5.98 (d, *J* = 1.5 Hz, 4H). HRMS (ESI) calculated for (M^+) $C_{60}H_{34}F_{12}N_2$: 1010.2530; mass found: 1010.2480.

Synthesis of **4a** (e)[4]: **4-4Br** (0.446 mmol), 4-trifluoromethylphenyl boronic acid (3.57 mmol), and a stir bar were added to a 100mL Schlenk tube. The Schlenk tube was put under vacuum then backfilled with N_2 (three cycles) before transferring it to an N_2 filled glovebox. $Pd(PPh_3)_4$ (0.067 mmol) and 30.0 mL of THF were added. The storage tube was taken out of the glove box then 9.00 mL of 2.00 M aqueous K_2CO_3 that had been sparged with N_2 for >30 min was added to the storage tube under N_2. The mixture was heated to 100 °C and stirred for 48 hours. After allowing the reaction mixture to cool, the reaction mixture was transferred to a round bottom flask using THF and 100 mL of water, the THF was then removed via rotary evaporation and dark green/yellow solids crashed out into the water. The solids were recovered by vacuum filtration, then hot DCM was added until the solids were almost entirely dissolved ~400 mL). The solution was then filtered and small amounts of silver/grey solids were recovered. The filtrate was then rotovapped down to yield bright yellow solids (Yield: 80%). Although the 1H-NMR looked relatively clean, we attempted to further recrystallize the yellow powder. The bright yellow powder was then redissolved in warm DCM which was layered with methanol (x2 volume relative to DCM) and yellow solids started to crash out. The yellow solids were recovered via vacuum filtration then dissolved in ~300 mL of toluene. Warm hexanes in three times the volume of toluene was then layered on top of the solution. The solution was transferred to the freezer and allowed to recrystallize. Bright yellow solids were then recovered via vacuum filtration (Yield: 16 %) ^{1}H NMR (400 MHz, DMSO) δ 7.48 (dd, *J* = 8.6, 3.5 Hz, 13H), 7.20 (d, *J* = 8.9 Hz, 4H), 6.99 (d, *J* = 8.0 Hz, 8H), 5.57 (s, 4H), 3.80 (s, 6H). ^{1}H NMR (400 MHz, C_6D_6) δ 7.29 (d, *J* = 8.8 Hz, 4H), 6.94 – 6.78 (m, 20H), 6.12 (s, 4H), 3.11 (s, 6H). HRMS (ESI) calculated for (M^+) $C_{54}H_{34}F_{12}N_2O_2$: 970.2428; mass found: Not detected.

Synthesis of **5a** (e)[4]: **5-4Br** (0.533 mmol) and 4-trifluoromethylphenyl boronic acid (4.27 mmol) were added to a 100mL storage tube. The storage tube was put under vacuum then backfilled with N_2 (3 cycles) before transferring it to an N_2 filled glovebox. $Pd(PPh_3)_4$ (0.080 mmol) and 40.0

mL of THF was added. The storage tube was then taken out of the glove box then 12.0 mL of 2.00 M aqueous K_2CO_3 that had been sparged with N_2 for >30 min was added to the storage tube under N_2. The mixture was heated to 100 °C and refluxed for 24 hours. After allowing the reaction mixture to cool, the reaction mixture was transferred to a round bottom flask using THF, then THF was removed via rotary evaporation. DCM was added until the solids were almost entirely dissolved. The solution was then washed with eqivolume of water three times then the organic layer was washed with an equivolume of brine two times. The solution was then dried with sodium sulfate and concentrated via rotary evaporation. The recovered yellow/green solids were then stirred in ~300 mL of hot toluene until almost everything had dissolved, then, after allowing it to cool, the solution was filtered. Small amounts of silver/grey solids were recovered from the product solution during this step. Warm hexanes in three times the volume of toluene was then layered on top of the solution. The solution was transferred to the freezer and allowed to recrystallize. Bright yellow solids were recovered via vacuum filtration. (Yield: 83 %) ^{1}H NMR (400 MHz, C_6D_6) δ 7.97 (d, *J* = 2.0 Hz, 2H), 7.77 (d, *J* = 8.6 Hz, 2H), 7.58 (dt, *J* = 7.2, 3.6 Hz, 2H), 7.55 – 7.46 (m, 4H), 6.75 (q, *J* = 8.4 Hz, 16H), 6.18 (s, 4H). HRMS (ESI) calculated for (M^+) $C_{60}H_{34}F_{12}N_2$: 1010.2530; mass found: 1010.2517.

Synthesis of **3b** (e)[4]: **3-4Br** (0.175 mmol), 4-methoxyphenyl boronic acid (0.00140 mol), and a stir bar were added to a 100mL storage tube. The storage tube was put under vacuum then backfilled with N_2 (three cycles) before transferring it to an N_2 filled glovebox. $Pd(PPh_3)_4$ (0.026 mol) and 10 mL of anhydrous Sure/seal THF was added. The storage tube was then taken out of the glove box then 6 mL of 2M aqueous K_2CO_3 that had been sparged with N_2 for >30 min was added to the storage tube under N_2. The mixture was heated to 110 °C and stirred for 48 hours. After allowing the reaction mixture to cool, THF was used to transfer the mixture to a round bottom flask. 100 mL of DI H_2O was added to the round bottom flask and then the THF was then removed via rotary evaporation—yellow solids precipitated into the water. The solids were recovered by

vacuum filtration, rinsed with ~100 mL of methanol, then dissolved in hot DCM until the solids were almost entirely dissolved ~400 mL). The solution was then filtered and small amounts of silver/grey solids were recovered. The filtrate was then layered with x2 volume of methanol and placed in the freezer to recrystallize. (Yield: 44%). ^{1}H NMR (400 MHz, $CDCl_3$) δ 9.00 (dd, *J* = 8.8, 4.0 Hz, 2H), 7.76 (t, *J* = 6.7 Hz, 2H), 7.65 (dd, *J* = 13.4, 8.0 Hz, 3H), 7.59 (d, *J* = 8.3 Hz, 2H), 6.86 (dd, *J* = 8.4, 6.4 Hz, 9H), 6.37 – 6.24 (m, 9H), 6.19 (d, *J* = 1.7 Hz, 4H), 3.08 (s, 14H). HRMS (ESI) calculated for (M^+) $C_{60}H_{46}N_2O_4$: 858.3458; mass found: 858.3441.

Synthesis of **5b** (e)[4]: **5-4Br** (0.667 mmol) and 4-methoxyphenyl boronic acid (5.33 mmol) were added to a 250 mL storage tube along with a stir bar. The storage tube was put under vacuum then backfilled with N_2 (x3) before transferring it to an N_2 filled glovebox. $Pd(PPh_3)_4$ (0.099 mmol) and 50.0 mL of THF were added. The storage tube was then taken out of the glove box then 15.0 mL of a 2.00 M aqueous K_2CO_3 that had been sparged with N_2 for >30 min was added to the storage tube under N_2. The mixture was heated to 100 °C and stirred for 24 h. After allowing the reaction mixture to cool, it was transferred to a round bottom flask using 100 mL of THF and 100 mL of water. The THF was then removed via rotary evaporation and yellow/green solids crashed out. The solids were then filtered off and the filtrate disposed of. Hot DCM was added to the until the solids were almost entirely dissolved. The solution was then washed with eqivolume of water three times then the organic layer was washed with brine. The solution was then dried with sodium sulfate, filtered, then concentrated via rotary evaporation. The solids were recrystallized by using hot dichloromethane to dissolve the solids, then adding three times that volume of methanol. The recovered yellow solids were then dissolved in warm toluene and filtered. Small amounts of silver/grey solids were recovered from the product solution during this step. The toluene was removed via rotary evaporation and the remaining solids were recrystallized again from hot DCM/MeOH in a ratio of 1:3 yielding bright yellow solids. (Yield: 84%) ^{1}H NMR (400 MHz, C_6D_6) δ 8.00 (s, 2H), 7.80 – 7.45 (m, 7H), 6.46 – 6.21 (m, 12H), 3.06 (d, *J* = 3.6 Hz, 12H). ^{1}H NMR (400

MHz, DMSO) δ 8.26 (d, *J* = 8.7 Hz, 2H), 8.19 (d, *J* = 1.9 Hz, 2H), 8.05 (t, *J* = 7.6 Hz, 4H), 7.72 – 7.65 (m, 2H), 7.61 (q, *J* = 6.9 Hz, 4H), 6.66 – 6.53 (m, 18H), 5.54 (s, 4H). HRMS (ESI) calculated for (M^+) $C_{60}H_{46}N_2O_4$: 858.3458; mass found: 858.3435.

Polymer Synthesis:

Approximately 15.0 mg of the catalyst was weighed into a 20 mL scintillation vial. Each catalyst was then dissolved in DMAc to a known concentration. A specific volume of the catalyst stock solution was then dispensed into a 20 mL scintillation vials such that when 1.00 mL of monomer was added to the reaction vial, the catalyst would either be at a 500 ppm, 100 ppm, 50 ppm, or 10 ppm catalyst loading relative to monomer. After the catalyst solutions were dispensed into scintillation vials, the DMAc was removed via rotary evaporation and the sample was dried on a high vac line for 24 hours. The scintillation vials containing catalyst were then equipped with a stir bar and brought into a nitrogen-filled glovebox. 1.00 mL of monomer and 1.00 mL of solvent was then added using Hamilton gas tight syringes and the solution stirred in the dark for 2 minutes. 17.8 μL of initiator (diethyl-2-bromo-2-methylmalonate) was then added using a Hamilton gas tight syringe and the reaction vessel was immediately placed in the center of an LED beaker, the latter of which had been turned on for at least 5 minutes. The initial time for the start of the polymerization was noted at the moment the reaction vessel was transferred to the LED beaker and the polymerizations were allowed to proceed for eight hours. Polymerizations were run according to previously described methods.[3,4]

CHARACTERIZATION OF CATALYST PROPERTIES

Table A1.1. Select experimentally determined and computationally predicted photophysical and electrochemical properties of PCs.

PC	$\lambda_{max,abs}$ (nm)[a]	ε_{max} ($M^{-1}s^{-1}$)[b]	$\lambda_{max,em}$ (nm)[c]	$E_{S1,exp}$ (eV)[d]	$E_{T1,comp}$ (eV)[e]	Stokes Shift (nm)	ϕ_f (%)[f]	$E_{1/2}$ ($^2PC^{\bullet+}/^1PC$) (V vs SCE)[g]	$E^0_{ox,comp}$ ($^2PC^{\bullet+}/^1PC$) (V vs SCE)[e]	$E^{0*}_{S1,exp}$ ($^2PC^{\bullet+}/^1PC^*$) (V vs SCE)[h]	$E^{0*}_{T1,comp}$ ($^2PC^{\bullet+}/^3PC^*$) (V vs SCE)[e]
3	366	5,500	663	1.87	2.23	297	1.32	0.23	0.10	-1.64	-2.13
3a	385	21,900	586	2.12	1.91	201	9.00	0.34	0.24	-1.78	-1.67
3b	385	13,100	636	1.95	2.07	251	4.31	0.23	0.00	-1.72	-2.06
4	373	5,500	467	2.66	2.29	94.0	23.0	0.16	0.01	-2.50	-2.29
4a	392	21,000	599	2.07	1.82	207	36.0	0.34	0.16	-1.73	-1.66
5	343	5,900	654	1.90	2.19	311	0.72	0.21[i]	0.06	-1.69	-2.12
5a	373	27,400	587	2.11	1.89	214	35.0	0.38	0.15	-1.73	-1.75
5b	371	16,000	621	2.00	1.99	250	4.00	0.38	0.00	-1.62	-2.00

[a]Maximum wavelength of absorption was measured using UV-Vis in DMAc. [b]Molar absorptivity calculated at λ_{max} in DMAc. [c] Maximum wavelength of emission was measured using steady-state fluorescence spectroscopy in DMAc. [d]Singlet energies were calculated using the maximum wavelength of emission (E(eV)=1239.8 / λ (nm)). [e]DFT calculations were performed at the uM06/6-311+G(d,p)//uM06/6-31+G(d,p) level of theory with CPCM-described solvation in DMAc. [f]Quantum yield of fluorescence was measured in DMAc using absolute methods. [g]All measurements were performed in a 3-compartment electrochemical cell with an Ag/ AgNO3 reference electrode in MeCN (0.01 M) and 0.1 M NBu4PF6 electrolyte solution. DMAc was used to solvate the PCs and in the working electrode compartment, while platinum was used as both the working and counter electrodes. E (V vs SCE) = E (V vs Ag/AgNO3 [0.01 M]) + 0.298 V. [h]Singlet excited state reduction potentials were calculated using the singlet energies (estimated from the maximum wavelength of emission) and the $E_{1/2}$. [i]Values were taken from ref. 2.

Table A1.2. Experimentally determined singlet and triplet excited state lifetimes of PCs.

PC	τ_{S1} (ns)[a]	τ_{T1} (µs)[b]	$\lambda_{kinetic\ em}$ (nm)[c]	$\lambda_{kinetic\ abs}$ (nm)[d]
3	9	0.63	617	445
3a	17	144	569	440
3b	11	42	608	593
4	37	88	466	450
4a	13	NA[e]	585	NA[e]
5	NA[f]	3.5	600	450
5a	17	NA[e]	575	NA[e]
5b	11	108	598	550

[a]Singlet excited state lifetime determined by kinetic emission. [b]Triplet excited state lifetime determined by kinetic absorption. [c]Wavelength at which kinetic emission was measured. [d]Wavelength at which kinetic absorption was measured. [e]Excited state absorption signal was too weak to measure kinetic decay of excited state absorption, therefore a triplet excited state lifetime was not measured for this PC. [f]Kinetic emission measured at 600nm was determined to be 6.3 ns which is too close to the limit of detection for the instrument (6 ns) to be measured accurately, therefore this data is not included in the above table.

Ultraviolet-Visible Spectroscopy

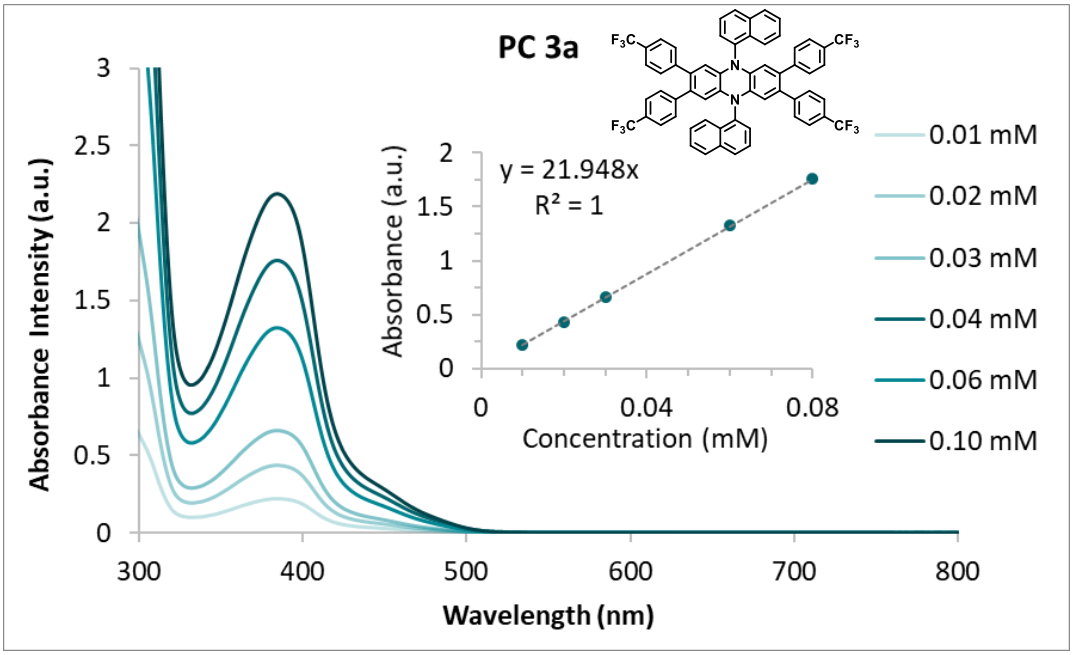

Figure A1.4. UV-Vis spectra of 3a at varied concentrations in DMAc in a quartz cuvette with a pathlength of 1cm. Secondary graph demonstrates the Beer-Lambert law relationship between concentration and absorbance at 385 nm.

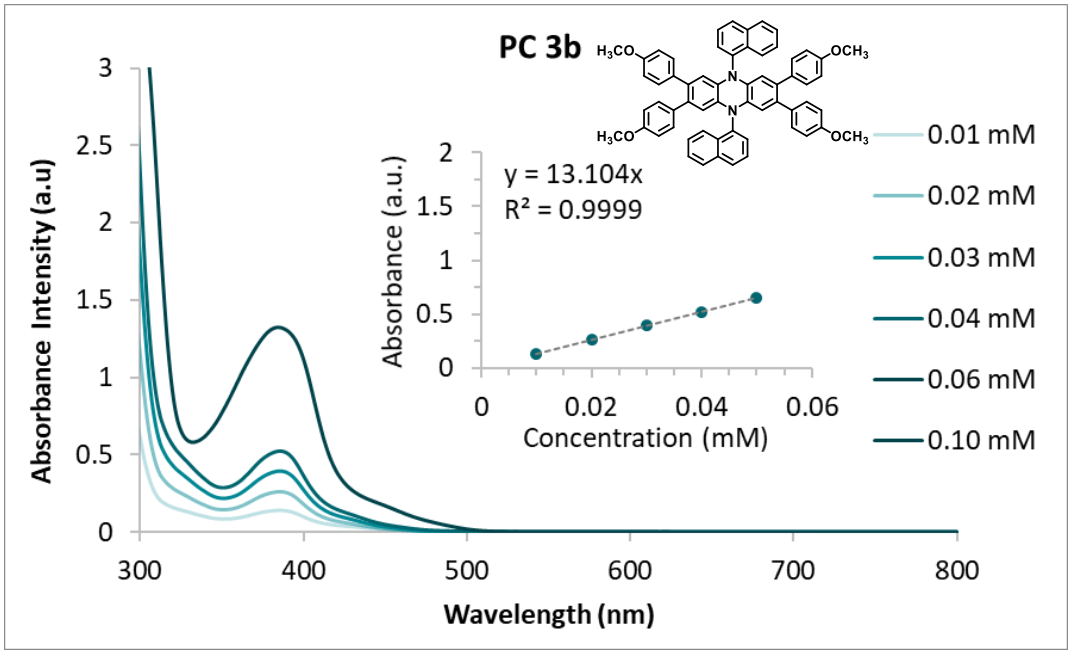

Figure A1.5. UV-Vis spectra of 3b at varied concentrations in DMAc in a quartz cuvette with a pathlength of 1cm. Secondary graph demonstrates the Beer-Lambert law relationship between concentration and absorbance at 385 nm.

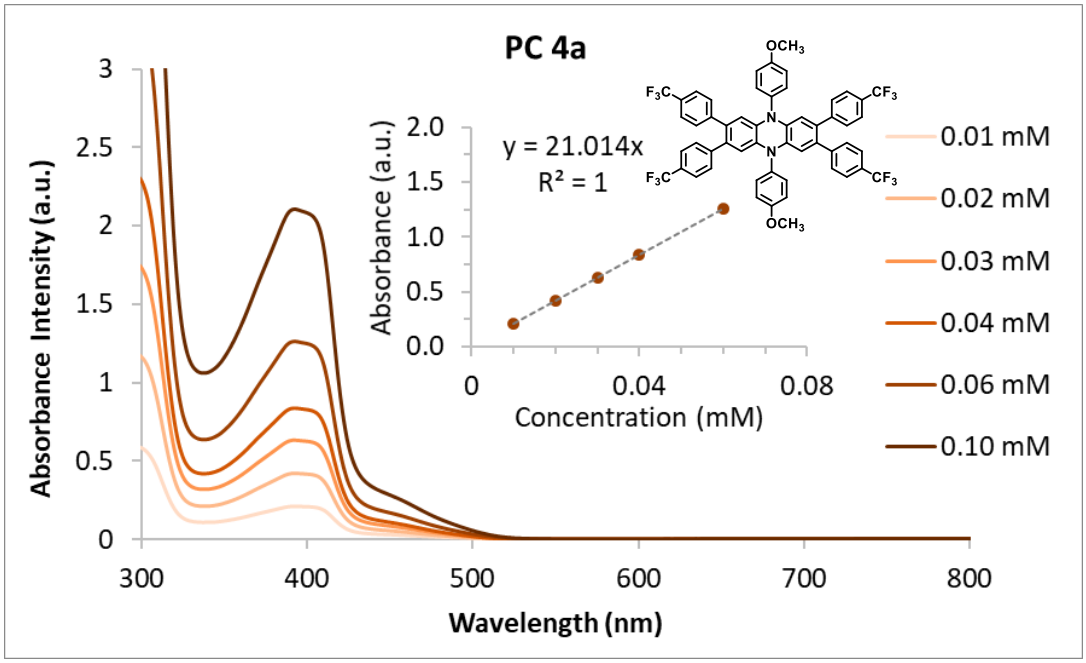

Figure A1.6. UV-Vis spectra of 4a at varied concentrations in DMAc in a quartz cuvette with a pathlength of 1cm. Secondary graph demonstrates the Beer-Lambert law relationship between concentration and absorbance at 392 nm.

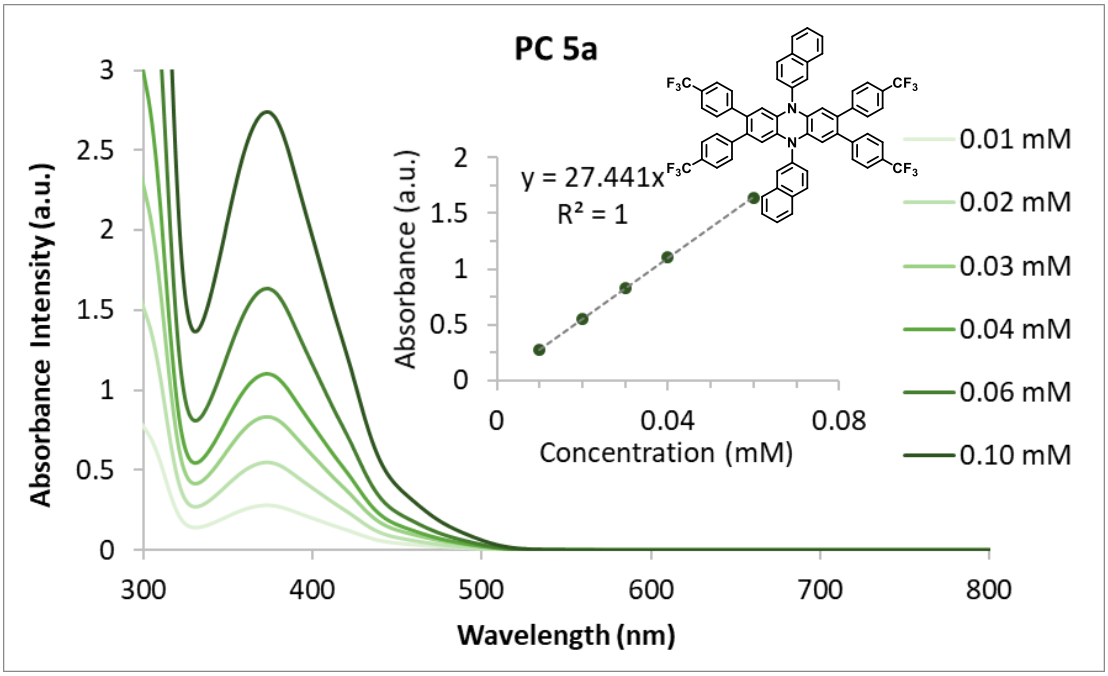

Figure A1.7. UV-Vis spectra of **5a** at varied concentrations in DMAc in a quartz cuvette with a pathlength of 1cm. Secondary graph demonstrates the Beer-Lambert law relationship between concentration and absorbance at 373 nm.

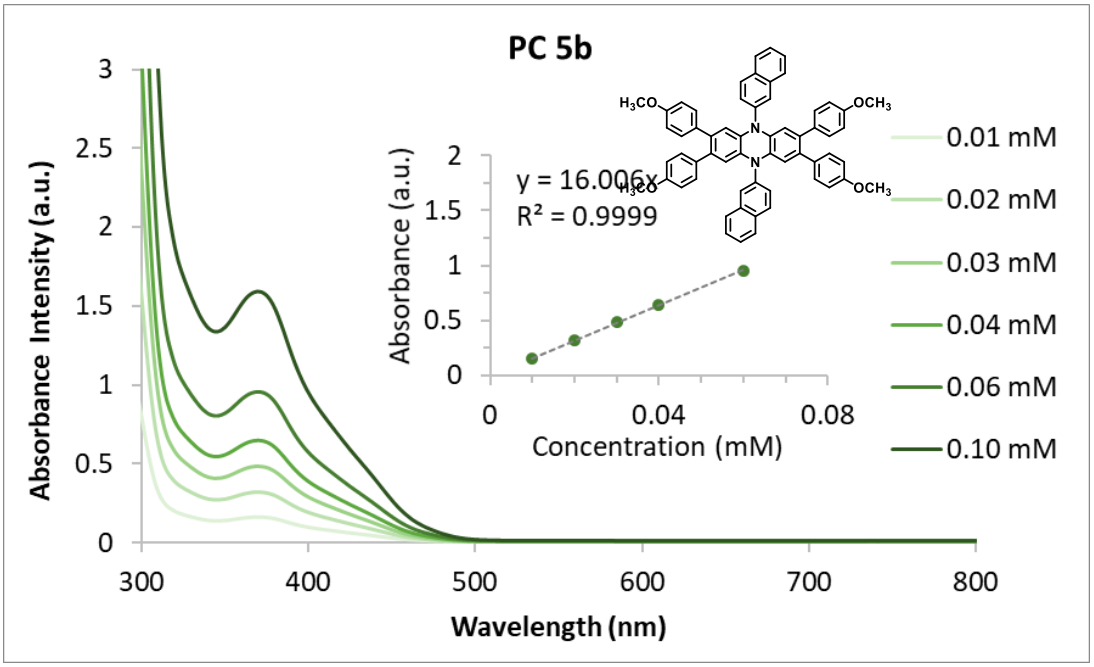

Figure A1.8. UV-Vis spectra of **5b** at varied concentrations in DMAc in a quartz cuvette with a pathlength of 1cm. Secondary graph demonstrates the Beer-Lambert law relationship between concentration and absorbance at 371 nm.

Fluorescence Spectroscopy

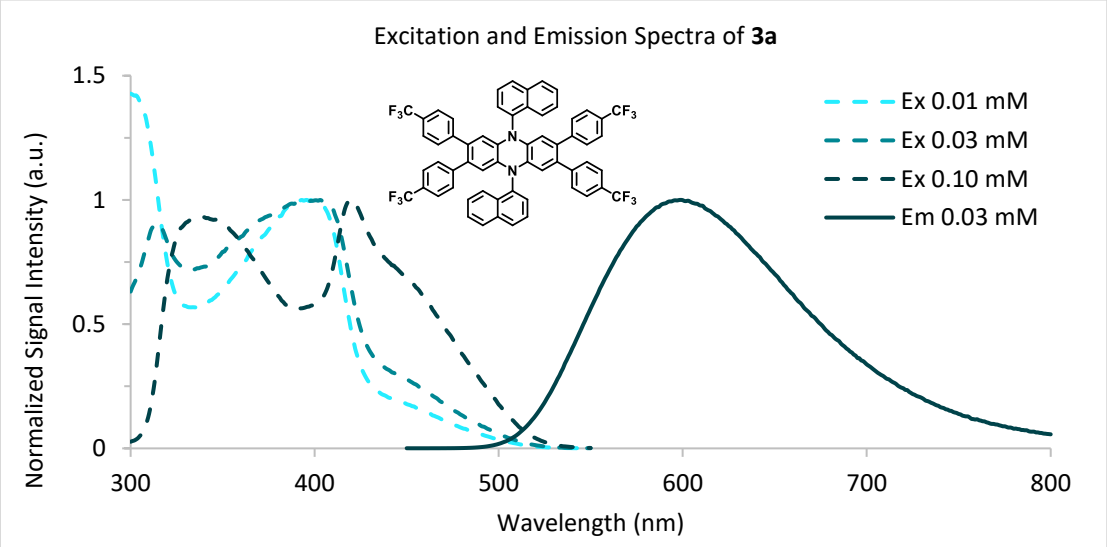

Figure A1.9. Fluorescence spectra of PC **3a**. Dashed lines are the excitation spectra at varying concentrations in DMAc and the solid line is the emission spectrum at 0.03 mM in DMAc. Emission spectra was collected using an excitation wavelength of 385 nm and is representative of emission profiles at all concentrations between 0.01 mM and 0.10 mM. Excitation spectra were collected for emission at 586 nm.

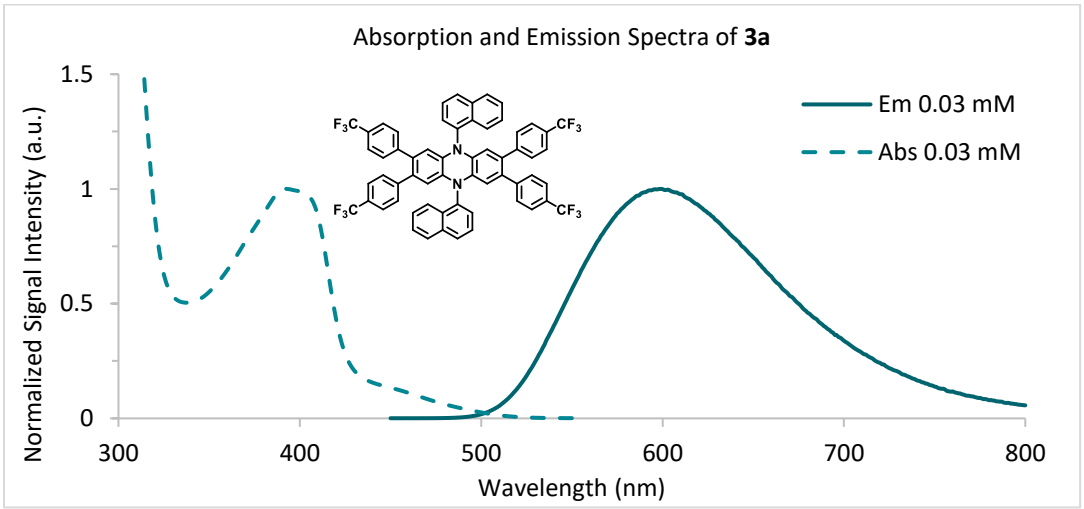

Figure A1.10. Emission spectra of PC **3a** (solid) and absorption spectra of **3a** (dashed) at 0.03 mM in DMAc. Absorption spectra was measured using UV-Vis and emission spectra was measured using fluorimetry. Emission spectra was collected using an excitation wavelength of 385 nm.

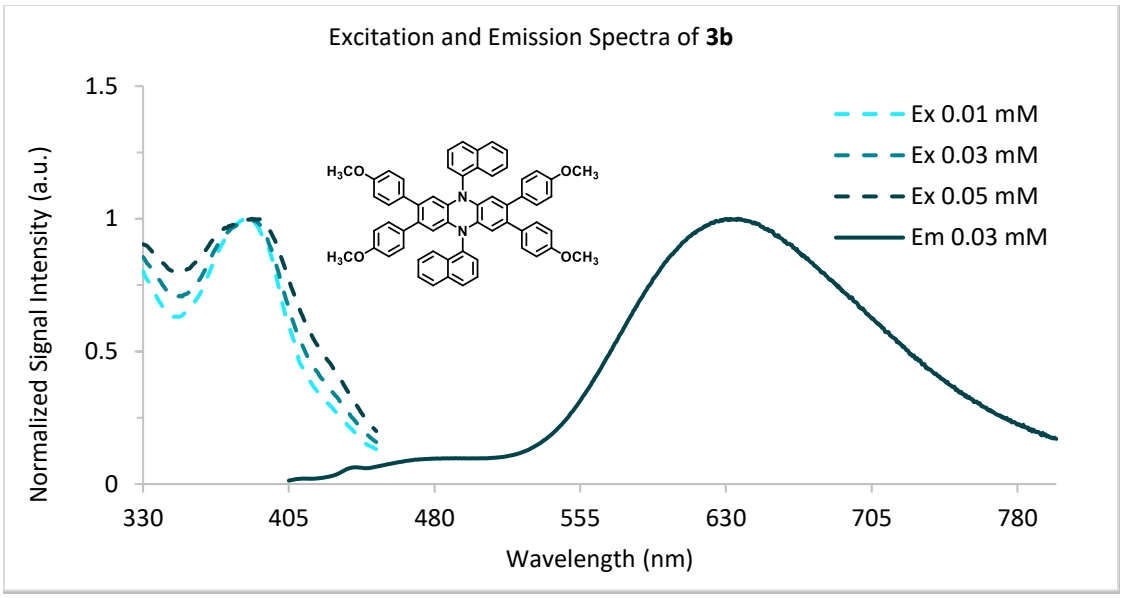

Figure A1.11. Fluorescence spectra of PC **3b**. Dashed lines are the excitation spectra at varying concentrations in DMAc and the solid line is the emission spectrum at 0.03 mM in DMAc. Emission spectra was collected using an excitation wavelength of 385 nm and is representative of emission profiles at all concentrations between 0.01 mM and 0.10 mM. Excitation spectra were collected for emission at 636 nm.

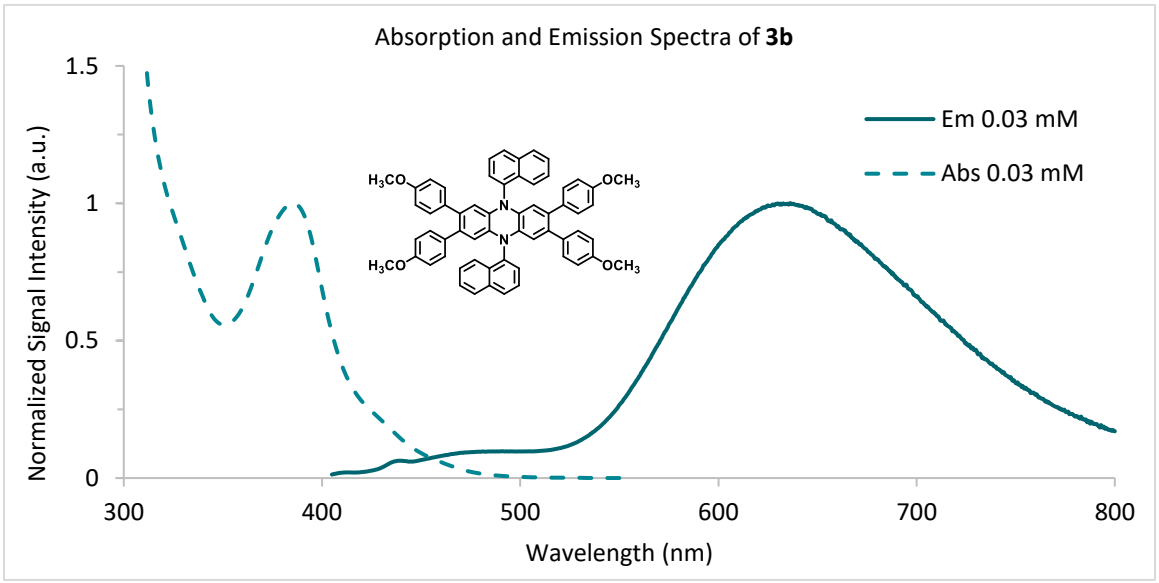

Figure A1.12. Emission spectra of PC **3b** (solid) and absorption spectra of **3b** (dashed) at 0.03 mM in DMAc. Absorption spectra was measured using UV-Vis and emission spectra was measured using fluorimetry. Emission spectra was collected using an excitation wavelength of 385 nm.

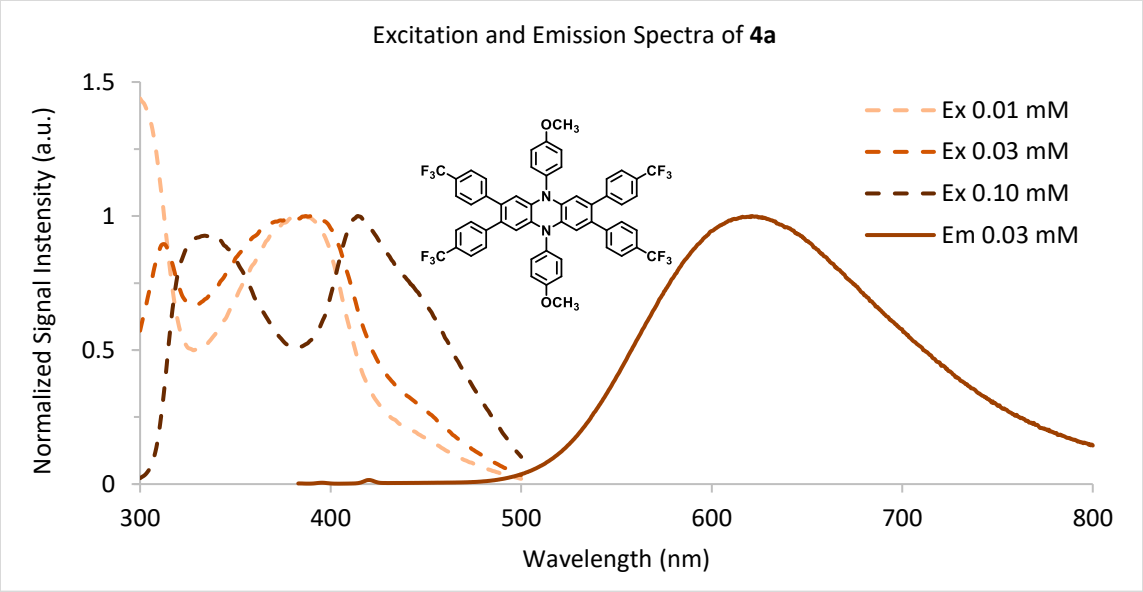

Figure A1.13. Fluorescence spectra of PC **4a**. Dashed lines are the excitation spectra at varying concentrations in DMAc and the solid line is the emission spectrum at 0.03 mM in DMAc. Emission spectra was collected using an excitation wavelength of 392 nm and is representative of emission profiles at all concentrations between 0.01 mM and 0.10 mM. Excitation spectra were collected for emission at 599 nm.

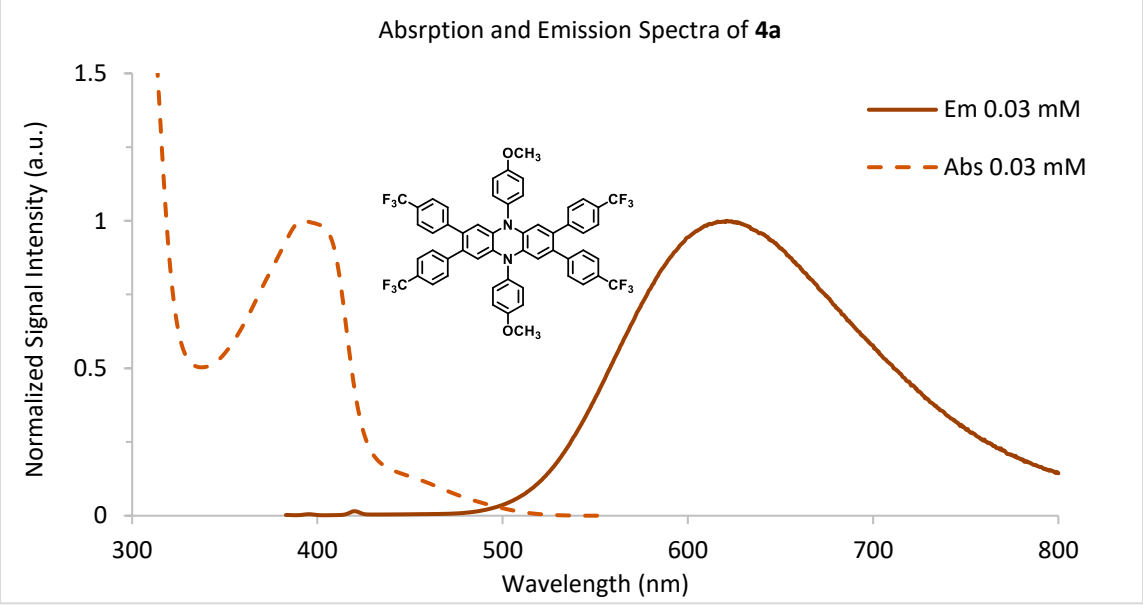

Figure A1.14. Emission spectra of PC **4a** (solid) and absorption spectra of **4a** (dashed) at 0.03 mM in DMAc. Absorption spectra was measured using UV-Vis and emission spectra was measured using fluorimetry. Emission spectra was collected using an excitation wavelength of 392 nm.

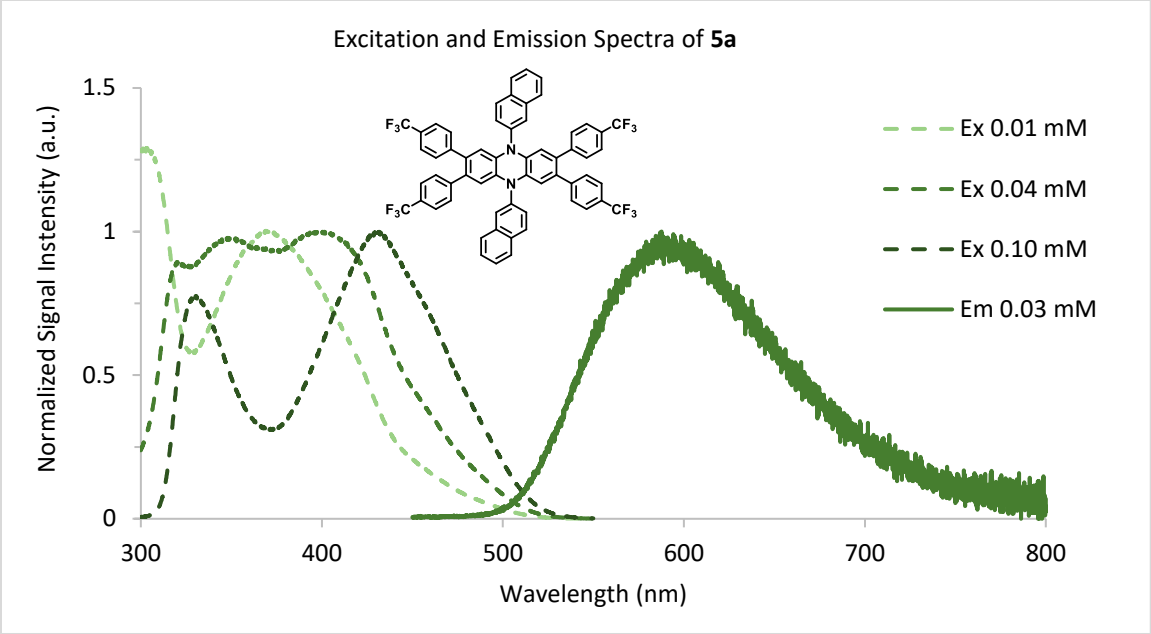

Figure A1.15. Fluorescence spectra of PC **5a**. Dashed lines are the excitation spectra at varying concentrations in DMAc and the solid line is the emission spectrum at 0.03 mM in DMAc. Emission spectra was collected using an excitation wavelength of 373 nm and is representative of emission profiles at all concentrations between 0.01 mM and 0.10 mM. Excitation spectra were collected for emission at 587 nm.

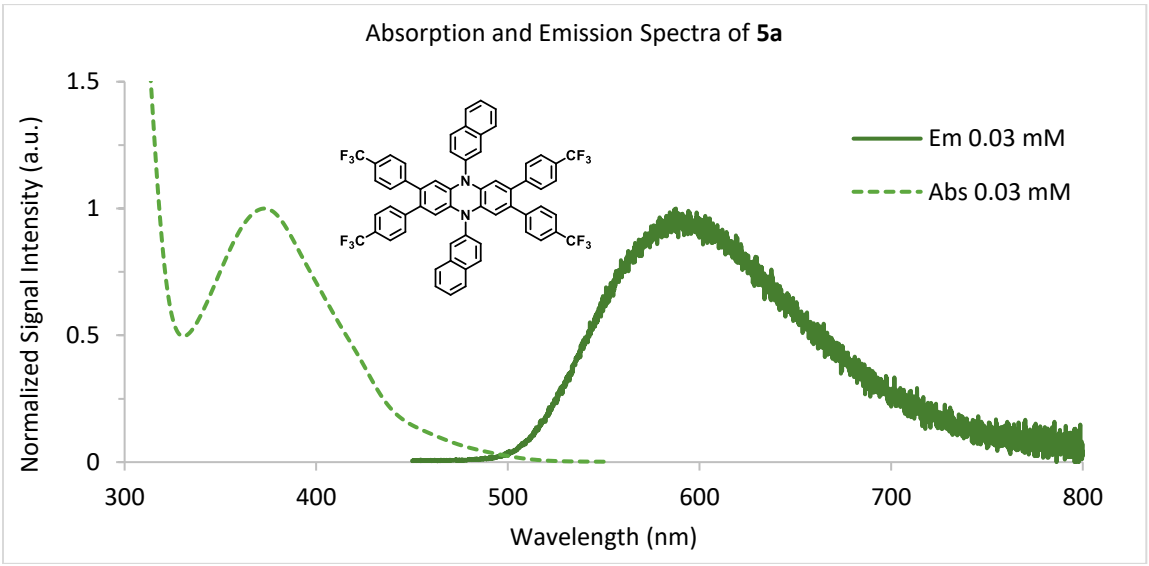

Figure A1.16. Emission spectra of PC **5a** (solid) and absorption spectra of **5a** (dashed) at 0.03 mM in DMAc. Absorption spectra was measured using UV-Vis and emission spectra was measured using fluorimetry. Emission spectra was collected using an excitation wavelength of 373 nm.

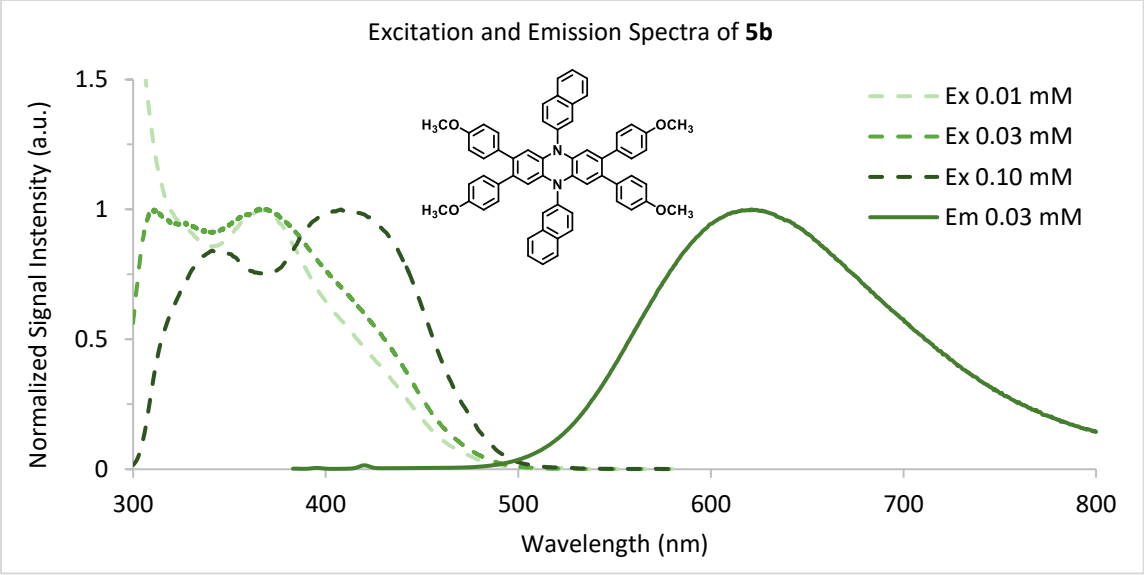

Figure A1.17. Fluorescence spectra of PC **5b**. Dashed lines are the excitation spectra at varying concentrations in DMAc and the solid line is the emission spectrum at 0.03 mM in DMAc. Emission spectra was collected using an excitation wavelength of 371 nm and is representative of emission profiles at all concentrations between 0.01 mM and 0.10 mM. Excitation spectra were collected for emission at 621 nm.

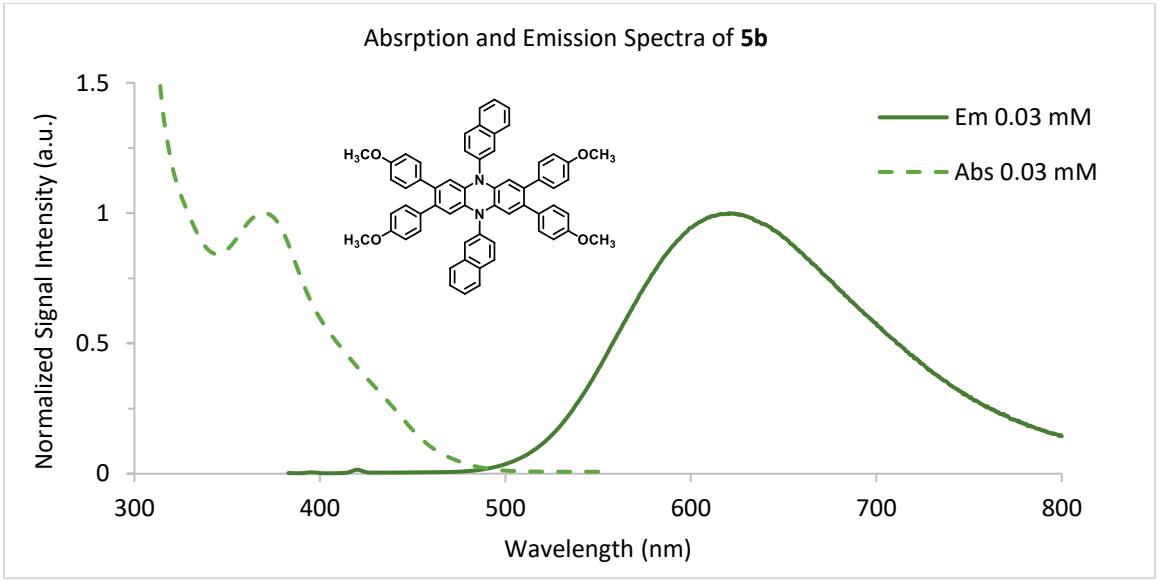

Figure A1.18. Emission spectra of PC **5b** (solid) and absorption spectra of **5b** (dashed) at 0.03 mM in DMAc. Absorption spectra was measured using UV-Vis and emission spectra was measured using fluorimetry. Emission spectra was collected using an excitation wavelength of 371 nm.

Transient Absorption Spectroscopy

Spectral Absorption Data

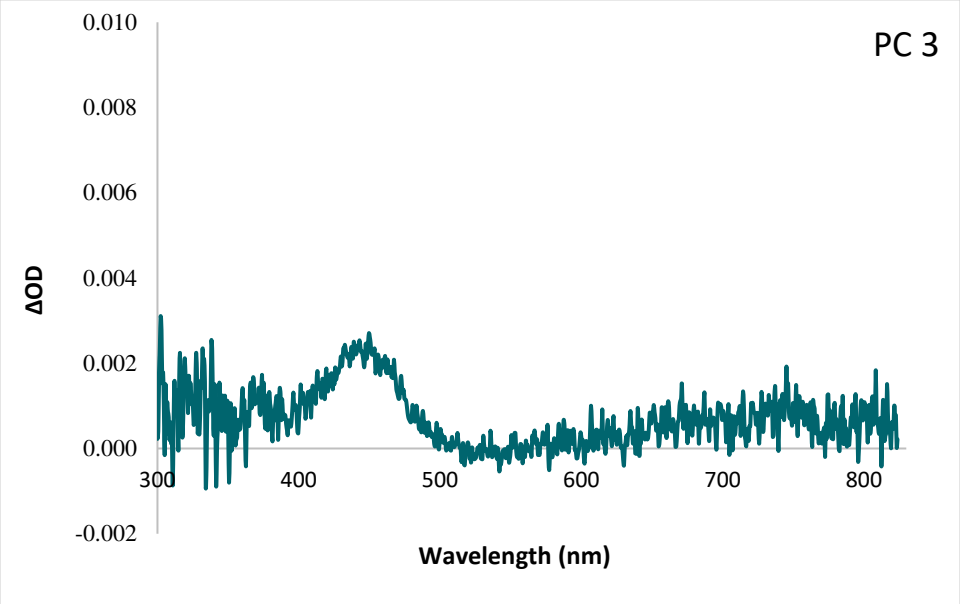

Figure A1.19. Spectral absorption of PC **3** in DMAc at a 200 ns time delay, with no emission subtraction. The excited state absorption (ESA) feature visible at λ = 445 nm was followed by kinetic absorption. The spectral absorption data was offset corrected using kinetic data acquired at λ = 445 nm.

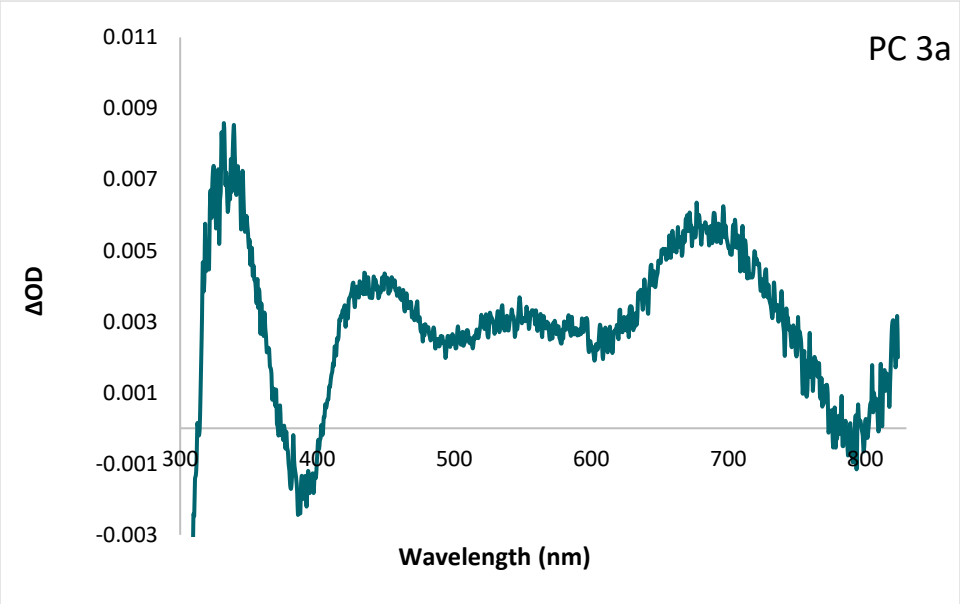

Figure A1.20. Spectral absorption of PC **3a** in DMAc with no time delay (t = 0 ns) and with emission subtraction. The ESA feature visible at λ = 440 nm was followed by kinetic absorption. The spectral absorption data was offset corrected using kinetic data acquired at λ = 440 nm.

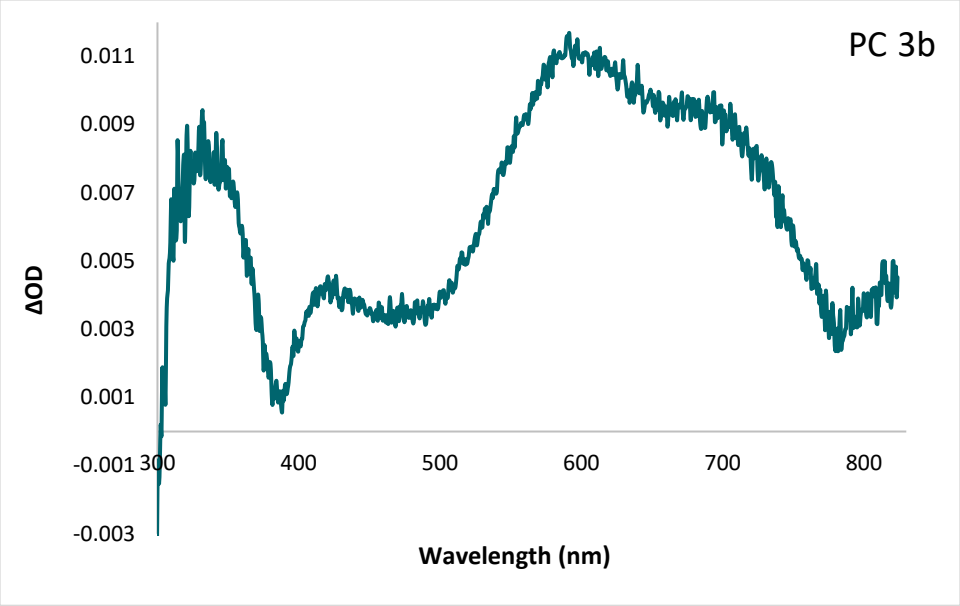

Figure A1.21. Spectral absorption of PC **3b** in DMAc at a 200 ns time delay, with no emission subtraction. The ESA feature visible at λ = 593 nm was followed by kinetic absorption. The spectral absorption data was offset corrected using kinetic data acquired at λ = 593 nm.

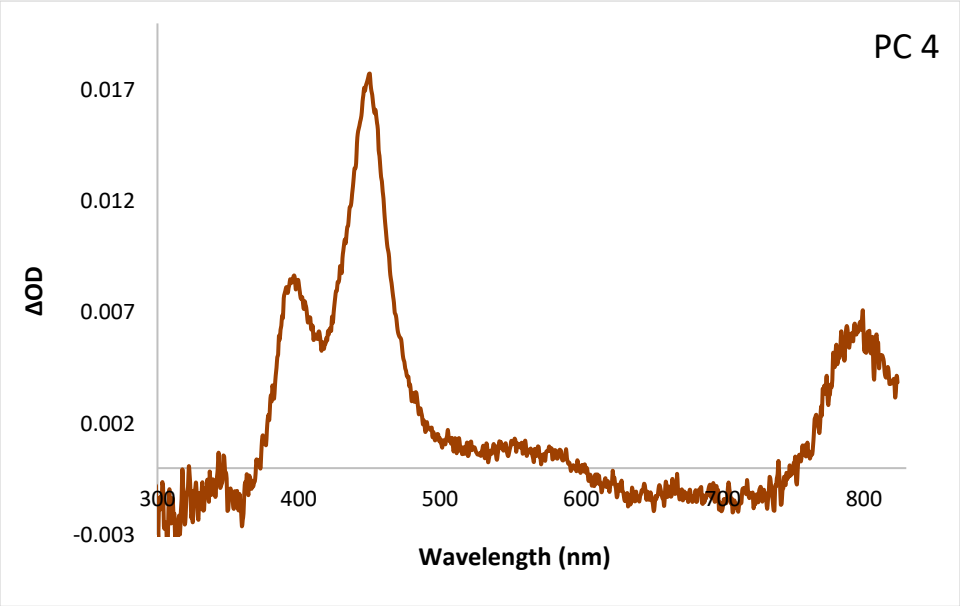

Figure A1.22. Spectral absorption of PC **4** in DMAc at a 400 ns time delay, with no emission subtraction. The ESA feature visible at λ = 450 nm was followed by kinetic absorption. The spectral absorption data was offset corrected using kinetic data acquired at λ = 450 nm.

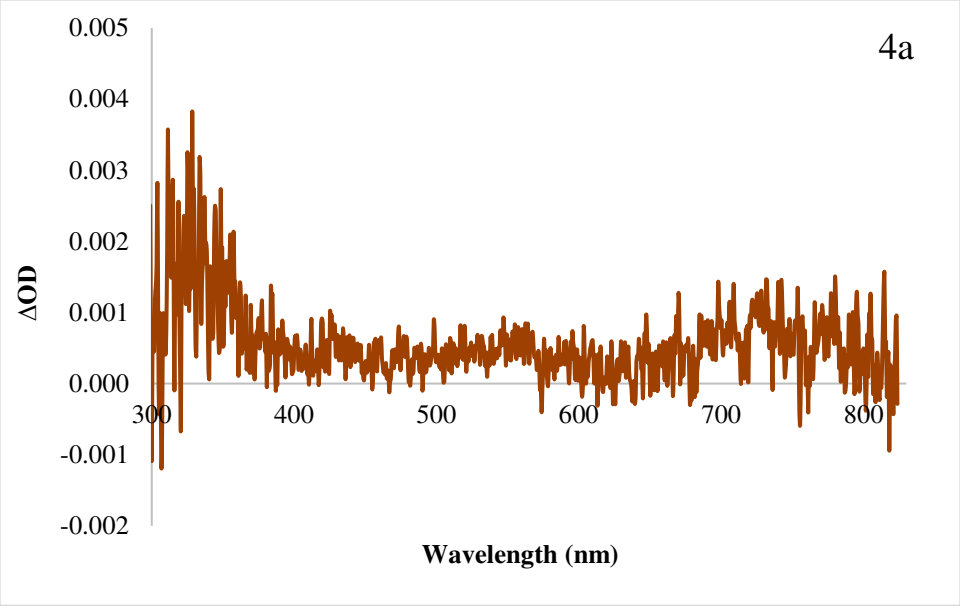

Figure A1.23. Spectral absorption of PC **4a** in DMAc at a 200 ns time delay, with no emission subtraction. There are no distinguishable features that can be followed by kinetic absorption. The spectral absorption data was offset corrected using kinetic data acquired at λ = 450 nm.

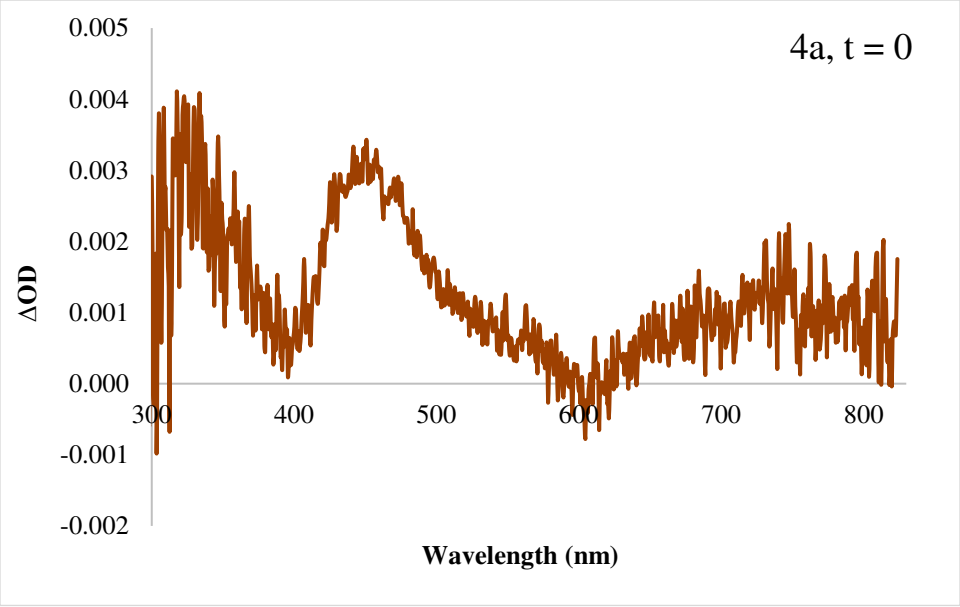

Figure A1.24. Spectral absorption of PC **4a** in DMAc with a 0 ns time delay and with emission subtraction. The ESA feature at λ = 450 nm was followed by kinetic absorption and fit with an exponential tail fit, resulting in determination of τ_{S1}= 14 ns, in agreement with τ_{S1} determined by kinetic emission (13 ns). The spectral absorption data was offset corrected using kinetic data acquired at λ = 450 nm.

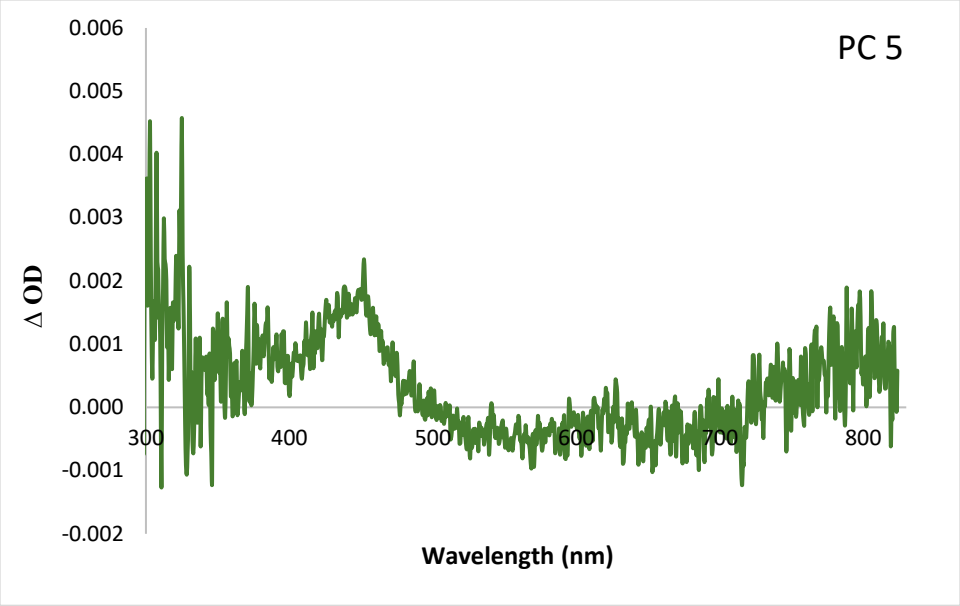

Figure A1.25. Spectral absorption of PC **5** in DMAc at a 200 ns time delay, with no emission subtraction. The ESA feature visible at λ = 450 nm was followed by kinetic absorption. The spectral absorption data was offset corrected using kinetic data acquired at λ = 450 nm.

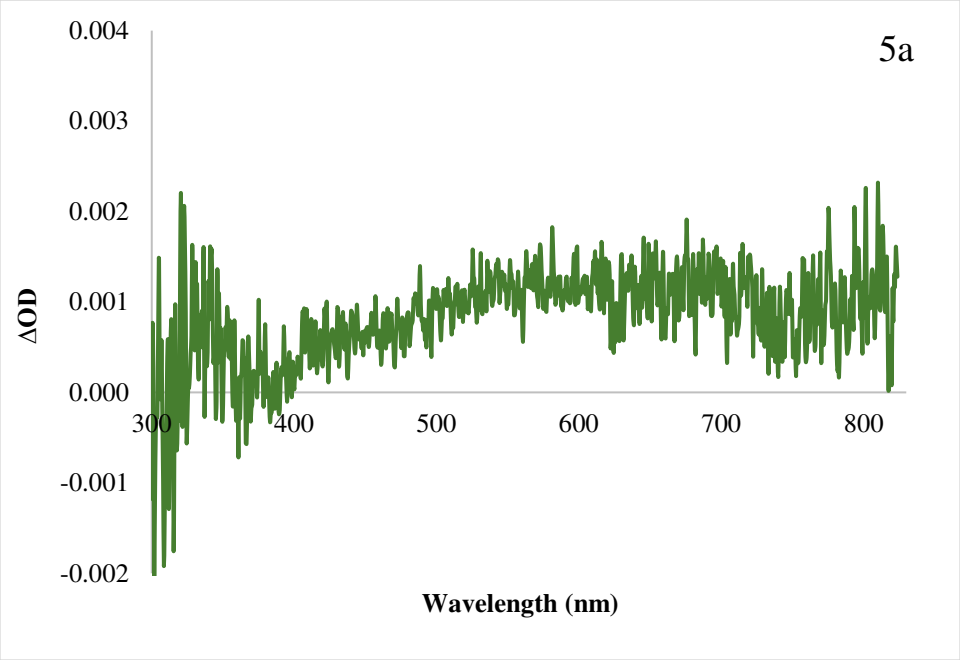

Figure A1.26. Spectral absorption of PC **5a** in DMAc at a 200 ns time delay, with no emission subtraction. There are no features that can be followed by kinetic absorption – the weak ESA at 570 nm was followed but no triplet single was detected. The spectral absorption data was offset corrected using kinetic data acquired at λ = 570 nm.

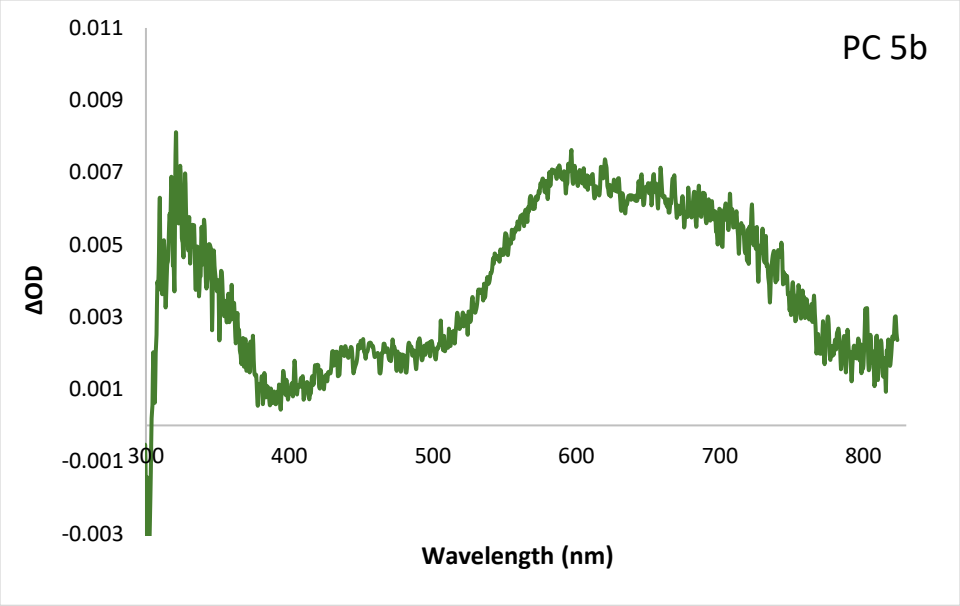

Figure A1.27. Spectral absorption of PC **5b** in DMAc at a 200 ns time delay, with no emission subtraction. The ESA feature visible at λ = 550 nm was followed by kinetic absorption. The spectral absorption data was offset corrected using kinetic data acquired at λ = 550 nm.

Kinetic Emission Data

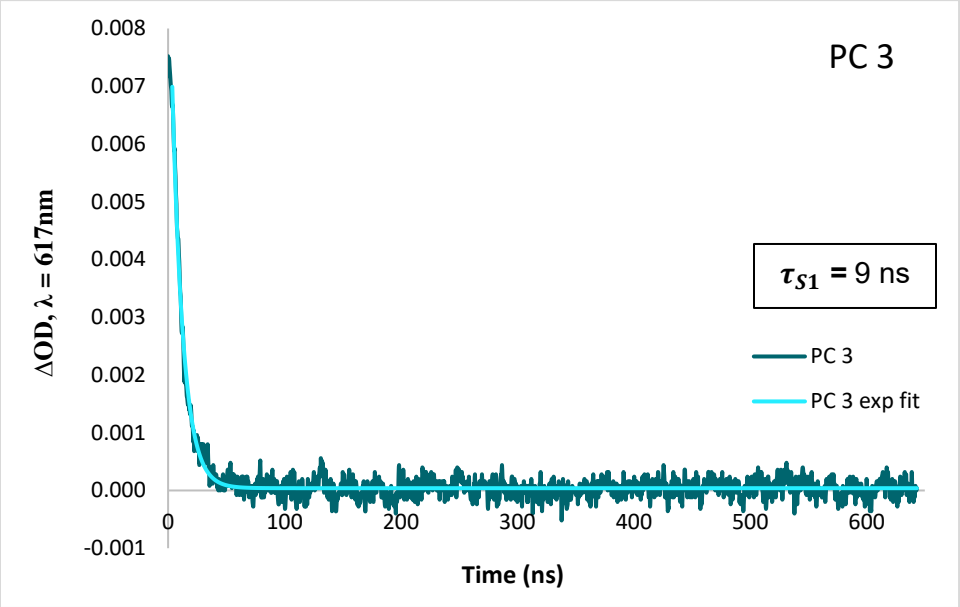

Figure A1.28. Kinetic emission trace for PC **3** in DMAc at 617 nm with an exponential tail fit for determination of τ_{S1}.

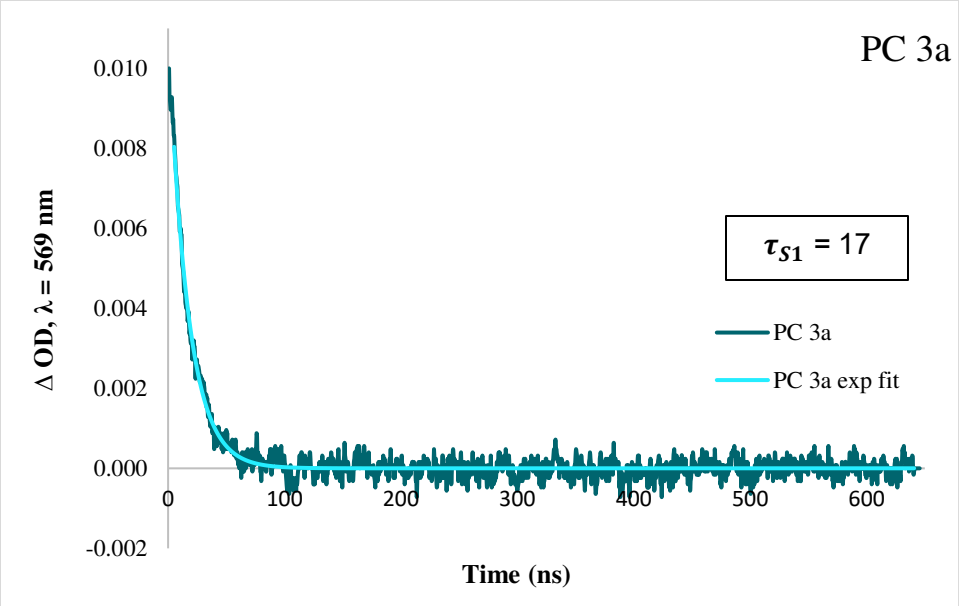

Figure A1.29. Kinetic emission trace for PC **3a** in DMAc at 569 nm with an exponential tail fit for determination of τ_{S1}.

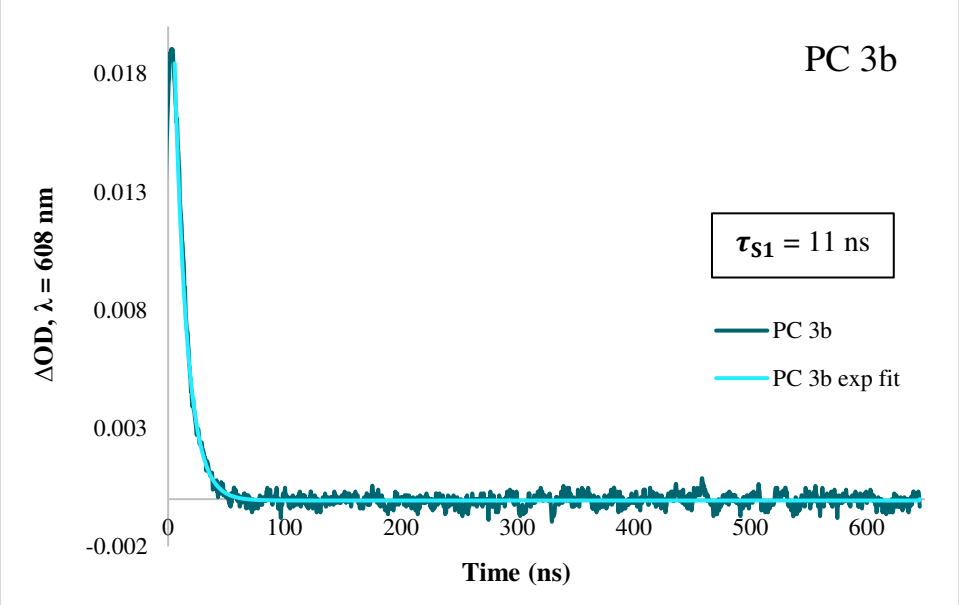

Figure A1.30. Kinetic emission trace for PC **3b** in DMAc at 608 nm with an exponential tail fit for determination of τ_{S1}. Kinetic emission was also measured at 462 nm, but τ_{S1} was found to be less than the 6 ns duration of the instrument laser pulse (below limit of detection).

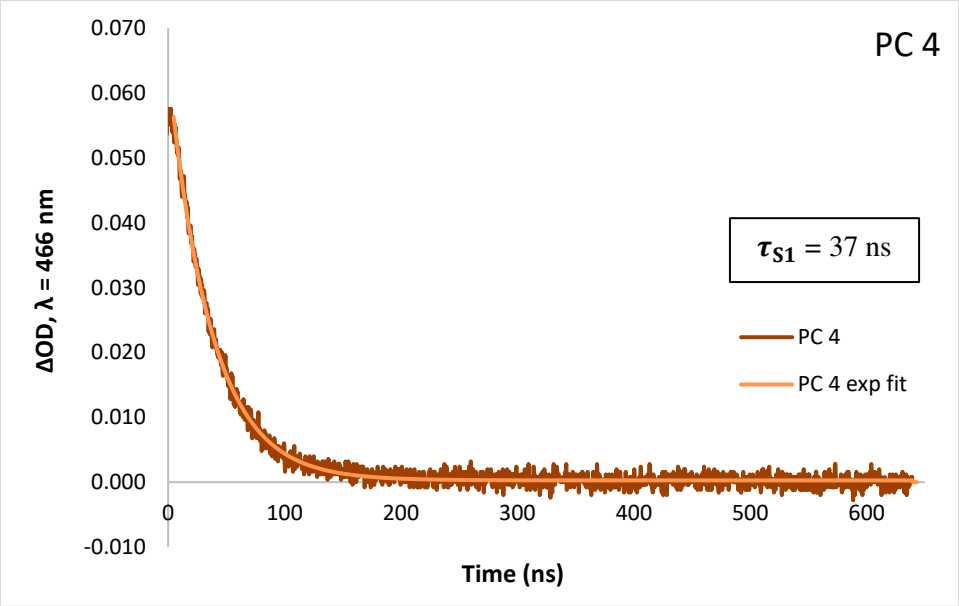

Figure A1.31. Kinetic emission trace for PC **4** in DMAc at 466 nm with an exponential tail fit for determination of τ_{S1}.

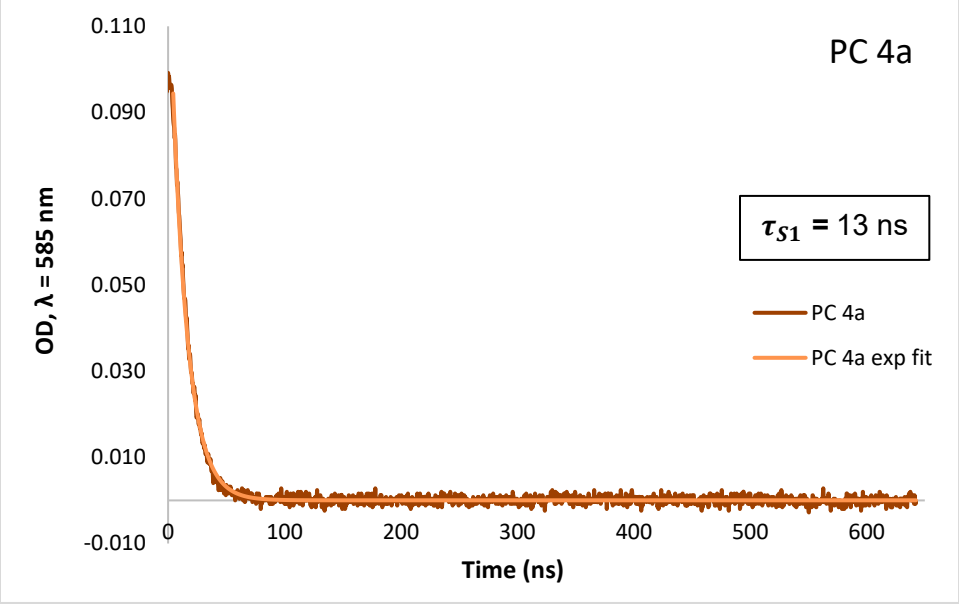

Figure A1.32. Kinetic emission trace for PC **4a** in DMAc at 585 nm with an exponential tail fit for determination of τ_{S1}.

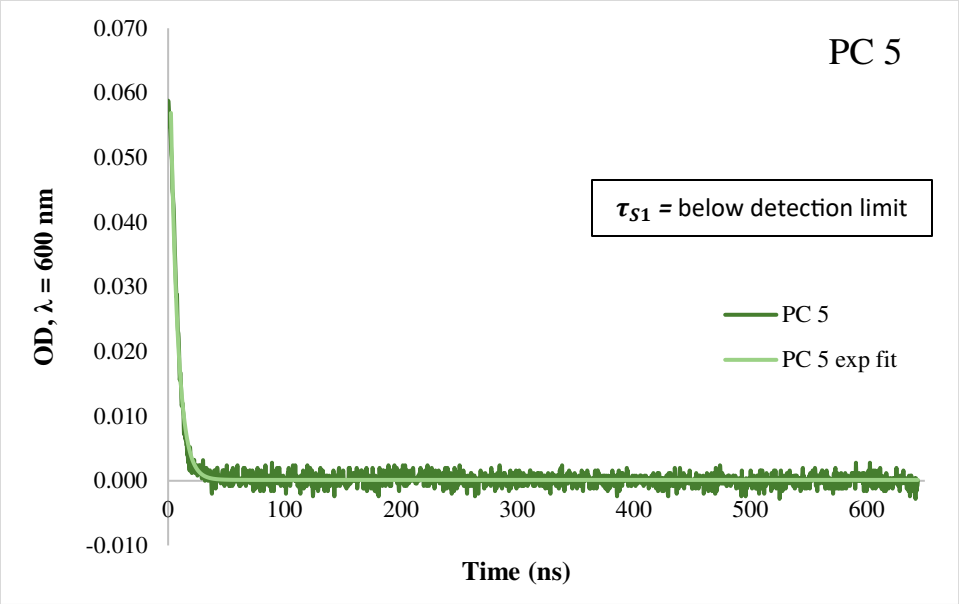

Figure A1.33. Kinetic emission trace for PC **5** in DMAc at 600 nm with an exponential tail fit for determination of τ_{S1} is shown above, however τ_{S1} was not reported because it was found to be less than the 6 ns duration of the instrument laser pulse (below limit of detection).

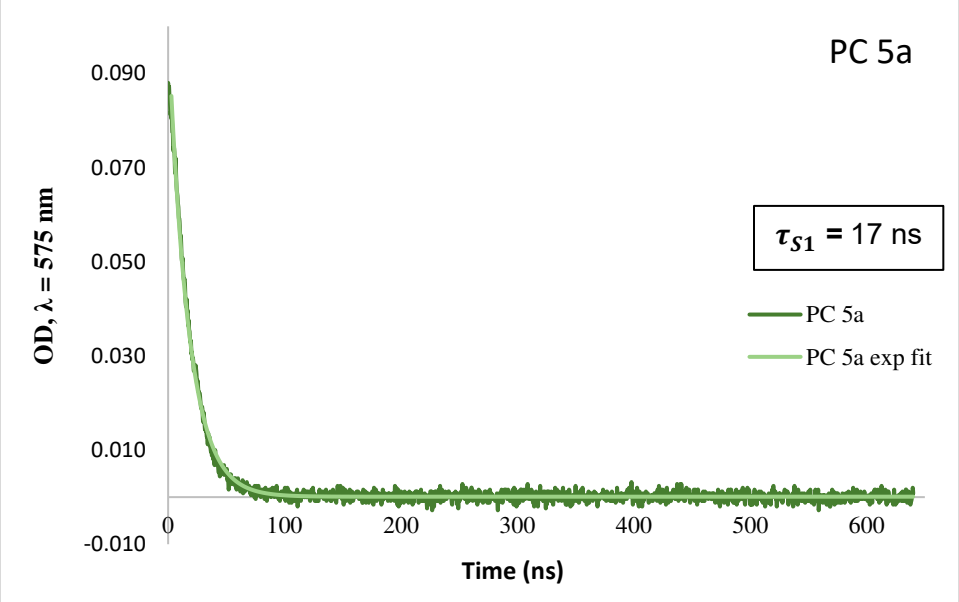

Figure A1.34. Kinetic emission trace for PC 5a in DMAc at 575 nm with an exponential tail fit for determination of τ_{S1}.

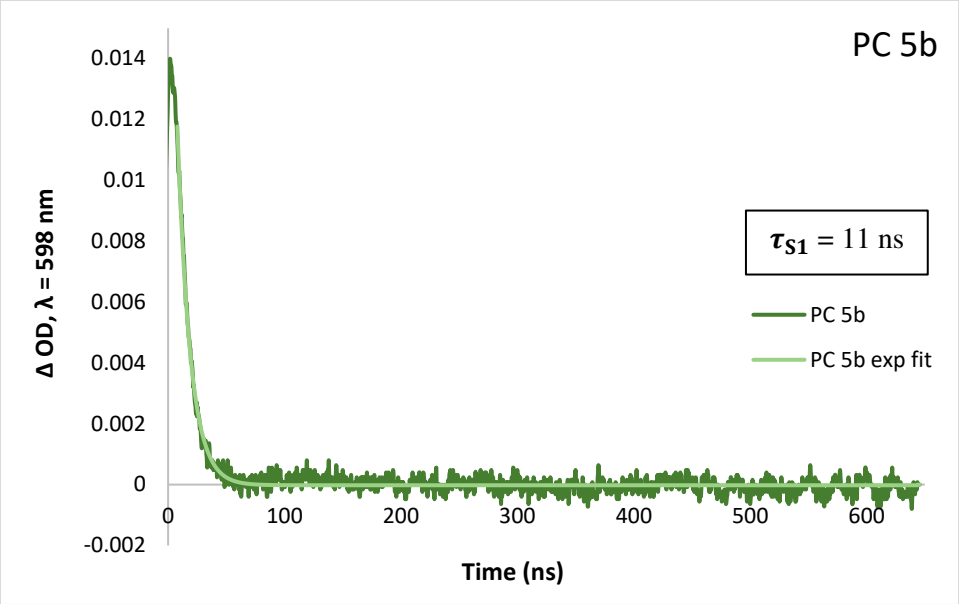

Figure A1.35. Kinetic emission trace for PC **5b** in DMAc at 598 nm with an exponential tail fit for determination of τ_{S1}. Kinetic emission was also measured at 457 nm, but τ_{S1} was found to be less than the 6 ns duration of the instrument laser pulse (below limit of detection).

Kinetic Absorption Data

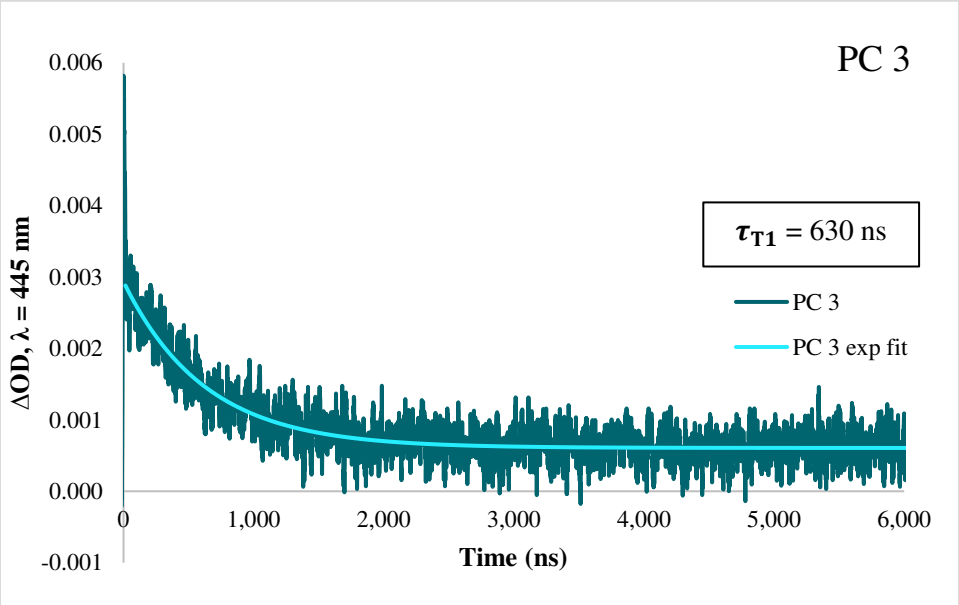

Figure A1.36. Kinetic absorption trace for PC **3** in DMAc at 445 nm with an exponential tail fit for determination of τ_{T1}.

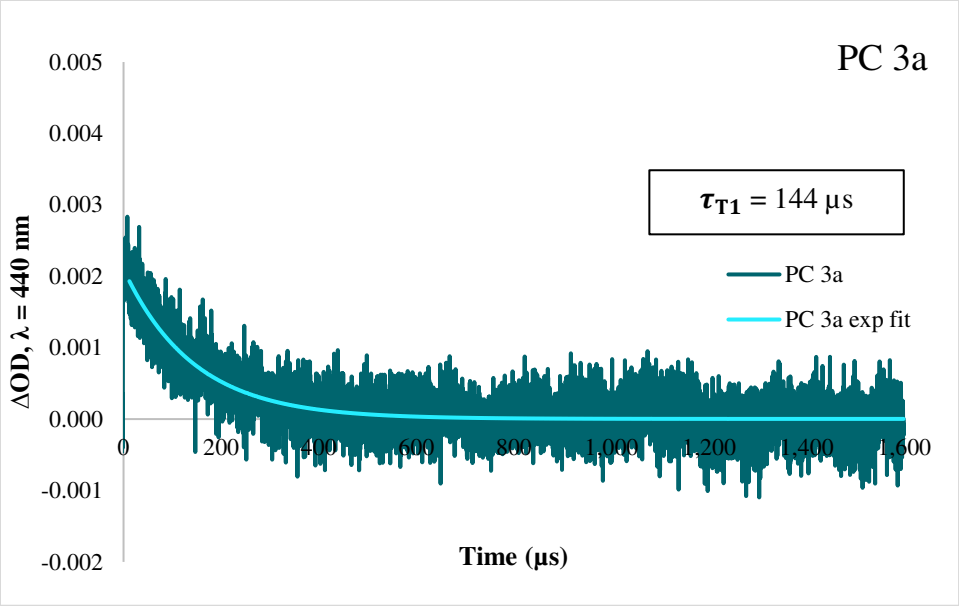

Figure A1.37. Kinetic absorption trace for PC **3a** in DMAc at 440 nm with an exponential tail fit for determination of τ_{T1}.

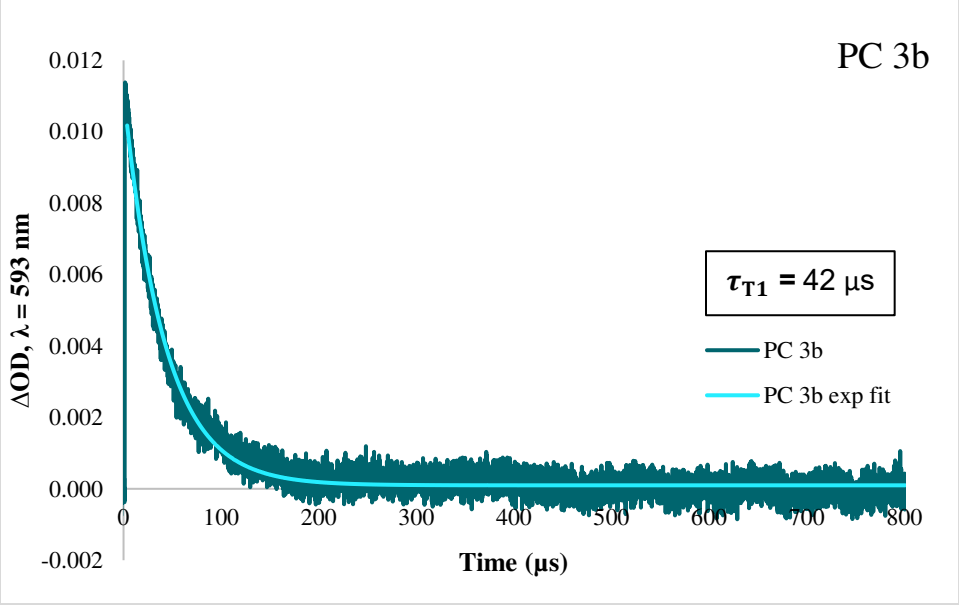

Figure A1.38. Kinetic absorption trace for PC **3b** in DMAc at 593 nm with an exponential tail fit for determination of τ_{T1}.

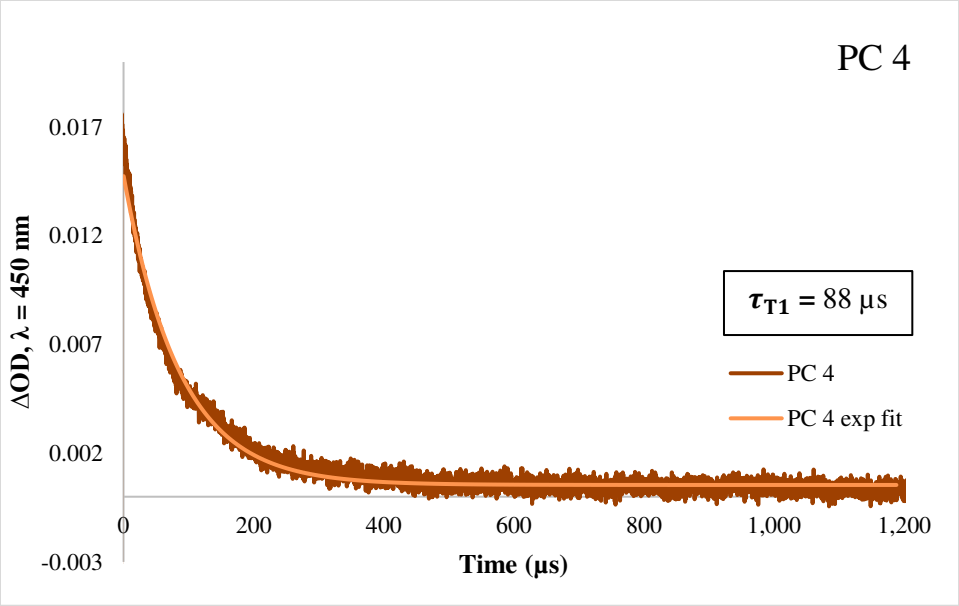

Figure A1.39. Kinetic absorption trace for PC **4** in DMAc at 450 nm with an exponential tail fit for determination of τ_{T1}.

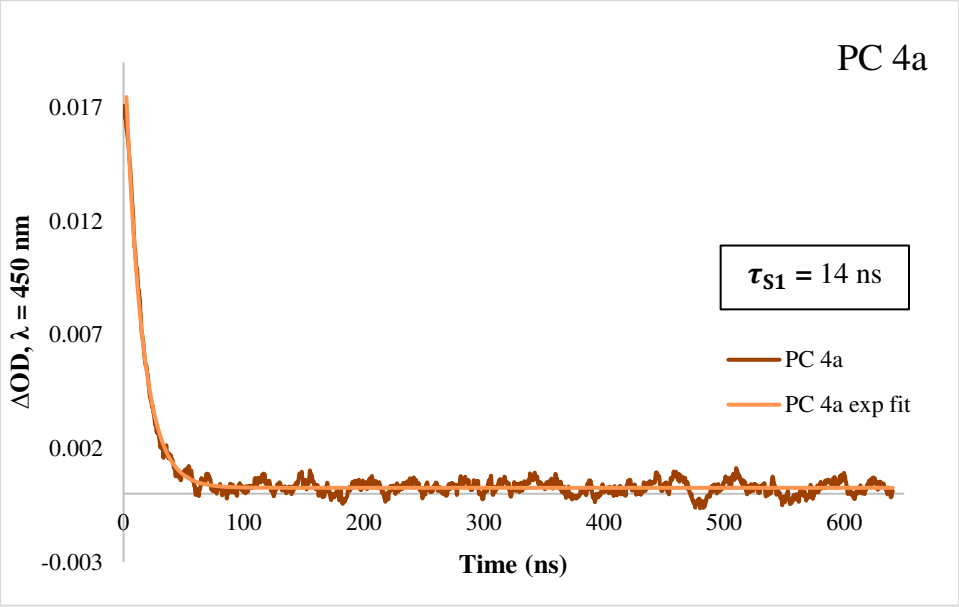

Figure A1.40. Kinetic absorption trace for PC **4a** in DMAc at 450 nm with an exponential tail fit for determination of τ_{S1}. By kinetic absorption τ_{S1}= 14 ns, in good agreement with τ_{S1} determined by kinetic emission (τ_{S1}=13 ns).

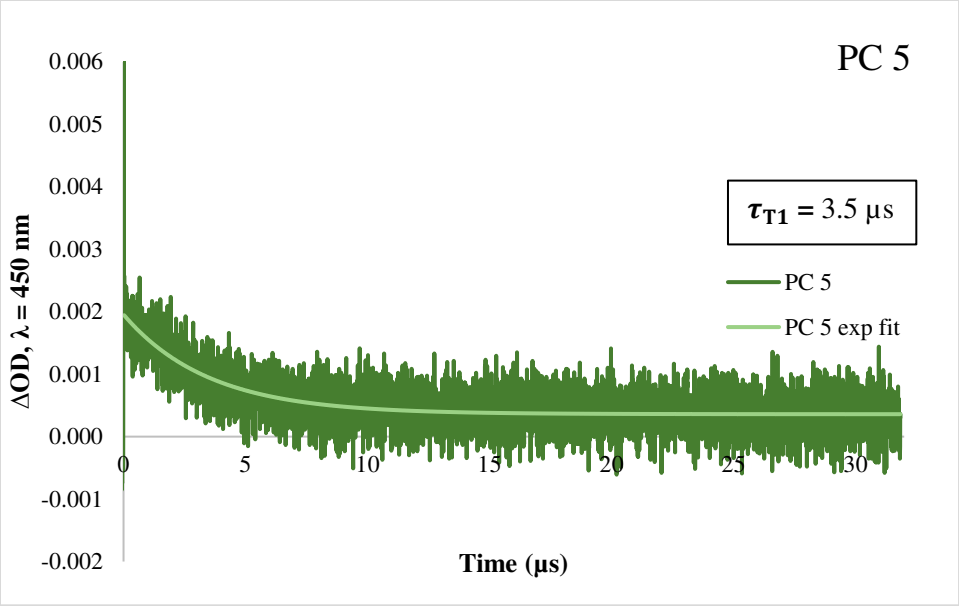

Figure A1.41. Kinetic absorption trace for PC **5** in DMAc at 450 nm with an exponential tail fit for determination of τ_{T1}.

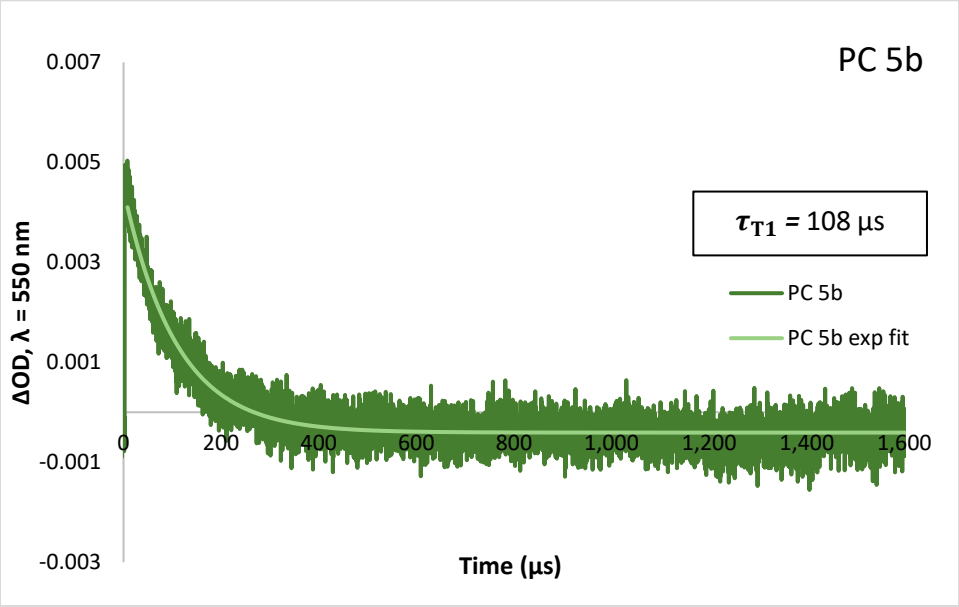

Figure A1.42. Kinetic absorption trace for PC **5b** in DMAc at 550 nm with an exponential tail fit for determination of τ_{T1}.

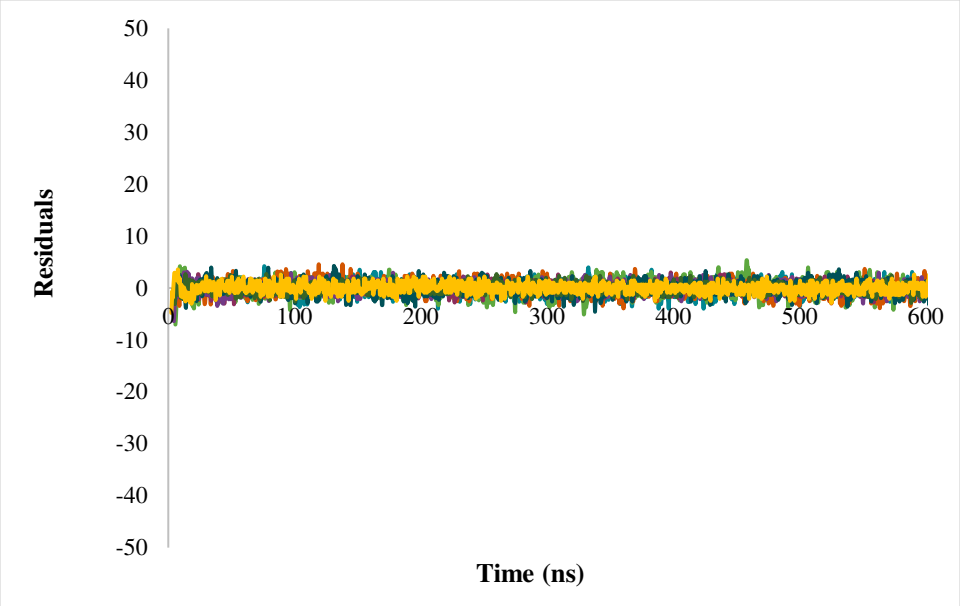

Figure A1.43. Overlayed residuals for exponential tail fits of the kinetic emission traces included in this work.

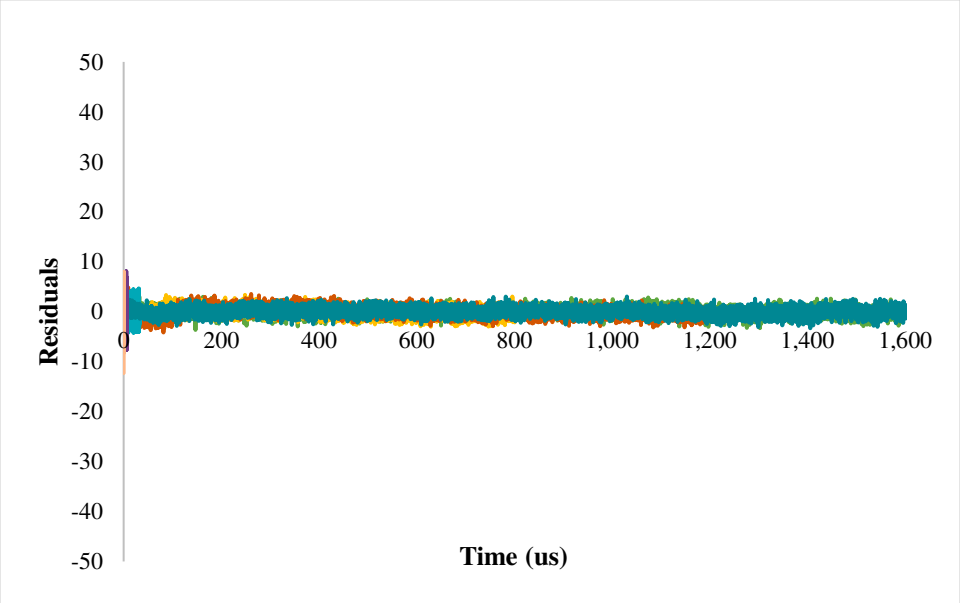

Figure A1.44. Overlayed residuals for exponential tail fits of the kinetic absorption traces included in this work.

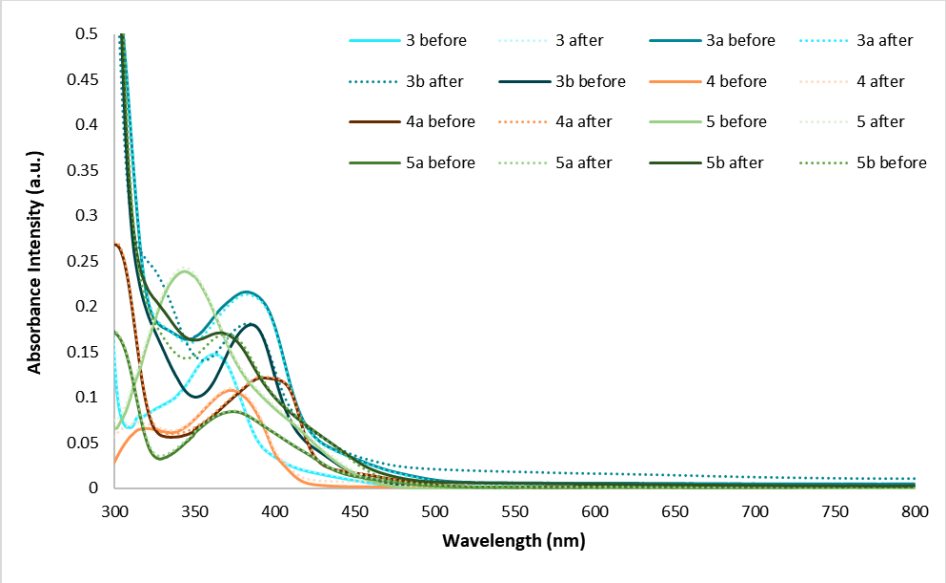

Figure A1.45. Overlaid UV-vis spectra of PC solutions used for TA spectroscopy, taken before and after TA spectroscopy was performed to monitor if PC degradation occurred. The PC solutions analyzed in this work did not show evidence of degradation after TA, indicated by no significant observable change in the UV-vis spectra before and after TA spectroscopy was performed.

Solvatochromism

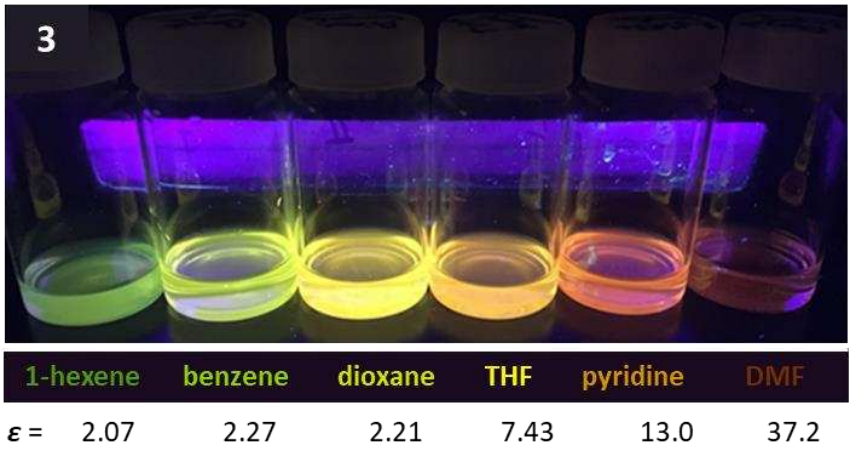

Figure A1.46. Previously reported photograph of PC **3** dissolved in solvents of increasing polarity (from left to right) while under irradiation with 365 nm light. (*J. Am. Chem. Soc.* **2017**, *139*, 348−355)

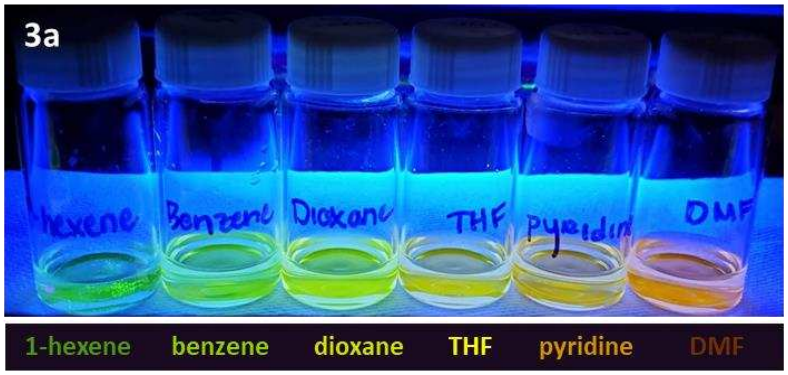

Figure A1.47. Photograph of PC **3a** dissolved in solvents of increasing polarity (from left to right) while under irradiation with 365 nm light.

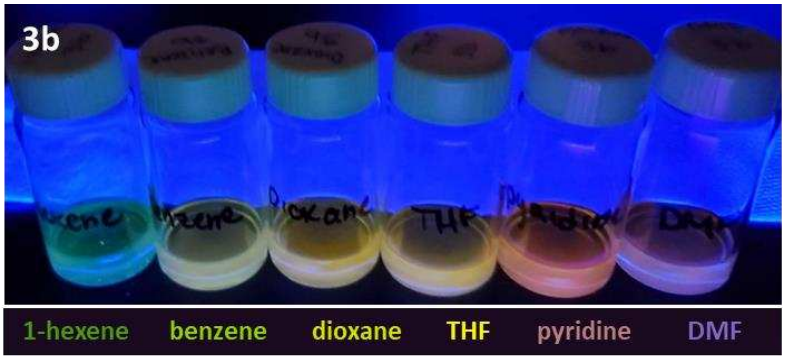

Figure A1.48. Photograph of PC **3b** dissolved in solvents of increasing polarity (from left to right) while under irradiation with 365 nm light.

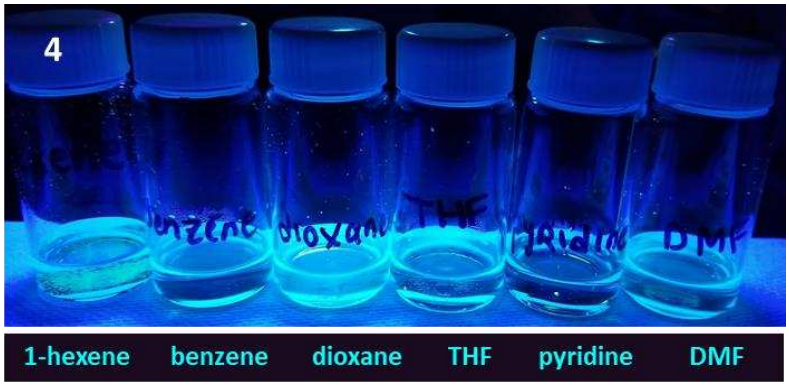

Figure A1.49. Photograph of PC **4** dissolved in solvents of increasing polarity (from left to right) while under irradiation with 365 nm light.

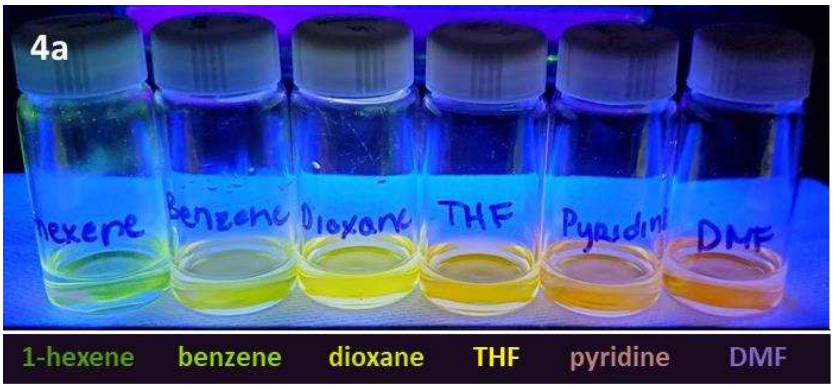

Figure A1.50. Photograph of PC **4** dissolved in solvents of increasing polarity (from left to right) while under irradiation with 365 nm light.

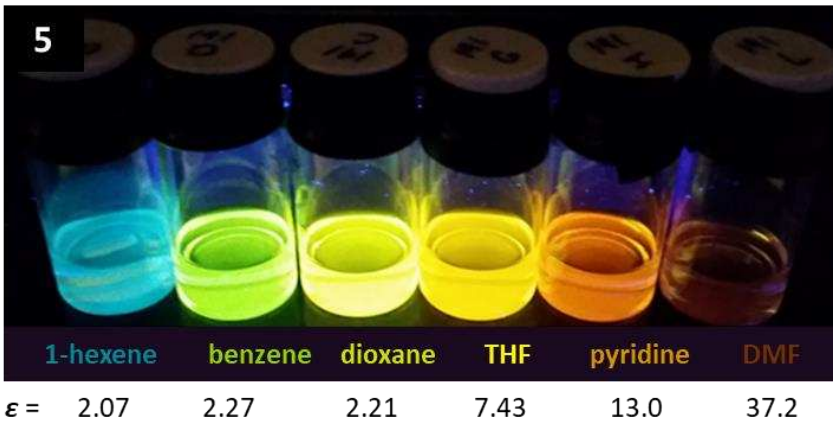

Figure A1.51. Previously reported Photograph of PC **5** dissolved in solvents of increasing polarity (from left to right) while under irradiation with 365 nm light. (*J. Am. Chem. Soc.* **2017**, *139*, 348−355)

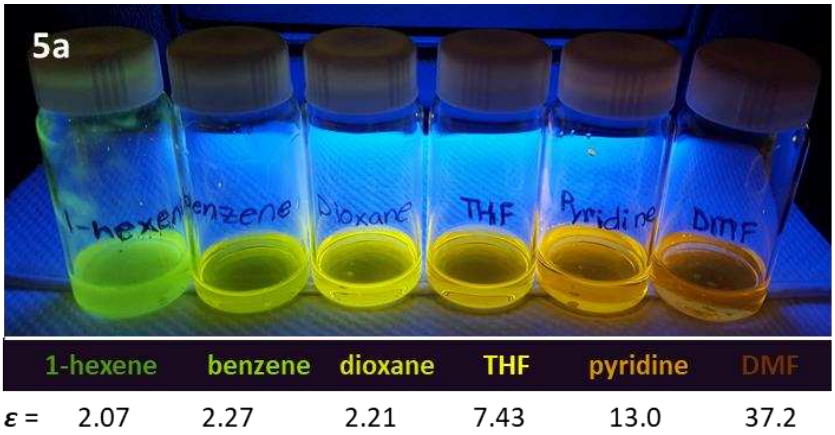

Figure A1.52. Photograph of PC **5a** dissolved in solvents of increasing polarity (from left to right) while under irradiation with 365 nm light.

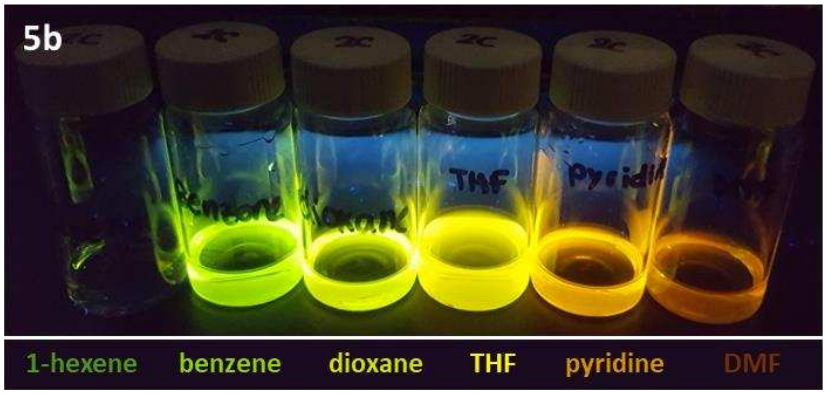

Figure A1.53. Photograph of PC **5b** dissolved in solvents of increasing polarity (from left to right) while under irradiation with 365 nm light.

Cyclic Voltammetry

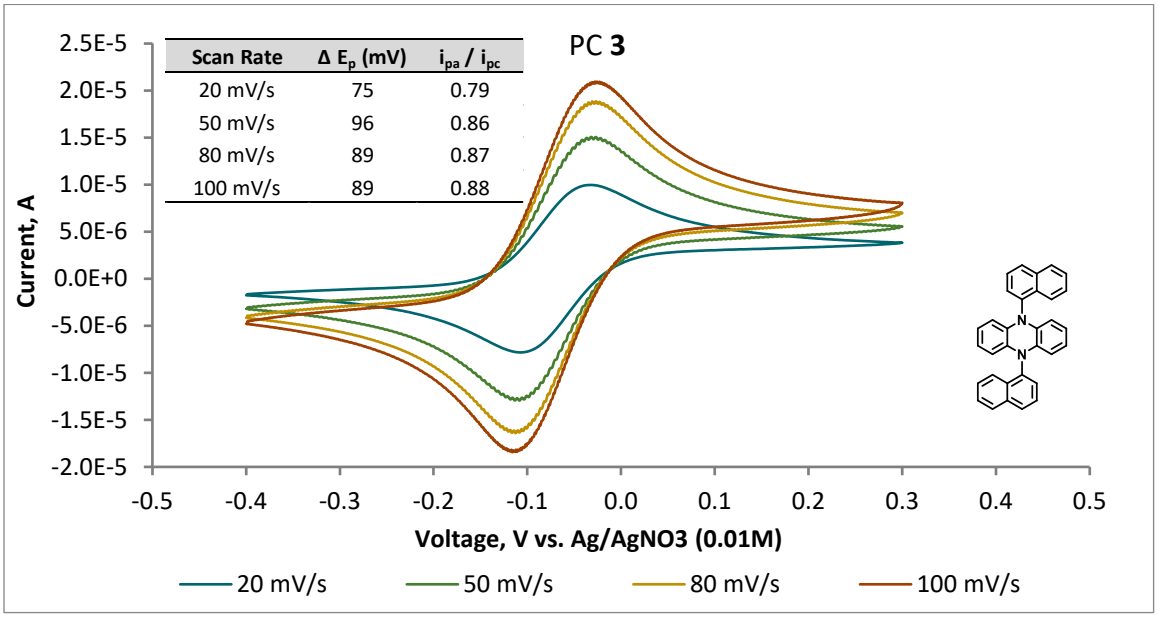

Figure A1.54. Cyclic voltammogram of PC **3** in DMAc at 20 mV/s, 50 mV/s, 80 mV/s, and 100 mV/s scan rates. Inserted into the graph is a chart showing the ratios of peak anodic current to peak cathodic current (i_{pa}/i_{pc}) and the difference between peak anodic and peak cathodic current (ΔE_p) at each scan rate.

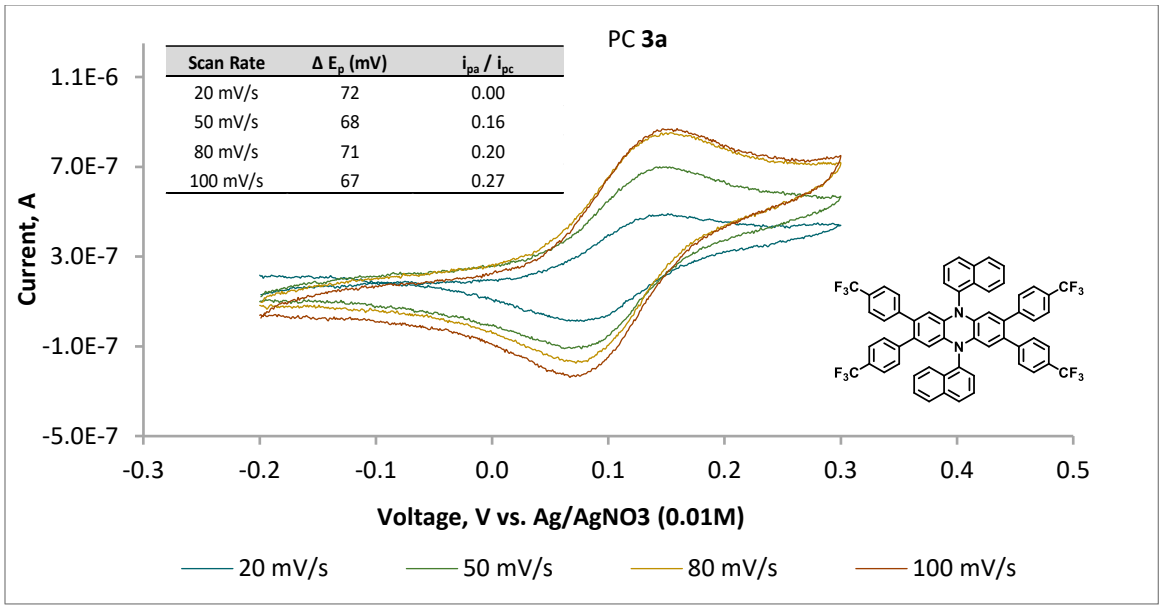

Figure A1.55. Cyclic voltammogram of PC **3a** in DMAc at 20 mV/s, 50 mV/s, 80 mV/s, and 100 mV/s scan rates. Inserted into the graph is a chart showing the ratios of peak anodic current to peak cathodic current (i_{pa}/i_{pc}) and the difference between peak anodic and peak cathodic current (ΔE_p) at each scan rate.

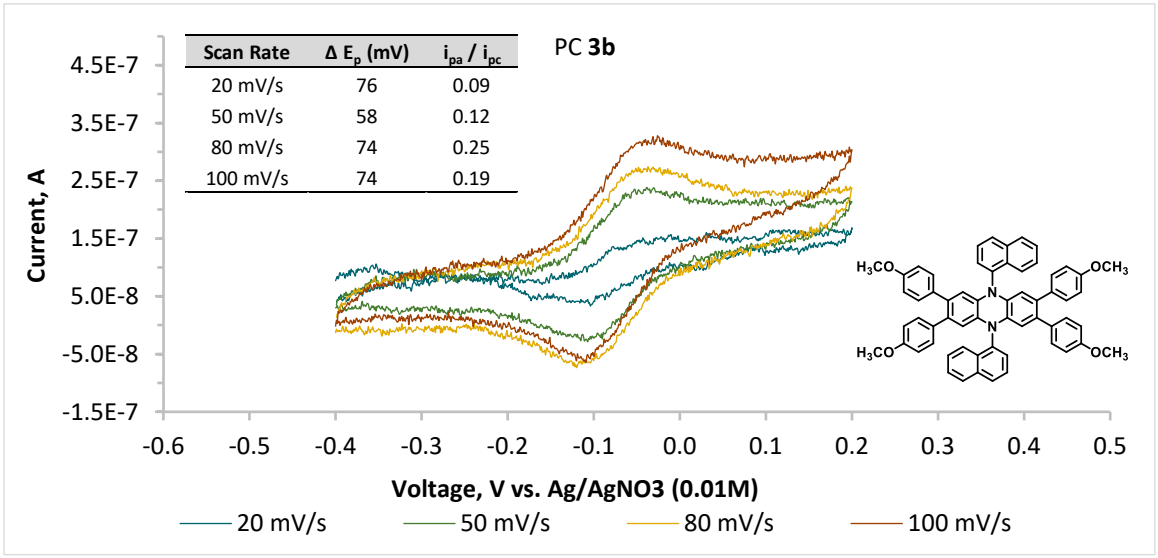

Figure A1.56. Cyclic voltammogram of PC **3b** in DMAc at 20 mV/s, 50 mV/s, 80 mV/s, and 100 mV/s scan rates. Inserted into the graph is a chart showing the ratios of peak anodic current to peak cathodic current (i_{pa}/i_{pc}) and the difference between peak anodic and peak cathodic current (ΔE_p) at each scan rate.

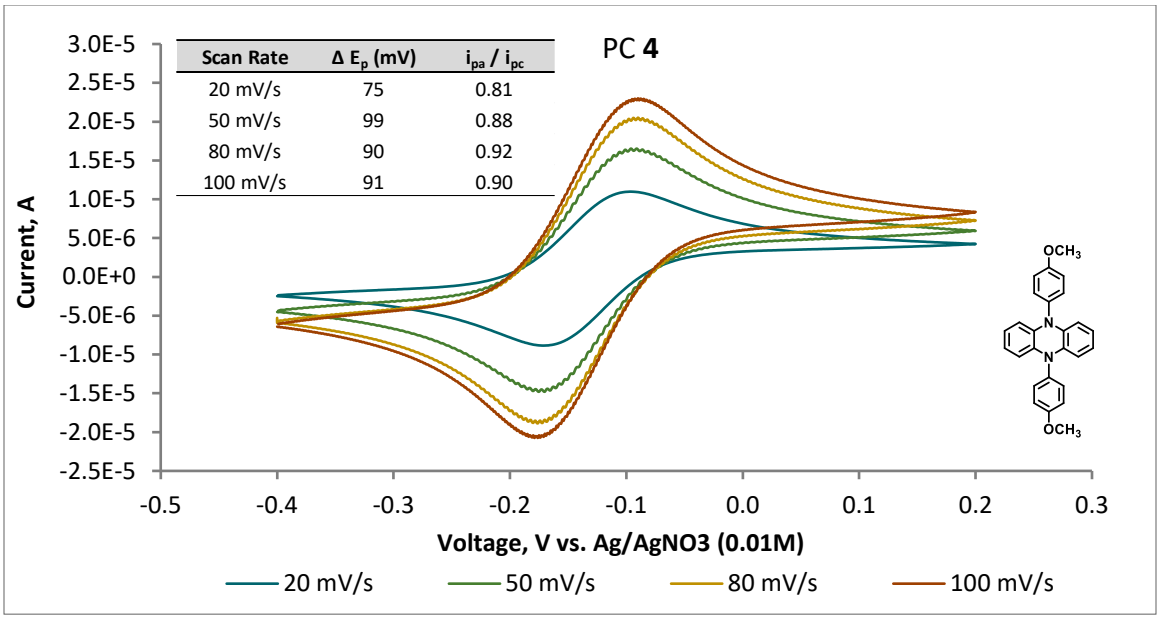

Figure A1.57. Cyclic voltammogram of PC **4** in DMAc at 20 mV/s, 50 mV/s, 80 mV/s, and 100 mV/s scan rates. Inserted into the graph is a chart showing the ratios of peak anodic current to peak cathodic current (i_{pa}/i_{pc}) and the difference between peak anodic and peak cathodic current (ΔE_p) at each scan rate.

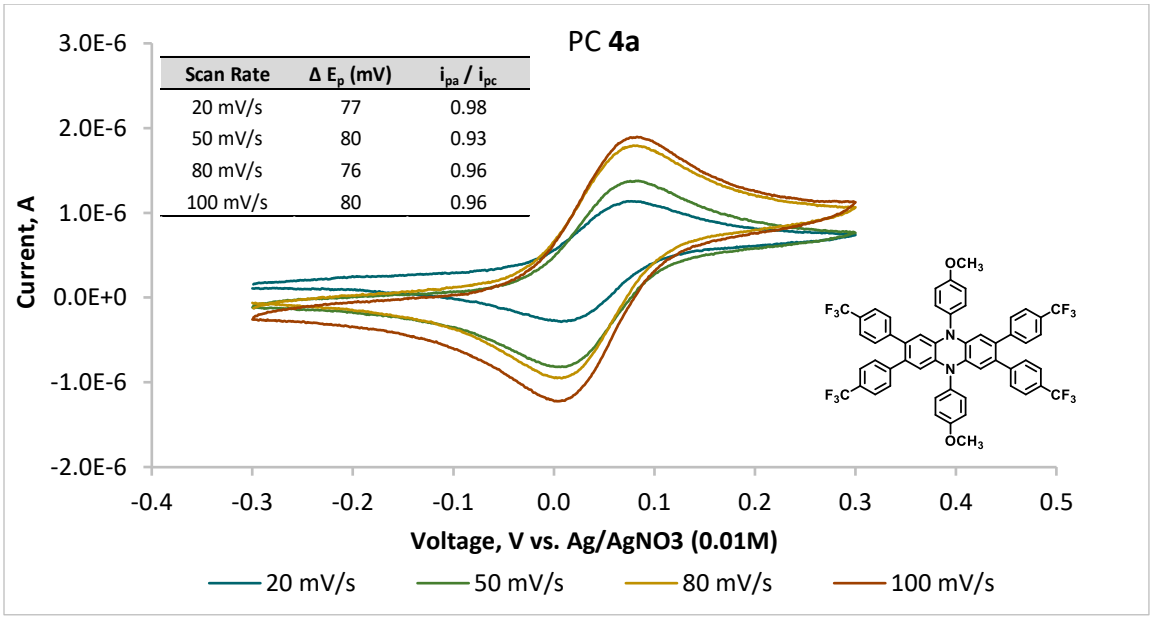

Figure A1.58. Cyclic voltammogram of PC **4a** in DMAc at 20 mV/s, 50 mV/s, 80 mV/s, and 100 mV/s scan rates. Inserted into the graph is a chart showing the ratios of peak anodic current to peak cathodic current (i_{pa}/i_{pc}) and the difference between peak anodic and peak cathodic current (ΔE_p) at each scan rate.

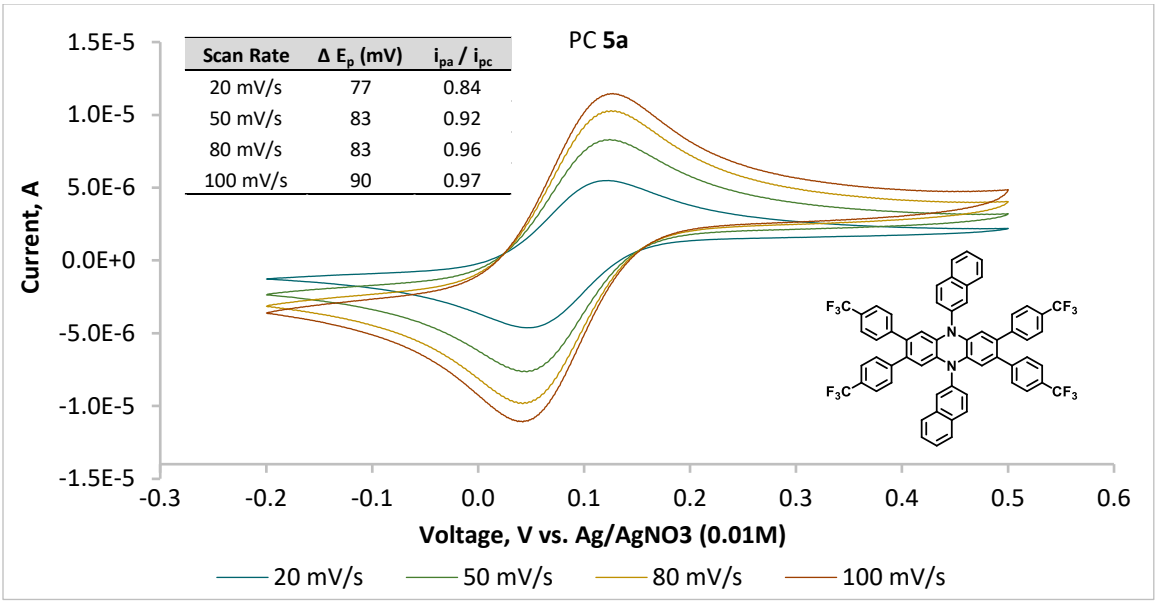

Figure A1.59. Cyclic voltammogram of PC **5a** in DMAc at 20 mV/s, 50 mV/s, 80 mV/s, and 100 mV/s scan rates. Inserted into the graph is a chart showing the ratios of peak anodic current to peak cathodic current (i_{pa}/i_{pc}) and the difference between peak anodic and peak cathodic current (ΔE_p) at each scan rate.

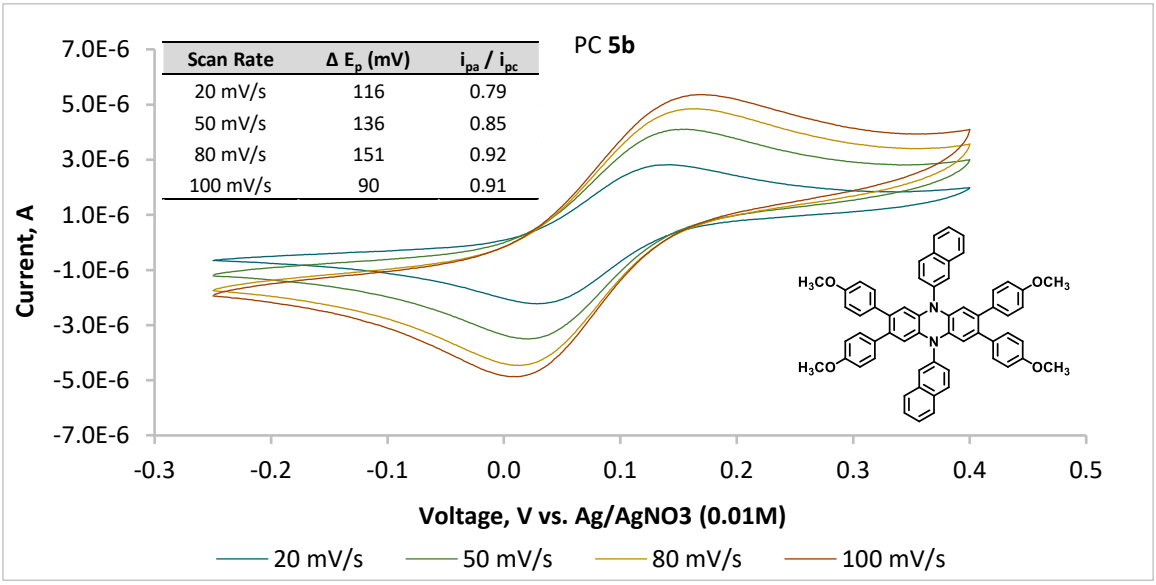

Figure A1.60. Cyclic voltammogram of PC **5b** in DMAc at 20 mV/s, 50 mV/s, 80 mV/s, and 100 mV/s scan rates. Inserted into the graph is a chart showing the ratios of peak anodic current to peak cathodic current (i_{pa}/i_{pc}) and the difference between peak anodic and peak cathodic current (ΔE_p) at each scan rate.

COMPUTATIONAL MODELING OF PCs

Excited State Calculations (TD-DFT)

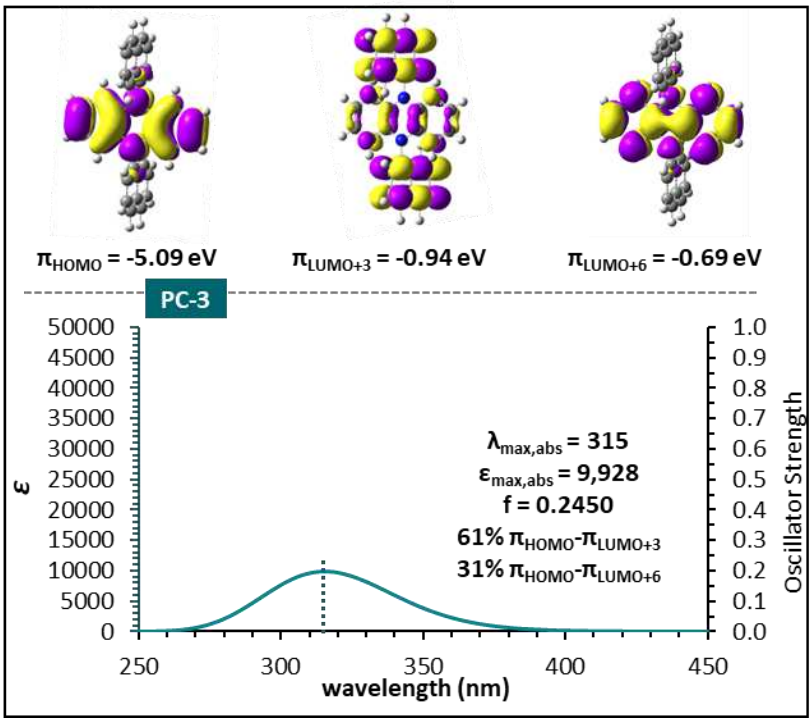

Figure A1.61: Computationally modeled molecular orbitals predicted to be involved in absorption transitions for PC **3** detailed below (top). Computationally predicted UV−vis spectrum of PCs **3** along with theoretically assigned percentage contributions (>15%) of various orbitals to the predicted absorption peaks. $\lambda_{max,abs}$ is the absorption maximum wavelength and is reported in units of nm, $\varepsilon_{max,abs}$ is the predicted molar extinction coefficient at $\lambda_{max,abs}$ and is reported in units of M^{-1} cm^{-1}, and *f* is the predicted oscillator strength; all of these values were predicted at the TD-DFT CAM-B3LYP/6-31+G(d,p)/CPCM-DMA level of theory (bottom).

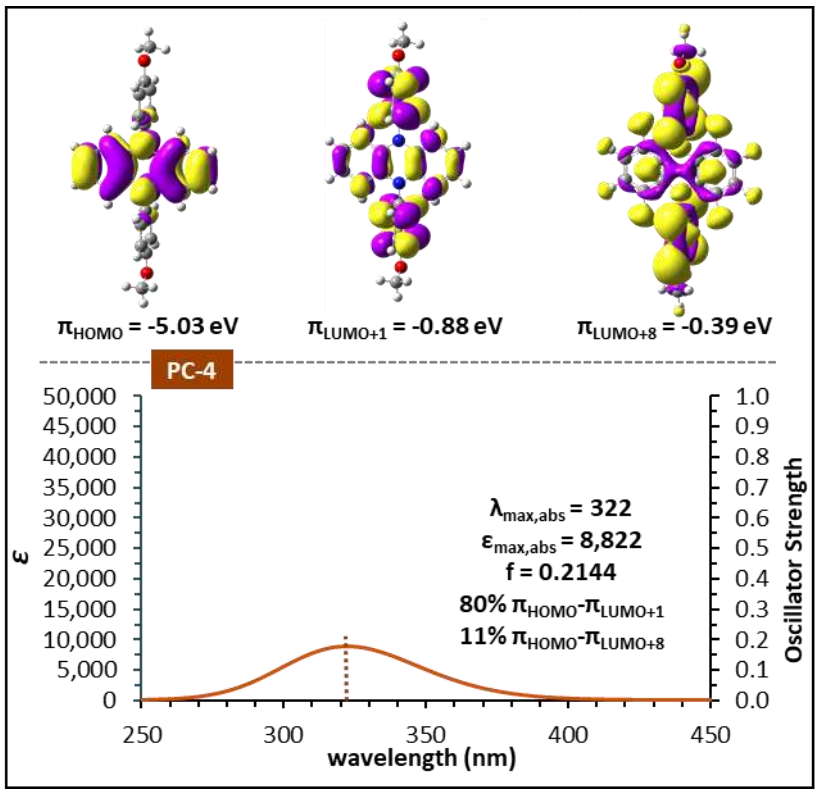

Figure A1.62: Computationally modeled molecular orbitals predicted to be involved in absorption transitions for PC **4** detailed below (top). Computationally predicted UV−vis spectrum of PCs **4** along with theoretically assigned percentage contributions (>15%) of various orbitals to the predicted absorption peaks. $\lambda_{max,abs}$ is the absorption maximum wavelength and is reported in units of nm, $\varepsilon_{max,abs}$ is the predicted molar extinction coefficient at $\lambda_{max,abs}$ and is reported in units of M^{-1} cm^{-1}, and f is the predicted oscillator strength; all of these values were predicted at the TD-DFT CAM-B3LYP/6-31+G(d,p)/CPCM-DMA level of theory (bottom).

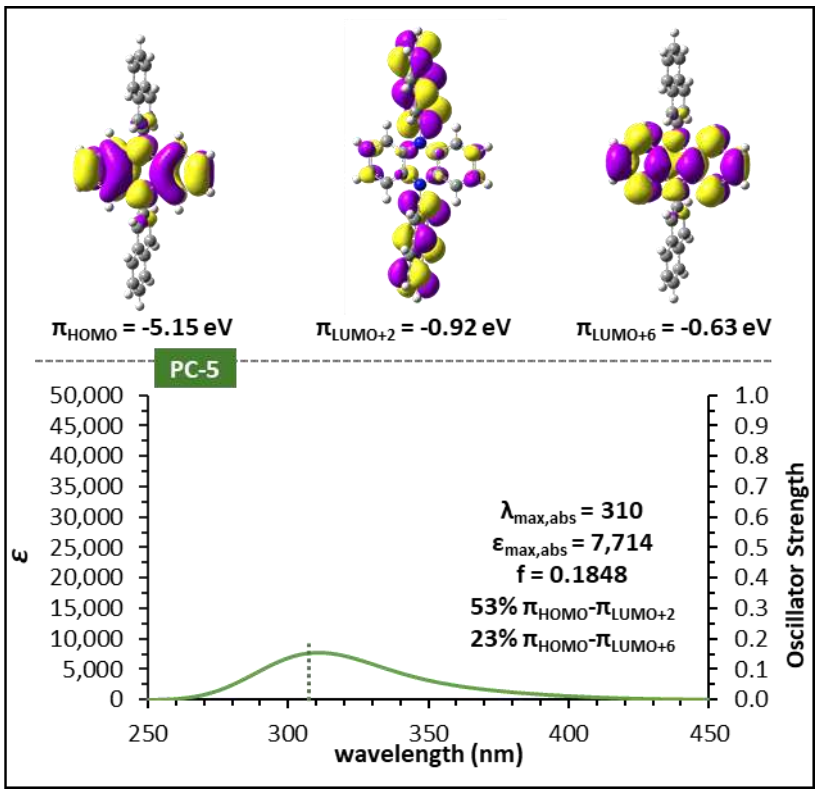

Figure A1.63: Computationally modeled molecular orbitals predicted to be involved in absorption transitions for PC **5** detailed below (top). Computationally predicted UV−vis spectrum of PCs **5** along with theoretically assigned percentage contributions (>15%) of various orbitals to the predicted absorption peaks. $\lambda_{max,abs}$ is the absorption maximum wavelength and is reported in units of nm, $\varepsilon_{max,abs}$ is the predicted molar extinction coefficient at $\lambda_{max,abs}$ and is reported in units of M^{-1} cm^{-1}, and f is the predicted oscillator strength; all of these values were predicted at the TD-DFT CAM-B3LYP/6-31+G(d,p)/CPCM-DMA level of theory (bottom).

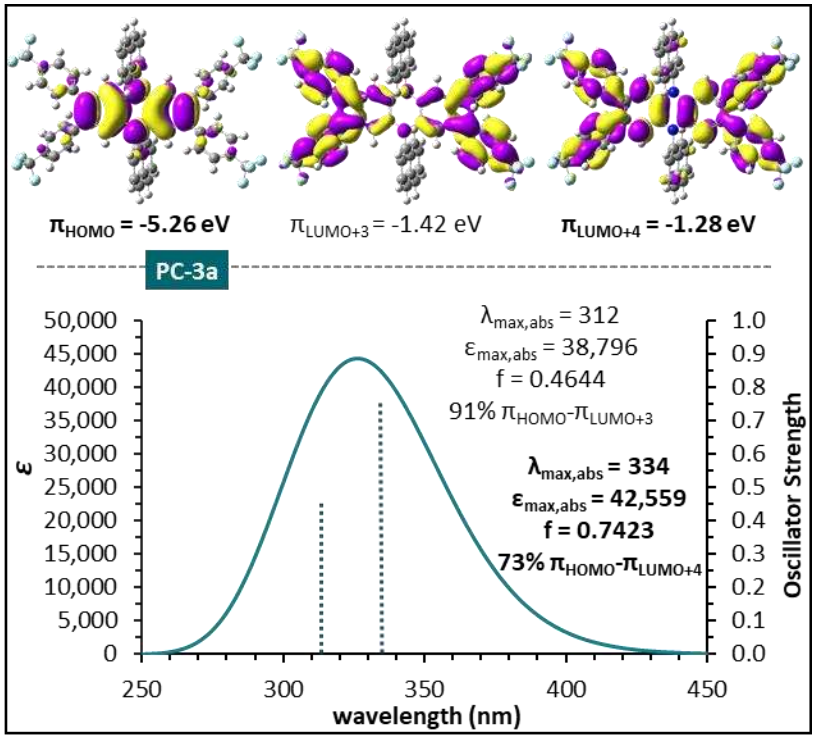

Figure A1.64: Computationally modeled molecular orbitals predicted to be involved in absorption transitions for PC **3a** detailed below (top). Computationally predicted UV−vis spectrum of PCs **3a** along with theoretically assigned percentage contributions (>15%) of various orbitals to the predicted absorption peaks. $\lambda_{max,abs}$ is the predicted absorption maximum wavelength and is reported in units of nm, $\varepsilon_{max,abs}$ is the predicted molar extinction coefficient at the predicted $\lambda_{max,abs}$ and is reported in units of M^{-1} cm^{-1}, and f is the predicted oscillator strength; all of these values were predicted at the TD-DFT CAM-B3LYP/6-31+G(d,p)/CPCM-DMA level of theory (bottom).

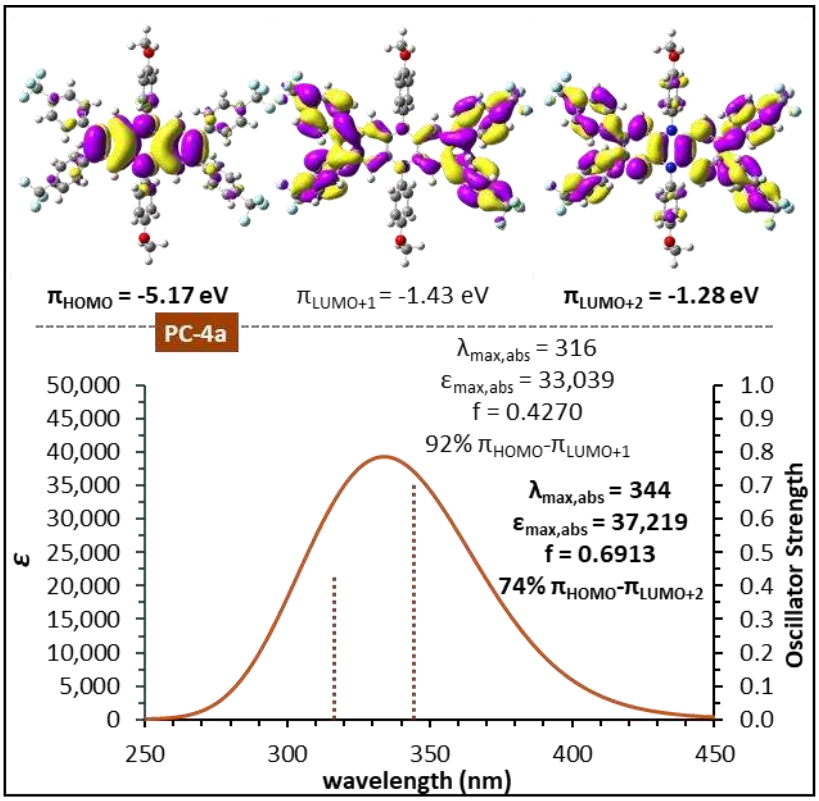

Figure A1.65: Computationally modeled molecular orbitals predicted to be involved in absorption transitions for PC **4a** detailed below (top). Computationally predicted UV−vis spectrum of PCs **4a** along with theoretically assigned percentage contributions (>15%) of various orbitals to the predicted absorption peaks. $\lambda_{max,abs}$ is the predicted absorption maximum wavelength and is reported in units of nm, $\varepsilon_{max,abs}$ is the predicted molar extinction coefficient at the predicted $\lambda_{max,abs}$ and is reported in units of M^{-1} cm^{-1}, and *f* is the predicted oscillator strength; all of these values were predicted at the TD-DFT CAM-B3LYP/6-31+G(d,p)/CPCM-DMA level of theory (bottom).

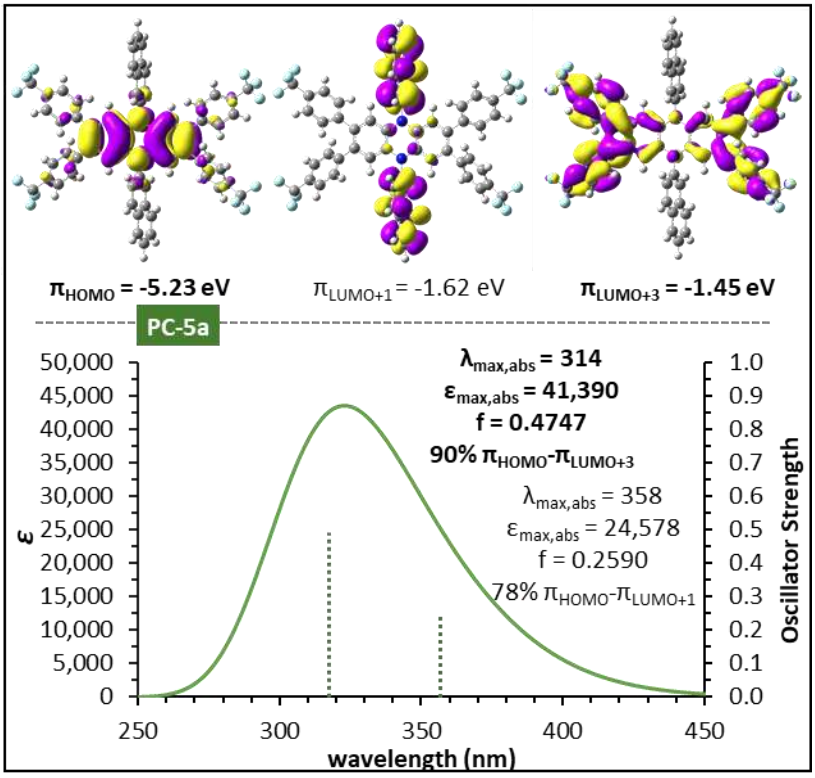

Figure A1.66: Computationally modeled molecular orbitals predicted to be involved in absorption transitions for PC **5a** detailed below (top). Computationally predicted UV−vis spectrum of PCs **5a** along with theoretically assigned percentage contributions (>15%) of various orbitals to the predicted absorption peaks. $\lambda_{max,abs}$ is the predicted absorption maximum wavelength and is reported in units of nm, $\varepsilon_{max,abs}$ is the predicted molar extinction coefficient at the predicted $\lambda_{max,abs}$ and is reported in units of M^{-1} cm^{-1}, and f is the predicted oscillator strength; all of these values were predicted at the TD-DFT CAM-B3LYP/6-31+G(d,p)/CPCM-DMA level of theory (bottom).

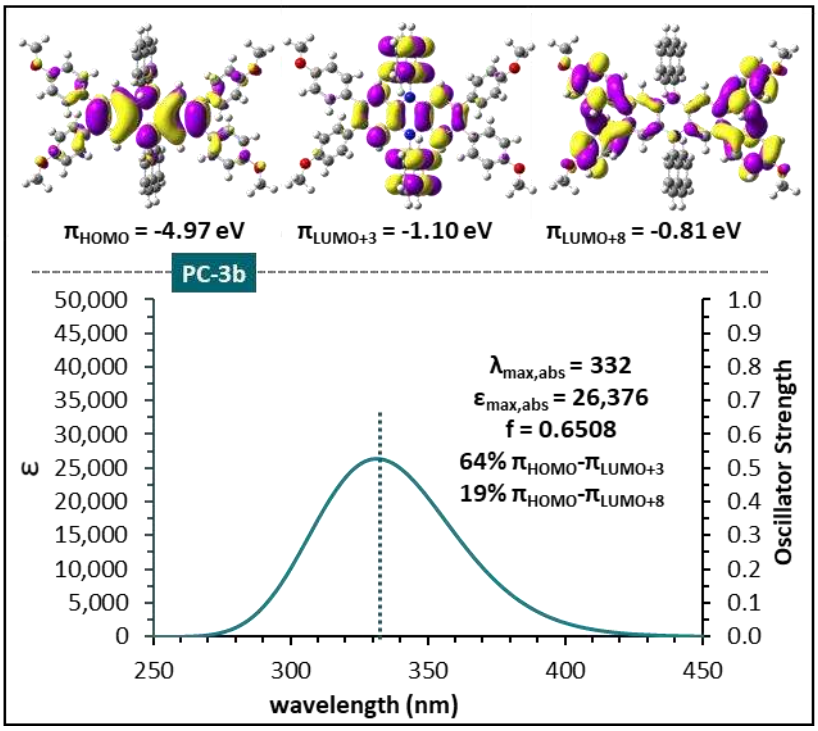

Figure A1.67: Computationally modeled molecular orbitals predicted to be involved in absorption transitions for PC **3b** detailed below (top). Computationally predicted UV−vis spectrum of PCs **3b** along with theoretically assigned percentage contributions (>15%) of various orbitals to the predicted absorption peaks. $\lambda_{max,abs}$ is the predicted absorption maximum wavelength and is reported in units of nm, $\varepsilon_{max,abs}$ is the predicted molar extinction coefficient at the predicted $\lambda_{max,abs}$ and is reported in units of M^{-1} cm^{-1}, and f is the predicted oscillator strength; all of these values were predicted at the TD-DFT CAM-B3LYP/6-31+G(d,p)/CPCM-DMA level of theory (bottom).

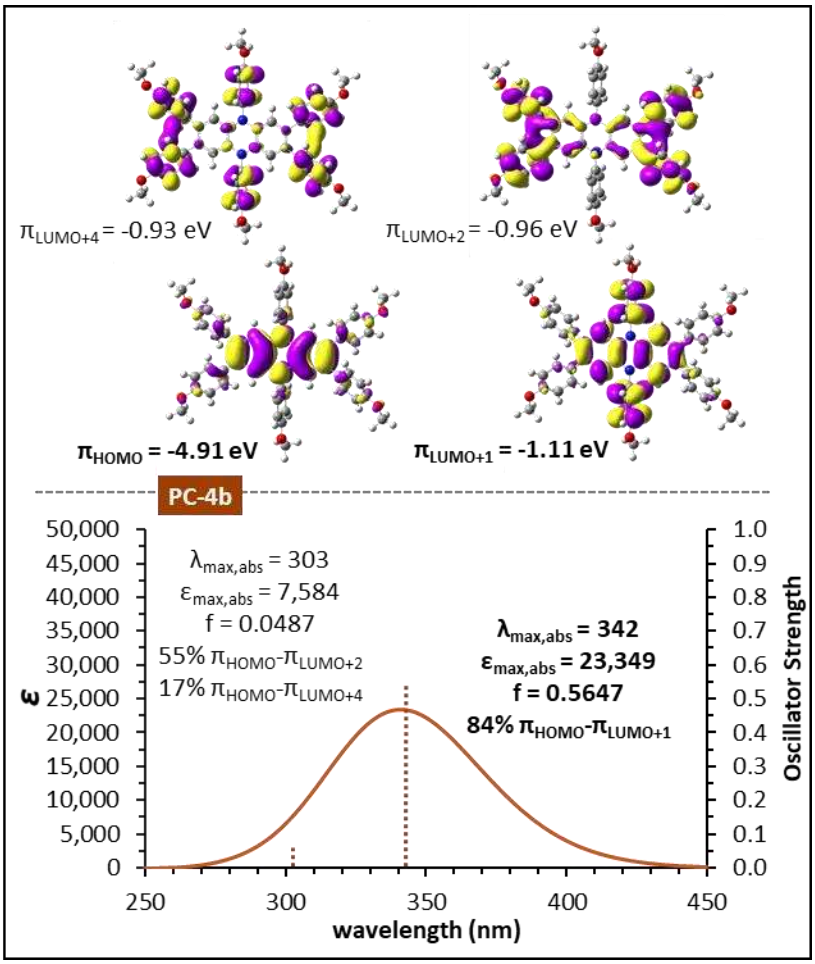

Figure A1.68: Computationally modeled molecular orbitals predicted to be involved in absorption transitions for PC **4b** detailed below (top). Computationally predicted UV−vis spectrum of PCs **4b** along with theoretically assigned percentage contributions (>15%) of various orbitals to the predicted absorption peaks. $\lambda_{max,abs}$ is the predicted absorption maximum wavelength and is reported in units of nm, $\varepsilon_{max,abs}$ is the predicted molar extinction coefficient at the predicted $\lambda_{max,abs}$ and is reported in units of M^{-1} cm^{-1}, and f is the predicted oscillator strength; all of these values were predicted at the TD-DFT CAM-B3LYP/6-31+G(d,p)/CPCM-DMA level of theory (bottom).

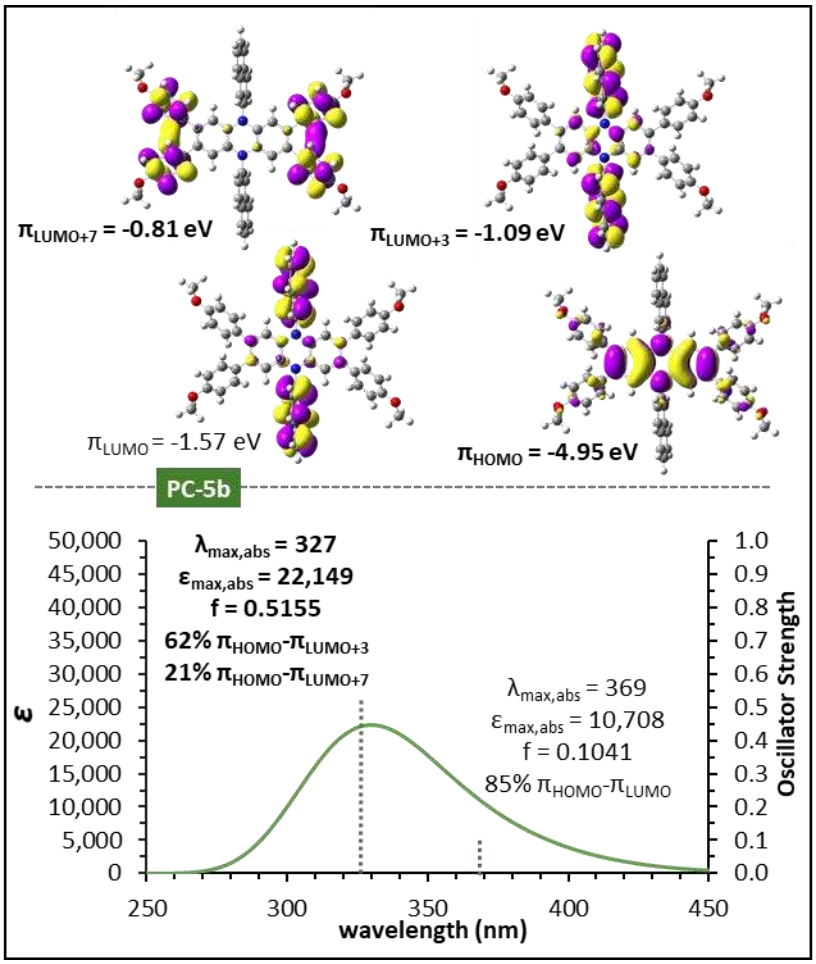

Figure A1.69: Computationally modeled molecular orbitals predicted to be involved in absorption transitions for PC **5b** detailed below (top). Computationally predicted UV−vis spectrum of PCs **5b** along with theoretically assigned percentage contributions (>15%) of various orbitals to the predicted absorption peaks. $\lambda_{max,abs}$ is the predicted absorption maximum wavelength and is reported in units of nm, $\varepsilon_{max,abs}$ is the predicted molar extinction coefficient at the predicted $\lambda_{max,abs}$ and is reported in units of M^{-1} cm^{-1}, and f is the predicted oscillator strength; all of these values were predicted at the TD-DFT CAM-B3LYP/6-31+G(d,p)/CPCM-DMA level of theory (bottom).

Computationally Modeled Singly Occupied Molecular Orbitals (SOMOs) of PCs

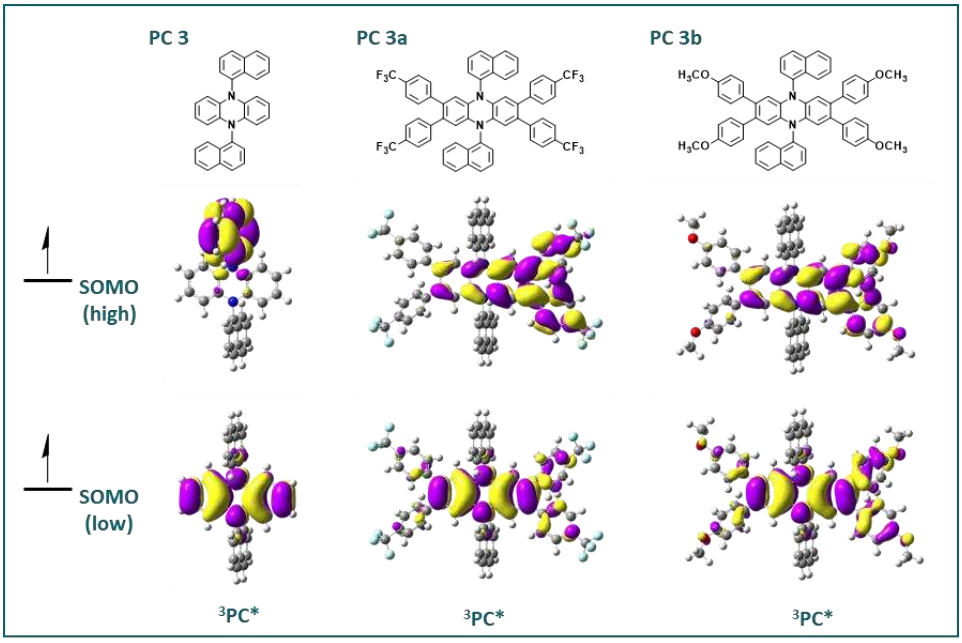

Figure A1.70. Computational modeling of the singularly occupied molecular orbitals (SOMOs) for PCs **3**, **3a**, and **3b** (from left to right); the lower lying SOMO (bottom row) and higher lying SOMO (top row) for each PC in the triplet excited state are shown.

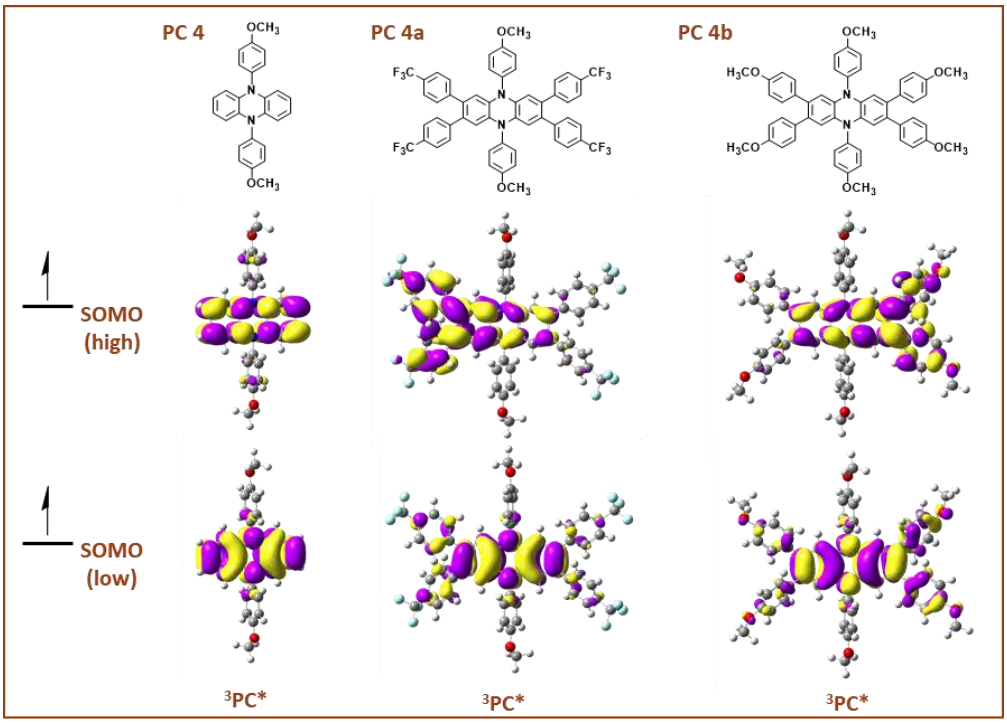

Figure A1.71. Computational modeling of the singularly occupied molecular orbitals (SOMOs) for PCs **4, 4a**, and **4b** (from left to right); the lower lying SOMO (bottom row) and higher lying SOMO (top row) for each PC in the triplet excited state are shown.

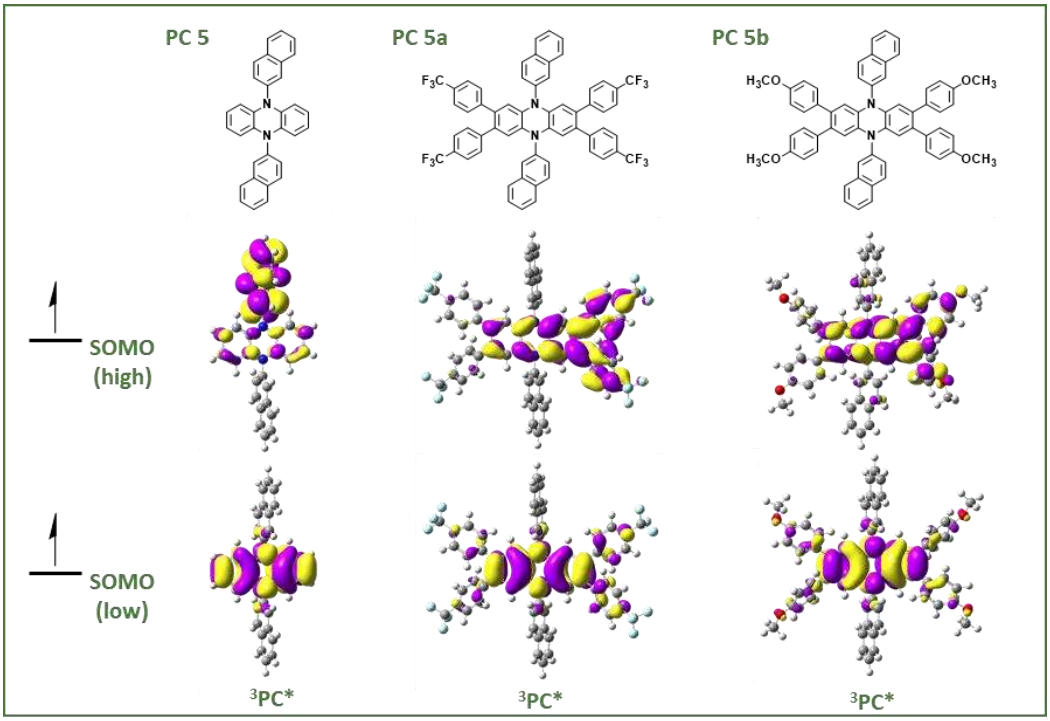

Figure A1.72. Computational modeling of the singularly occupied molecular orbitals (SOMOs) for PCs **5**, **5a**, and **5b** (from left to right); the lower lying SOMO (bottom row) and higher lying SOMO (top row) for each PC in the triplet excited state are shown.

Computationally Modeled Electrostatic Potential (ESP) Maps of PCs

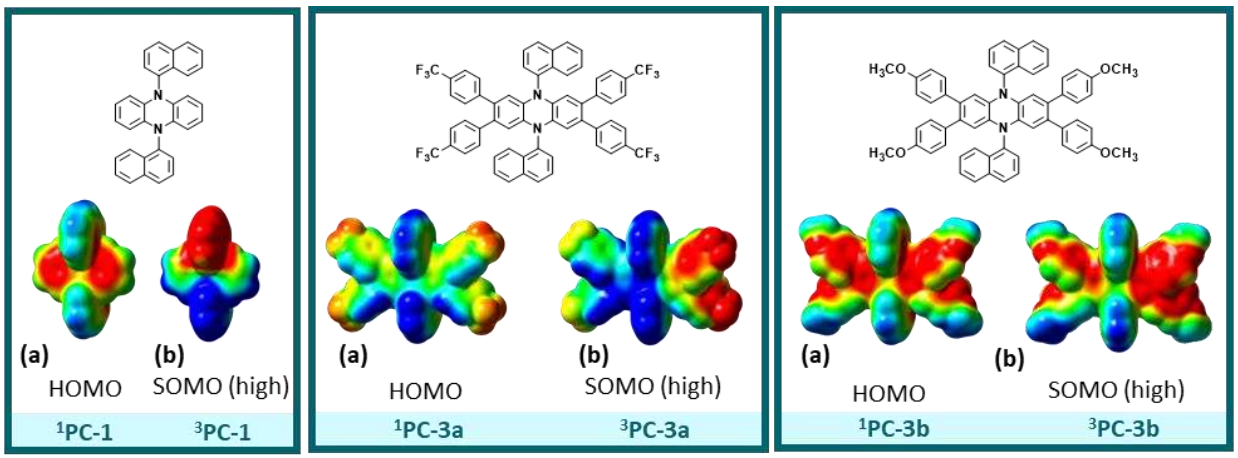

Figure A1.73. Electrostatic potential (ESP) mapped electron density for PCs **3**, **3a**, and **3b** (from left to right) in the ground state (a) and triplet excited state (b) are shown. Red color represents electron rich regions and blue color represents electron deficient regions.

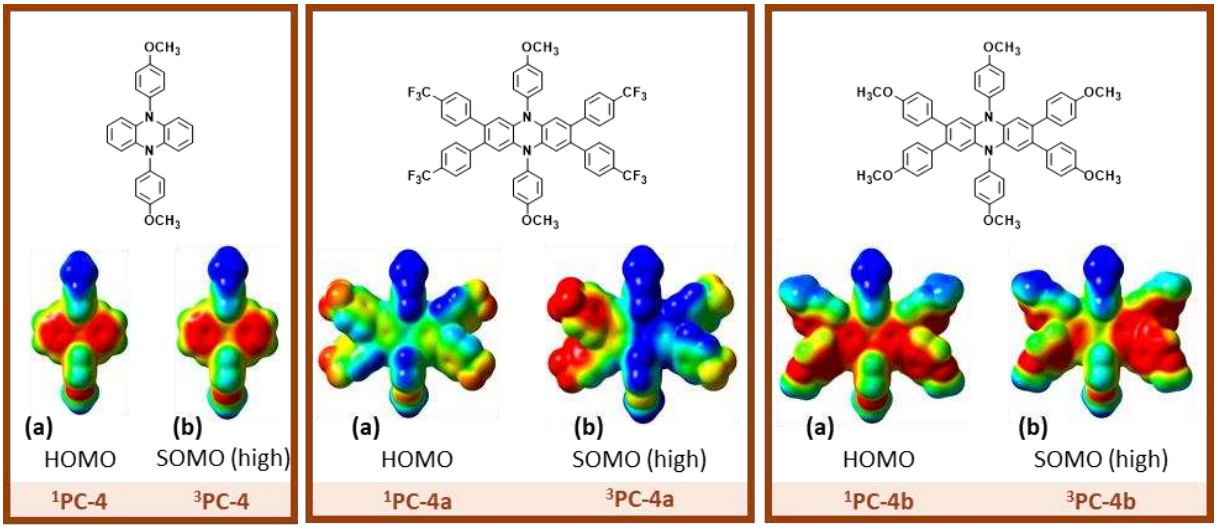

Figure A1.74. Electrostatic potential (ESP) mapped electron density for PCs **4, 4a**, and **4b** (from left to right) in the ground state (a) and triplet excited state (b) are shown. Red color represents electron rich regions and blue color represents electron deficient regions.

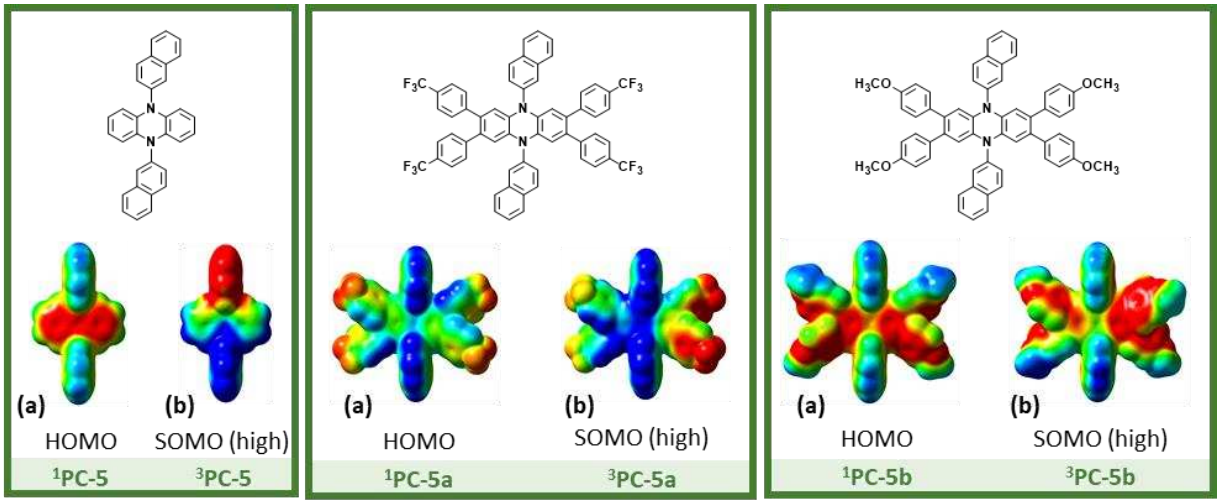

Figure A1.75. Electrostatic potential (ESP) mapped electron density for PCs **5**, **5a**, and **5b** (from left to right) in the ground state (a) and triplet excited state (b) are shown. Red color represents electron rich regions and blue color represents electron deficient regions.

POLYMERIZATION DATA

Table A1.3. O-ATRP Results from Employing PCs for the Polymerization of MMA at Varied Catalyst Loadings[a]

Run	PC	PC Loading (ppm)[b]	Conv. [c]	M_n (kDa)[d]	M_w (kDa)[d]	$Đ$ (M_w/M_n) [d]	I^*[e]
1	**3**	500	42.9%	5.71	6.37	1.12	79.5%
2	**3**	100	67.5%	8.97	9.63	1.07	78.1%
3	**3**	50	84.6%	8.26	9.87	1.19	105%
4	**3a**	500	67.7%	7.53	7.76	1.07	93.4%
5	**3a**	100	64.5%	7.71	8.93	1.16	87.0%
6	**3a**	50	85.8%	8.80	9.46	1.07	91.9%
7	**3a**	10	66.8%	7.17	10.7	1.49	96.8%
8	**3b**	100	51.2%	5.32	8.33	1.57	101%
10	**4a**	100	65.4%	7.57	8.70	1.15	89.8%
11	**4a**	50	75.5%	7.53	9.55	1.27	104%
12	**4a**	10	66.8%	7.17	10.7	1.49	96.8%
13	**5**	500	84.3%	10.2	11.7	1.15	85.6%
14	**5**	100	77.1%	8.74	10.4	1.18	91.2%
15	**5**	50	86.6%	12.8	15.3	1.20	69.9%
16	**5**	10	62.4%	7.43	13.3	1.79	87.5%
17	**5a**	500	60.5%	9.00	9.76	1.08	70.1%
18	**5a**	100	72.7%	8.08	8.87	1.09	93.2%
19	**5a**	50	79.5%	7.34	9.42	1.28	112%
20	**5a**	10	69.9%	7.54	10.71	1.42	96.1%
21	**5b**	500	52.4%	5.45	9.20	1.69	101%
22	**5b**	100	73.3%	8.25	12.7	1.54	92.1%
34	**PhenO**[f]	50	56.3%	6.77	12.2	1.81	87.0%

[a]All polymerizations were conducted using MMA as the monomer and DBMM as the initiator in a ratio of [1000]:[100] with DMAc as the solvent. [b]PC loading is relative to mols of monomer. [c]Conversion was determined by ^{1}H-NMR spectroscopy. [d]Measured using GPC. [e]Initiator efficiency (I^*) calculated by ((theoretical M_n/observed M_n)*100). [f]3,7-Di([1,1'-biphenyl]-4-yl)-10-(naphthalen-1-yl)-10*H*-phenoxazine

Table A1.4. Summary of results of O-ATRP of MMA in varied solvents using 50 ppm of 3b, O-ATRP of varied monomers in benzene using 50ppm of 3b, and O-ATRP with other PCs using optimized conditions. [a]

Run	PC	PC Loading (ppm)[b]	Monomer	Solvent	Conv. [c]	M_n (kDa)[d]	M_W (kDa)[d]	$Đ$ (M_w/M_n)[d]	I^*[e]
6	**3a**	50	MMA	DMAc	85.8%	8.80	9.46	1.07	91.9%
23	**3a**	50	MMA	THF	77.7%	9.88	11.5	1.17	81.0%
24	**3a**	50	MMA	EtOAc	86.9%	8.79	10.8	1.23	102%
25	**3a**	50	MMA	Benz	89.2%	10.0	10.6	1.06	92.0%
26	**3a**	50	MMA	DCM	94.1%	8.88	11.0	1.24	109%
27	**3a**	10	MMA	Benz	83.2%	7.24	10.9	1.51	119%
28	**3a**	50	nBA	Benz	93.3%	14.4	24.4	1.69	85.0%
29[f]	**3a**	50	DMA	Benz	85.8%	na	na	na	na
30[g]	**3a**	50	VA	Benz	0.00%	na	na	na	na
31[g]	**3a**	50	styrene	Benz	0.00%	na	na	na	na
32	**4a**	50	nBA	Benz	87.3%	11.9	28.8	2.41	96.0%
33	**4a**	10	MMA	Benz	51.9%	5.34	7.11	1.33	102%

[a]All polymerizations were conducted using DBMM as the initiator in a ratio of [1000]:[100] for [monomer]:[DBMM]. [b]PC loading is relative to mols of monomer. [c]Conversion was determined by ^{1}H-NMR spectroscopy. [d]Measured using GPC. [e]Initiator efficiency (I^*) calculated by ((theoretical M_n/observed M_n)*100). [f]Molecular weight data was not obtained for this polymer. [g]Molecular weight data was not obtained as there was no conversion observed.

Polymerization Kinetics

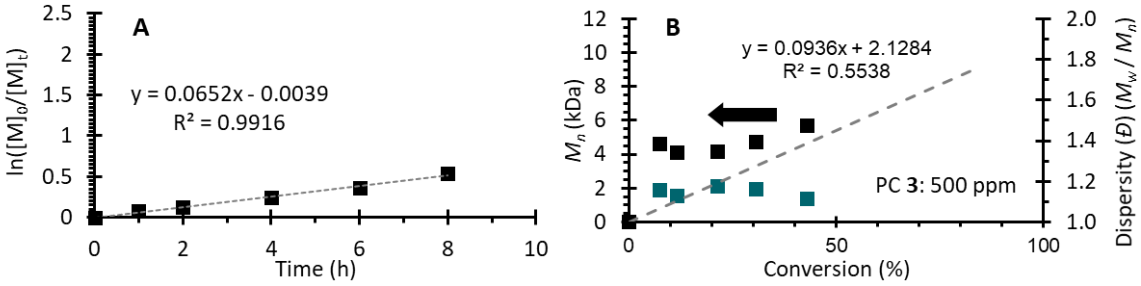

Figure A1.76. Polymerization data from Run 1 (Table A1.3). [MMA]:[DMAc]:[DBMM]:[**3**] = [1000]:[1000]:[10]:[500]. (A) First order kinetic plot of the natural log of monomer consumption as a function of time. (B) Plot of molecular weight (M_n) growth as a function of monomer conversion (black squares), theoretical M_n growth as a function of monomer conversion (dashed grey line), and dispersity as a function of monomer conversion (blue squares). Equation on chart (B) represents the trendline for the measured M_n growth as a function of conversion.

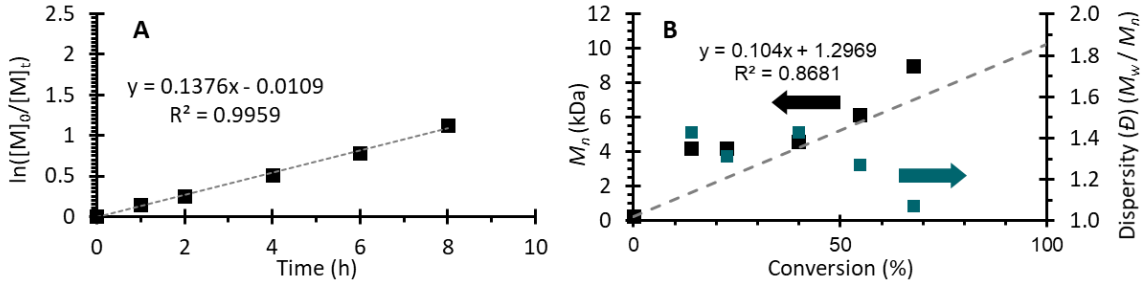

Figure A1.77. Polymerization data from Run 2 (Table A1.3). [MMA]:[DMAc]:[DBMM]:[**3**] = [1000]:[1000]:[10]:[100]. (A) First order kinetic plot of the natural log of monomer consumption as a function of time. (B) Plot of molecular weight (M_n) growth as a function of monomer conversion (black squares), theoretical M_n growth as a function of monomer conversion (dashed grey line), and dispersity as a function of monomer conversion (blue squares). Equation on chart (B) represents the trendline for the measured M_n growth as a function of conversion.

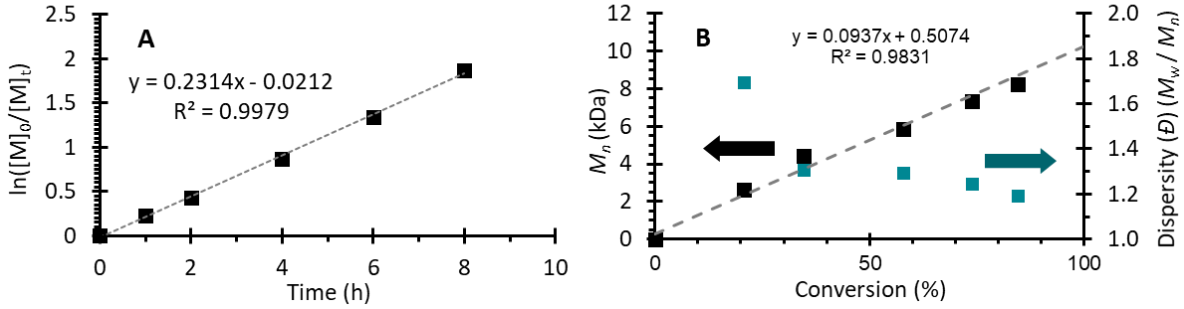

Figure A1.78. Polymerization data from Run 3 (Table A1.3). [MMA]:[DMAc]:[DBMM]:[**3**] = [1000]:[1000]:[10]:[50]. (A) First order kinetic plot of the natural log of monomer consumption as a function of time. (B) Plot of molecular weight (M_n) growth as a function of monomer conversion (black squares), theoretical M_n growth as a function of monomer conversion (dashed grey line), and dispersity as a function of monomer conversion (blue squares). Equation on chart (B) represents the trendline for the measured M_n growth as a function of conversion.

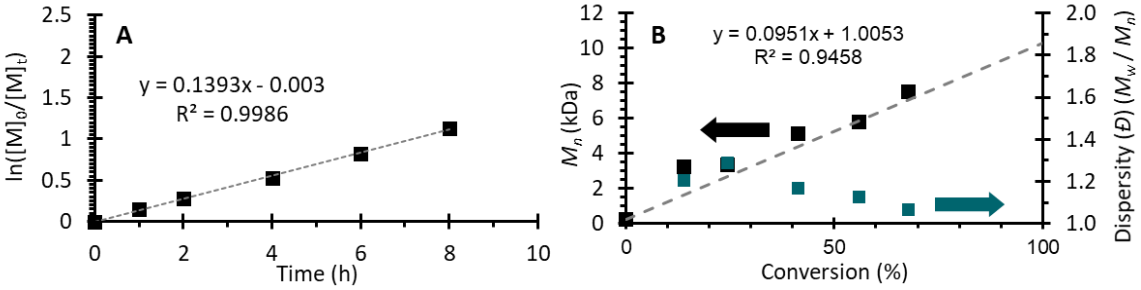

Figure A1.79. Polymerization data from Run 4 (Table A1.3). [MMA]:[DMAc]:[DBMM]:[**3a**] = [1000]:[1000]:[10]:[500]. (A) First order kinetic plot of the natural log of monomer consumption as a function of time. (B) Plot of molecular weight (M_n) growth as a function of monomer conversion (black squares), theoretical M_n growth as a function of monomer conversion (dashed grey line), and dispersity as a function of monomer conversion (blue squares). Equation on chart (B) represents the trendline for the measured M_n growth as a function of conversion.

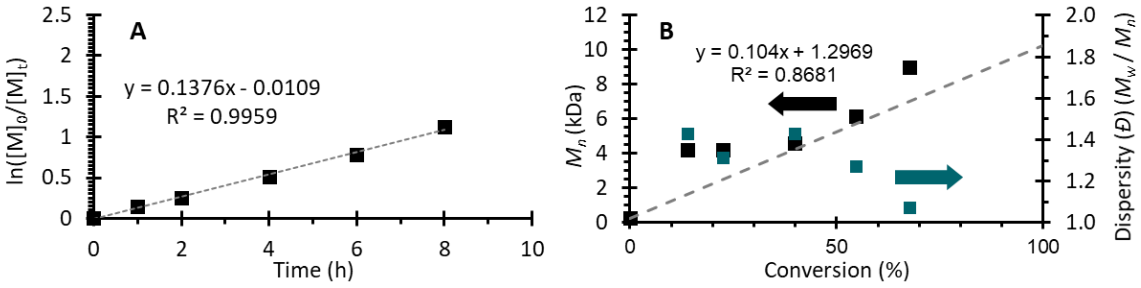

Figure A1.80. Polymerization data from Run 5 (Table A1.3). [MMA]:[DMAc]:[DBMM]:[**3a**] = [1000]:[1000]:[10]:[100]. (A) First order kinetic plot of the natural log of monomer consumption as a function of time. (B) Plot of molecular weight (M_n) growth as a function of monomer conversion (black squares), theoretical M_n growth as a function of monomer conversion (dashed grey line), and dispersity as a function of monomer conversion (blue squares). Equation on chart (B) represents the trendline for the measured M_n growth as a function of conversion.

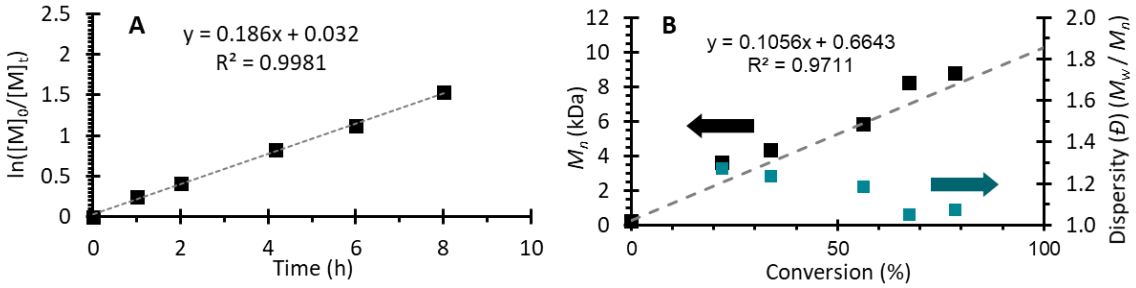

Figure A1.81. Polymerization data from Run 6 (Table A1.3). [MMA]:[DMAc]:[DBMM]:[**3a**] = [1000]:[1000]:[10]:[50]. (A) First order kinetic plot of the natural log of monomer consumption as a function of time. (B) Plot of molecular weight (M_n) growth as a function of monomer conversion (black squares), theoretical M_n growth as a function of monomer conversion (dashed grey line), and dispersity as a function of monomer conversion (blue squares). Equation on chart (B) represents the trendline for the measured M_n growth as a function of conversion.

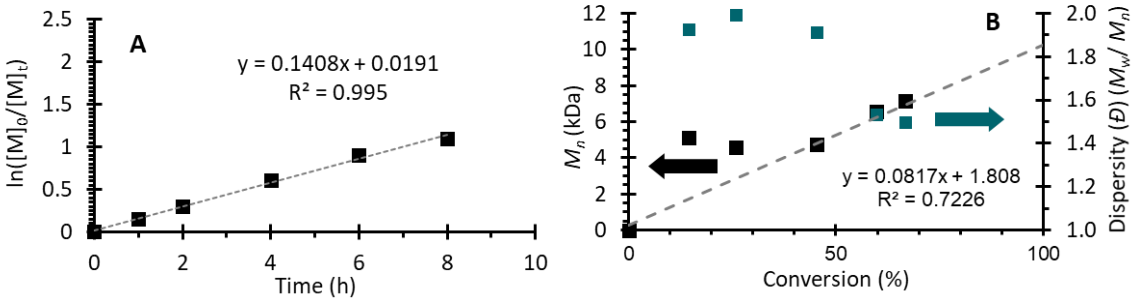

Figure A1.82. Polymerization data from Run 7 (Table A1.3). [MMA]:[DMAc]:[DBMM]:[**3a**] = [1000]:[1000]:[10]:[10]. (A) First order kinetic plot of the natural log of monomer consumption as a function of time. (B) Plot of molecular weight (M_n) growth as a function of monomer conversion (black squares), theoretical M_n growth as a function of monomer conversion (dashed grey line), and dispersity as a function of monomer conversion (blue squares). Equation on chart (B) represents the trendline for the measured M_n growth as a function of conversion.

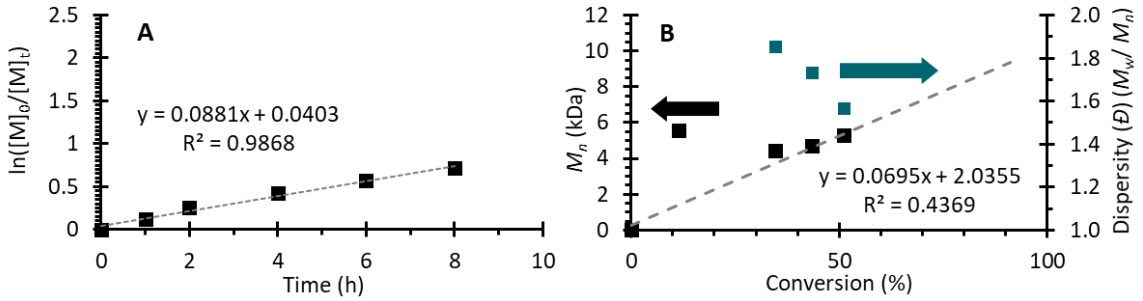

Figure A1.83. Polymerization data from Run 8 (Table A1.3). [MMA]:[DMAc]:[DBMM]:[**3b**] = [1000]:[1000]:[10]:[100]. (A) First order kinetic plot of the natural log of monomer consumption as a function of time. (B) Plot of molecular weight (M_n) growth as a function of monomer conversion (black squares), theoretical M_n growth as a function of monomer conversion (dashed grey line), and dispersity as a function of monomer conversion (blue squares). Equation on chart (B) represents the trendline for the measured M_n growth as a function of conversion.

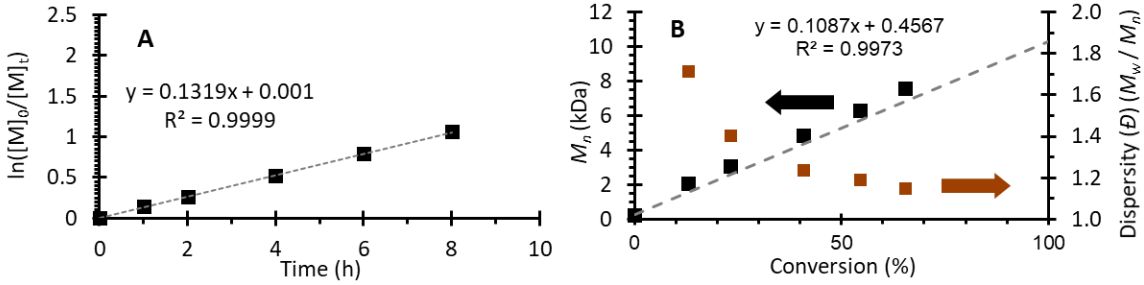

Figure A1.84. Polymerization data from Run 10 (Table A1.3). [MMA]:[DMAc]:[DBMM]:[**4a**] = [1000]:[1000]:[10]:[100]. (A) First order kinetic plot of the natural log of monomer consumption as a function of time. (B) Plot of molecular weight (M_n) growth as a function of monomer conversion (black squares), theoretical M_n growth as a function of monomer conversion (dashed grey line), and dispersity as a function of monomer conversion (orange squares). Equation on chart (B) represents the trendline for the measured M_n growth as a function of conversion.

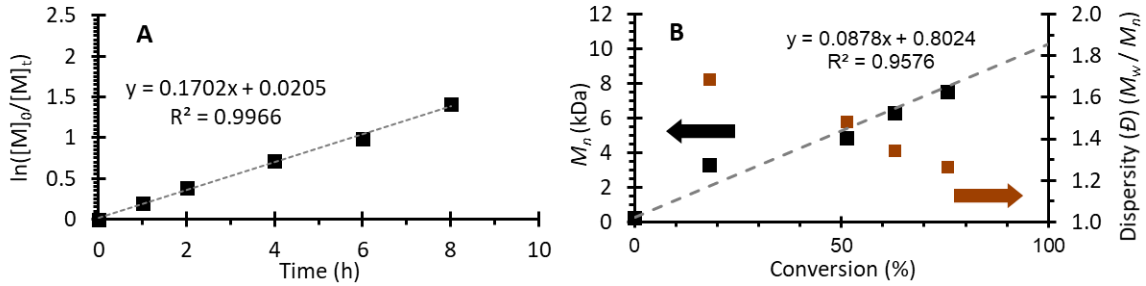

Figure A1.85. Polymerization data from Run 11 (Table A1.3). [MMA]:[DMAc]:[DBMM]:[**4a**] = [1000]:[1000]:[10]:[50]. (A) First order kinetic plot of the natural log of monomer consumption as a function of time. (B) Plot of molecular weight (M_n) growth as a function of monomer conversion (black squares), theoretical M_n growth as a function of monomer conversion (dashed grey line), and dispersity as a function of monomer conversion (orange squares). Equation on chart (B) represents the trendline for the measured M_n growth as a function of conversion.

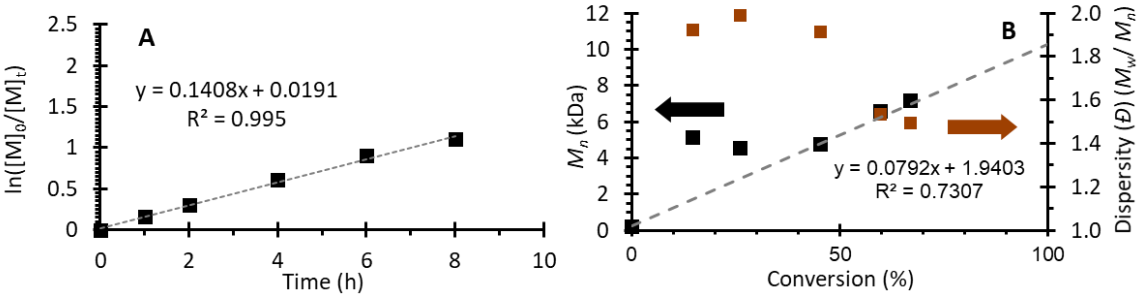

Figure A1.86. Polymerization data from Run 12 (Table A1.3). [MMA]:[DMAc]:[DBMM]:[**4a**] = [1000]:[1000]:[10]:[10]. (A) First order kinetic plot of the natural log of monomer consumption as a function of time. (B) Plot of molecular weight (M_n) growth as a function of monomer conversion (black squares), theoretical M_n growth as a function of monomer conversion (dashed grey line), and dispersity as a function of monomer conversion (orange squares). Equation on chart (B) represents the trendline for the measured M_n growth as a function of conversion.

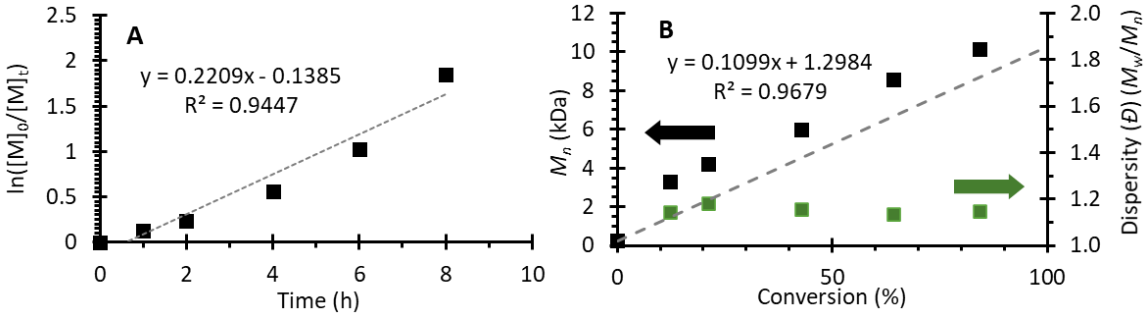

Figure A1.87. Polymerization data from Run 13 (Table A1.3). [MMA]:[DMAc]:[DBMM]:[**5**] = [1000]:[1000]:[10]:[500]. (A) First order kinetic plot of the natural log of monomer consumption as a function of time. (B) Plot of molecular weight (M_n) growth as a function of monomer conversion (black squares), theoretical M_n growth as a function of monomer conversion (dashed grey line), and dispersity as a function of monomer conversion (green squares). Equation on chart (B) represents the trendline for the measured M_n growth as a function of conversion.

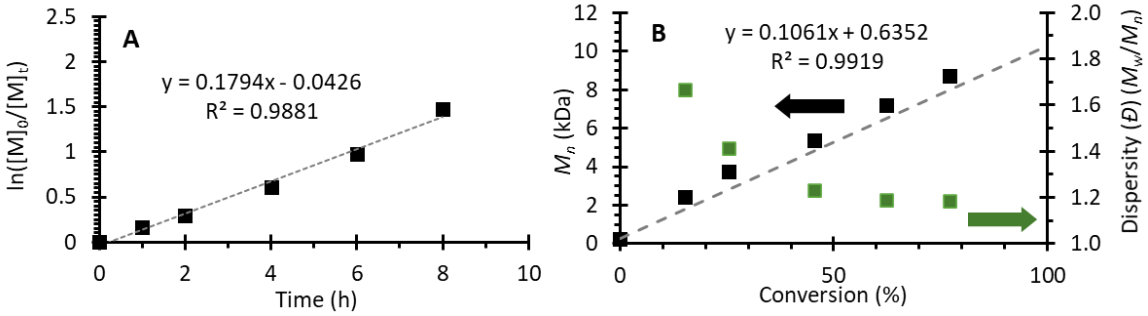

Figure A1.88. Polymerization data from Run 14 (Table A1.3). [MMA]:[DMAc]:[DBMM]:[**5**] = [1000]:[1000]:[10]:[100]. (A) First order kinetic plot of the natural log of monomer consumption as a function of time. (B) Plot of molecular weight (M_n) growth as a function of monomer conversion (black squares), theoretical M_n growth as a function of monomer conversion (dashed grey line), and dispersity as a function of monomer conversion (green squares). Equation on chart (B) represents the trendline for the measured M_n growth as a function of conversion.

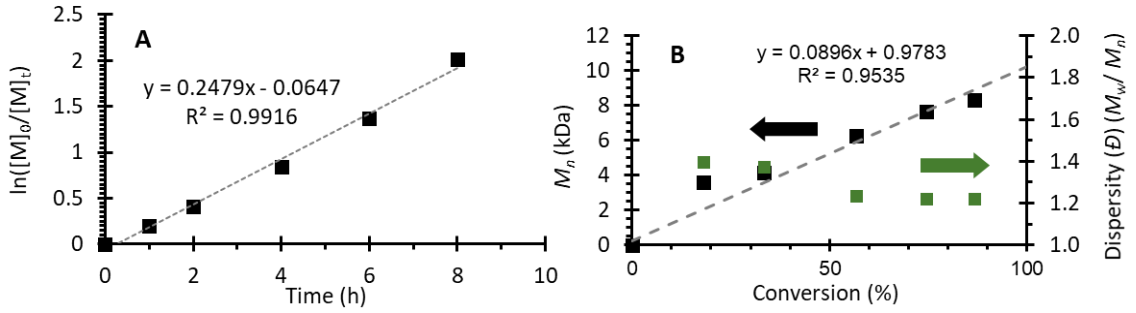

Figure A1.89. Polymerization data from Run 15 (Table A1.3). [MMA]:[DMAc]:[DBMM]:[**5**] = [1000]:[1000]:[10]:[50]. (A) First order kinetic plot of the natural log of monomer consumption as a function of time. (B) Plot of molecular weight (M_n) growth as a function of monomer conversion (black squares), theoretical M_n growth as a function of monomer conversion (dashed grey line), and dispersity as a function of monomer conversion (green squares). Equation on chart (B) represents the trendline for the measured M_n growth as a function of conversion.

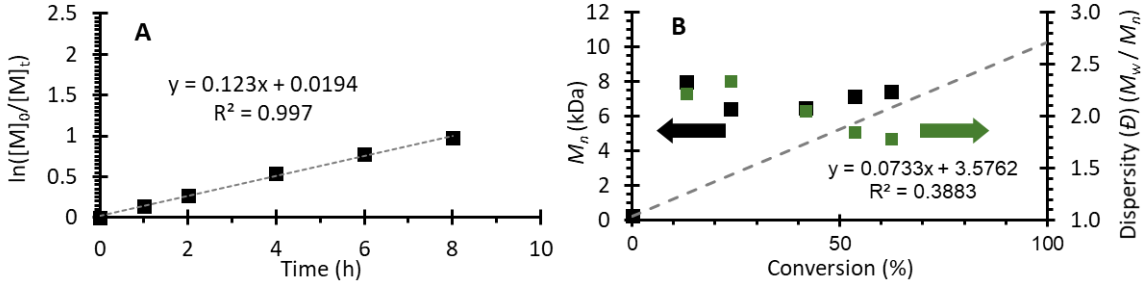

Figure A1.90. Polymerization data from Run 16 (Table A1.3). [MMA]:[DMAc]:[DBMM]:[**5**] = [1000]:[1000]:[10]:[10]. (A) First order kinetic plot of the natural log of monomer consumption as a function of time. (B) Plot of molecular weight (M_n) growth as a function of monomer conversion (black squares), theoretical M_n growth as a function of monomer conversion (dashed grey line), and dispersity as a function of monomer conversion (green squares). Equation on chart (B) represents the trendline for the measured M_n growth as a function of conversion.

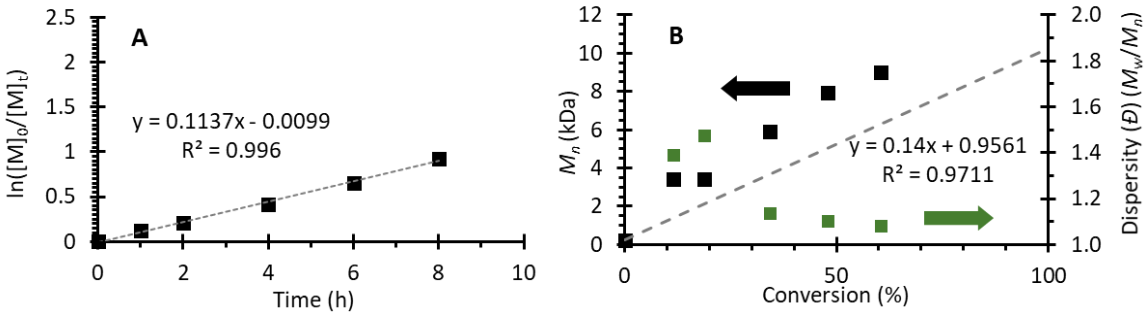

Figure A1.91. Polymerization data from Run 17 (Table A1.3). [MMA]:[DMAc]:[DBMM]:[**5a**] = [1000]:[1000]:[10]:[500]. (A) First order kinetic plot of the natural log of monomer consumption as a function of time. (B) Plot of molecular weight (M_n) growth as a function of monomer conversion (black squares), theoretical M_n growth as a function of monomer conversion (dashed grey line), and dispersity as a function of monomer conversion (green squares). Equation on chart (B) represents the trendline for the measured M_n growth as a function of conversion.

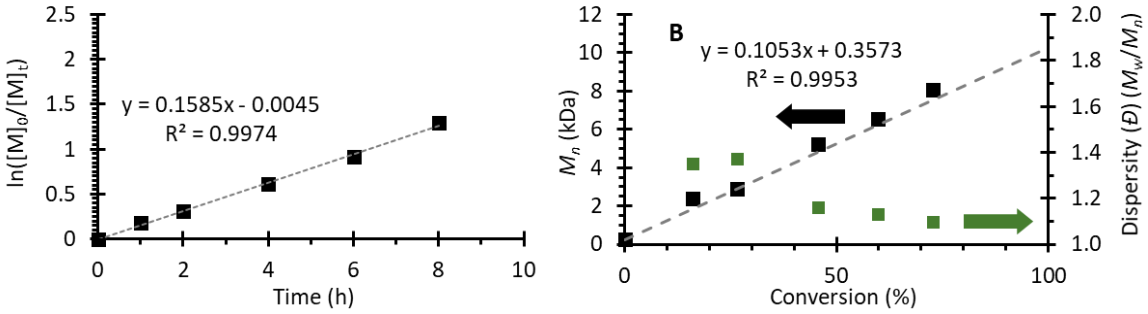

Figure A1.92. Polymerization data from Run 18 (Table A1.3). [MMA]:[DMAc]:[DBMM]:[**5a**] = [1000]:[1000]:[10]:[100]. (A) First order kinetic plot of the natural log of monomer consumption as a function of time. (B) Plot of molecular weight (M_n) growth as a function of monomer conversion (black squares), theoretical M_n growth as a function of monomer conversion (dashed grey line), and dispersity as a function of monomer conversion (green squares). Equation on chart (B) represents the trendline for the measured M_n growth as a function of conversion.

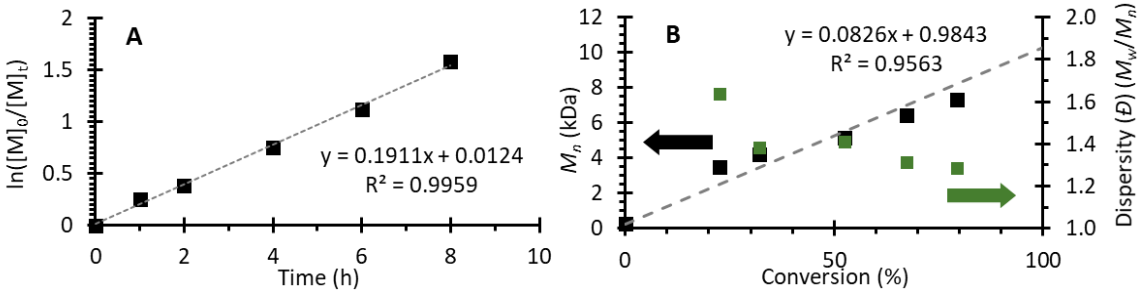

Figure A1.93. Polymerization data from Run 19 (Table A1.3). [MMA]:[DMAc]:[DBMM]:[**5a**] = [1000]:[1000]:[10]:[50]. (A) First order kinetic plot of the natural log of monomer consumption as a function of time. (B) Plot of molecular weight (M_n) growth as a function of monomer conversion (black squares), theoretical M_n growth as a function of monomer conversion (dashed grey line), and dispersity as a function of monomer conversion (green squares). Equation on chart (B) represents the trendline for the measured M_n growth as a function of conversion.

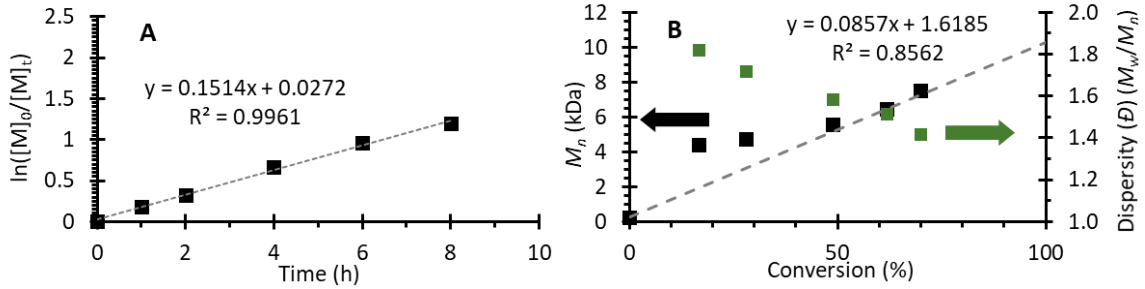

Figure A1.94. Polymerization data from Run 20 (Table A1.3). [MMA]:[DMAc]:[DBMM]:[**5a**] = [1000]:[1000}:[10]:[10]. (A) First order kinetic plot of the natural log of monomer consumption as a function of time. (B) Plot of molecular weight (M_n) growth as a function of monomer conversion (black squares), theoretical M_n growth as a function of monomer conversion (dashed grey line), and dispersity as a function of monomer conversion (green squares). Equation on chart (B) represents the trendline for the measured M_n growth as a function of conversion.

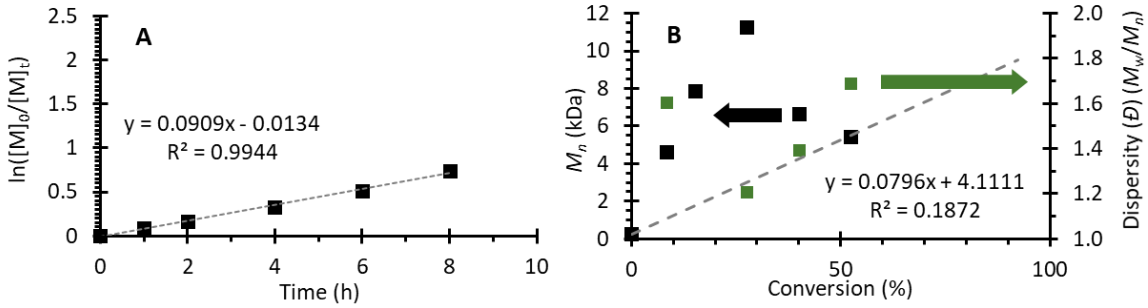

Figure A1.95. Polymerization data from Run 21 (Table A1.3). [MMA]:[DMAc]:[DBMM]:[**5b**] = [1000]:[1000]:[10]:[500]. (A) First order kinetic plot of the natural log of monomer consumption as a function of time. (B) Plot of molecular weight (M_n) growth as a function of monomer conversion (black squares), theoretical M_n growth as a function of monomer conversion (dashed grey line), and dispersity as a function of monomer conversion (green squares). Equation on chart (B) represents the trendline for the measured M_n growth as a function of conversion.

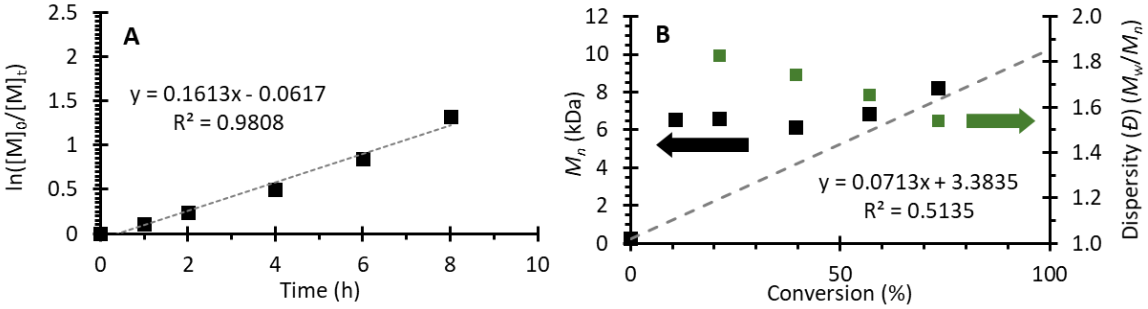

Figure A1.96. Polymerization data from Run 22 (Table A1.3). [MMA]:[DMAc]:[DBMM]:[**5b**] = [1000]:[1000]:[10]:[100]. (A) First order kinetic plot of the natural log of monomer consumption as a function of time. (B) Plot of molecular weight (M_n) growth as a function of monomer conversion (black squares), theoretical M_n growth as a function of monomer conversion (dashed grey line), and dispersity as a function of monomer conversion (green squares). Equation on chart (B) represents the trendline for the measured M_n growth as a function of conversion.

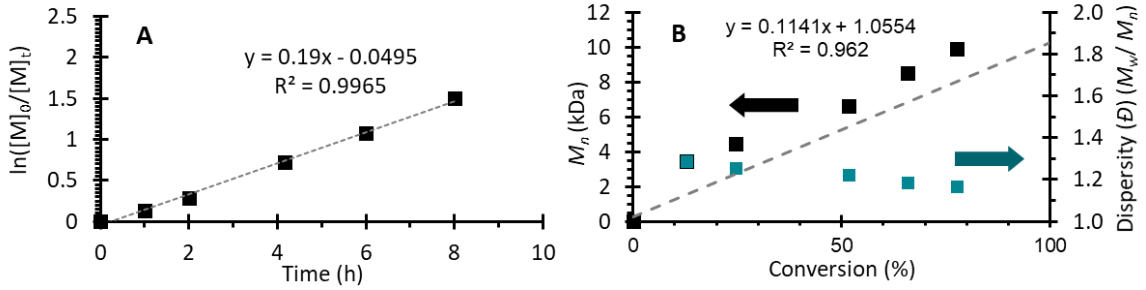

Figure A1.97. Polymerization data from Run 23 (Table A1.4). [MMA]:[THF]:[DBMM]:[**3a**] = [1000]:[1000]:[10]:[50]. (A) First order kinetic plot of the natural log of monomer consumption as a function of time. (B) Plot of molecular weight (M_n) growth as a function of monomer conversion (black squares), theoretical M_n growth as a function of monomer conversion (dashed grey line), and dispersity as a function of monomer conversion (blue squares). Equation on chart (B) represents the trendline for the measured M_n growth as a function of conversion.

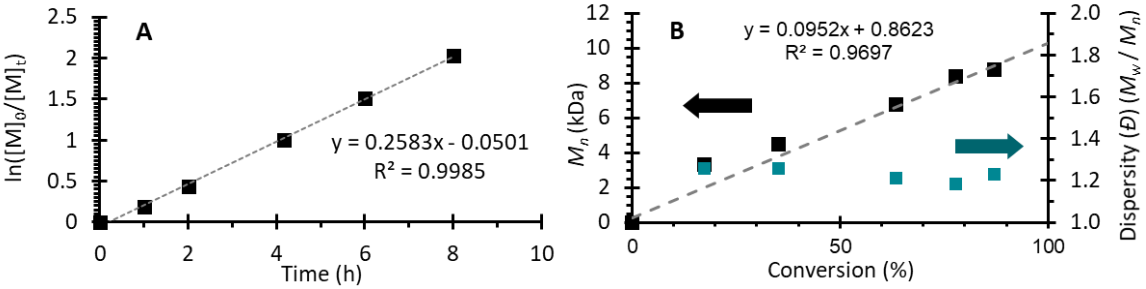

Figure A1.98. Polymerization data from Run 24 (Table A1.4). [MMA]:[EtOAc]:[DBMM]:[**3a**] = [1000]:[1000]:[10]:[50]. (A) First order kinetic plot of the natural log of monomer consumption as a function of time. (B) Plot of molecular weight (M_n) growth as a function of monomer conversion (black squares), theoretical M_n growth as a function of monomer conversion (dashed grey line), and dispersity as a function of monomer conversion (blue squares). Equation on chart (B) represents the trendline for the measured M_n growth as a function of conversion.

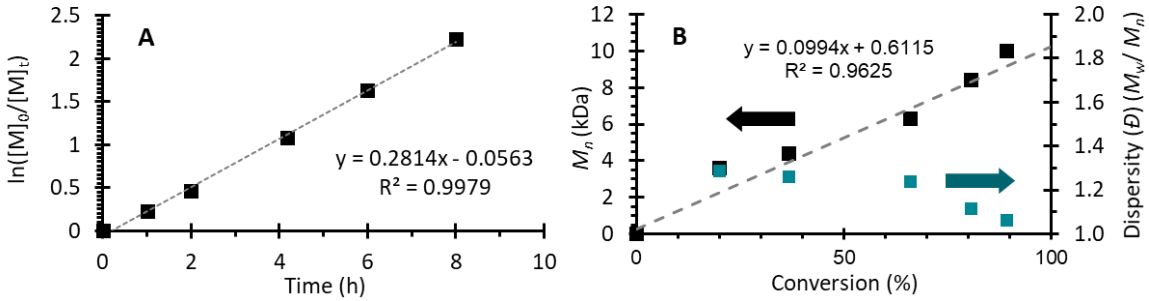

Figure A1.99. Polymerization data from Run 25 (Table A1.4). [MMA]:[Benz]:[DBMM]:[**3a**] = [1000]:[1000]:[10]:[50]. (A) First order kinetic plot of the natural log of monomer consumption as a function of time. (B) Plot of molecular weight (M_n) growth as a function of monomer conversion (black squares), theoretical M_n growth as a function of monomer conversion (dashed grey line), and dispersity as a function of monomer conversion (blue squares). Equation on chart (B) represents the trendline for the measured M_n growth as a function of conversion.

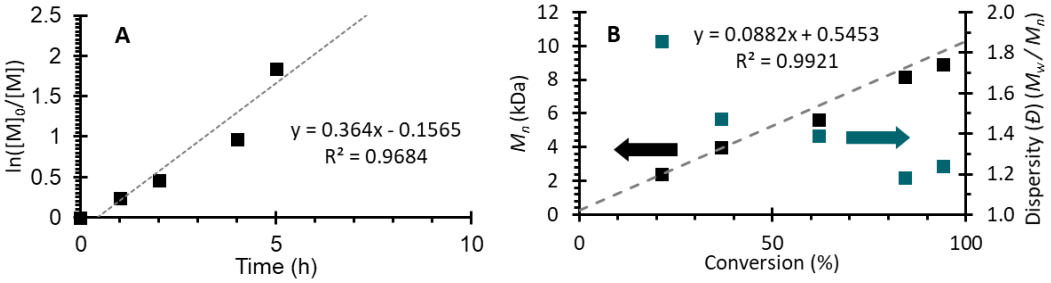

Figure A1.100. Polymerization data from Run 26 (Table A1.4). [MMA]:[DCM]:[DBMM]:[**3a**] = [1000]:[1000]:[10]:[50]. (A) First order kinetic plot of the natural log of monomer consumption as a function of time. (B) Plot of molecular weight (M_n) growth as a function of monomer conversion (black squares), theoretical M_n growth as a function of monomer conversion (dashed grey line), and dispersity as a function of monomer conversion (blue squares). Equation on chart (B) represents the trendline for the measured M_n growth as a function of conversion.

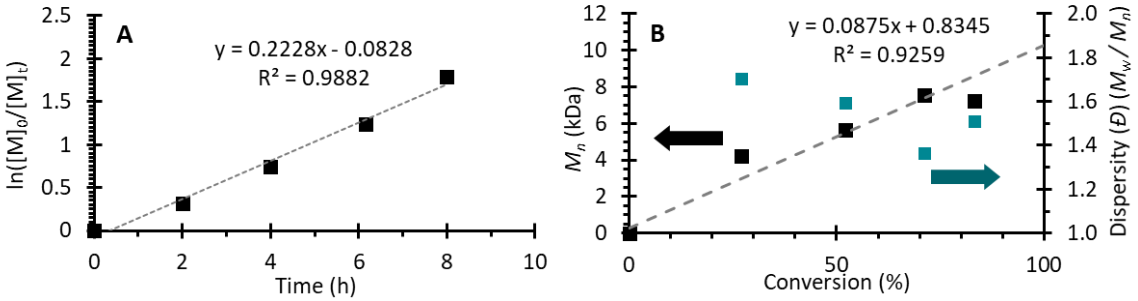

Figure A1.101. Polymerization data from Run 27 (Table A1.4). [MMA]:[Benz]:[DBMM]:[**3a**] = [1000]:[1000]:[10]:[10]. (A) First order kinetic plot of the natural log of monomer consumption as a function of time. (B) Plot of molecular weight (M_n) growth as a function of monomer conversion (black squares), theoretical M_n growth as a function of monomer conversion (dashed grey line), and dispersity as a function of monomer conversion (blue squares). Equation on chart (B) represents the trendline for the measured M_n growth as a function of conversion.

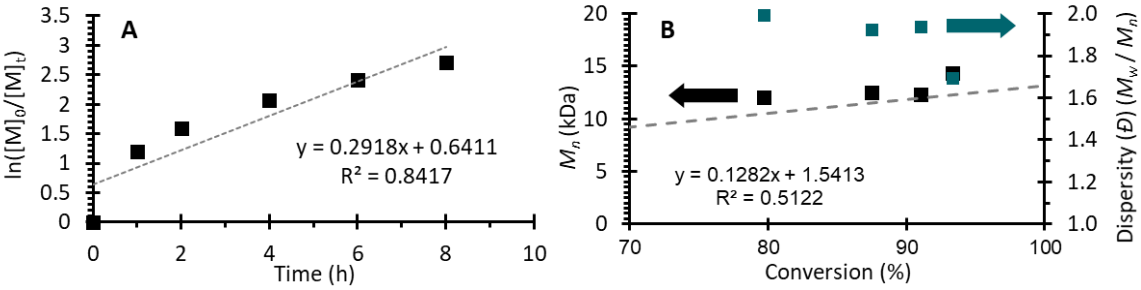

Figure A1.102. Polymerization data from Run 28 (Table A1.4). [nBA]:[Benz]:[DBMM]:[**3a**] = [1000]:[1000]:[10]:[50]. (A) First order kinetic plot of the natural log of monomer consumption as a function of time. (B) Plot of molecular weight (M_n) growth as a function of monomer conversion (black squares), theoretical M_n growth as a function of monomer conversion (dashed grey line), and dispersity as a function of monomer conversion (blue squares). Equation on chart (B) represents the trendline for the measured M_n growth as a function of conversion.

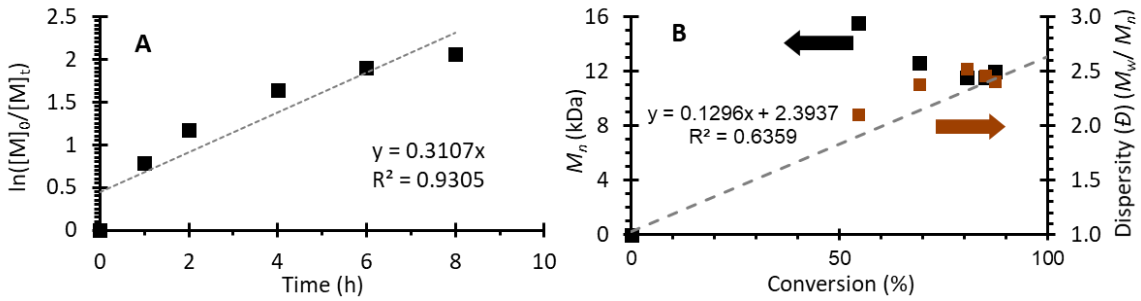

Figure A1.103. Polymerization data from Run 32 (Table A1.4). [nBA]:[Benz]:[DBMM]:[**4a**] = [1000]:[1000]:[10]:[50]. (A) First order kinetic plot of the natural log of monomer consumption as a function of time. (B) Plot of molecular weight (M_n) growth as a function of monomer conversion (black squares), theoretical M_n growth as a function of monomer conversion (dashed grey line), and dispersity as a function of monomer conversion (orange squares). Equation on chart (B) represents the trendline for the measured M_n growth as a function of conversion.

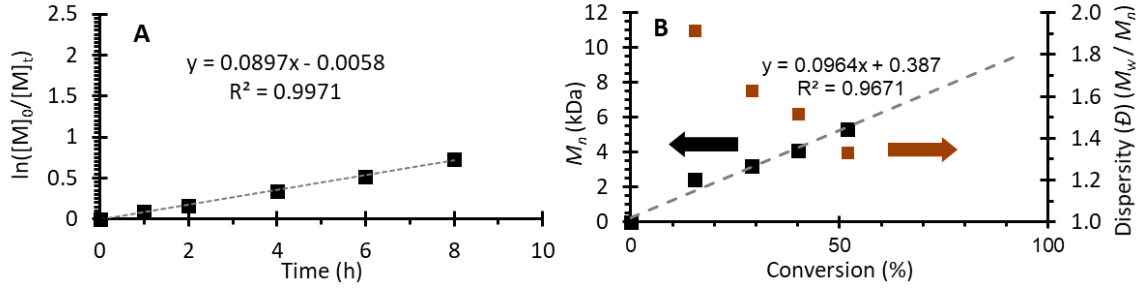

Figure A1.104. Polymerization data from Run 33 (Table A1.4). [MMA]:[Benz]:[DBMM]:[**4a**] = [1000]:[1000]:[10]:[10]. (A) First order kinetic plot of the natural log of monomer consumption as a function of time. (B) Plot of molecular weight (M_n) growth as a function of monomer conversion (black squares), theoretical M_n growth as a function of monomer conversion (dashed grey line), and dispersity as a function of monomer conversion (orange squares). Equation on chart (B) represents the trendline for the measured M_n growth as a function of conversion.

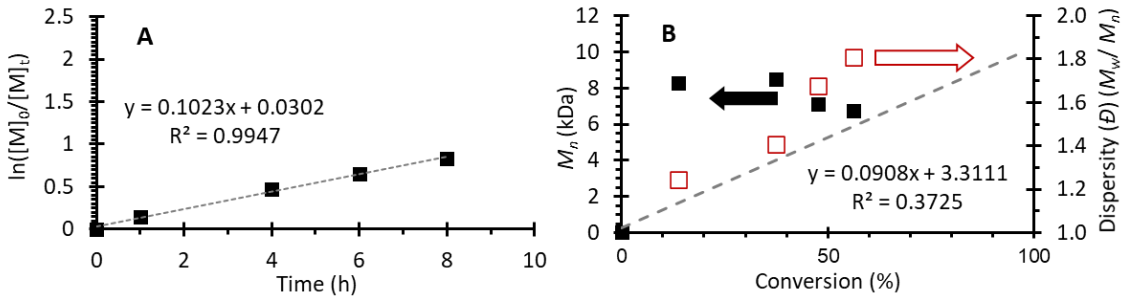

Figure A1.105. Polymerization data from Run 34 (Table A1.4). [MMA]:[DMAc]:[DBMM]:[**PhenO***] = [1000]:[1000]:[10]:[50]. (A) First order kinetic plot of the natural log of monomer consumption as a function of time. (B) Plot of molecular weight (M_n) growth as a function of monomer conversion (black squares), theoretical M_n growth as a function of monomer conversion (dashed grey line), and dispersity as a function of monomer conversion (orange squares). Equation on chart (B) represents the trendline for the measured M_n growth as a function of conversion. *(**PhenO**: 3,7-Di([1,1'-biphenyl]-4-yl)-10-(naphthalen-1-yl)-10*H*-phenoxazine).

Chain Extension Experiment

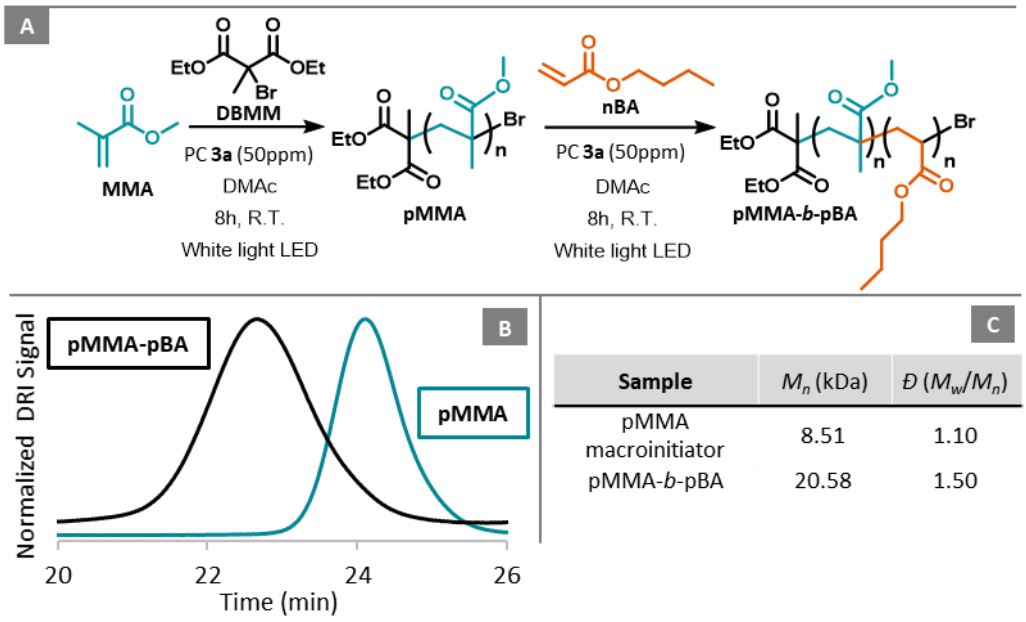

Sample	M_n (kDa)	Đ (M_w/M_n)
pMMA macroinitiator	8.51	1.10
pMMA-*b*-pBA	20.58	1.50

Figure A1.106. (**A**) Reaction scheme for chain extension of pMMA macroinitiator with nBA to form pMMA-*b*-pBA. The polymerization of the macromonomer was run in DMAc using DBMM as the initiator and MMA as the monomer in a ratio of [MMA]:[DBMM]:[**3a**] = [1000]:[10]:[0.05]. (**B**) Overlaid GPC traces of the isolated pMMA macroinitator and the isolated pMMA-*b*-pBA block copolymer. (**C**) Molecular weight data (obtained using GPC) for the isolated pMMA macroinitiator and the isolated pMMA-*b*-nBA block copolymer.

^{1}H-NMR SPECTRA OF CATALYSTS & RELEVANT INTERMEDIATES

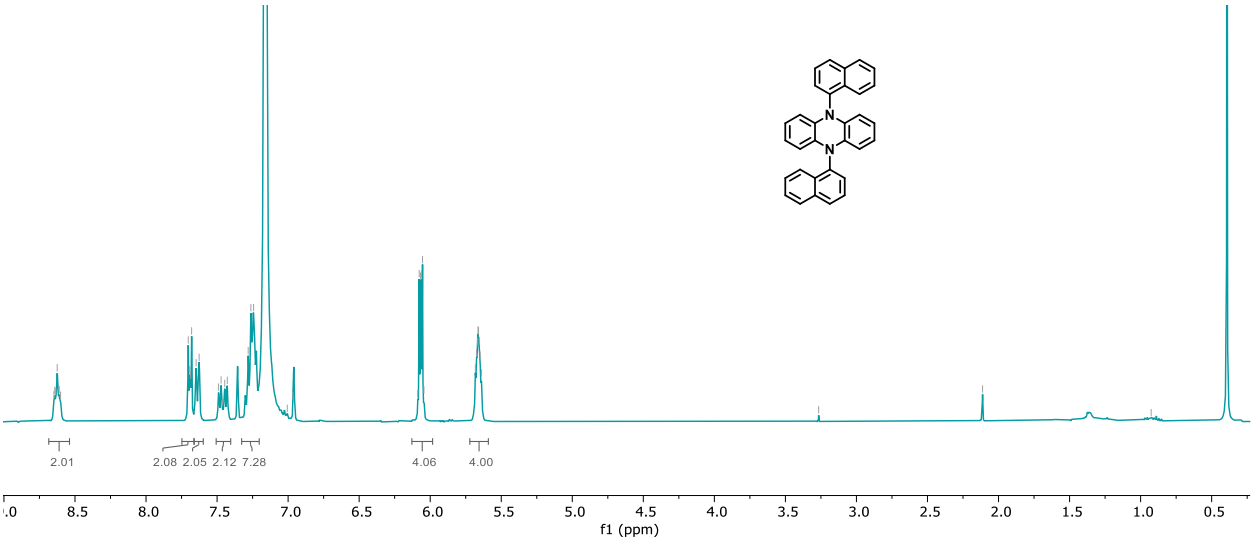

Figure A1.107. ^{1}H-NMR spectrum of **PC 3** in C_6D_6 after recrystallization.

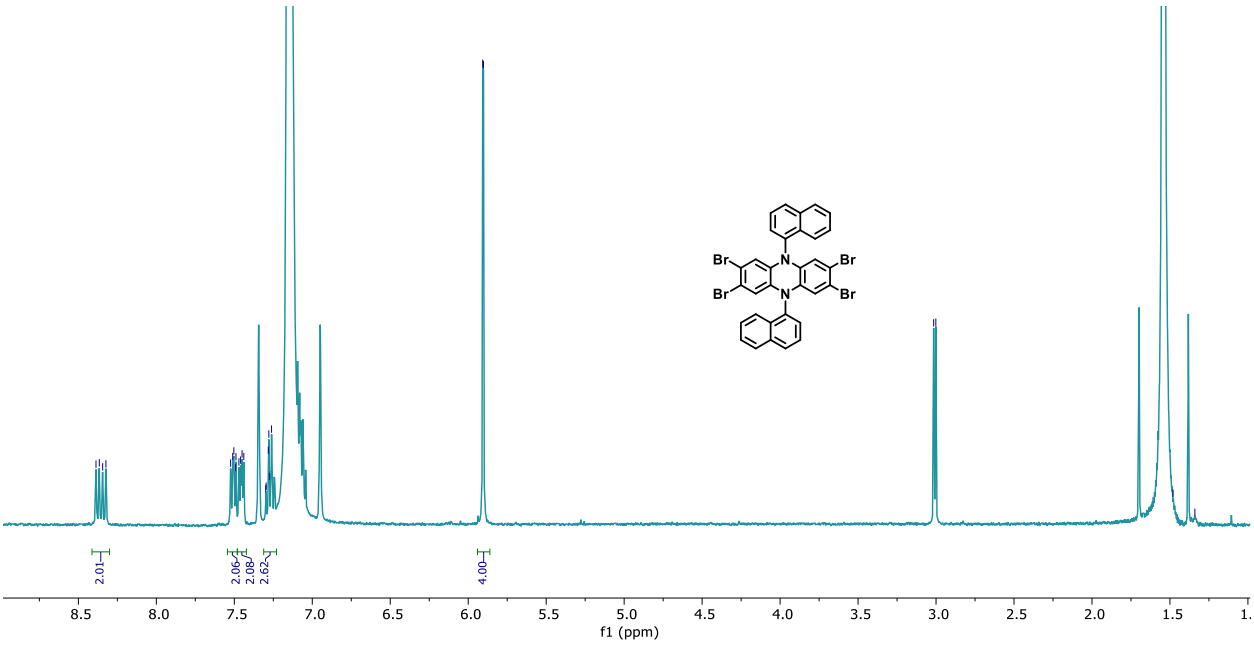

Figure A1.108. ^{1}H-NMR spectrum of unpurified **PC 3-4Br** in C_6D_6.

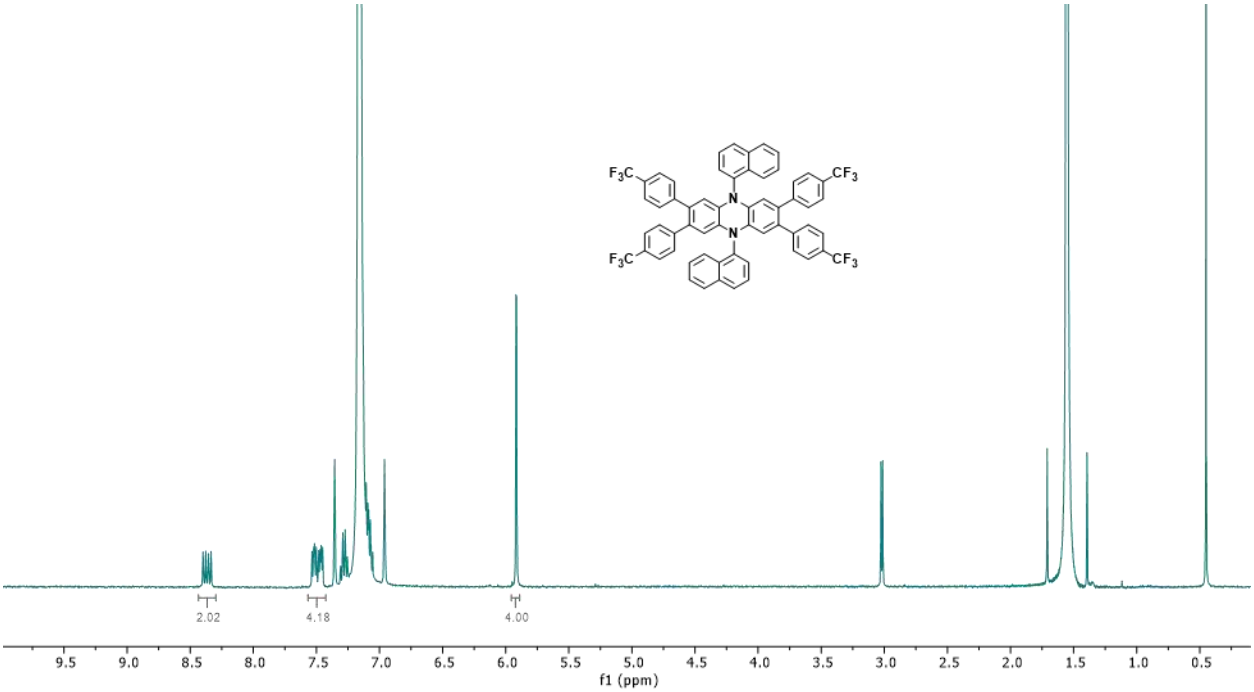

Figure A1.109. ^{1}H-NMR spectrum of **PC 3a** in C_6D_6 after recrystallization.

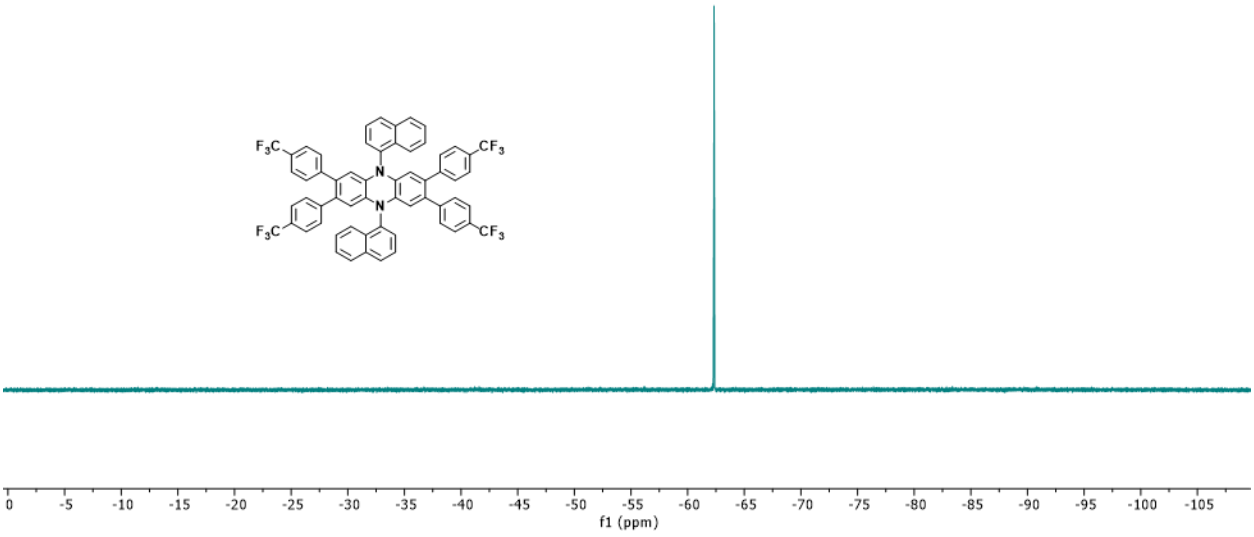

Figure A1.110. ^{19}F-NMR spectrum of **PC 3a** in C_6D_6.

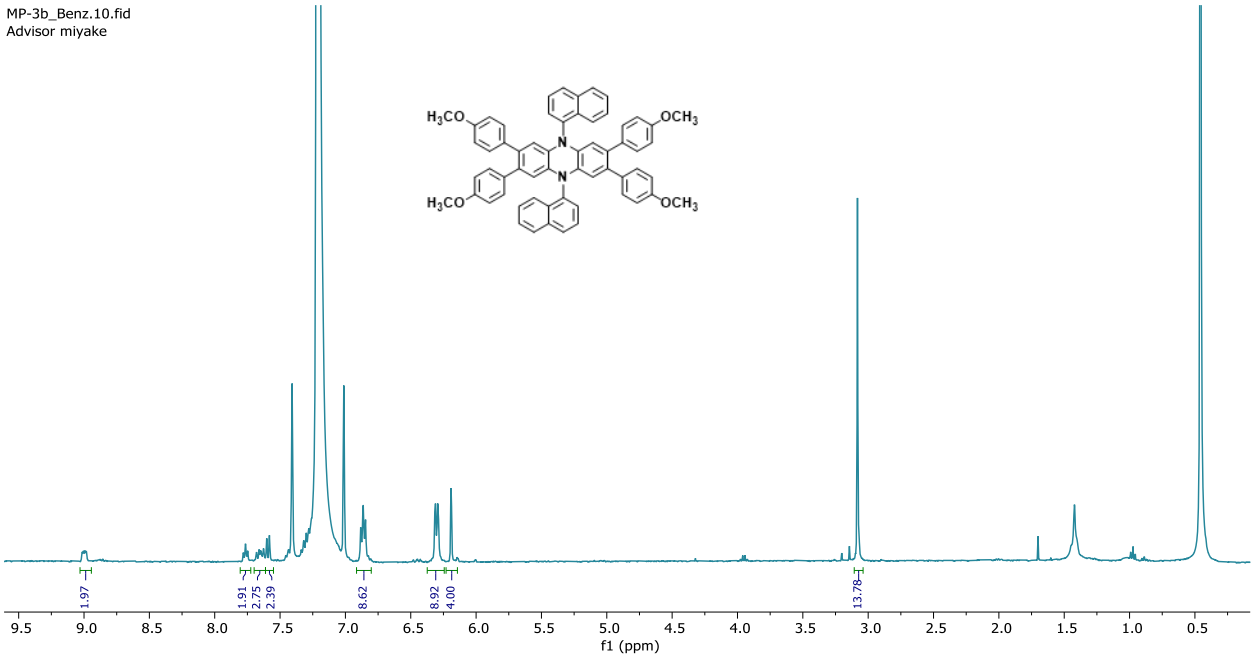

Figure A1.111. ^{1}H-NMR spectrum of **PC 3b** in C_6D_6.

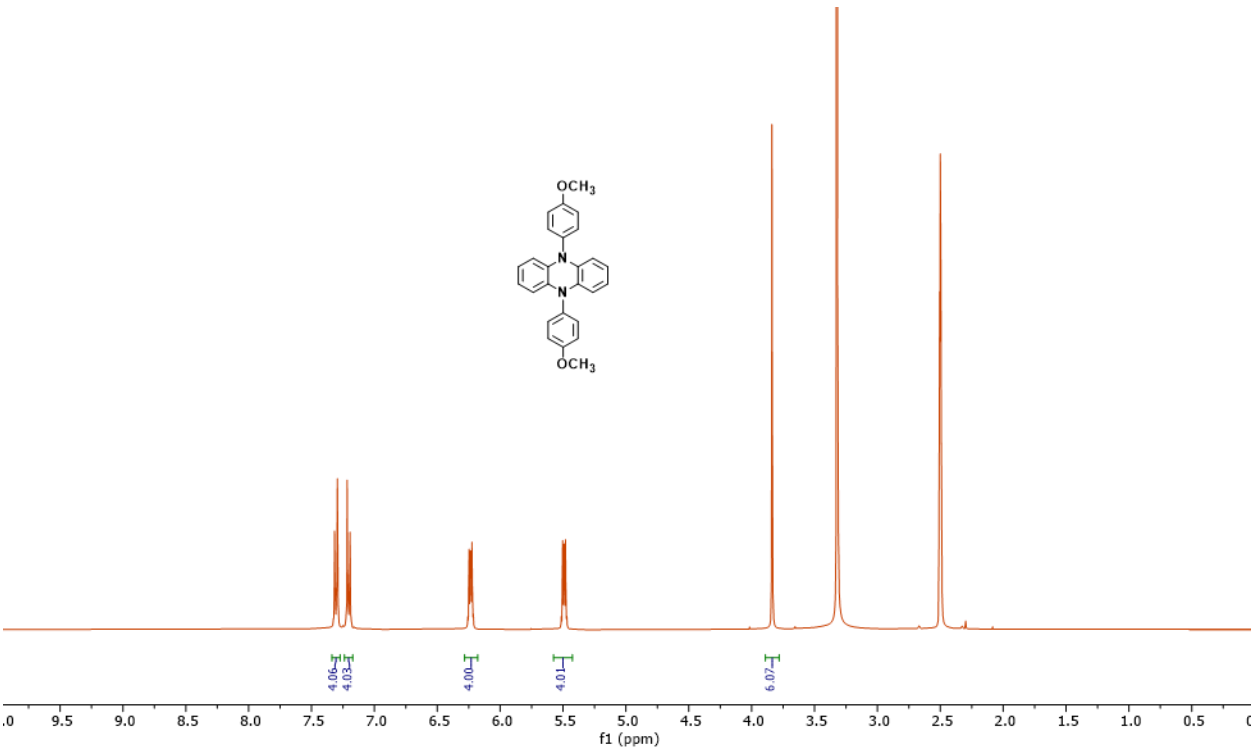

Figure A1.112. ^{1}H-NMR spectrum of PC **4** recrystallization from toluene-hexanes DMSO-d_6.

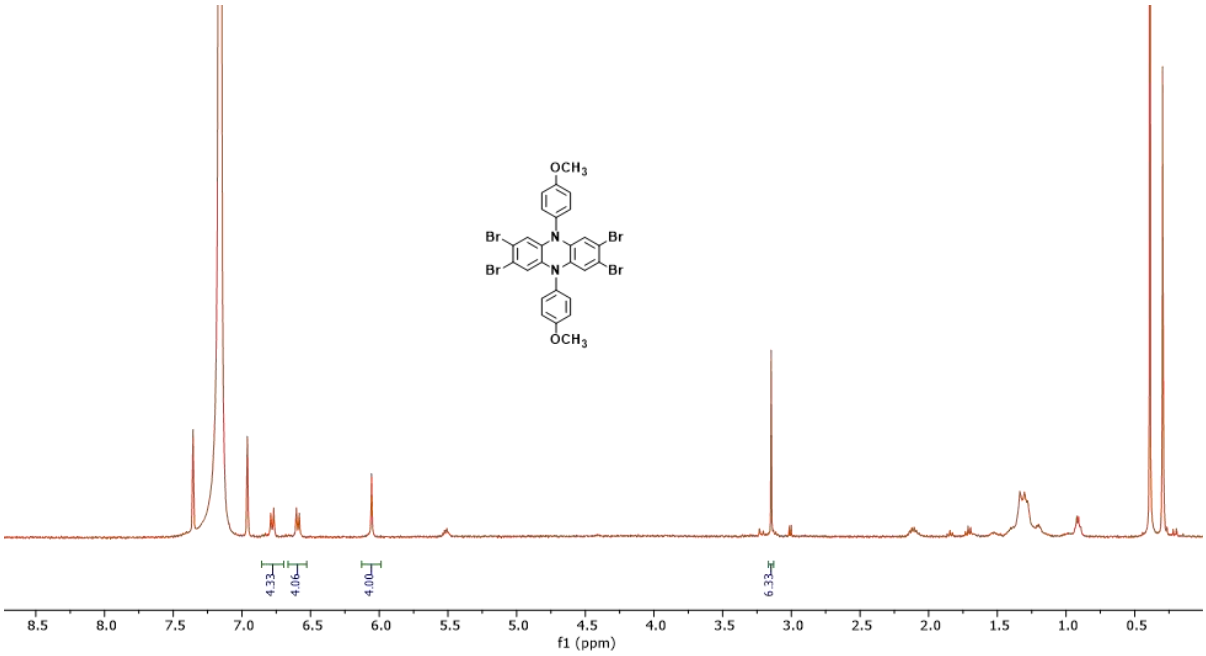

Figure A1.113. ^{1}H-NMR spectrum of unpurified **4-4Br** in C_6D_6.

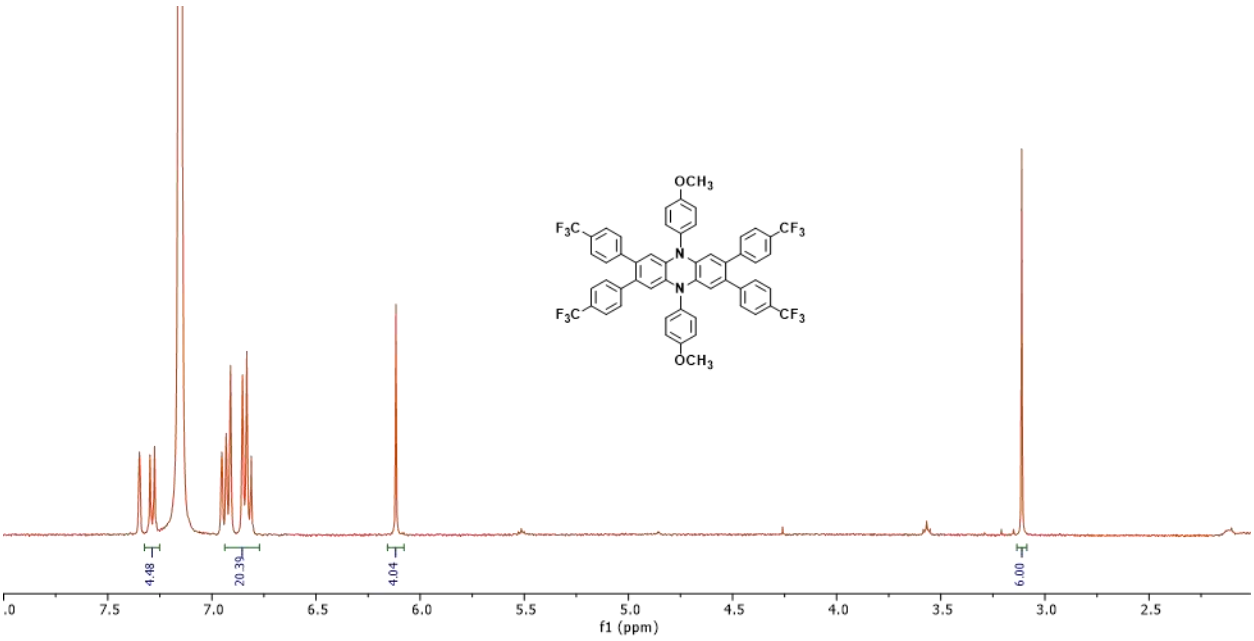

Figure A1.114. ^{1}H-NMR spectrum of **4a** in C_6D_6 after recrystallization.

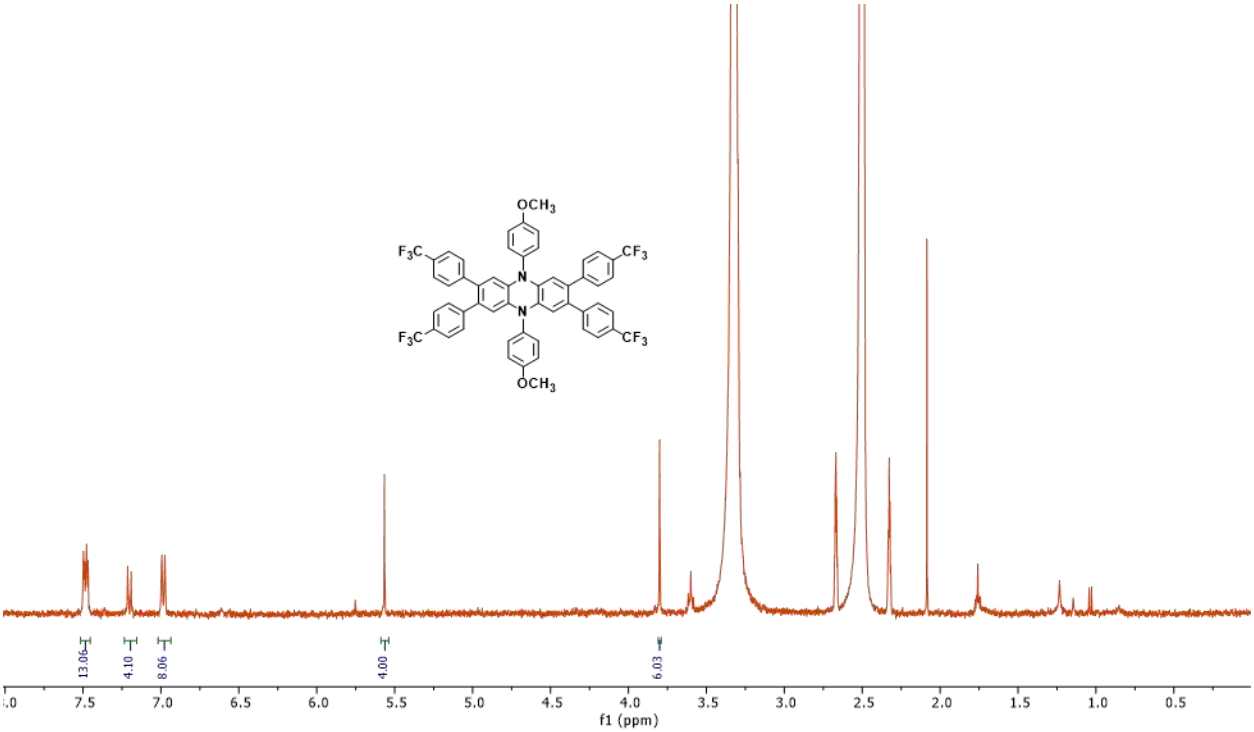

Figure A1.115. ^{1}H-NMR spectrum of **4a** in DMSO-d_6 after recrystallization.

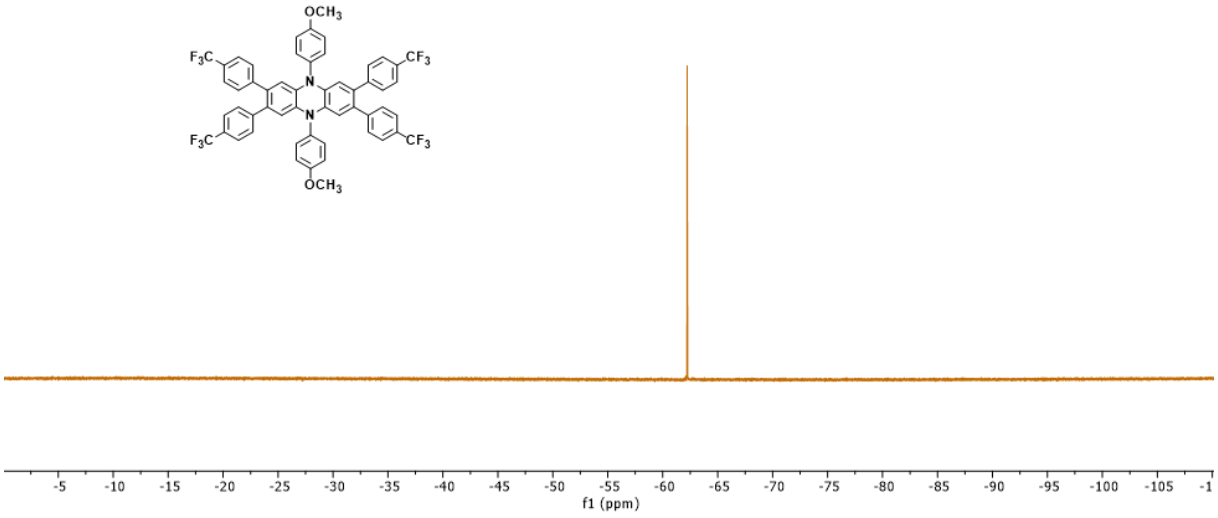

Figure A1.116. ^{19}F-NMR spectrum of **PC 4a** in C_6D_6 after recrystallization.

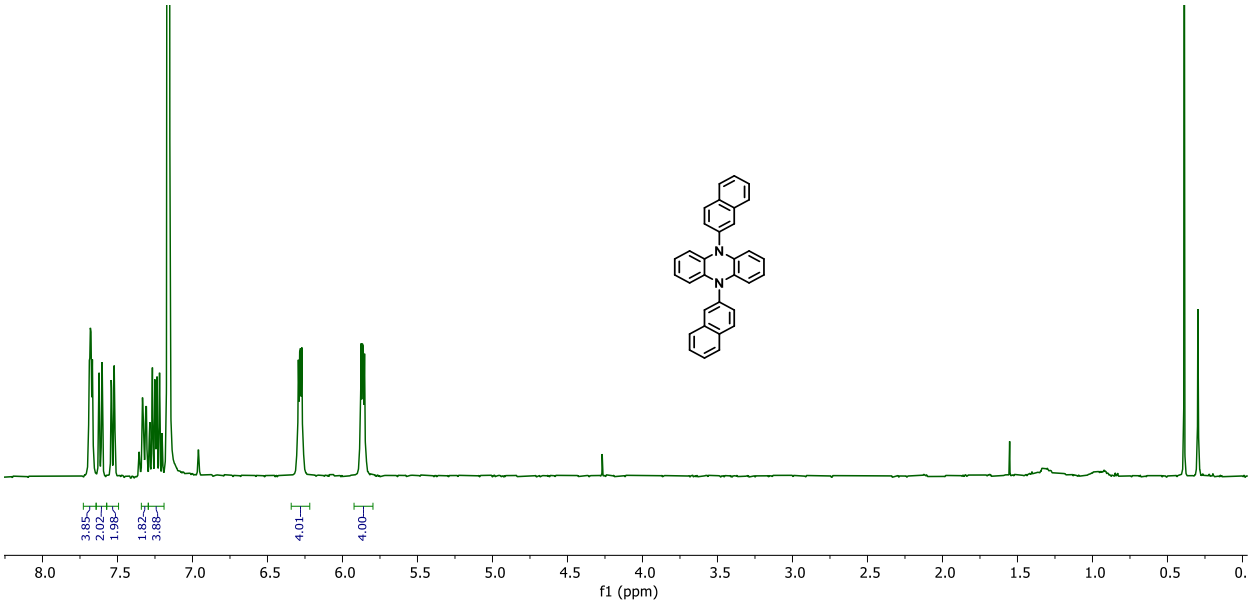

Figure A1.117. ^{1}H-NMR spectrum of PC **5** in C_6D_6 after recrystallization.

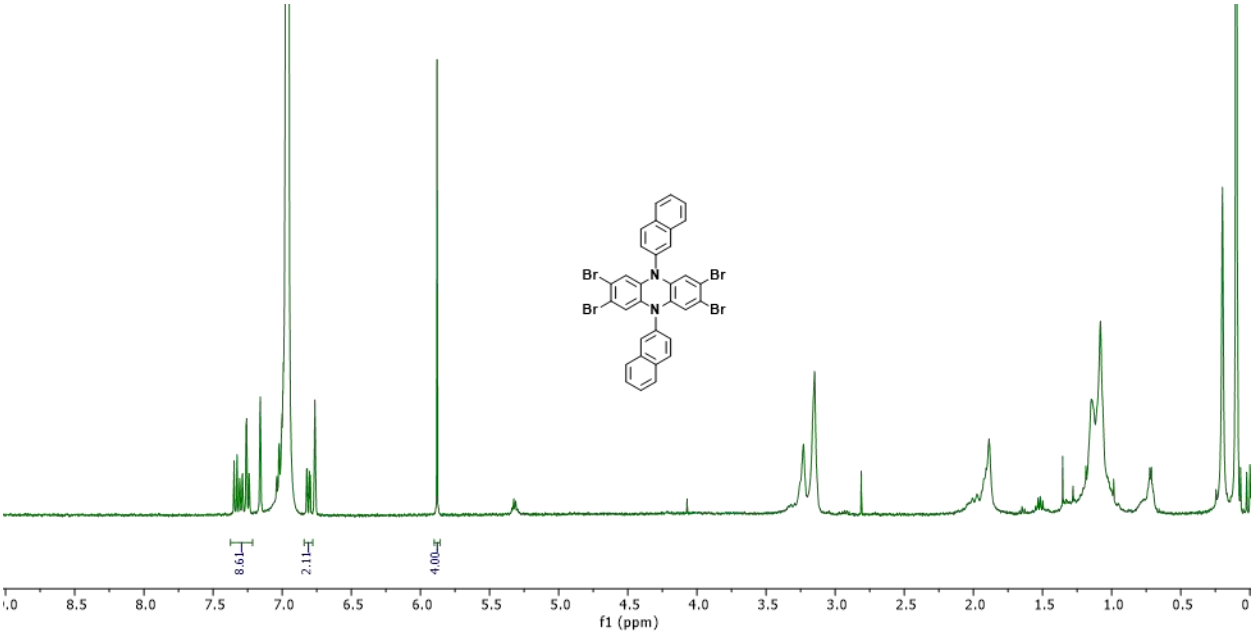

Figure A1.118. ^{1}H-NMR spectrum of unpurified **5-4Br** in C_6D_6.

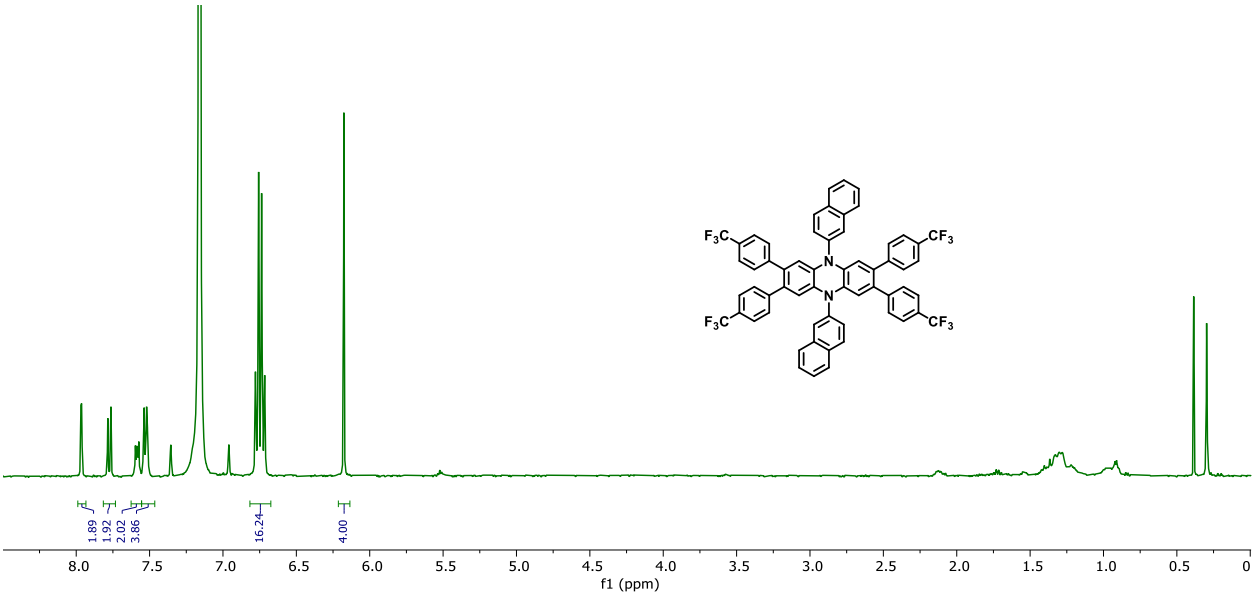

Figure A1.119. ^{1}H-NMR spectrum of PC **5a** in C_6D_6 after recrystallization.

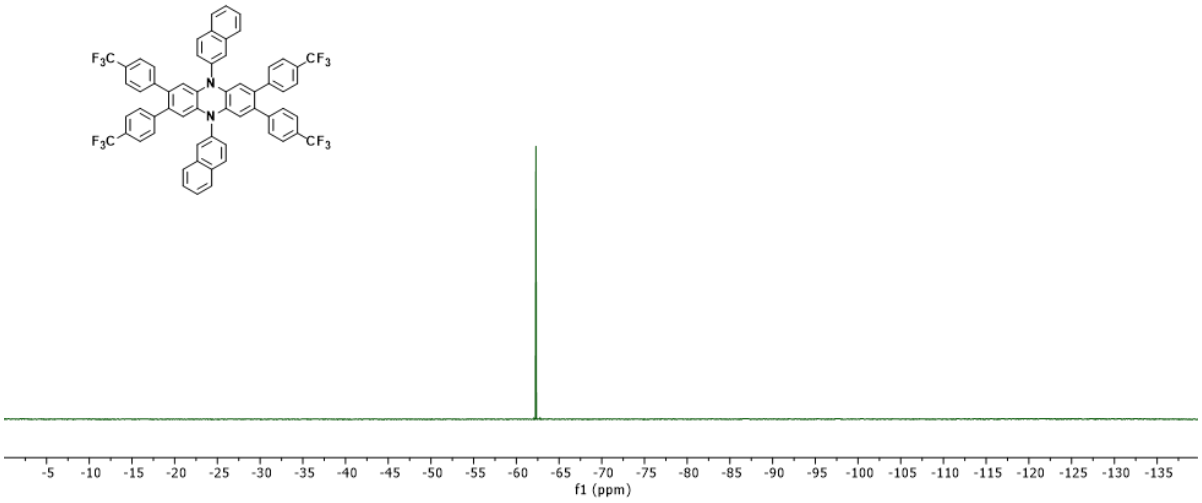

Figure A1.120. ^{19}F-NMR spectrum of **PC 5a** in C_6D_6 after recrystallization.

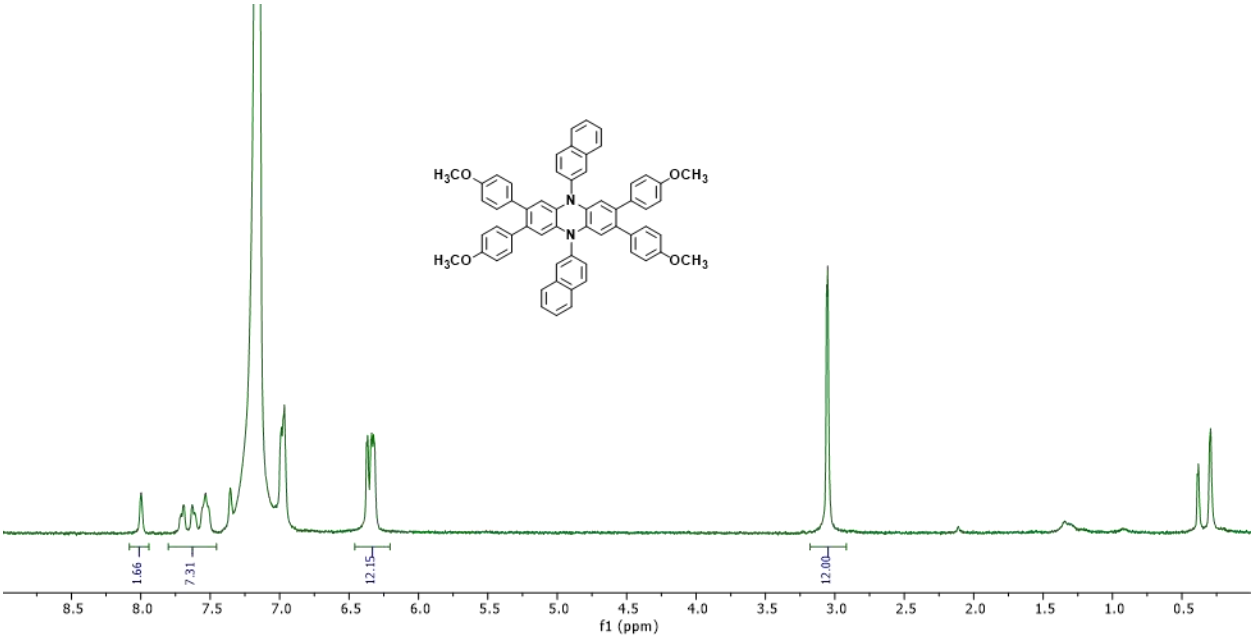

Figure A1.121. ^{1}H-NMR spectrum of PC **5b** in C_6D_6 after recrystallization.

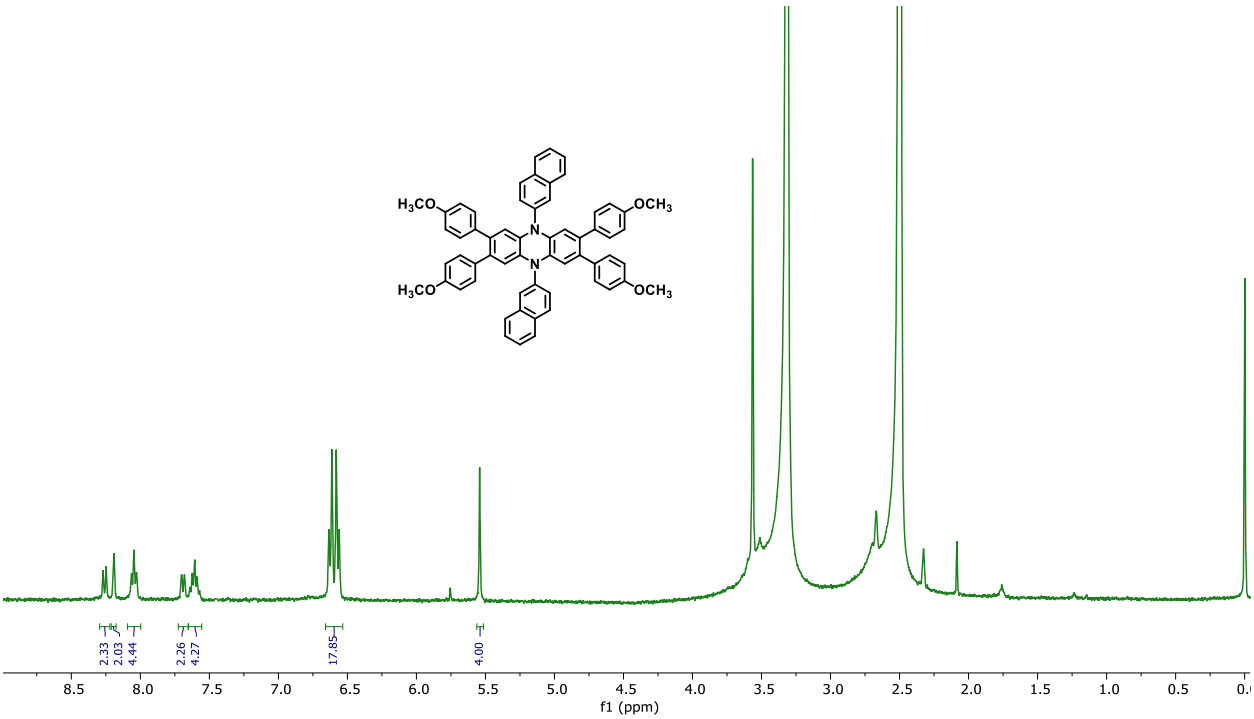

Figure A1.121. ^{1}H-NMR spectrum of PC **5b** in DMSO-d6 after recrystallization.

COMPUTATIONAL DETAILS

All calculations were performed using computational chemistry software package Gaussian 16. This work used the Extreme Science and Engineering Discovery Environment (XSEDE).

Reduction Potentials

Standard reduction potentials (E^0) of **3**, **4, 5, 3a, 3b, 4a, 4b** and **5a, 5b** were calculated following previously reported procedures.[5,6,7,8] A value of -100.5 kcal/mol was assumed for the reduction free energy of the standard hydrogen electrode (SHE). Thus, $E^{0*}_{T1,comp}$ ($^2PC^{\bullet+}/^3PC^*$) was calculated as $E^{0*}_{T1,comp}$ = (-100.5 - ΔG_{red})/23.06 (V vs. SHE) where ΔG_{red} = G($^3PC^*$) – G($^2PC^{\bullet+}$). $E^0_{ox,comp}$ ($^2PC^{\bullet+}/^1PC$) was calculated as ΔG_{red} = G(^1PC) – G($^2PC^{\bullet+}$).

For **3**, **4, 5, 3a, 3b, 4a, 4b** and **5a, 5b** Gibbs free energies of $^3PC^*$, $^2PC^{\bullet+}$, and ^1PC were calculated at the unrestricted M06/6-311+G** level of theory in CPCM-H_2O solvent (single point energy) using geometries optimized at the unrestricted M06/6-31G** level of theory in CPCM-H_2O solvent. Values were converted from V vs. SHE to V vs. SCE by E^0 (V vs. SCE) = E^0 (V vs. SHE) – 0.24 V. The triplet energies ($E_{T1,comp}$) of DHPs and CE-DHPs were obtained by $E_{T1,comp}$(kcal/mol) = [G($^3PC^*$) – G(^1PC)] then converted from kcal/mol to eV by dividing $E_{T1,comp}$(kcal/mol) by 23.06. A CPCM-H_2O solvation model was chosen based on the results of previous work where the computed reduction potential approximates the experimental values within ~0.2 V to ~0.4 V.

Excited State Calculations (TD-DFT)

Using optimized ground state geometries, single point time dependent density functional theory (TD-DFT) calculations were performed using the rCAM-B3LYP/6- 31+G(d,p)/CPCM-DMA level of theory.[9] rCAM-B3LYP was chosen because it gave better λ_{max} predictions that are closer to experimental values in comparison to rωB97xd level of theory.[10]

Electrostatic Potential (ESP) Calculations

For geometries optimized using uM06/6-31G** (ground state singlets and excited state triplets), single point energy calculations with CHELPG[11] ESP population analyses were performed at uM06/6-31G** level of theory using a CPCM-DMAc solvation model. Total electron density of ^{1}PC and ^{3}PC* were first plotted and then were mapped with ESP derived charges to show distribution of charges on the dihydrophenazine derivatives. Molecular orbitals of ^{1}PC (highest occupied molecular orbital (HOMO) and lowest unoccupied molecular orbital (LUMO)) and molecular orbitals of ^{3}PC* (high lying singly occupied molecular orbitals (SOMOs)) were mapped then visualized.

Molecular Coordinates

All coordinates are reported as XYZ Cartesian coordinates. Energies (E_{0K} (not ZPE and thermally corrected)) are computed at uM06/6-311+G**/CPCM-H2O level of theory and are reported in parentheses. Energies are reported in Hartrees units.

PC 3 – (ground state)
(-1341.480383)

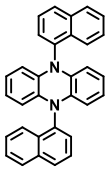

C	-0.62404400	-7.97622400	-0.86454800
C	0.10437400	-6.85423600	-0.46515200
C	0.82601300	-6.85128900	0.72477600
C	0.80991900	-8.00140600	1.54129300
C	0.08422200	-9.11518900	1.12996800
C	-0.63151100	-9.10764700	-0.06859700
C	2.26948800	-6.87543500	3.15480600
C	2.28550900	-5.72529300	2.33831900
C	3.01109400	-4.61145600	2.74971300
H	3.02034300	-3.72623400	2.11958000
C	3.72686600	-4.61901300	3.94825100
C	3.71954300	-5.75049200	4.74412400
C	2.99120100	00	4.34468700
H	0.11702900	-5.96660800	-1.09176600
H	0.07489800	- DC6014600	
H	2.97867700	-7.76018800	4.97123800
N	1.57040300	-5.72795600	1.12746900
N	1.52509800	-7.99878000	2.75210100
H	-1.18992200	-9.99239500	-0.36275200
H	-1.17685000	-7.94909400	-1.79982100
H	4.28518800	-3.73422600	4.24246100
H	4.27242000	-5.77764700	5.67935400
C	1.50356600	-4.53359700	0.35095400
C	0.47380500	-3.58694800	0.61468100
C	2.42550400	-4.31319300	-0.64293200
C	-0.49338500	-3.77674800	1.63097000
C	0.42156300	-2.40543000	-0.18155600
C	2.36880600	-3.14091200	-1.42619500
H	3.19809200	-5.05938900	-0.81621400
C	-1.46942300	-2.83605400	1.84763900
H	-0.45042900	-4.67937900	2.23718500
C	-0.59962400	-1.45633700	0.06847500
C	1.38731400	-2.20982200	-1.19935400
H	3.10607300	-2.98318600	-2.20871900
C	-1.52480500	-1.66508400	1.05983200
H	-2.20722300	-2.99132800	2.63087700
H	-0.63440400	-0.55670600	-0.54370200
H	1.33458600	-1.30306500	-1.79945500
H	-2.30418100	-0.92975300	1.24294600

C	1.59195100	-9.19315300	3.52859900
C	0.67013700	-9.41347900	4.52261900
C	2.62159300	-10.13988500	3.26471900
C	0.72686100	-10.58575400	5.30589000
H	-0.10236400	-8.66721800	4.69600700
C	2.67385900	-11.32139900	4.06096200
C	3.58864700	-9.95017200	2.24828600
C	1.70825100	-11.51691900	5.07891400
H	-0.01030800	-10.74341800	6.08851800
C	3.69493100	-12.27057700	3.81078700
C	4.56457700	-10.89094900	2.03148000
H	3.54568200	-9.04753900	1.64207600
H	1.76101100	-12.42367200	5.67901700
C	4.61998000	-12.06191500	2.81928800
H	3.72973400	-13.17020300	4.42297100
H	5.30227200	-10.73574200	1.24813000
H	5.39927100	-12.79731100	2.63606800

PC 3 – (radical cation)

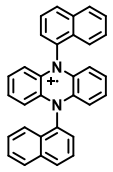

(-1341.309566)

C	-0.63362100	-7.94070200	-0.82768400
C	0.05562400	-6.81439900	-0.43210200
C	0.80845900	-6.82855100	0.75158300
C	0.84544500	-8.00671800	1.53988800
C	0.14076400	-9.14289800	1.11547500
C	-0.58833300	-9.10851200	-0.05389200
C	2.28701200	-6.89823400	3.12783900
C	2.25002500	-5.72006700	2.33953500
C	2.95469200	-4.58388100	2.76395600
H	2.92186200	-3.68218300	2.16154800
C	3.68378300	-4.61826500	3.93332700
C	3.72907500	-5.78607600	4.70711700
C	3.03983800	-6.91238200	4.31153000
H	0.02495000	-5.91124800	-1.03241200
H	0.17358700	-10.04459400	1.71788700
H	3.07051000	-7.81553200	4.91184100
N	1.51472300	-5.71269700	1.16681300
N	1.58074600	-8.01408700	2.71261200
H	-1.13011500	-9.99378800	-0.37198900
H	-1.21223000	-7.91835900	-1.74587400
H	4.22555500	-3.73298500	4.25143000
H	4.30767800	-5.80841700	5.62531000
C	1.46551000	-4.51150600	0.37009300
C	0.44011200	-3.56455400	0.62798700
C	2.40522400	-4.32774900	-0.61166300

C	-0.53924400	-3.73303200	1.63575000
C	0.41406800	-2.39198900	-0.18319200
C	2.36692900	-3.16258800	-1.40453700
H	3.16981100	-5.08498300	-0.76895100
C	-1.50369800	-2.77577200	1.82881800
H	-0.52492600	-4.62551600	2.25778000
C	-0.59658700	-1.42707400	0.04514300
C	1.39258900	-2.22035700	-1.19250300
H	3.11259300	-3.02098200	-2.18109300
C	-1.53469300	-1.61326700	1.02827500
H	-2.25186500	-2.91306100	2.60496500
H	-0.61202200	-0.53447400	-0.57721700
H	1.35634900	-1.31934800	-1.80163800
H	-2.30609600	-0.86632700	1.19502200
C	1.62992800	-9.21526300	3.50935500
C	0.69019600	-9.39897700	4.49110200
C	2.65531100	-10.16224200	3.25150100
C	0.72845400	-10.56411900	5.28400600
H	-0.07437800	-8.64172400	4.64836000
C	2.68131900	-11.33478700	4.06271100
C	3.63469000	-9.99381000	2.24375000
C	1.70277800	-11.50637500	5.07201000
H	-0.01722500	-10.70569000	6.06055300
C	3.69195900	-12.29972800	3.83441900
C	4.59912800	-10.95109400	2.05072500
H	3.62040100	-9.10134200	1.62169700
H	1.73899100	-12.40736900	5.68116900
C	4.63008700	-12.11357800	2.85130000
H	3.70736600	-13.19231100	4.45680400
H	5.34731300	-10.81384000	1.27458800
H	5.40147800	-12.86053900	2.68458600

PC 3 – (neutral triplet)

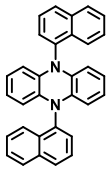

(-1341.394364)

C	-0.64449500	-7.93339200	-0.81949700
C	0.02882400	-6.80218600	-0.41152600
C	0.79837100	-6.82139000	0.76229800
C	0.86474100	-8.01124600	1.53108500
C	0.17989400	-9.15468700	1.09134700
C	-0.56128100	-9.11693000	-0.07005900
C	2.29685000	-6.90536300	3.11743500
C	2.23044400	-5.71553500	2.34860600
C	2.91534200	-4.57209200	2.78823900
H	2.85093000	-3.66541900	2.19497900
C	3.65656200	-4.60979100	3.94961300
C	3.73982100	-5.79329400	4.69910000
C	3.06649400	-6.92452800	4.29120400
H	-0.02047800	-5.88406000	-0.98830400
H	0.24427900	-10.06142400	1.68451300
H	3.11590000	-7.84261700	4.86803100
N	1.50305800	-5.70211700	1.17099200
N	1.59219700	-8.02466500	2.70868100
H	-1.08334500	-10.00948800	-0.40174000
H	-1.23938300	-7.90467700	-1.72750600
H	4.17865400	-3.71722200	4.28122000
H	4.33476800	-5.82197200	5.60707100
C	1.46459300	-4.50599900	0.36835100
C	0.43974100	-3.55687700	0.62637000
C	2.41823700	-4.33067500	-0.62864900
C	-0.53726200	-3.71850300	1.63297200
C	0.41603100	-2.38042900	-0.19394300
C	2.37856000	-3.17894100	-1.41615000
H	3.17844900	-5.09433800	-0.77984600
C	-1.51265500	-2.75090400	1.83192900
H	-0.52135500	-4.61105000	2.25613400
C	-0.59442400	-1.41843700	0.03969000
C	1.39655600	-2.22055400	-1.20460200
H	3.12146500	-3.03681300	-2.19707600
C	-1.54096200	-1.60102400	1.03450600
H	-2.25814200	-2.88971800	2.61161000
H	-0.61222200	-0.52561700	-0.58406000
H	1.36404700	-1.32212700	-1.81903900
H	-2.30908500	-0.84797200	1.19652100
C	1.63083800	-9.22085500	3.51119700
C	0.67736500	-9.39637700	4.50814200
C	2.65568900	-10.16988700	3.25309900
C	0.71714200	-10.54824700	5.29559500
H	-0.08287700	-8.63277400	4.65941400
C	2.67952500	-11.34640800	4.07329500
C	3.63260100	-10.00806800	2.24646800

C	1.69911800	-11.50648600	5.08396000
H	-0.02569900	-10.69052400	6.07654000
C	3.68998600	-12.30833400	3.83958600
C	4.60795700	-10.97554600	2.04744300
H	3.61663100	-9.11548000	1.62337600
H	1.73170200	-12.40495600	5.69831700
C	4.63638300	-12.12556300	2.84479800
H	3.70788600	-13.20121100	4.46324000
H	5.35338100	-10.83659500	1.26774300
H	5.40453200	-12.87855400	2.68269800

PC 3a – (ground state)

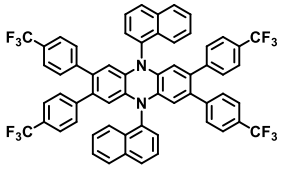

(-3613.344380)

C	-0.59185200	-7.99614500	-0.90141700
C	0.19802400	-6.90594500	-0.50791400
C	0.87661300	-6.87277200	0.70206200
C	0.76229700	-7.97356800	1.57430100
C	-0.01091000	-9.05769100	1.18407800
C	-0.68801700	-9.09954800	-0.04344400
C	2.21835500	-6.85377300	3.17781500
C	2.33267500	-5.75298000	2.30557300
C	3.10597100	-4.66890200	2.69574500
H	3.16647100	-3.80541000	2.03765000
C	3.78314400	-4.62707800	3.92323100
C	3.68697300	-5.73047900	4.78120800
C	2.89702400	-6.82064100	4.38774700
H	0.25819300	-6.04211600	-1.16553400
H	-0.07140600	-9.92118700	1.84216900
H	2.83684600	-7.68446700	5.04537100
N	1.66065500	-5.77028600	1.07421000
N	1.43420300	-7.95620300	2.80572900
C	1.62304200	-4.58477100	0.27804100
C	0.60863200	-3.61820500	0.52826000
C	2.55415300	-4.39550700	-0.71292300
C	-0.36685800	-3.77883500	1.54162200
C	0.58307900	-2.44445200	-0.28044800
C	2.52175600	-3.23073100	-1.50904600
H	3.31349100	-5.15770700	-0.87387100
C	-1.32481100	-2.81668200	1.74374400
H	-0.34767400	-4.67467800	2.15912400
C	-0.42004000	-1.47276400	-0.04493400
C	1.55719500	-2.27910300	-1.29579700
H	3.26495400	-3.09533900	-2.28993400
C	-1.35338700	-1.65299500	0.94430600
H	-2.06901100	-2.94960900	2.52491400
H	-0.43403800	-0.57904400	-0.66638200
H	1.52484300	-1.37806700	-1.90573800

H	-2.11864800	-0.90055500	1.11657900
C	1.47178100	-9.14170700	3.60192200
C	0.54064100	-9.33092800	4.59286400
C	2.48617600	-10.10830400	3.35174900
C	0.57298300	-10.49569400	5.38900500
H	-0.21868100	-8.56870600	4.75377900
C	2.51167000	-11.28204800	4.16047300
C	3.46170500	-9.94771800	2.33841700
C	1.53752000	-11.44735400	5.17579600
H	-0.17023900	-10.63105100	6.16987700
C	3.51476700	-12.25377000	3.92500300
C	4.41963500	-10.90990300	2.13633700
H	3.44257200	-9.05188500	1.72089900
H	1.56982700	-12.34838300	5.78575000
C	4.44815000	-12.07358200	2.93578900
H	3.52871700	-13.14748200	4.54646300
H	5.16386500	-10.77700700	1.35519000
H	5.21339200	-12.82604700	2.76354900
C	4.52498000	-3.39021100	4.25734300
C	5.40930000	-2.83023000	3.32607800
C	4.33435600	-2.73265400	5.47742900
C	6.09067700	-1.65717100	3.60986300
H	5.57363200	-3.33484900	2.37635600
C	5.01276700	-1.55680000	5.76710800
H	3.63805700	-3.14463300	6.20447000
C	5.89388200	-1.02073500	4.83377100
H	6.78317900	-1.23567100	2.88440100
H	4.85233900	-1.05280500	6.71556000
C	4.40955500	-5.83279700	6.06916500
C	5.78042600	-5.56835700	6.16030100
C	3.72861600	-6.24122100	7.22358000
C	6.45263600	-5.69637100	7.36805400
H	6.32795800	-5.26692400	5.27007600
C	4.39377200	-6.36988200	8.43252100
H	2.66075100	-6.44218900	7.17003800
C	5.75794100	-6.09486500	8.50526000
H	7.51799800	-5.49339600	7.42428700
H	3.85417300	-6.67781700	9.32561900
C	-1.42977800	-10.33645000	-0.37759300
C	-1.23902400	-10.99403400	-1.59764400
C	-2.31417700	-10.89642400	0.55360200
C	-1.91738400	-12.16991100	-1.88735400
H	-0.54266800	-10.58205900	-2.32463100
C	-2.99550800	-12.06950200	0.26978200
H	-2.47861200	-10.39178200	1.50329200
C	-2.79858400	-12.70596500	-0.95409200
H	-1.75685800	-12.67392500	-2.83578000
H	-3.68807400	-12.49099100	0.99518800
C	-1.31436900	-7.89385900	-2.18941200
C	-2.68521900	-8.15839300	-2.28062000
C	-0.63340600	-7.48535700	-3.34378200

C	-3.35737900	-8.03040200	-3.48840300
H	-3.23277500	-8.45987700	-1.39042700
C	-1.29851400	-7.35671100	-4.55275200
H	0.43444200	-7.28431300	-3.29018600
C	-2.66265900	-7.63182200	-4.62556400
H	-4.42272600	-8.23344400	-3.54469200
H	-0.75889800	-7.04869700	-5.44581300
C	6.43993900	-6.25001000	9.82476900
C	6.63810900	0.24633900	5.10014200
C	-3.54271600	-13.97308900	-1.22049300
C	-3.34457500	-7.47679700	-5.94512900
F	6.29997800	1.21036800	4.22787500
F	6.41583400	0.72796800	6.32717300
F	7.96394300	0.07585600	4.97269600
F	7.73692300	-5.92968300	9.77812000
F	5.87240200	-5.47900400	10.76658700
F	6.35823300	-7.51225800	10.27662500
F	-4.86855500	-13.80273800	-1.09295100
F	-3.32047000	-14.45461700	-2.44756900
F	-3.20443300	-14.93714600	-0.34831400
F	-4.64164300	-7.79676900	-5.89844500
F	-2.77722000	-8.24818400	-6.88674900
F	-3.26251300	-6.21467900	-6.39727900

PC 3a – radical cation

(-3613.167923)

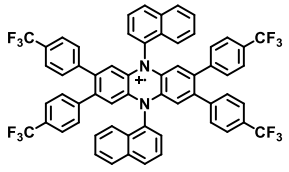

C	-0.66910600	-7.99179700	-0.84901300
C	0.09092800	-6.90013500	-0.45864600
C	0.80099000	-6.88948000	0.74542000
C	0.72548400	-8.01732300	1.59726400
C	-0.02121600	-9.12640400	1.18982400
C	-0.70525300	-9.14374200	-0.01576800
C	2.16053100	-6.91404500	3.18500000
C	2.23610400	-5.78624800	2.33310200
C	2.98296000	-4.67724400	2.74046700
H	2.99646200	-3.79269200	2.11018300
C	3.66701600	-4.65992900	3.94604400
C	3.63065200	-5.81175900	4.77942800
C	2.87051300	-6.90336200	4.38911200
H	0.10683600	-6.01393600	-1.08650800
H	-0.03459300	-10.01100100	1.82004200
H	2.85446400	-7.78950300	5.01704200
N	1.55759200	-5.79692700	1.12826900
N	1.40390700	-8.00659300	2.80216400
C	1.64849600	-4.65569100	0.25085500
C	0.69458100	-3.61295800	0.38153600
C	2.65244700	-4.62232600	-0.68301800
C	-0.34766800	-3.62509800	1.33899200

C	0.81250800	-2.50656300	-0.51043600
C	2.75659500	-3.52043300	-1.55588700
H	3.35703300	-5.44868100	-0.74060400
C	-1.23639100	-2.58106700	1.40523100
H	-0.44183200	-4.46563400	2.02349300
C	-0.12306600	-1.44868600	-0.41197500
C	1.85507600	-2.49001100	-1.46866200
H	3.55244100	-3.49744300	-2.29420100
C	-1.12552000	-1.48392700	0.52351100
H	-2.03381300	-2.59802100	2.14337400
H	-0.02844700	-0.60720100	-1.09543700
H	1.92719100	-1.63654100	-2.13989200
H	-1.83877200	-0.66687000	0.59056100
C	1.31298500	-9.14784700	3.67954300
C	0.30897400	-9.18125800	4.61335400
C	2.26691500	-10.19055800	3.54886000
C	0.20478600	-10.28320300	5.48615700
H	-0.39562200	-8.35491300	4.67093500
C	2.14893500	-11.29701100	4.44075500
C	3.30921100	-10.17836300	2.59145700
C	1.10631100	-11.31362000	5.39891700
H	-0.59109100	-10.30623800	6.22443700
C	3.08451400	-12.35488200	4.34228000
C	4.19794300	-11.22238500	2.52521000
H	3.40340700	-9.33778800	1.90700900
H	1.03414200	-12.16713800	6.07008000
C	4.08702500	-12.31958000	3.40685700
H	2.98985200	-13.19641200	5.02568200
H	4.99541400	-11.20537700	1.78712100
H	4.80027600	-13.13663600	3.33978900
C	4.37442700	-3.41619100	4.32312800
C	5.22190100	-2.79062200	3.40099500
C	4.17663700	-2.82443600	5.57450600
C	5.86497200	-1.60711400	3.72691600
H	5.39169800	-3.24988000	2.42975700
C	4.81313600	-1.63518800	5.90138100
H	3.50842000	-3.29198200	6.29383800
C	5.65960500	-1.03080000	4.97840800
H	6.53174200	-1.13062700	3.01206100
H	4.64855300	-1.17672600	6.87163800
C	4.40586300	-5.91946900	6.03505400
C	5.76972200	-5.61290200	6.06768800
C	3.78401700	-6.37989100	7.20181500
C	6.49852600	-5.75972200	7.23960500
H	6.26812000	-5.26929600	5.16431900
C	4.50703700	-6.52014200	8.37579900
H	2.72093800	-6.60962300	7.18943800
C	5.86488900	-6.20943300	8.39280800
H	7.55912700	-5.52841300	7.25509500
H	4.01756700	-6.86729700	9.28282200
C	-1.41238000	-10.38757500	-0.39304600

C	-1.21470000	-10.97888600	-1.64464300
C	-2.25945200	-11.01369900	0.52909800
C	-1.85088100	-12.16825100	-1.97173000
H	-0.54680400	-10.51091600	-2.36399700
C	-2.90217600	-12.19733500	0.20298200
H	-2.42919200	-10.55477900	1.50050400
C	-2.69689400	-12.77321700	-1.04872700
H	-1.68636400	-12.62636400	-2.94216300
H	-3.56861300	-12.67428000	0.91784400
C	-1.44446200	-7.88408400	-2.10454800
C	-2.80824200	-8.19103800	-2.13701000
C	-0.82291600	-7.42332400	-3.27132200
C	-3.53726600	-8.04425300	-3.30879200
H	-3.30639400	-8.53493400	-1.23361600
C	-1.54616200	-7.28310300	-4.44517600
H	0.24009900	-7.19328300	-3.25906300
C	-2.90392600	-7.59419100	-4.46202600
H	-4.59780300	-8.27586500	-3.32415900
H	-1.05692800	-6.93567200	-5.35222200
C	6.61152200	-6.38072000	9.67728300
C	6.36528600	0.25062300	5.28913400
C	-3.40241500	-14.05465800	-1.35973300
C	-3.65079500	-7.42292700	-5.74636600
F	5.99617200	1.22896800	4.44804000
F	6.12715500	0.68200800	6.53074700
F	7.69409500	0.12123100	5.15727700
F	7.89629400	-6.02899000	9.57760000
F	6.06949500	-5.64522200	10.65982900
F	6.57662400	-7.65492100	10.09657200
F	-4.73131900	-13.92514000	-1.22888700
F	-3.16340300	-14.48629300	-2.60108700
F	-3.03400100	-15.03286000	-0.51817300
F	-4.93545300	-7.77504000	-5.64654400
F	-3.10870500	-8.15812700	-6.72910000
F	-3.61632300	-6.14865600	-6.16547400

PC 3a – neutral triplet

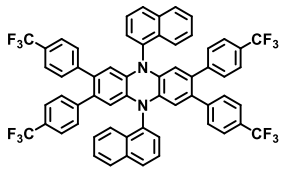

(-3613.271630)

C	-0.55555200	-7.96619300	-0.88116200
C	0.23542000	-6.89090500	-0.50166200
C	0.90766300	-6.85223700	0.72449100
C	0.76812400	-7.94716400	1.61328200
C	-0.02003000	-9.03482500	1.22268600
C	-0.67358300	-9.07648700	-0.00081600
C	2.21346300	-6.85301700	3.21652300
C	2.35131400	-5.72700900	2.30756000
C	3.09474900	-4.62990800	2.71119900
H	3.08645500	-3.74957100	2.07426000

C	3.73830600	-4.56098100	3.95063200
C	3.75246700	-5.78126900	4.78675000
C	2.92125200	-6.83954400	4.40794900
H	0.30668100	-6.03272100	-1.16468300
H	-0.09161500	-9.89331100	1.88535100
H	2.90571900	-7.73860100	5.01822000
N	1.68884200	-5.76961300	1.09241300
N	1.42279400	-7.92341900	2.83312800
C	1.79723900	-4.64853200	0.19953200
C	0.83893900	-3.60457600	0.29128200
C	2.81977700	-4.61653800	-0.71386900
C	-0.22045300	-3.60891800	1.23027700
C	0.96630900	-2.50905900	-0.61225300
C	2.93645700	-3.52617400	-1.60074200
H	3.53080800	-5.43902500	-0.74420700
C	-1.11671300	-2.57022700	1.26775400
H	-0.31643600	-4.44228800	1.92312300
C	0.02196300	-1.45571800	-0.54523300
C	2.02824200	-2.49910600	-1.54922000
H	3.74783400	-3.50893000	-2.32264000
C	-0.99697100	-1.48440000	0.37248400
H	-1.92661600	-2.58134500	1.99255300
H	0.12366800	-0.62259900	-1.23823800
H	2.11019700	-1.65504400	-2.23140800
H	-1.71620000	-0.67072100	0.41531700
C	1.30221400	-9.04931000	3.71836900
C	0.31189100	-9.05120600	4.66713400
C	2.22231900	-10.12348000	3.59070800
C	0.18504600	-10.14437100	5.54911500
H	-0.36676500	-8.20347900	4.72815700
C	2.08391000	-11.22242500	4.48841700
C	3.25649500	-10.14413500	2.62419700
C	1.05272400	-11.20330500	5.45897000
H	-0.60248400	-10.13901100	6.29711500
C	2.98848300	-12.30717500	4.38397400
C	4.11550700	-11.21207500	2.55203500
H	3.36477200	-9.30509900	1.94004700
H	0.96232700	-12.05047400	6.13621200
C	3.98183600	-12.30366400	3.43824500
H	2.87750800	-13.14337000	5.07182300
H	4.90695700	-11.21941700	1.80709600
H	4.67085000	-13.14114500	3.36703400
C	4.23287000	-3.27441700	4.40717000
C	4.72537500	-2.31176100	3.49326000
C	4.21183600	-2.90908900	5.77300000
C	5.15812100	-1.07151600	3.91462800
H	4.79920200	-2.56308000	2.43747400
C	4.63476600	-1.66055700	6.19468200
H	3.82220800	-3.60956100	6.50666400
C	5.11413200	-0.73163700	5.27213100
H	5.54580400	-0.35613600	3.19167900

H	4.58511200	-1.40087300	7.24867400
C	4.68064600	-5.98292400	5.88521600
C	5.96439800	-5.39071700	5.89131000
C	4.35168200	-6.81413800	6.98262300
C	6.86559800	-5.62792000	6.91423700
H	6.26592200	-4.76256600	5.05743300
C	5.24539400	-7.04097100	8.00908000
H	3.36046000	-7.25863600	7.04036700
C	6.51527500	-6.45223100	7.98296400
H	7.85371200	-5.17702700	6.87982700
H	4.96025500	-7.67242700	8.84840900
C	-1.41843900	-10.30740800	-0.34487700
C	-1.22307400	-10.95825900	-1.56820500
C	-2.30899400	-10.86836000	0.57983400
C	-1.89955900	-12.13328000	-1.86424200
H	-0.52390300	-10.54466300	-2.29143500
C	-2.98921500	-12.03994400	0.28795400
H	-2.48049200	-10.36551600	1.52911500
C	-2.78559100	-12.67204500	-0.93699600
H	-1.73466700	-12.63386700	-2.81363400
H	-3.68668200	-12.46278400	1.00768400
C	-1.27736600	-7.87382200	-2.16897600
C	-2.64837600	-8.14061200	-2.25643800
C	-0.59645300	-7.47100200	-3.32534900
C	-3.32172600	-8.01466500	-3.46339300
H	-3.19581400	-8.43904800	-1.36524500
C	-1.26363900	-7.34584900	-4.53342200
H	0.47194100	-7.27261900	-3.27469400
C	-2.62822400	-7.61905300	-4.60251900
H	-4.38731900	-8.21656700	-3.51751500
H	-0.72529800	-7.04038900	-5.42793800
C	7.43920800	-6.69443100	9.12206100
C	5.60827400	0.60715300	5.68817700
C	-3.52930900	-13.93802600	-1.21221800
C	-3.30849200	-7.48951100	-5.92615000
F	4.99449600	1.59996100	5.01775300
F	5.42879200	0.84432000	6.99338000
F	6.92338200	0.76062000	5.43944900
F	8.66769500	-6.20802800	8.90588200
F	6.99327700	-6.13448900	10.26365100
F	7.57403600	-8.00628000	9.38949400
F	-4.85505300	-13.76774100	-1.08681500
F	-3.30373600	-14.41242300	-2.44123200
F	-3.19247600	-14.90603000	-0.34428000
F	-4.62616800	-7.70083500	-5.85304000
F	-2.81496900	-8.36194400	-6.82008000
F	-3.12846000	-6.26900600	-6.45543800

PC 3b – ground state

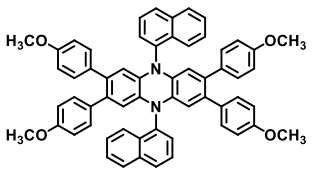

(-2723.174535)

C	-0.69255400	-7.98979900	-0.84839500
C	0.03416200	-6.87325900	-0.40600800
C	0.79224700	-6.88288000	0.75638100
C	0.81039100	-8.05157100	1.54239900
C	0.11610300	-9.16664900	1.09497200
C	-0.62983900	-9.17060500	-0.09412600
C	2.26854300	-6.94326900	3.15627400
C	2.25040600	-5.77458000	2.37025400
C	2.94471100	-4.65951000	2.81767200
H	2.88289800	-3.73926600	2.24108500
C	3.69068100	-4.65556100	4.00675600
C	3.75337900	-5.83637000	4.76102700
C	3.02663200	-6.95289300	4.31866100
H	-0.02691500	-5.95320700	-0.98296100
H	0.17792100	-10.08689300	1.67155800
H	3.08770000	-7.87293400	4.89563200
N	1.51954100	-5.75635900	1.17195300
N	1.54113900	-8.06974100	2.74076500
C	1.60060700	-4.61759700	0.31556000
C	0.64638900	-3.57084600	0.44577000
C	2.59915700	-4.55004100	-0.62546800
C	-0.39546300	-3.60347800	1.40390100
C	0.75171000	-2.44969600	-0.42924900
C	2.69823200	-3.43725100	-1.48625800
H	3.31092100	-5.37007200	-0.69535300
C	-1.29427900	-2.56946500	1.48940700
H	-0.47000000	-4.46129200	2.06920300
C	-0.19305500	-1.40089800	-0.31318200
C	1.79269600	-2.41122900	-1.38879500
H	3.49409800	-3.40010300	-2.22515600
C	-1.19385600	-1.45793700	0.62338200
H	-2.09085200	-2.60360400	2.22848300
H	-0.10753700	-0.54789200	-0.98417300
H	1.85940700	-1.54836700	-2.04916700
H	-1.91372200	-0.64732900	0.70337200
C	1.46007800	-9.20851300	3.59714300
C	0.46146700	-9.27603500	4.53811000
C	2.41425900	-10.25530600	3.46698200
C	0.36226300	-10.38882000	5.39888500
H	-0.25026300	-8.45596900	4.60794300
C	2.30879600	-11.37646300	4.34198200
C	3.45618900	-10.22273200	2.50893400
C	1.26774300	-11.41489200	5.30145800
H	-0.43366100	-10.42592800	6.13772200
C	3.25349200	-12.42532600	4.22597000
C	4.35494000	-11.25681000	2.42348800

H	3.53084900	-9.36491700	1.84364600
H	1.20095000	-12.27776900	5.96180200
C	4.25436800	-12.36834400	3.28948300
H	3.16786300	-13.27834000	4.89693800
H	5.15157500	-11.22271400	1.68447600
H	4.97418200	-13.17900300	3.20953500
C	4.32462100	-3.38309400	4.42128200
C	5.05579200	-2.61676000	3.51265600
C	4.16804500	-2.87601000	5.72062800
C	5.62375300	-1.39471400	3.86791600
H	5.20004200	-2.98842300	2.49918600
C	4.72310100	-1.66496900	6.09035400
H	3.59160600	-3.44383100	6.44854600
C	5.45775600	-0.91394500	5.16582000
H	6.19171500	-0.83637700	3.12994700
H	4.59435500	-1.26828900	7.09464200
C	4.58691700	-5.98976300	5.97534400
C	5.93339600	-5.59414900	5.99505200
C	4.07145800	-6.58414700	7.12793000
C	6.71966200	-5.77953000	7.11705700
H	6.36877700	-5.14038700	5.10676500
C	4.84839200	-6.77740100	8.26857900
H	3.02776000	-6.89474500	7.14412300
C	6.18218700	-6.37199800	8.26536900
H	7.76521800	-5.48085200	7.12887700
H	4.40267400	-7.23687900	9.14559300
C	-1.26377000	-10.44306500	-0.50868900
C	-1.10705600	-10.95018200	-1.80799700
C	-1.99511400	-11.20932900	0.39986300
C	-1.66217000	-12.16118500	-2.17778300
H	-0.53045600	-10.38243300	-2.53584300
C	-2.56312500	-12.43133000	0.04454300
H	-2.13945600	-10.83763300	1.41330700
C	-2.39699700	-12.91213500	-1.25333500
H	-1.53332500	-12.55789100	-3.18204900
H	-3.13120100	-12.98963300	0.78245000
C	-1.52609400	-7.83640100	-2.06271800
C	-2.87254800	-8.23198700	-2.08242900
C	-1.01058600	-7.24200800	-3.21530200
C	-3.65879700	-8.04666000	-3.20448300
H	-3.30794800	-8.68569000	-1.19412200
C	-1.78747900	-7.04879500	-4.35596500
H	0.03310900	-6.93140200	-3.23142100
C	-3.12128700	-7.45423700	-4.35278400
H	-4.70436100	-8.34529700	-3.21626900
H	-1.34180300	-6.58925800	-5.23296900
O	5.96201000	0.25903700	5.62393400
O	7.03240100	-6.50920800	9.31336500
O	-2.90134700	-14.08505400	-1.71152200
O	-3.97147300	-7.31700000	-5.40080600
C	6.70143600	1.05318100	4.71965200

H	7.59421200	0.52680600	4.35671300
H	6.09216700	1.35716300	3.85806000
H	7.01125900	1.94334700	5.26941200
C	6.53301500	-7.11199700	10.48907600
H	5.70457800	-6.53351100	10.91909500
H	6.19141700	-8.13881200	10.30227800
H	7.35920700	-7.13494700	11.20148400
C	-3.64083900	-14.87922800	-0.80732900
H	-3.03160000	-15.18333700	0.05423700
H	-4.53359900	-14.35284700	-0.44436200
H	-3.95071100	-15.76932800	-1.35717400
C	-3.47209300	-6.71416100	-6.57649900
H	-2.64368400	-7.29268800	-7.00656000
H	-3.13047100	-5.68738500	-6.38965900
H	-4.29828600	-6.69123400	-7.28890500

PC 3b – radical cation

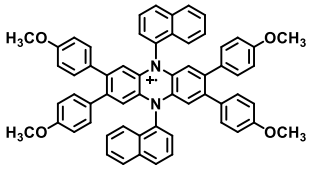

(-2723.007417)

C	-0.66955200	-7.96878000	-0.84112900
C	0.06362600	-6.86650100	-0.42172400
C	0.81542700	-6.87900600	0.75507200
C	0.80357200	-8.04094200	1.56294900
C	0.09663800	-9.16209200	1.12364500
C	-0.62134900	-9.16338900	-0.06505800
C	2.24528200	-6.94713700	3.15756600
C	2.25713700	-5.78520100	2.34968900
C	2.96407600	-4.66405400	2.78899000
H	2.91248600	-3.75017600	2.20401200
C	3.68206600	-4.66275700	3.97769100
C	3.73026900	-5.85736700	4.75376200
C	2.99708800	-6.95964400	4.33435900
H	0.01597600	-5.95023200	-1.00334200
H	0.14823000	-10.07597000	1.70862200
H	3.04473900	-7.87591400	4.91597500
N	1.54805500	-5.77617000	1.16045700
N	1.51265500	-8.04997400	2.75218000
C	1.61524200	-4.61884300	0.30521700
C	0.65285100	-3.58689400	0.45788400
C	2.61286500	-4.55630700	-0.63419800
C	-0.38466300	-3.62652500	1.42000600
C	0.75544600	-2.46283100	-0.41403100
C	2.70267300	-3.43829000	-1.48777400
H	3.32553900	-5.37433500	-0.71025900
C	-1.28311600	-2.59266100	1.51027800
H	-0.46520200	-4.48193500	2.08771000
C	-0.18961900	-1.41591200	-0.29096900
C	1.79255700	-2.41787700	-1.37725800
H	3.49447100	-3.39433700	-2.22965900

C	-1.18689000	-1.47810300	0.64860800
H	-2.07678700	-2.63092600	2.25176700
H	-0.10671800	-0.56076600	-0.95891500
H	1.85298200	-1.55117100	-2.03261300
H	-1.90745400	-0.66916900	0.73455600
C	1.44548100	-9.20730500	3.60741500
C	0.44786700	-9.26985500	4.54683700
C	2.40787900	-10.23924500	3.45473400
C	0.35807600	-10.38787900	5.40040800
H	-0.26481400	-8.45183400	4.62290900
C	2.30530300	-11.36331400	4.32664300
C	3.44538400	-10.19959700	2.49260200
C	1.26820100	-11.40828200	5.28987900
H	-0.43371500	-10.43184300	6.14230000
C	3.25037800	-12.41022200	4.20356700
C	4.34384600	-11.23345300	2.40231700
H	3.52590900	-9.34418300	1.82490300
H	1.20779000	-12.27499200	5.94522900
C	4.24763900	-12.34801600	3.26398100
H	3.16749100	-13.26537300	4.87150900
H	5.13751000	-11.19517500	1.66082100
H	4.96821100	-13.15694300	3.17802300
C	4.32254700	-3.40206900	4.40110900
C	5.04380400	-2.62906300	3.48902800
C	4.17564000	-2.91181200	5.70897400
C	5.61502800	-1.41329600	3.85172900
H	5.18381300	-2.99331300	2.47270900
C	4.72666100	-1.70171400	6.08082000
H	3.60635000	-3.48532000	6.43730800
C	5.45468400	-0.94287700	5.15556700
H	6.18050000	-0.84994400	3.11622400
H	4.60343700	-1.31169000	7.08792200
C	4.56242900	-5.99475600	5.96509000
C	5.90399400	-5.57978000	5.98017300
C	4.04990100	-6.59711800	7.11569900
C	6.69205800	-5.76245700	7.09905100
H	6.33494900	-5.12117400	5.09280400
C	4.82792300	-6.77735300	8.25508700
H	3.00892000	-6.91527500	7.13395700
C	6.15926000	-6.35955600	8.24864900
H	7.73476200	-5.45554300	7.11041600
H	4.38703200	-7.23671200	9.13413300
C	-1.26182500	-10.42407800	-0.48847900
C	-1.11491900	-10.91432800	-1.79634700
C	-1.98307800	-11.19709100	0.42359900
C	-1.66593500	-12.12442700	-2.16819800
H	-0.54563300	-10.34081400	-2.52467900
C	-2.55429700	-12.41285900	0.06089400
H	-2.12308700	-10.83284600	1.43992000
C	-2.39395300	-12.88327100	-1.24294600
H	-1.54271200	-12.51444600	-3.17530200

H	-3.11976600	-12.97621600	0.79639600
C	-1.50170600	-7.83139500	-2.05246200
C	-2.84326700	-8.24638300	-2.06755300
C	-0.98917600	-7.22902900	-3.20306700
C	-3.63132600	-8.06371100	-3.18643600
H	-3.27422400	-8.70499400	-1.18018700
C	-1.76719300	-7.04879900	-4.34245900
H	0.05180300	-6.91086400	-3.22131800
C	-3.09852600	-7.46660600	-4.33602900
H	-4.67402700	-8.37063300	-3.19780700
H	-1.32630000	-6.58943600	-5.22150200
O	5.95862500	0.22280600	5.61793900
O	7.00834600	-6.48664000	9.29242600
O	-2.89789000	-14.04895400	-1.70532300
O	-3.94760700	-7.33952800	-5.37981200
C	6.69267300	1.03023700	4.71771700
H	7.58476500	0.50936300	4.34685500
H	6.07696700	1.34116400	3.86389000
H	7.00138000	1.91423600	5.27727600
C	6.51981900	-7.09276300	10.47354100
H	5.68849400	-6.52026800	10.90468600
H	6.18918800	-8.12294300	10.28875000
H	7.35038600	-7.10473800	11.18058100
C	-3.63191800	-14.85639900	-0.80509700
H	-3.01620100	-15.16731700	0.04872500
H	-4.52401700	-14.33554200	-0.43422800
H	-3.94061400	-15.74040300	-1.36465500
C	-3.45907900	-6.73339300	-6.56092000
H	-2.62774800	-7.30587800	-6.99206600
H	-3.12845600	-5.70321200	-6.37611900
H	-4.28964400	-6.72141800	-7.26796300

PC 3b – neutral triplet

(-2723.094158)

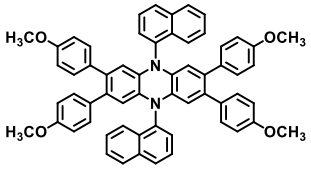

C	-0.59033900	-7.99113900	-0.87037500
C	0.18686200	-6.91121900	-0.47051700
C	0.88822700	-6.89156000	0.73992100
C	0.78896000	-8.01495500	1.60045000
C	0.02287300	-9.10993400	1.18691600
C	-0.65817900	-9.13535100	-0.02372400
C	2.23980700	-6.93265700	3.21463400
C	2.32944700	-5.77004200	2.33592800
C	3.03873000	-4.66016700	2.77128800
H	2.98863500	-3.75644200	2.16826400
C	3.70084700	-4.61051700	3.99990400
C	3.77321100	-5.86405200	4.79666500
C	2.97410300	-6.93589900	4.39140600
H	0.21868600	-6.02972100	-1.10613300

H	-0.01001700	-9.99238700	1.82119600
H	3.00136500	-7.85587000	4.97071000
N	1.65589200	-5.80245000	1.12506000
N	1.46270400	-8.00764600	2.81260300
C	1.75228300	-4.67115300	0.24799400
C	0.78622800	-3.63490300	0.34809600
C	2.77406300	-4.61762800	-0.66575600
C	-0.27305000	-3.65876100	1.28713000
C	0.90313500	-2.52869100	-0.54399700
C	2.88188100	-3.51769400	-1.54170000
H	3.49236600	-5.43353200	-0.70459300
C	-1.17943500	-2.62924600	1.33606900
H	-0.35822800	-4.50181500	1.96963900
C	-0.05162800	-1.48512300	-0.46581200
C	1.96466700	-2.49885800	-1.48071900
H	3.69320800	-3.48601500	-2.26341500
C	-1.07004600	-1.53304100	0.45163900
H	-1.98910600	-2.65532800	2.06087800
H	0.04155700	-0.64377000	-1.15016100
H	2.03883400	-1.64713300	-2.15438900
H	-1.79708000	-0.72666500	0.50282500
C	1.35501900	-9.14434400	3.68132800
C	0.36726400	-9.16814800	4.63297700
C	2.28100700	-10.21191200	3.54063200
C	0.24888400	-10.27300800	5.50127800
H	-0.31743400	-8.32609700	4.70590400
C	2.15301500	-11.32353300	4.42446700
C	3.31342900	-10.21222000	2.57185000
C	1.12376000	-11.32504700	5.39693400
H	-0.53771100	-10.28288200	6.25046000
C	3.06621100	-12.39978100	4.30398200
C	4.18118000	-11.27199100	2.48389200
H	3.41066300	-9.36202000	1.89988900
H	1.04068500	-12.18162300	6.06336100
C	4.05770100	-12.37604700	3.35664200
H	2.96343000	-13.24596600	4.98095500
H	4.97133900	-11.26367800	1.73746400
H	4.75326100	-13.20713500	3.27342900
C	4.15894300	-3.32343400	4.50290800
C	4.62677000	-2.31527900	3.63816300
C	4.11942700	-3.00057200	5.87969200
C	5.01923600	-1.06369900	4.09544400
H	4.71353300	-2.52445300	2.57324900
C	4.50085900	-1.75726600	6.34523500
H	3.75062200	-3.73783700	6.58864000
C	4.95774100	-0.77402800	5.46065400
H	5.38330900	-0.32966600	3.38233500
H	4.44712100	-1.51572200	7.40465800
C	4.72738400	-6.06161500	5.87774900
C	5.99166700	-5.42615400	5.88698200
C	4.45709500	-6.92906900	6.95398100

C	6.91466100	-5.65974100	6.88764800
H	6.25765700	-4.75858700	5.07101300
C	5.37496500	-7.16667100	7.96897300
H	3.48454100	-7.41433700	7.01662200
C	6.61820100	-6.52999200	7.94245100
H	7.89021700	-5.17840500	6.87244900
H	5.10525900	-7.83662200	8.78030100
C	-1.37970000	-10.37357200	-0.38872900
C	-1.22665700	-10.97402600	-1.64900000
C	-2.20557700	-11.01469400	0.53664700
C	-1.87167300	-12.15556700	-1.96282200
H	-0.58055600	-10.50623400	-2.38925800
C	-2.86492100	-12.20429900	0.23647300
H	-2.35365500	-10.56485700	1.51717300
C	-2.69893200	-12.78040400	-1.02233200
H	-1.74550700	-12.62554100	-2.93525300
H	-3.50458600	-12.66284600	0.98443600
C	-1.34866000	-7.87166800	-2.13428600
C	-2.71500900	-8.18788700	-2.20775400
C	-0.73411200	-7.38793300	-3.29083300
C	-3.42536400	-8.02801000	-3.38259500
H	-3.22702100	-8.55635300	-1.32097800
C	-1.43410400	-7.22296500	-4.48368600
H	0.32755000	-7.14701400	-3.26703400
C	-2.78964400	-7.54566200	-4.53261600
H	-4.48558000	-8.26350300	-3.43671400
H	-0.91271900	-6.85206800	-5.36084000
O	5.31852800	0.41236700	6.01878900
O	7.58892400	-6.68366400	8.88232900
O	-3.28952000	-13.93202400	-1.42639400
O	-3.57015400	-7.42838500	-5.63504000
C	5.77836700	1.42749000	5.15337400
H	6.68791200	1.12253900	4.61811000
H	5.01272200	1.71011600	4.41803200
H	6.00704400	2.29176400	5.77937700
C	7.32287100	-7.55591500	9.95900500
H	6.46002000	-7.21924400	10.54968700
H	7.13669100	-8.58173400	9.61280200
H	8.21150600	-7.54994900	10.59261600
C	-4.12919200	-14.59733300	-0.50545400
H	-3.58056200	-14.89647300	0.39748100
H	-4.98306400	-13.97182500	-0.21331000
H	-4.49826200	-15.49093300	-1.01118500
C	-2.96861000	-6.93949500	-6.81611700
H	-2.15597500	-7.59512400	-7.15607400
H	-2.57344700	-5.92445700	-6.67710800
H	-3.75069100	-6.91701300	-7.57659600

PC 4 – ground state

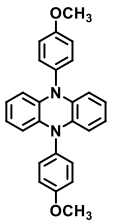

(-1263.349137)

C	-0.41653400	-7.87943900	-0.76039800
C	0.31590200	-6.76128700	-0.35521000
C	1.07631300	-6.78310400	0.80979400
C	1.10762000	-7.96097600	1.58713100
C	0.38134900	-9.07135400	1.16805200
C	-0.38333000	-9.03411300	-0.00007200
C	2.73085600	-6.92276900	3.09362300
C	2.70180900	-5.74556700	2.31461600
C	3.55222600	-4.69392200	2.64127800
H	3.52490100	-3.78729400	2.04332600
C	4.42597300	-4.78311100	3.72733600
C	4.45375300	-5.93533900	4.49124300
C	3.60959100	-7.00051400	4.16989500
H	0.28732700	-5.85264400	-0.95011200
H	0.40708400	-9.97547100	1.77027200
H	3.62835200	-7.90372500	4.77325700
N	1.79362900	-5.65437900	1.24455100
N	1.85555800	-7.97627700	2.77738200
C	1.82028100	-9.13278100	3.61145500
C	2.73694200	-10.17092500	3.42768500
C	0.86751600	-9.23146000	4.61753900
C	2.69848100	-11.28741000	4.24397100
H	3.48256200	-10.08699700	2.63913300
C	0.81568100	-10.35079700	5.44404000
H	0.15576300	-8.41976900	4.75303400
C	1.73653000	-11.38340000	5.25741000
H	0.06238900	-10.40732300	6.22371500
C	1.74833800	-4.46043000	0.46505100
C	0.80569000	-3.48091300	0.74945500
C	2.63975500	-4.27181500	-0.59430100
C	0.73632700	-2.31592100	-0.01056700
H	0.11499200	-3.63619100	1.57552700
C	2.58310800	-3.11839500	-1.35572700
H	3.37625100	-5.04340100	-0.81113100
C	1.62841100	-2.13451600	-1.06885800
H	3.26636300	-2.95227300	-2.18452300
H	-0.94744300	-9.91423100	-0.29772900
H	-1.00757100	-7.82921800	-1.67121200
H	5.07400500	-3.94266500	3.96193900
H	5.12503300	-6.02409900	5.34147100
H	3.40425200	-12.10446000	4.11895000
H	-0.00943200	-1.56344400	0.22663600
O	1.77901400	-12.51217600	6.00240100
O	1.64883600	-1.04602400	-1.87245700
C	0.83060300	-12.65101900	7.04167400

H	-0.19600800	-12.64298600	6.65318900
H	1.02653500	-13.61508100	7.51319500
H	0.93665100	-11.85547900	7.79066300
C	0.68868000	-0.03541900	-1.63650200
H	0.85545100	0.73320500	-2.39244100
H	-0.33362700	-0.42265900	-1.73642000
H	0.80827800	0.40833600	-0.63947300

PC 4 – radical cation

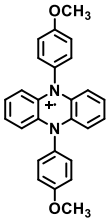

(-1263.181369)

C	-0.51661300	-7.80326800	-0.67567200
C	0.25298100	-6.71540100	-0.32235400
C	1.06441900	-6.76614800	0.82134500
C	1.07994500	-7.94511300	1.61085000
C	0.28973400	-9.04049200	1.23104900
C	-0.49743100	-8.96894800	0.10155700
C	2.66966400	-6.91893100	3.10925600
C	2.65790900	-5.74175700	2.31695700
C	3.46427600	-4.65413000	2.68494200
H	3.45490100	-3.75548900	2.07752100
C	4.26085100	-4.73026700	3.80751800
C	4.27058500	-5.89135600	4.59165300
C	3.48583400	-6.97190100	4.24948200
H	0.23781900	-5.81367500	-0.92505400
H	0.30524900	-9.94161400	1.83472200
H	3.49388300	-7.86979500	4.85793800
N	1.84613400	-5.68775300	1.19735800
N	1.87241900	-7.98991400	2.74456600
C	1.84843200	-9.16456200	3.57844300
C	2.78168200	-10.17890400	3.37255000
C	0.90049800	-9.26129200	4.58685500
C	2.75989400	-11.29502000	4.18816700
H	3.51871000	-10.08260200	2.57863600
C	0.87400200	-10.38225300	5.40868400
H	0.18195100	-8.45748500	4.73040500
C	1.80785300	-11.40318900	5.21110800
H	0.12876800	-10.44834900	6.19445500
C	1.80444500	-4.48120500	0.41107000
C	0.87764400	-3.49754300	0.72389100
C	2.68328700	-4.32467900	-0.65933200
C	0.81595200	-2.33580700	-0.03762700
H	0.20137900	-3.64213700	1.56321400
C	2.62566500	-3.17134900	-1.41922600
H	3.40131400	-5.10859300	-0.88860800
C	1.69161200	-2.17190000	-1.11457700
H	3.29440300	-3.01777300	-2.26131400

H	-1.10410200	-9.82343000	-0.18201800
H	-1.13961200	-7.75161400	-1.56324200
H	4.88129100	-3.88241800	4.08095900
H	4.89867400	-5.94552700	5.47546600
H	3.47436400	-12.10243000	4.05555200
H	0.08731200	-1.57158900	0.21235700
O	1.87160500	-12.52698500	5.95223800
O	1.71324600	-1.08969200	-1.91745000
C	0.93797000	-12.68239800	7.00586500
H	-0.09229400	-12.69336200	6.62897500
H	1.15893900	-13.64264500	7.47312800
H	1.04230200	-11.88491100	7.75221700
C	0.77579400	-0.05789400	-1.66765000
H	0.94610800	0.70356900	-2.42943900
H	-0.25427900	-0.42668800	-1.74990900
H	0.92365000	0.38518600	-0.67472200

PC 4 – neutral triplet

(-1263.259559)

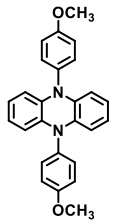

C	-0.55131200	-7.80770100	-0.67516600
C	0.20972400	-6.72148600	-0.31762800
C	1.04470100	-6.75479600	0.81841200
C	1.07414900	-7.96304500	1.62548800
C	0.28756900	-9.06419100	1.22868000
C	-0.50757000	-9.00552200	0.11027200
C	2.65229000	-6.91507900	3.13472200
C	2.64514900	-5.71737200	2.31141000
C	3.46353400	-4.63151300	2.68545000
H	3.46461600	-3.73895200	2.06509300
C	4.24936400	-4.68614400	3.81059800
C	4.24481300	-5.86103800	4.63099700
C	3.46309400	-6.93720800	4.28821200
H	0.17582200	-5.81580100	-0.91757400
H	0.31735900	-9.97089200	1.82750300
H	3.46540900	-7.82800700	4.91087900
N	1.83205400	-5.68543000	1.19605400
N	1.86646300	-7.98512200	2.75587800
C	1.85350300	-9.15618200	3.58416600
C	2.80301000	-10.15651600	3.38971900
C	0.89631200	-9.27797500	4.58017300
C	2.78977000	-11.28017500	4.19927500
H	3.54864200	-10.04271800	2.60588800
C	0.87452300	-10.40469000	5.39810400
H	0.16315900	-8.48571100	4.71560700

C	1.82622900	-11.40924900	5.20738500
H	0.11947200	-10.48688900	6.17321300
C	1.79384300	-4.49035000	0.40375700
C	0.90532200	-3.47841700	0.73410000
C	2.63953800	-4.35963700	-0.69535800
C	0.84941300	-2.31675400	-0.03220600
H	0.25381900	-3.60111700	1.59649600
C	2.58966800	-3.20901500	-1.46424100
H	3.32757900	-5.16567800	-0.94039100
C	1.69454100	-2.18306600	-1.13632500
H	3.23516200	-3.07823900	-2.32844900
H	-1.10336100	-9.86817000	-0.17477500
H	-1.18527200	-7.75568600	-1.55595900
H	4.87189200	-3.83633500	4.07634800
H	4.86087500	-5.90475300	5.52484400
H	3.51843600	-12.07615500	4.07193100
H	0.14982500	-1.53147200	0.23575100
O	1.89675900	-12.54048800	5.94502000
O	1.72097800	-1.10181700	-1.94813100
C	0.95057300	-12.71254900	6.98203700
H	-0.07449000	-12.73802400	6.59062700
H	1.17762600	-13.67046900	7.45194800
H	1.02909200	-11.91542400	7.73253100
C	0.82975900	-0.04100400	-1.66429500
H	0.99862600	0.71808400	-2.42926000
H	-0.21580700	-0.37180400	-1.71041400
H	1.02477100	0.39432200	-0.67564300

PC 4a – ground state

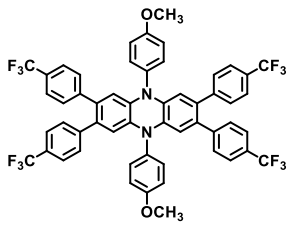

(-3535.213942)

C	-9.32889400	-3.09819400	-0.97163000
C	-8.71760300	-2.89942300	0.27577600
C	-7.57698600	-3.58577600	0.66703400
C	-7.02175100	-4.53679100	-0.21412900
C	-7.61220500	-4.72103200	-1.45617500
C	-8.75288300	-4.01253600	-1.86312500
C	-5.29012000	-5.04302400	1.42458400
C	-5.83877400	-4.08401700	2.30120700
C	-5.21961000	-3.86527300	3.52338900
H	-5.61106900	-3.08888800	4.17594300
C	-4.07992200	-4.57493200	3.93147400
C	-3.55979600	-5.55682000	3.07833300
C	-4.17590400	-5.76141100	1.83420500
H	-9.17609000	-2.20552600	0.97591800
H	-7.15258600	-5.41481700	-2.15568800
H	-3.78425000	-6.53628100	1.17987900
C	-7.51340700	-2.36863000	2.78548500

C	-8.43065900	-2.71442500	3.76978400
C	-7.11497500	-1.03777200	2.64601900
C	-8.95625700	-1.74674400	4.62147000
H	-8.73400600	-3.75459100	3.87031300
C	-7.63350200	-0.06675700	3.48367300
H	-6.39706000	-0.77601600	1.87135500
C	-8.55683400	-0.41617600	4.47699000
H	-9.67049200	-2.03830000	5.38488800
H	-7.33921800	0.97548700	3.39252100
C	-5.31151600	-6.20884400	-0.72378900
C	-5.77669800	-7.52488600	-0.74199600
C	-4.28570400	-5.82796000	-1.57985900
C	-5.21806300	-8.44590300	-1.61037000
H	-6.58089000	-7.81434900	-0.06866100
C	-3.71342100	-6.74639100	-2.45522300
H	-3.93017000	-4.79973600	-1.55665800
C	-4.18206300	-8.06218700	-2.47082500
H	-2.91200300	-6.42772000	-3.11399500
H	-5.56411200	-9.47566300	-1.64247200
N	-6.97968200	-3.36781100	1.91579100
N	-5.88515500	-5.25801300	0.17424300
C	-3.46119300	-4.19672700	5.22177400
C	-4.25113300	-4.04788600	6.36593500
C	-2.08764400	-3.93051200	5.31834100
C	-3.69268000	-3.65511500	7.57643800
H	-5.31714700	-4.25793500	6.30898000
C	-1.52548900	-3.53815100	6.52085900
H	-1.46110200	-4.02279700	4.43409100
C	-2.32886100	-3.40178000	7.65336500
H	-4.31722800	-3.55085600	8.45873500
H	-0.46029600	-3.32597400	6.58433600
C	-2.42329700	-6.43359100	3.43832100
C	-1.38081900	-6.64798200	2.52694000
C	-2.38128400	-7.09851900	4.66889000
C	-0.32436700	-7.48853400	2.84096000
H	-1.39538800	-6.13275500	1.56878600
C	-1.32636100	-7.94161500	4.98928200
H	-3.19213100	-6.95859600	5.38019900
C	-0.29533500	-8.13395400	4.07569900
H	0.48584100	-7.64027500	2.13095800
H	-1.30840500	-8.45468400	5.94626900
C	-9.24551500	-4.23363600	-3.24106900
C	-9.41046200	-5.53225200	-3.73265900
C	-9.51052700	-3.15549500	-4.09775500
C	-9.83806100	-5.75614100	-5.03589000
H	-9.21520100	-6.37892600	-3.07781600
C	-9.93552000	-3.37182600	-5.39724000
H	-9.36884300	-2.13891300	-3.73783600
C	-10.10164800	-4.67481300	-5.86752000
H	-9.96963300	-6.77020000	-5.40168500
H	-10.13092000	-2.52933200	-6.05726400

C	-10.58640100	-2.36851200	-1.24776700
C	-11.72181000	-3.03734900	-1.72782800
C	-10.67999500	-0.99757800	-0.98863100
C	-12.90499000	-2.35421700	-1.94998300
H	-11.67241900	-4.10735900	-1.91667000
C	-11.86470600	-0.30581200	-1.21055400
H	-9.80588600	-0.46294200	-0.62272000
C	-12.97667300	-0.98473300	-1.69312400
H	-13.78264000	-2.88311000	-2.31559200
H	-11.92065200	0.76063000	-1.01317900
C	-14.26985000	-0.28420500	-1.95083300
C	0.85654400	-9.03562100	4.37579500
C	-1.68226200	-2.97701800	8.93043100
C	-10.56993100	-4.86416000	-7.27271700
F	0.91265600	-10.06810500	3.51828400
F	2.02945300	-8.39182500	4.26170900
F	0.80396600	-9.54846400	5.60924600
F	-0.73228700	-3.84497600	9.31536000
F	-1.07108300	-1.78794900	8.80142400
F	-2.55162300	-2.86845700	9.94008400
F	-11.78621300	-4.32706900	-7.46391800
F	-9.75277400	-4.25966600	-8.15049200
F	-10.64669800	-6.15173800	-7.62379100
F	-14.63572400	-0.38172800	-3.23957900
F	-14.22177900	1.01751100	-1.65036300
F	-15.27266500	-0.82111600	-1.23663800
O	-3.70100900	-9.03459200	-3.27747000
O	-9.00380500	0.60255000	5.24520000
C	-9.94079700	0.30389000	6.26186700
H	-10.86468900	-0.11773100	5.84537300
H	-9.52557700	-0.39658700	6.99788500
H	-10.17025700	1.24837900	6.75699700
C	-2.65016200	-8.70124700	-4.16366600
H	-2.95558400	-7.92230400	-4.87410000
H	-1.75852700	-8.36283500	-3.62025400
H	-2.40963000	-9.61214000	-4.71345700

PC 4a – radical cation

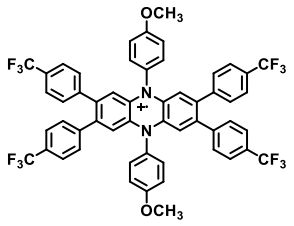

(-3535.039672)

C	-8.37507200	-6.24385700	3.38951100
C	-7.94176600	-4.93899300	3.21394400
C	-7.11234400	-4.57302200	2.14957000
C	-6.67531800	-5.57165600	1.24526000
C	-7.14053900	-6.88009400	1.40606700
C	-7.98811600	-7.23383100	2.44419500
C	-5.40212700	-3.92349900	0.04087000
C	-5.86506200	-2.91934300	0.92582000

C	-5.48103300	-1.59322600	0.70463400
H	-5.89128600	-0.81468100	1.34072700
C	-4.63694300	-1.23905700	-0.33619400
C	-4.11261800	-2.25780200	-1.17933700
C	-4.51527600	-3.56913400	-0.98017300
H	-8.22532000	-4.18559900	3.94280000
H	-6.85968900	-7.63093800	0.67360900
H	-4.10278500	-4.35034100	-1.61151700
C	-7.14716600	-2.24916900	2.89023200
C	-6.33722200	-1.89198600	3.95858100
C	-8.38611800	-1.64109900	2.69389000
C	-6.75961000	-0.91311600	4.85076400
H	-5.37417700	-2.37948700	4.09202600
C	-8.81060800	-0.66860900	3.57942300
H	-9.00505800	-1.93493500	1.84931600
C	-8.00077900	-0.29816300	4.66201900
H	-6.12033300	-0.64213800	5.68449400
H	-9.77032700	-0.17512000	3.45525000
C	-5.37417000	-6.24375400	-0.70774900
C	-6.01146700	-6.37167400	-1.94140000
C	-4.31707800	-7.07258200	-0.36109300
C	-5.58002700	-7.33858500	-2.82944400
H	-6.83782900	-5.71159200	-2.19465500
C	-3.88234600	-8.04900500	-1.25016600
H	-3.83420500	-6.95458200	0.60629900
C	-4.51399500	-8.18313900	-2.48996300
H	-3.05371800	-8.68938800	-0.96806400
H	-6.05427100	-7.46528200	-3.79856600
N	-6.70014100	-3.26516600	1.97194600
N	-5.81844600	-5.23064700	0.21481100
C	-4.36357000	0.19966900	-0.54646700
C	-3.98786600	1.00753600	0.52937900
C	-4.52616800	0.78268100	-1.81020000
C	-3.76685700	2.36829500	0.35222100
H	-3.84857200	0.56232400	1.51213000
C	-4.31636600	2.13899200	-1.98836700
H	-4.83337000	0.16853700	-2.65335000
C	-3.93208000	2.93145900	-0.90655600
H	-3.46425600	2.98468800	1.19307300
H	-4.45454300	2.58877300	-2.96899100
C	-3.11639800	-1.99615800	-2.24098200
C	-3.28269900	-2.56395900	-3.51006200
C	-1.97479500	-1.22968100	-1.98586900
C	-2.33430900	-2.36511300	-4.50079200
H	-4.17285000	-3.15187800	-3.72302500
C	-1.01964000	-1.03397600	-2.97354100
H	-1.82416000	-0.79461700	-1.00058300
C	-1.20114800	-1.60075200	-4.23036800
H	-2.47424300	-2.80198600	-5.48694400
H	-0.13210700	-0.44607600	-2.76147800
C	-8.48445600	-8.62699400	2.48810300

C	-7.59010600	-9.69206200	2.35458700
C	-9.85263500	-8.90061400	2.61945200
C	-8.04391700	-11.00545000	2.36577800
H	-6.52509000	-9.49098400	2.26230900
C	-10.30874600	-10.20718100	2.62415200
H	-10.56226500	-8.08146300	2.70785500
C	-9.40230300	-11.26046800	2.50365200
H	-7.33928800	-11.82599500	2.27253100
H	-11.37196300	-10.41461300	2.71938500
C	-9.19604300	-6.54736400	4.58228800
C	-8.87494700	-7.61896000	5.42653900
C	-10.28751500	-5.73613600	4.90225800
C	-9.63194800	-7.87183800	6.55735400
H	-8.01944300	-8.24983600	5.19668900
C	-11.05498400	-5.99207200	6.03214800
H	-10.55174900	-4.90831100	4.24799500
C	-10.72665000	-7.06065100	6.85646100
H	-9.37314000	-8.70000300	7.21307800
H	-11.90931800	-5.36405300	6.26610600
C	-11.51444200	-7.36680300	8.09031200
C	-0.20235500	-1.40829500	-5.32725600
C	-3.71205900	4.39117400	-1.14791000
C	-9.94100300	-12.65555600	2.50733300
F	0.24201800	-2.58447300	-5.79538100
F	-0.74325400	-0.76535400	-6.37343500
F	0.86521500	-0.70600900	-4.93763100
F	-2.77520700	4.59486400	-2.08646500
F	-4.82890400	4.98666000	-1.59339900
F	-3.32425300	5.04493800	-0.04937700
F	-10.70290100	-12.88222400	3.58817700
F	-10.72448000	-12.87881300	1.44051300
F	-8.97880600	-13.58220000	2.49514500
F	-11.95522100	-8.63362600	8.08865900
F	-12.58033300	-6.57408400	8.23247700
F	-10.76408500	-7.22928200	9.19480500
O	-4.17087000	-9.09211400	-3.42276700
O	-8.50271200	0.66035200	5.46447300
C	-7.72024300	1.08343800	6.56700700
H	-7.54522300	0.26178800	7.27257900
H	-6.75631900	1.49134400	6.23819700
H	-8.29046600	1.86818300	7.06513500
C	-3.11053100	-9.98504400	-3.12936700
H	-2.16805500	-9.44747000	-2.96733800
H	-3.33672600	-10.59566600	-2.24634200
H	-3.00857200	-10.63504700	-3.99879600

PC 4a – neutral triplet

(-3535.141948)

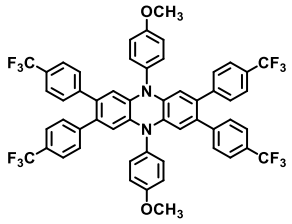

C	-8.43126100	-6.25069400	3.39858300
C	-8.06817400	-4.92556500	3.14515600
C	-7.26102100	-4.55494500	2.07988000
C	-6.75122900	-5.59111200	1.19861800
C	-7.19446800	-6.89175600	1.37106800
C	-8.08249200	-7.26826000	2.38500300
C	-5.47235900	-3.92261300	0.00462400
C	-5.98752000	-2.90715400	0.85143500
C	-5.59992800	-1.58186000	0.62254200
H	-6.04710000	-0.79513800	1.22406200
C	-4.70197800	-1.23269500	-0.37551400
C	-4.13358500	-2.26014800	-1.18024700
C	-4.54384800	-3.57020100	-0.98071000
H	-8.33121300	-4.16213600	3.87218600
H	-6.90566500	-7.62533100	0.62395300
H	-4.09404600	-4.35742000	-1.57956600
C	-7.37486600	-2.21758800	2.72971100
C	-6.62136500	-1.80202500	3.81821300
C	-8.62670100	-1.65804500	2.47915000
C	-7.10914900	-0.81654200	4.67021100
H	-5.64714800	-2.25161700	3.99828400
C	-9.11901300	-0.67906200	3.32317600
H	-9.20507900	-1.99698700	1.62270800
C	-8.36369300	-0.25301800	4.42353300
H	-6.50821500	-0.50289600	5.51703500
H	-10.09083200	-0.22362400	3.15345000
C	-5.36011700	-6.25671900	-0.67780300
C	-5.95957900	-6.47691400	-1.91686400
C	-4.27959800	-7.02586700	-0.27002900
C	-5.46963000	-7.46925200	-2.74634700
H	-6.80722200	-5.86617900	-2.21983100
C	-3.78352300	-8.02816400	-1.09720900
H	-3.82712900	-6.84121500	0.70184300
C	-4.38080500	-8.25200300	-2.34055400
H	-2.93721600	-8.62199200	-0.76740800
H	-5.91571200	-7.66303700	-3.71794000
N	-6.86861000	-3.24482100	1.86299600
N	-5.87296100	-5.23401100	0.19027000
C	-4.42214400	0.20359800	-0.58798000
C	-4.11796800	1.03304800	0.49574000
C	-4.49136400	0.77113000	-1.86879700
C	-3.87548600	2.38913700	0.31194600
H	-4.04818600	0.60455100	1.49333500
C	-4.25522700	2.12167800	-2.05654800
H	-4.74590500	0.14573500	-2.72134800

C	-3.94008800	2.93209500	-0.96523600
H	-3.62684900	3.01834500	1.16117500
H	-4.32042900	2.55414900	-3.05254900
C	-3.06992400	-2.01527700	-2.17777500
C	-3.14646400	-2.59756800	-3.45010300
C	-1.94557700	-1.24470200	-1.86042500
C	-2.13232800	-2.41258400	-4.37643600
H	-4.02073400	-3.18807300	-3.71576400
C	-0.92590200	-1.05860800	-2.78323500
H	-1.86257300	-0.79755700	-0.87236000
C	-1.01968500	-1.64294500	-4.04230900
H	-2.20538200	-2.86282600	-5.36410300
H	-0.05420600	-0.46705800	-2.51961400
C	-8.69413200	-8.58264900	2.32230300
C	-8.01801600	-9.67891800	1.73436600
C	-9.99893200	-8.82903800	2.81564900
C	-8.60071000	-10.92710000	1.64078000
H	-6.99745000	-9.55267400	1.37967900
C	-10.58592700	-10.07592000	2.71382100
H	-10.56269600	-8.01483100	3.26297900
C	-9.89123300	-11.14171400	2.13554800
H	-8.04563700	-11.75190700	1.20097900
H	-11.59529600	-10.22822400	3.08958100
C	-8.99048700	-6.57509800	4.70071600
C	-8.68297700	-7.79188100	5.35551200
C	-9.82565600	-5.66822700	5.39057500
C	-9.15953700	-8.06636500	6.62151300
H	-8.02855500	-8.50905600	4.86744600
C	-10.31300300	-5.94780500	6.65492800
H	-10.11961500	-4.73853900	4.90781000
C	-9.98166000	-7.14863700	7.28355900
H	-8.88698000	-8.99898200	7.11263100
H	-10.96366100	-5.23680200	7.15663400
C	-10.48106600	-7.49083900	8.64173100
C	0.05007500	-1.46640400	-5.07005700
C	-3.69299100	4.38467600	-1.21282100
C	-10.54286900	-12.47022100	1.99240500
F	0.51244900	-2.64948100	-5.50511700
F	-0.40865500	-0.82200800	-6.15522100
F	1.09860100	-0.77427800	-4.61347500
F	-2.72973200	4.57022300	-2.12922100
F	-4.78861900	4.99635400	-1.69120000
F	-3.32331600	5.04303100	-0.10977300
F	-11.38442100	-12.73524200	3.00457400
F	-11.27575000	-12.56604900	0.86468400
F	-9.65127900	-13.47205300	1.94481400
F	-11.22594900	-8.61202000	8.63829400
F	-11.23412600	-6.52285800	9.17836100
F	-9.47336000	-7.72796400	9.50277600
O	-3.98104800	-9.19694600	-3.21756900
O	-8.92946500	0.70609000	5.18673500

C	-8.20603000	1.17568700	6.30938600
H	-8.02758500	0.37282200	7.03590500
H	-7.24475100	1.61322100	6.01142600
H	-8.82308700	1.94667500	6.77219500
C	-2.89438000	-10.02619700	-2.85060800
H	-1.97808000	-9.44279900	-2.69537500
H	-3.11680500	-10.59806400	-1.94074100
H	-2.74180000	-10.71855300	-3.67936300

PC 4b – ground state

(-2645.043127)

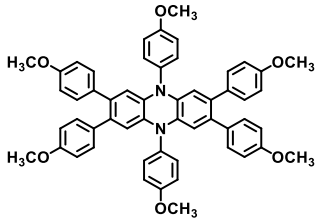

C	-3.32726200	-2.62009100	-2.39196800
C	-2.15348800	-2.55900600	-1.62343300
C	-1.83708900	-1.47626400	-0.81592900
C	-2.73907400	-0.39388700	-0.75291400
C	-3.89236700	-0.44362000	-1.52225600
C	-4.20980700	-1.53091700	-2.35345600
C	-1.31829200	0.69162900	0.90727500
C	-0.41875800	-0.39280400	0.84736600
C	0.67497000	-0.39840300	1.70128900
H	1.34114000	-1.25796300	1.69145600
C	0.93570300	0.63697600	2.61374200
C	0.06424100	1.73547200	2.64376500
C	-1.05064300	1.72828800	1.78957400
H	-1.48124800	-3.41359400	-1.63985400
H	-4.56309400	0.41217100	-1.51358400
H	-1.71143200	2.59160600	1.79872300
C	0.31013700	-2.47678000	-0.20463100
C	1.32287100	-2.35905900	-1.15817300
C	0.25371000	-3.60761800	0.60148000
C	2.26640700	-3.36130700	-1.29882300
H	1.35979700	-1.47091000	-1.78560700
C	1.19701500	-4.62299600	0.46998800
H	-0.53882200	-3.69070800	1.34279900
C	2.20891700	-4.49870600	-0.48454800
H	3.06374900	-3.28871800	-2.03385100
H	1.13696900	-5.49744100	1.11044100
C	-3.34598600	1.80826000	0.12462800
C	-3.20434300	2.87887400	-0.75963300
C	-4.36614100	1.82635300	1.06851000
C	-4.07253800	3.95433900	-0.69493400
H	-2.40390700	2.85559200	-1.49612700
C	-5.24429000	2.90366000	1.14622300

H	-4.46762700	0.98750000	1.75449900
C	-5.09522500	3.97375100	0.26086900
H	-6.03379200	2.90170400	1.89153800
O	3.17682200	-5.42014800	-0.69473400
H	-3.97997200	4.79886600	-1.37276100
O	-5.88653000	5.07075900	0.24986400
N	-0.65508800	-1.43583200	-0.06112100
N	-2.43875300	0.70878300	0.06173800
C	-6.92026700	5.14844300	1.21146300
H	-7.41755000	6.10652700	1.05406900
H	-7.65035700	4.33870900	1.08393200
H	-6.52124600	5.11374800	2.23350600
C	3.15973500	-6.58806300	0.10220700
H	4.01034600	-7.19243800	-0.21587800
H	3.26730400	-6.34901600	1.16811100
H	2.23523700	-7.16110700	-0.04545600
C	2.08421800	0.47093900	3.53365400
C	1.94879100	0.66972900	4.91683100
C	3.32871500	0.05266600	3.06081500
C	3.01006700	0.46652400	5.77887800
H	0.98725300	0.98550200	5.31746800
C	4.41013300	-0.15620600	3.91469400
H	3.46478400	-0.10411600	1.99174100
C	4.25224300	0.05346100	5.28379000
H	2.90244800	0.61292700	6.85105400
H	5.36216900	-0.47582800	3.50181600
C	0.26871200	2.92906800	3.49552400
C	-0.79182200	3.47922500	4.21744300
C	1.51132200	3.57777900	3.57361200
C	-0.63874100	4.62276000	4.99882300
H	-1.76642700	2.99457500	4.18099700
C	1.68184400	4.71311400	4.34354100
H	2.35513400	3.18326900	3.01088000
C	0.60707800	5.24471300	5.06547500
H	-1.49020300	5.01090800	5.54975300
H	2.64305000	5.21884300	4.39784700
C	-5.43954100	-1.43496900	-3.17287100
C	-5.44384500	-1.74563700	-4.54209400
C	-6.63371600	-0.97837300	-2.61229400
C	-6.58853700	-1.61150300	-5.30551500
H	-4.52583100	-2.09491100	-5.01135600
C	-7.79687400	-0.83699500	-3.36592300
H	-6.66337900	-0.73682400	-1.55087500
C	-7.77672600	-1.15598100	-4.72279800
H	-6.58867000	-1.84597600	-6.36737700
H	-8.70515900	-0.48559600	-2.88566600
C	-3.57800000	-3.85996200	-3.16179000
C	-2.58018700	-4.40942100	-3.96775500
C	-4.79714100	-4.55018600	-3.07522000
C	-2.77294700	-5.59402800	-4.67565500
H	-1.62639900	-3.89144200	-4.05749000

C	-5.00548800	-5.72801900	-3.76881800
H	-5.59085400	-4.15371700	-2.44453600
C	-3.99439200	-6.25850600	-4.57808200
H	-1.97255000	-5.98226700	-5.29834600
H	-5.94729000	-6.26672300	-3.69565300
O	5.23150900	-0.11449000	6.20748800
O	0.87549600	6.35916300	5.79068300
O	-8.84438500	-1.05839600	-5.55392600
O	-4.29488600	-7.41525700	-5.22030400
C	-0.18396300	6.93128900	6.52910300
H	-0.57509000	6.23274400	7.28081600
H	0.22666100	7.80676700	7.03449400
H	-1.00744500	7.24694600	5.87480600
C	6.49905300	-0.53599900	5.74867700
H	6.92749800	0.17958100	5.03429300
H	7.14434600	-0.59341300	6.62667000
H	6.44765900	-1.52520100	5.27444500
C	-3.29713700	-7.98528300	-6.04144400
H	-2.39904600	-8.24368600	-5.46467200
H	-3.72413700	-8.89668900	-6.46302100
H	-3.01268500	-7.31015100	-6.85944500
C	-10.05968400	-0.58927000	-5.00800600
H	-10.78123500	-0.57069100	-5.82620800
H	-10.43070700	-1.25507000	-4.21752100
H	-9.95386400	0.42450300	-4.59941300

PC 4b – radical cation

(-2644.878597)

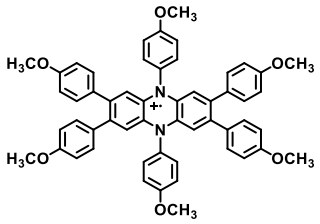

C	-3.30267200	-2.61800100	-2.37988300
C	-2.14923600	-2.57459600	-1.60762600
C	-1.85860000	-1.50301600	-0.76038100
C	-2.77865500	-0.42871900	-0.67759000
C	-3.92439400	-0.45914500	-1.47488600
C	-4.20553000	-1.51605900	-2.33152300
C	-1.37380100	0.64676400	0.96005600
C	-0.45713000	-0.43067100	0.88231200
C	0.66990700	-0.41778100	1.70719300
H	1.33678500	-1.27493300	1.69542900
C	0.93033800	0.62137100	2.59116600
C	0.03984900	1.73398600	2.62505600
C	-1.09044600	1.71136300	1.81838200
H	-1.47416100	-3.42502500	-1.62736900
H	-4.59690000	0.39327800	-1.45630200
H	-1.75628400	2.56901400	1.82677900
C	0.25694800	-2.53434100	-0.12120200
C	1.27110900	-2.41408900	-1.06983200
C	0.17444300	-3.65362000	0.69449500

C	2.20611800	-3.42412900	-1.19648300
H	1.31787600	-1.52847900	-1.69934000
C	1.11263300	-4.67312100	0.57098500
H	-0.62435200	-3.72724200	1.42912300
C	2.13293800	-4.55841700	-0.37710500
H	3.00938000	-3.36007600	-1.92504200
H	1.04198400	-5.54454400	1.21375900
C	-3.42942500	1.73754600	0.23887300
C	-3.28557000	2.80032300	-0.65182300
C	-4.43485500	1.74054600	1.19462300
C	-4.15581500	3.87132800	-0.57698200
H	-2.49116700	2.77759900	-1.39425100
C	-5.31270400	2.81653800	1.27543100
H	-4.52808200	0.90132700	1.88019100
C	-5.17147200	3.88726300	0.38836400
H	-6.09639600	2.81246400	2.02615800
O	3.09263100	-5.48414200	-0.57606400
H	-4.07057900	4.71586100	-1.25494200
O	-5.96181000	4.97927500	0.38347300
N	-0.71001600	-1.47655000	0.01141200
N	-2.51111800	0.63144200	0.17113700
C	-6.99203100	5.05875000	1.35166700
H	-7.48785400	6.01727100	1.19472600
H	-7.72237800	4.24954200	1.22628000
H	-6.58601600	5.02492500	2.37048700
C	3.06499500	-6.65233200	0.22379100
H	3.91515600	-7.25951300	-0.08888800
H	3.16733900	-6.41023300	1.28906900
H	2.13892000	-7.22009100	0.06902800
C	2.09278200	0.48737300	3.49189300
C	1.97808500	0.72349100	4.87178800
C	3.32634000	0.05366400	3.00247500
C	3.05197000	0.53143600	5.71788600
H	1.02521100	1.04823800	5.28427300
C	4.42097100	-0.13398500	3.84069400
H	3.44416100	-0.12499200	1.93506800
C	4.28494800	0.10420900	5.20881200
H	2.96372800	0.69950700	6.78819700
H	5.36645000	-0.46048700	3.41913200
C	0.27230900	2.93474200	3.45200500
C	-0.77417900	3.50018900	4.18390900
C	1.52225500	3.57453200	3.49020000
C	-0.59825500	4.65410100	4.94075900
H	-1.74954200	3.01663000	4.18187100
C	1.71010900	4.72578500	4.22885500
H	2.35280800	3.16748000	2.91765000
C	0.65159200	5.27393300	4.96443100
H	-1.43325000	5.05520300	5.50676500
H	2.67238600	5.23093800	4.25056000
C	-5.41123800	-1.41686400	-3.17796800
C	-5.37545800	-1.70756100	-4.55188000

C	-6.61756500	-0.96713300	-2.63624100
C	-6.49735200	-1.55154000	-5.34129300
H	-4.44668500	-2.04749500	-5.00524700
C	-7.75892000	-0.81407600	-3.41627600
H	-6.67567600	-0.74852500	-1.57142500
C	-7.70054400	-1.10522600	-4.77964500
H	-6.47028200	-1.76314300	-6.40714400
H	-8.68088900	-0.47457600	-2.95468300
C	-3.54838500	-3.83371200	-3.18133300
C	-2.53000700	-4.37917100	-3.96517700
C	-4.78080400	-4.50602500	-3.14093800
C	-2.71785700	-5.54585600	-4.69967000
H	-1.56963800	-3.86963400	-4.02235400
C	-4.97888400	-5.67104800	-3.85516600
H	-5.58830000	-4.11190100	-2.52746300
C	-3.94951600	-6.19883000	-4.64498800
H	-1.90640000	-5.93147700	-5.30893900
H	-5.92666900	-6.20190700	-3.81646400
O	5.27560300	-0.04694900	6.11599600
O	0.93706600	6.39772300	5.65913800
O	-8.74159400	-0.98944200	-5.63374700
O	-4.24318100	-7.33779900	-5.31154700
C	-0.10449600	6.99119200	6.41001200
H	-0.48151300	6.30825100	7.18222200
H	0.32323300	7.87296200	6.88887800
H	-0.93835400	7.29888000	5.76599200
C	6.53755500	-0.48351900	5.64949600
H	6.96045500	0.21924300	4.92002300
H	7.19041600	-0.52949900	6.52214000
H	6.47370000	-1.47996100	5.19351800
C	-3.23039100	-7.91034500	-6.11591900
H	-2.35292200	-8.18914700	-5.51823100
H	-3.65996100	-8.80853800	-6.56157300
H	-2.91693500	-7.22582100	-6.91469400
C	-9.97388300	-0.52758100	-5.11494500
H	-10.66956100	-0.49532700	-5.95441800
H	-10.36641800	-1.20759500	-4.34798500
H	-9.87724900	0.47890200	-4.68779700

PC 4b – neutral triplet

(-2644.964206)

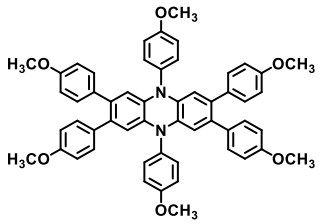

C	-3.28410500	-2.58163500	-2.39761900
C	-2.13476000	-2.53831700	-1.61958500
C	-1.85965900	-1.49353300	-0.73020800
C	-2.81325100	-0.44709200	-0.59671100
C	-3.95861700	-0.48002900	-1.40029600

C	-4.21338800	-1.50085400	-2.30693800
C	-1.41872000	0.63587300	1.06333600
C	-0.42969500	-0.42660200	0.90974400
C	0.71407500	-0.38930600	1.69494200
H	1.38494200	-1.24398000	1.65761300
C	0.98084200	0.62590200	2.61615000
C	0.04951700	1.78053600	2.65699800
C	-1.13268600	1.68992900	1.92206000
H	-1.43919900	-3.37181000	-1.67455600
H	-4.65370100	0.35412300	-1.34886000
H	-1.81960200	2.53263400	1.94104500
C	0.26949100	-2.50394300	-0.12773900
C	1.29052100	-2.36079100	-1.06576600
C	0.19814300	-3.64001100	0.66519500
C	2.23742100	-3.35958100	-1.20649400
H	1.33260900	-1.46230600	-1.67762000
C	1.14623000	-4.65058100	0.52989600
H	-0.60351900	-3.73294400	1.39475200
C	2.17091300	-4.50887500	-0.40852600
H	3.04444500	-3.27482100	-1.92915900
H	1.07963600	-5.53409400	1.15668400
C	-3.56927800	1.59743500	0.47915700
C	-3.54636600	2.74515000	-0.31147800
C	-4.55217200	1.42909900	1.44361200
C	-4.51196900	3.72075200	-0.13281900
H	-2.76918000	2.86269500	-1.06357600
C	-5.52694900	2.40425000	1.62966700
H	-4.55483100	0.52679500	2.05138100
C	-5.50615500	3.55620600	0.83958200
H	-6.28991800	2.25618800	2.38666800
O	3.14361100	-5.42348300	-0.61766000
H	-4.51935100	4.62492300	-0.73545200
O	-6.40115000	4.56394800	0.94147800
N	-0.70197700	-1.46075600	0.02920900
N	-2.57341500	0.58091700	0.30030800
C	-7.42504900	4.44262900	1.91040300
H	-8.02671200	5.34964100	1.83960100
H	-8.06190100	3.57084500	1.71297000
H	-7.01063300	4.36331700	2.92361100
C	3.12227800	-6.60136900	0.16554400
H	3.98111900	-7.19642000	-0.14763100
H	3.21321900	-6.37358700	1.23530600
H	2.20355500	-7.17776100	-0.00278700
C	2.06511500	0.43813700	3.57075300
C	1.98705900	0.91098400	4.90227000
C	3.23295900	-0.27021500	3.22786300
C	2.99453800	0.67453100	5.81738200
H	1.10055300	1.45330200	5.22259200
C	4.25408400	-0.51082600	4.13844500
H	3.36144000	-0.62376400	2.20619700
C	4.14113700	-0.03682500	5.44739900

H	2.91399200	1.02979800	6.84257100
H	5.13742000	-1.05450900	3.81542900
C	0.37251200	3.04651200	3.30450300
C	-0.62623500	3.85671800	3.87569900
C	1.69281700	3.55021300	3.34899300
C	-0.34735100	5.09377500	4.44443800
H	-1.65363500	3.49718300	3.89939300
C	1.98189200	4.78048700	3.90704300
H	2.49853800	2.96947200	2.90622900
C	0.96635800	5.56647900	4.46340300
H	-1.15690500	5.67124200	4.88147800
H	2.99932600	5.16554100	3.91855500
C	-5.39773100	-1.37232500	-3.18212100
C	-5.31371700	-1.59304500	-4.56743100
C	-6.62990800	-0.96164100	-2.66850100
C	-6.40771600	-1.40868800	-5.39112700
H	-4.36577100	-1.90564300	-5.00142900
C	-7.74301900	-0.77207400	-3.48408000
H	-6.73028800	-0.79683000	-1.59686400
C	-7.63377200	-0.99642300	-4.85585400
H	-6.33857100	-1.56890300	-6.46444800
H	-8.68313800	-0.45820600	-3.04052200
C	-3.50644100	-3.77693800	-3.23821900
C	-2.47680300	-4.30015900	-4.02340800
C	-4.73551300	-4.45770000	-3.24260500
C	-2.64554800	-5.45119800	-4.78955400
H	-1.51747100	-3.78584400	-4.05254000
C	-4.91956000	-5.60187400	-3.99534700
H	-5.55581800	-4.08305100	-2.63334800
C	-3.87515200	-6.10814400	-4.77794400
H	-1.82001900	-5.81789000	-5.39222200
H	-5.86787400	-6.13397400	-3.99003700
O	5.08031600	-0.20635000	6.41672600
O	1.35475500	6.75573900	4.99700800
O	-8.64681300	-0.84573000	-5.74450600
O	-4.15507700	-7.23291200	-5.48175500
C	0.35405000	7.57604000	5.55938900
H	-0.15031200	7.08147400	6.40073900
H	0.85496000	8.47462700	5.92382200
H	-0.40015200	7.86340200	4.81419500
C	6.24962200	-0.91616600	6.07132300
H	6.80010500	-0.41877500	5.26114900
H	6.87604000	-0.94055100	6.96475300
H	6.02233700	-1.94615100	5.76403900
C	-3.12572600	-7.77901300	-6.28030600
H	-2.25707800	-8.07006000	-5.67477600
H	-3.54137400	-8.66714400	-6.75872300
H	-2.79832500	-7.07286000	-7.05491300
C	-9.89596200	-0.41293200	-5.24665700
H	-10.56852300	-0.35391000	-6.10375500
H	-10.30675800	-1.12254400	-4.51620200

H	-9.82124500	0.57765500	-4.77859600

PC 5 – ground state

(-1341.477327)

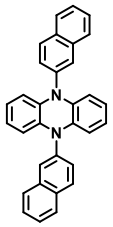

C	4.44053200	-5.39924000	2.62577000
C	3.22674700	-4.75461100	2.38107700
C	2.01768400	-5.33443700	2.75289700
C	2.02500400	-6.59653500	3.38405200
C	3.24113800	-7.23169100	3.61648400
C	4.44773700	-6.63729700	3.24280800
C	-0.41364200	-6.65121500	3.30261800
C	-0.42104400	-5.39051600	2.66878700
C	-1.62718300	-4.86696200	2.21322200
H	-1.63425400	-3.89395100	1.73025200
C	-2.82442700	-5.56564100	2.37797700
C	-2.81725400	-6.80142300	2.99946700
C	-1.61314500	-7.33966700	3.45672500
H	3.22170200	-3.78014900	1.90089500
H	3.24788100	-8.20128600	4.10663100
H	-1.60952300	-8.30765300	3.95003700
N	0.78815800	-4.67950100	2.54566700
N	0.80266400	-7.16378800	3.79655100
C	0.78587200	-3.44807400	1.82177100
C	0.81656400	-3.47092700	0.40556100
C	0.75816000	-2.25679200	2.49973700
H	0.83855600	-4.43454800	-0.10032200
C	0.76030500	-1.02785700	1.79497100
H	0.73586500	-2.25640900	3.58840600
H	5.38238000	-7.15439300	3.44351100
H	5.36929200	-4.91891900	2.32927100
H	-3.75178600	-5.12911400	2.01652500
H	-3.73900900	-7.35998400	3.13930500
C	0.81773100	-2.29689000	-0.30034900
C	0.79037300	-1.04713400	0.36968200
C	0.79261900	0.18203400	-0.33350200
C	0.76693100	1.37557600	0.34366700
H	0.76920600	2.31360400	-0.20587400
C	0.73721700	1.39408400	1.75604600
H	0.71681500	2.34655000	2.27975100
C	0.73398500	0.21932900	2.46549700
H	0.81557100	0.16031400	-1.42169200
H	0.71108800	0.22716400	3.55373700
H	0.84096400	-2.30678800	-1.38853600
C	0.81427600	-8.49480500	4.31583400
C	0.77142100	-8.70693600	5.66940200
C	0.86758900	-9.58670900	3.41491200
C	0.77772900	-10.02466900	6.19127000

H	0.73104100	-7.85541400	6.34696100
C	0.87567200	-10.87010100	3.89213900
H	0.90028700	-9.37958300	2.34685400
C	0.73147400	-10.28073900	7.58333800
C	0.83056000	-11.12561200	5.28642000
H	0.91556600	-11.71498200	3.20692400
C	0.73675500	-11.56848500	8.05808000
H	0.69155800	-9.43590300	8.26881400
C	0.83517300	-12.44192500	5.80764000
C	0.78917800	-12.65948000	7.16194700
H	0.70059800	-11.75397800	9.12865300
H	0.87548200	-13.27818900	5.11173100
H	0.79292200	-13.67440400	7.55144500

PC 5 – radical cation

(-1341.307624)

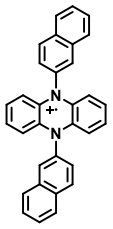

C	4.42469300	-5.38246900	2.65938800
C	3.23399300	-4.76931500	2.33208500
C	2.01485800	-5.40757900	2.60426500
C	2.01920400	-6.68508300	3.22072600
C	3.24245700	-7.28927400	3.54664400
C	4.42895300	-6.64494600	3.26753700
C	-0.39346700	-6.73155100	3.14172100
C	-0.39782600	-5.45430700	2.52472000
C	-1.62007500	-4.86287400	2.17270400
H	-1.62305700	-3.88543500	1.70219500
C	-2.80535400	-5.52084400	2.42381400
C	-2.80107900	-6.78262300	3.03341600
C	-1.61151900	-7.38170000	3.38960900
H	3.23028700	-3.79176300	1.86182700
H	3.24521700	-8.26624900	4.01813700
H	-1.60778200	-8.35786200	3.86278900
N	0.80582900	-4.81564200	2.28525500
N	0.81436500	-7.30969700	3.48924300
C	0.80179100	-3.51623000	1.66003700
C	0.84971100	-3.44590700	0.25144700
C	0.75270000	-2.39426300	2.44474300
H	0.88799300	-4.36566200	-0.32719100
C	0.74939100	-1.11612600	1.83803600
H	0.71637200	-2.48402800	3.52918600
H	5.36946500	-7.12334100	3.52262900
H	5.36186900	-4.87944300	2.44229000
H	-3.74496500	-5.05352000	2.14587500
H	-3.73732300	-7.29603600	3.22914100
C	0.84719400	-2.21554700	-0.35295900
C	0.79749000	-1.02598300	0.41533700
C	0.79420600	0.25415100	-0.18947600

C	0.74567000	1.38941400	0.57949100
H	0.74365900	2.36758900	0.10562000
C	0.69815100	1.29813400	1.98871900
H	0.66015700	2.20657900	2.58412300
C	0.69987600	0.07268800	2.60534200
H	0.83091000	0.31854000	-1.27523600
H	0.66348400	-0.00553300	3.69015500
H	0.88372200	-2.13785900	-1.43750600
C	0.81783600	-8.60241600	4.12816200
C	0.77841400	-8.67266800	5.49588500
C	0.86102100	-9.75714300	3.31806300
C	0.78030500	-9.93629600	6.13178000
H	0.74556100	-7.76163800	6.09123300
C	0.86305000	-10.98988300	3.91806100
H	0.89153200	-9.64893100	2.23655800
C	0.74065300	-10.06064200	7.54144300
C	0.82297500	-11.11446700	5.32892700
H	0.89575600	-11.89320300	3.31267900
C	0.74321500	-11.29981700	8.13008300
H	0.70821200	-9.15660100	8.14627100
C	0.82411600	-12.37791800	5.96780400
C	0.78523500	-12.46816900	7.33639700
H	0.71272700	-11.38773500	9.21293000
H	0.85640700	-13.27465500	5.35192400
H	0.78652200	-13.44287500	7.81736700

PC 5 – neutral triplet

(-1341.391719)

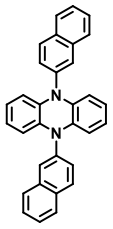

C	4.40399500	-5.21764800	2.98497000
C	3.21044700	-4.62273400	2.63744300
C	1.99481700	-5.28654200	2.86959900
C	2.00679900	-6.57406400	3.46953700
C	3.23604800	-7.16905500	3.80136200
C	4.41580100	-6.49874700	3.56286300
C	-0.40678300	-6.62537500	3.38530100
C	-0.40746900	-5.33696300	2.78699400
C	-1.63109800	-4.72301600	2.47369900
H	-1.61361800	-3.73421600	2.02699900
C	-2.81966500	-5.36805200	2.73871400
C	-2.81753600	-6.65086700	3.31309700
C	-1.62988400	-7.27213400	3.63179500
H	3.18253600	-3.63599100	2.18681700
H	3.24616300	-8.15814500	4.24760900
H	-1.62927800	-8.26204000	4.07632200
N	0.79247600	-4.71888900	2.49860700
N	0.80371200	-7.21944400	3.69839800

C	0.79378400	-3.49817300	1.73038000
C	0.83133100	-3.58437500	0.34624700
C	0.75803900	-2.26944800	2.40860700
H	0.85798100	-4.56350200	-0.13008300
C	0.76168800	-1.05954400	1.66365600
H	0.72905600	-2.24582100	3.49737400
H	5.35901600	-6.96820500	3.82623100
H	5.33756800	-4.69235200	2.80744100
H	-3.76008900	-4.88096900	2.49910700
H	-3.75610300	-7.16009800	3.51088300
C	0.83452400	-2.40945600	-0.40673800
C	0.80111900	-1.12991700	0.22338300
C	0.80537300	0.07284300	-0.50866000
C	0.77284100	1.31926100	0.12786600
H	0.77739800	2.23162200	-0.46620100
C	0.73466500	1.38640100	1.51578600
H	0.70915300	2.35277600	2.01711400
C	0.72906500	0.21218700	2.27510600
H	0.83550000	0.01440100	-1.59737700
H	0.69922600	0.26282800	3.36401400
H	0.86442100	-2.45523000	-1.49451300
C	0.81432600	-8.56592700	4.20783400
C	0.77336700	-8.78376800	5.55995600
C	0.86687900	-9.62966400	3.28133500
C	0.78344700	-10.10872000	6.05768800
H	0.73329300	-7.94201000	6.24950700
C	0.87730000	-10.91951900	3.74438300
H	0.89796600	-9.40567300	2.21763200
C	0.74252200	-10.38482600	7.44569100
C	0.83621400	-11.19426100	5.13384600
H	0.91748400	-11.75319700	3.04637200
C	0.75333000	-11.68010800	7.89828700
H	0.70238300	-9.55100700	8.14397600
C	0.84600300	-12.51877500	5.63342600
C	0.80558500	-12.75631700	6.98426700
H	0.72169100	-11.88370200	8.96547800
H	0.88636500	-13.34343200	4.92424000
H	0.81358100	-13.77705000	7.35777900

PC 5a – ground state

(-3613.340800)

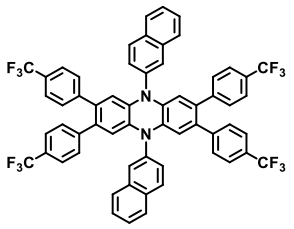

C	-1.55468200	2.30948400	-2.07708700
C	-0.55755400	1.42664400	-1.63459900
C	0.60365200	1.85939200	-1.01216100
C	0.80613300	3.24399500	-0.83985400
C	-0.18105800	4.12000000	-1.26713100

C	-1.36953800	3.68343100	-1.87294200
H	-0.68645800	0.36294500	-1.81782900
H	-0.05082900	5.18489300	-1.09108000
N	1.58697000	0.95838300	-0.57831900
N	1.98751500	3.69813600	-0.23770000
C	2.68728500	1.40790600	0.16641800
C	3.57864700	0.52510500	0.75939000
C	2.89800300	2.79256400	0.32570100
C	4.69924300	0.95550000	1.48586700
H	3.38492900	-0.54233100	0.68797200
C	4.02060400	3.22140700	1.01851800
C	4.93896000	2.33206200	1.59676100
H	4.21500400	4.28848800	1.09081400
C	2.16952700	5.09945800	-0.02268500
C	1.73850600	5.67639200	1.14623500
C	2.79911100	5.87384400	-1.02387800
C	1.92459400	7.06006000	1.37372600
H	1.25494300	5.06306000	1.90603700
C	2.98848100	7.21819400	-0.82855000
H	3.12495000	5.38238700	-1.93788700
C	1.49683600	7.68661000	2.57006400
C	2.56214900	7.84595000	0.36797200
H	3.47357400	7.82265600	-1.59269800
C	1.69335200	9.03048200	2.76284300
H	1.01015700	7.08077800	3.33234500
C	2.74997100	9.23100700	0.59807500
C	2.32642200	9.80992500	1.76766900
H	1.36197800	9.50260000	3.68427900
H	3.23778800	9.82596400	-0.17208000
H	2.47618800	10.87370800	1.93420900
C	1.33255800	-0.44519300	-0.66555900
C	1.88637400	-1.18095400	-1.68165300
C	0.51449000	-1.05933300	0.31316600
C	1.65094900	-2.57484900	-1.76721900
H	2.51528000	-0.69063200	-2.42341600
C	0.26643200	-2.40530800	0.24918900
H	0.09278500	-0.44259600	1.10434100
C	2.21110400	-3.36673800	-2.79910600
C	0.82461300	-3.19803700	-0.78539300
H	-0.36145500	-2.88686900	0.99651200
C	1.96486900	-4.71543800	-2.85577400
H	2.84052500	-2.88452400	-3.54491200
C	0.58920000	-4.59166400	-0.87259200
C	1.14632200	-5.33352800	-1.88364600
H	2.40008600	-5.31530500	-3.65101100
H	-0.04212000	-5.06232100	-0.12092100
H	0.95997100	-6.40297000	-1.94094700
C	6.13556700	2.91110300	2.24673300
C	6.00597800	3.99412400	3.12239200
C	7.42254600	2.42825600	1.96816000
C	7.12080100	4.57774400	3.71156900

H	5.01390300	4.37569800	3.35484800
C	8.53693500	3.00477500	2.55293700
H	7.54665200	1.60156200	1.27258700
C	8.38692500	4.08171600	3.42705900
H	7.00290100	5.41359800	4.39461700
H	9.53184100	2.62827700	2.32501100
C	5.52553800	-0.07805600	2.14823400
C	5.86668000	0.02958100	3.50436000
C	5.94115200	-1.21208400	1.44409800
C	6.60327200	-0.96102600	4.13045200
H	5.53766100	0.89791400	4.07097600
C	6.68154500	-2.20981600	2.06683000
H	5.69224800	-1.30592000	0.38918300
C	7.01214300	-2.08399800	3.41029200
H	6.85502100	-0.87095800	5.18509600
H	7.00314600	-3.08286500	1.50675100
C	-2.72192900	1.72756800	-2.77569500
C	-3.18156700	2.25063400	-3.99300700
C	-3.36357100	0.60086600	-2.25097200
C	-4.25020700	1.67054900	-4.65535300
H	-2.68290200	3.11369400	-4.42833800
C	-4.43492800	0.01320200	-2.91174200
H	-3.02396000	0.18683300	-1.30371700
C	-4.87922300	0.54891400	-4.11435500
H	-4.59396900	2.08091900	-5.60254600
H	-4.92504600	-0.85839300	-2.48866800
C	-2.38556900	4.70964200	-2.19745500
C	-2.01883700	5.87056600	-2.88468900
C	-3.71722300	4.57068200	-1.78026700
C	-2.94916200	6.86710800	-3.15478900
H	-0.99142200	5.98719800	-3.22301900
C	-4.64763500	5.56141700	-2.04311700
H	-4.01592400	3.68119700	-1.22998600
C	-4.26364700	6.71168300	-2.73300700
H	-2.65344100	7.76128300	-3.69567500
H	-5.67519400	5.45015200	-1.70333800
C	-5.29515300	7.76289900	-2.98048200
C	-6.03081700	-0.04732700	-4.85555400
C	7.80297000	-3.13248200	4.12140800
C	9.61504500	4.66252300	4.04707000
F	-4.81651400	8.80837100	-3.66235800
F	-5.79923400	8.23649100	-1.82897100
F	-6.33852800	7.27914500	-3.67388700
F	-5.69111400	-0.38071000	-6.11115100
F	-7.05157900	0.81905700	-4.96189200
F	-6.50814000	-1.14939800	-4.26863100
F	8.09914400	-4.17639400	3.34052700
F	7.14093600	-3.60823200	5.18874300
F	8.96355600	-2.64415300	4.58882500
F	10.23390900	3.77113200	4.83900800
F	10.51443300	5.02255500	3.11700500

F	9.36003900	5.74271700	4.79252300

PC 5a – radical cation

(-3613.165563)

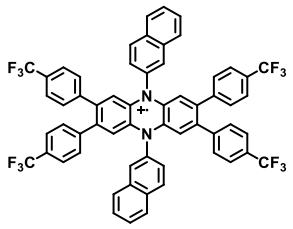

C	-1.51107100	2.21214000	-2.07937000
C	-0.57473800	1.35053300	-1.52936700
C	0.53765600	1.82107800	-0.82618700
C	0.72833500	3.21798700	-0.69658000
C	-0.22843200	4.08467600	-1.23352900
C	-1.34771300	3.61424000	-1.90318200
H	-0.68835500	0.28113500	-1.67997700
H	-0.11403200	5.15415600	-1.08272200
N	1.46000600	0.95475400	-0.27007500
N	1.83922400	3.69208900	-0.02399200
C	2.56627900	1.42877800	0.40913300
C	3.48508200	0.56003600	1.00519200
C	2.76631200	2.82593400	0.52513600
C	4.60217200	1.02742700	1.67963100
H	3.29643000	-0.50891900	0.97041100
C	3.90948900	3.29428500	1.18012000
C	4.83584300	2.42938300	1.74203200
H	4.09549300	4.36370100	1.21552000
C	2.04004700	5.11566800	0.09281500
C	1.58887000	5.76781800	1.21014100
C	2.69762800	5.78965100	-0.95816200
C	1.78073000	7.16483900	1.32828100
H	1.08438900	5.21730700	2.00261500
C	2.89149500	7.14303700	-0.85999600
H	3.03682000	5.22553900	-1.82355700
C	1.33237800	7.88521900	2.46205600
C	2.44268100	7.86339400	0.27494400
H	3.39654500	7.68313500	-1.65796000
C	1.53173300	9.23965100	2.54745100
H	0.82816500	7.34469400	3.26069400
C	2.63250200	9.26165300	0.39510800
C	2.18729200	9.93321300	1.50532700
H	1.18566500	9.78657900	3.42057300
H	3.13817000	9.79082500	-0.41029100
H	2.33737900	11.00646000	1.58843000
C	1.23916900	-0.46736200	-0.36201900
C	1.82256600	-1.17641200	-1.37881600
C	0.41964200	-1.08047600	0.61024700
C	1.60600100	-2.57190200	-1.47024100
H	2.44882100	-0.67087900	-2.11215600
C	0.19856500	-2.43088600	0.53597700
H	-0.01929800	-0.47264900	1.39773000
C	2.18651900	-3.35042000	-2.50069200

C	0.77944900	-3.20871400	-0.49639300
H	-0.42881000	-2.92491400	1.27469700
C	1.95837300	-4.70156000	-2.56271400
H	2.81503400	-2.85688800	-3.23925000
C	0.56400900	-4.60503000	-0.58992200
C	1.14022500	-5.33383600	-1.59916400
H	2.40788800	-5.29299200	-3.35599100
H	-0.06686600	-5.08708500	0.15430900
H	0.96942000	-6.40534100	-1.66233700
C	6.05553600	3.01346500	2.34242400
C	5.95407300	4.07076000	3.25007900
C	7.32655200	2.54979400	1.97748900
C	7.09403400	4.64904800	3.79528500
H	4.97203000	4.43095900	3.54848300
C	8.46413100	3.12931400	2.51207700
H	7.42182000	1.74027200	1.25776200
C	8.34670100	4.17773200	3.42425000
H	7.00571400	5.46306000	4.50811800
H	9.44944100	2.77539000	2.21805500
C	5.47517900	0.03399800	2.34272600
C	5.85012300	0.18896300	3.68426700
C	5.89604800	-1.10250200	1.64791200
C	6.62168000	-0.77353500	4.31210400
H	5.51978600	1.06340800	4.24014900
C	6.67773800	-2.06653300	2.27266200
H	5.62295300	-1.22469500	0.60220400
C	7.03584800	-1.90176500	3.60439800
H	6.89849100	-0.65481300	5.35718400
H	7.00779000	-2.94352500	1.72439800
C	-2.62096400	1.61807700	-2.85687000
C	-2.94090900	2.08748700	-4.13803500
C	-3.33877300	0.54088200	-2.33105900
C	-3.95628400	1.49378900	-4.86811000
H	-2.38021000	2.91403700	-4.56797900
C	-4.36267500	-0.05325000	-3.05845900
H	-3.10503600	0.17700900	-1.33299800
C	-4.67007200	0.42559400	-4.32549500
H	-4.19462000	1.85592100	-5.86548300
H	-4.92235800	-0.88372500	-2.63924300
C	-2.34882700	4.60309100	-2.36020300
C	-1.94296400	5.73630500	-3.06895300
C	-3.70670900	4.44333900	-2.05168500
C	-2.87045200	6.68761100	-3.47631200
H	-0.89278500	5.86372000	-3.32209500
C	-4.63202500	5.39252800	-2.44910400
H	-4.03290900	3.57303700	-1.48707800
C	-4.21313100	6.51324800	-3.16619300
H	-2.55005000	7.55949100	-4.03841200
H	-5.68365400	5.26746000	-2.20139800
C	-5.24709700	7.50626500	-3.59277800
C	-5.76122500	-0.18653300	-5.14505500

C	7.86371900	-2.92164900	4.31926300
C	9.60036600	4.75008800	4.00452900
F	-4.72627500	8.53780900	-4.26278800
F	-5.90985900	8.00705700	-2.53907100
F	-6.17000200	6.93963800	-4.38489900
F	-5.28742200	-0.68588800	-6.29682600
F	-6.68880300	0.72262700	-5.48183400
F	-6.38862900	-1.17882000	-4.50831500
F	8.17067800	-3.96833800	3.54797600
F	7.22621500	-3.39406800	5.40129800
F	9.01743600	-2.39702200	4.75960100
F	10.22960800	3.85432100	4.78128200
F	10.47199000	5.09581700	3.04545500
F	9.37551600	5.83446900	4.75208600

PC 5a – neutral triplet

(-3613.268850)

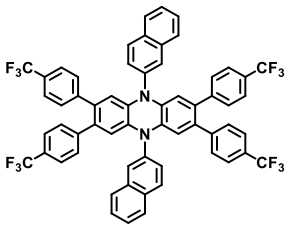

C	-1.52800800	2.30139700	-2.05097800
C	-0.57070900	1.42023400	-1.56912700
C	0.53957000	1.84639200	-0.83268800
C	0.70704600	3.23492800	-0.59453400
C	-0.27667400	4.11784700	-1.05227800
C	-1.39250000	3.68946100	-1.75789300
H	-0.65947000	0.36508400	-1.81327200
H	-0.18616700	5.17227800	-0.80595400
N	1.48227400	0.95497200	-0.35370700
N	1.81661000	3.67517300	0.10365900
C	2.61007500	1.37850400	0.32761500
C	3.54521800	0.49506200	0.84549200
C	2.78453300	2.80105500	0.56704900
C	4.66923900	0.91124500	1.56316600
H	3.33777200	-0.56871900	0.76919500
C	3.93804400	3.23379800	1.20397200
C	4.93661400	2.36151700	1.64374600
H	4.11404200	4.30414200	1.26663600
C	1.98951300	5.08379900	0.32944600
C	1.56304400	5.63591800	1.50882000
C	2.60956900	5.86118300	-0.67317600
C	1.74145500	7.01980600	1.74475200
H	1.08947900	5.01057800	2.26411300
C	2.79174400	7.20399300	-0.46409800
H	2.93263000	5.37883900	-1.59290500
C	1.31679200	7.63300300	2.94837400
C	2.36816200	7.81719400	0.74121800
H	3.26856400	7.81837100	-1.22511500
C	1.50652800	8.97664600	3.15044200

H	0.83857000	7.01805900	3.70845700
C	2.54908100	9.20113100	0.98109800
C	2.12883200	9.76760600	2.15803900
H	1.17772100	9.43926800	4.07747000
H	3.02850000	9.80527500	0.21305700
H	2.27317700	10.83082200	2.33226100
C	1.24295200	-0.45477000	-0.49677700
C	1.81788500	-1.14640000	-1.53017000
C	0.41130000	-1.08968300	0.45187200
C	1.57952500	-2.53576000	-1.66617800
H	2.45662600	-0.62940200	-2.24461400
C	0.16477200	-2.43275700	0.33635700
H	-0.02004800	-0.49814100	1.25611200
C	2.15189500	-3.29322900	-2.71667800
C	0.73697500	-3.18860500	-0.71710900
H	-0.47458000	-2.93877000	1.05683100
C	1.90130200	-4.63807400	-2.82254600
H	2.79338600	-2.78819400	-3.43636800
C	0.49806100	-4.57750800	-0.85551200
C	1.06683800	-5.28563700	-1.88368900
H	2.34573400	-5.21205600	-3.63152500
H	-0.14534000	-5.07102700	-0.12944400
H	0.87774000	-6.35168800	-1.98057300
C	6.22450000	2.91915100	2.02269500
C	6.32200100	4.18569500	2.64117500
C	7.43736400	2.24257900	1.74933700
C	7.54583700	4.74730600	2.95885700
H	5.41406700	4.72376900	2.90563400
C	8.65911900	2.80777600	2.05501800
H	7.40914400	1.27396300	1.25725100
C	8.72668900	4.06346400	2.66792000
H	7.58664900	5.71717500	3.44698000
H	9.57702900	2.27575300	1.81119000
C	5.43671100	-0.08468200	2.29242100
C	6.03321000	0.20547500	3.54321500
C	5.58841800	-1.39982700	1.79862400
C	6.71921700	-0.75993100	4.25217500
H	5.92249100	1.19891300	3.97008700
C	6.28566000	-2.36449700	2.50347000
H	5.17942800	-1.65623600	0.82366600
C	6.85575800	-2.05358100	3.73881100
H	7.15011600	-0.51799100	5.22187600
H	6.40031500	-3.36273500	2.08963300
C	-2.60238900	1.74650000	-2.90164900
C	-2.93757100	2.33675600	-4.12963900
C	-3.27018000	0.57964800	-2.51578700
C	-3.90464200	1.77225100	-4.94332000
H	-2.41935400	3.23714800	-4.45165000
C	-4.24269200	0.01027600	-3.32788800
H	-3.03234200	0.12032900	-1.55874600
C	-4.55759800	0.60598500	-4.54304500

H	-4.14863300	2.22853100	-5.90016200
H	-4.75694900	-0.89329700	-3.01403700
C	-2.41294800	4.69852400	-2.11154400
C	-2.02742200	5.92883100	-2.65426300
C	-3.77609000	4.47084900	-1.86909000
C	-2.96912600	6.90585000	-2.95274100
H	-0.97570800	6.11590900	-2.86045800
C	-4.71795800	5.44113100	-2.16407000
H	-4.09478600	3.52775300	-1.43122700
C	-4.31472600	6.66075300	-2.70853700
H	-2.65715900	7.85423900	-3.38009100
H	-5.77161800	5.25804000	-1.96474100
C	-5.36589800	7.67183300	-3.03161800
C	-5.60018500	0.03200000	-5.44594600
C	7.65283800	-3.04473500	4.50872500
C	10.06484800	4.62516700	2.99236200
F	-4.85607300	8.82365000	-3.47950000
F	-6.12113800	7.95975200	-1.95973600
F	-6.20954800	7.21716900	-3.97236300
F	-5.12117000	-0.17068400	-6.68333300
F	-6.64865800	0.86028900	-5.58139000
F	-6.07592800	-1.13751600	-5.00716600
F	7.57926100	-4.28073700	4.00006400
F	7.25669500	-3.12011800	5.79210400
F	8.95904000	-2.71702600	4.55064700
F	10.76209800	3.82145500	3.81726800
F	10.82987600	4.76834100	1.89329500
F	9.99761300	5.82581000	3.58100000

PC 5b – ground state

(-2723.170996)

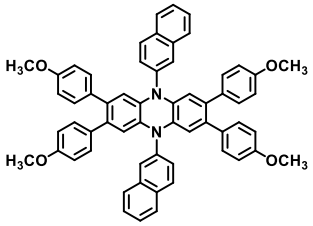

C	-2.05882500	2.16036100	1.14833300
C	-0.98940300	1.31691400	0.80511500
C	0.04107800	1.71122000	-0.03544400
C	0.00422700	3.00675300	-0.58944800
C	-1.04513000	3.84747200	-0.24725100
C	-2.07647800	3.46082400	0.62420600
H	-0.98660300	0.30129800	1.19337300
H	-1.05461800	4.86104300	-0.64171700
N	1.10438900	0.85275800	-0.35561700
N	1.02288500	3.41302200	-1.46460100
C	2.12364300	1.25942100	-1.22987200
C	3.17343800	0.41898000	-1.57139500
C	2.08681400	2.55496300	-1.78385800
C	4.20525000	0.80590200	-2.44217400
H	3.18286400	-0.59462300	-1.17701000
C	3.11781000	2.94958500	-2.62363900

C	4.18765900	2.10640500	-2.96620200
H	3.11506100	3.96522400	-3.01183500
C	1.01575800	4.74305300	-1.98134800
C	0.44326200	5.00616000	-3.20060500
C	1.61320800	5.77936800	-1.22517500
C	0.44659400	6.32049800	-3.72659400
H	-0.01191600	4.19611300	-3.76931000
C	1.62634200	7.06124200	-1.71008900
H	2.05557000	5.53429900	-0.26175500
C	-0.12866400	6.62537700	-4.98471300
C	1.04913700	7.36741600	-2.96811100
H	2.08479700	7.86421400	-1.13572500
C	-0.10631200	7.90826800	-5.47048100
H	-0.58783700	5.82159400	-5.55756400
C	1.05508200	8.68120600	-3.49698900
C	0.49138900	8.94596700	-4.71993500
H	-0.54955600	8.13178400	-6.43764300
H	1.51770100	9.47619600	-2.91457800
H	0.50221000	9.95786400	-5.11712400
C	1.11140900	-0.47735200	0.16091600
C	1.68399400	-0.74076000	1.38007300
C	0.51380600	-1.51343700	-0.59542000
C	1.68059200	-2.05520400	1.90579400
H	2.13930800	0.06913100	1.94890000
C	0.50061800	-2.79541600	-0.11077800
H	0.07136800	-1.26811200	-1.55873600
C	2.25590100	-2.36039100	3.16382100
C	1.07790000	-3.10190600	1.14713200
H	0.04204200	-3.59822700	-0.68527000
C	2.23346200	-3.64337800	3.64932200
H	2.71517900	-1.55676500	3.73680900
C	1.07188500	-4.41580800	1.67573800
C	1.63562800	-4.68086800	2.89859300
H	2.67672900	-3.86713800	4.61641800
H	0.60915500	-5.21063900	1.09319600
H	1.62475000	-5.69284700	3.29557000
C	-3.09891600	4.47196300	0.97843200
C	-3.75312600	5.20880100	-0.00947900
C	-3.41769200	4.75018200	2.31636200
C	-4.70384700	6.17902200	0.30307300
H	-3.52906700	5.00901600	-1.05642600
C	-4.35499400	5.71159700	2.64504400
H	-2.91288400	4.20230700	3.10995100
C	-5.00975900	6.43186600	1.63925500
H	-5.19707900	6.72018000	-0.49876200
H	-4.59745500	5.93271800	3.68186800
C	-3.12250000	1.60264700	2.01463500
C	-2.79653100	0.86651800	3.15482700
C	-4.48393900	1.74590400	1.70293800
C	-3.77155800	0.29290700	3.96789300
H	-1.74900300	0.74664000	3.42707300

C	-5.46513900	1.18291800	2.49765900
H	-4.77155100	2.30614700	0.81511700
C	-5.11692400	0.45116500	3.63874600
H	-3.47001700	-0.26559700	4.84887600
H	-6.51907800	1.28646300	2.25070300
C	5.22803600	-0.20506100	-2.79589700
C	5.54755900	-0.48323200	-4.13364100
C	5.88174300	-0.94190000	-1.80764200
C	6.48509100	-1.44459700	-4.46182300
H	5.04316700	0.06464800	-4.92749300
C	6.83268400	-1.91206100	-2.11967400
H	5.65706700	-0.74214700	-0.76082200
C	7.13933400	-2.16487500	-3.45570500
H	6.72812500	-1.66566800	-5.49852300
H	7.32544800	-2.45319600	-1.31754300
C	5.25178700	2.66446600	-3.83172700
C	4.92639400	3.40085000	-4.97192400
C	6.61305300	2.52147600	-3.51917600
C	5.90182300	3.97495800	-5.78416100
H	3.87902000	3.52055500	-5.24483300
C	7.59464800	3.08492700	-4.31308000
H	6.90023700	1.96109300	-2.63130900
C	7.24701400	3.81693900	-5.45417600
H	5.60072300	4.53366000	-6.66516700
H	8.64844200	2.98158400	-4.06542600
O	-5.91514400	7.34803400	2.06431400
O	-6.15086900	-0.06229700	4.35112600
O	8.28128000	4.33098300	-6.16565600
O	8.04492300	-3.08105300	-3.88032300
C	-6.61144000	8.08807600	1.08317900
H	-7.20365700	7.43411500	0.42933100
H	-7.28392400	8.75891800	1.62022000
H	-5.92766800	8.68508900	0.46532700
C	-5.84118900	-0.82021100	5.50200500
H	-5.30692600	-0.21932700	6.24979800
H	-6.79251500	-1.14987700	5.92260100
H	-5.23500500	-1.70161600	5.25363800
C	8.74099800	-3.82084800	-2.89883500
H	8.05712900	-4.41803500	-2.28125500
H	9.41392600	-4.49151100	-3.43553700
H	9.33272100	-3.16667600	-2.24475200
C	7.97216900	5.08918200	-7.31649600
H	7.36541000	5.97023500	-7.06827600
H	8.92367500	5.41941300	-7.73624200
H	7.43874300	4.48834200	-8.06492100

PC 5a – cation radical

(-2723.005097)

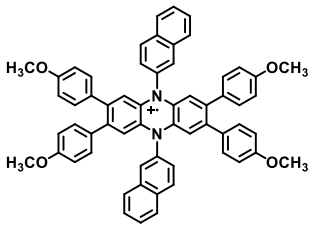

C	-2.04238400	2.13940300	1.12638900
C	-0.98891300	1.29813200	0.79242300
C	0.05084900	1.70353800	-0.04657600
C	0.01700800	3.00722600	-0.59801900
C	-1.03292000	3.86037000	-0.25063900
C	-2.04964200	3.46815200	0.61023000
H	-0.99391800	0.27760200	1.16366400
H	-1.02935000	4.87864100	-0.62896700
N	1.09808100	0.85713500	-0.36798300
N	1.03057500	3.40955900	-1.45003600
C	2.11164400	1.25946600	-1.22000700
C	3.16157200	0.40632000	-1.56738800
C	2.07780800	2.56315700	-1.77144300
C	4.17830200	0.79854800	-2.42824200
H	3.15800400	-0.61195100	-1.18905900
C	3.11757800	2.96856900	-2.61043300
C	4.17104500	2.12729500	-2.94439600
H	3.12258500	3.98909800	-2.98167300
C	1.00973100	4.74290400	-1.99396200
C	0.41908400	4.96676500	-3.21000900
C	1.61238000	5.78186800	-1.25212200
C	0.40849400	6.27320700	-3.75391200
H	-0.03766300	4.14373300	-3.75738600
C	1.60943100	7.05390900	-1.76202300
H	2.06779400	5.55440500	-0.29112700
C	-0.18368900	6.55353700	-5.00955000
C	1.01460600	7.33420400	-3.01764000
H	2.06968600	7.86840800	-1.20669500
C	-0.17363600	7.82918300	-5.51346700
H	-0.64482900	5.73889000	-5.56452100
C	1.00692900	8.63979800	-3.56586600
C	0.42690100	8.88112500	-4.78569300
H	-0.62917600	8.03599700	-6.47840800
H	1.47196700	9.44597600	-3.00170600
H	0.42686900	9.88653500	-5.19867500
C	1.11892600	-0.47620700	0.17594500
C	1.70958200	-0.70006600	1.39198800
C	0.51626700	-1.51517200	-0.56588600
C	1.72017200	-2.00650600	1.93589600
H	2.16633600	0.12296600	1.93935900
C	0.51921700	-2.78721200	-0.05598100
H	0.06084600	-1.28771100	-1.52687800
C	2.31236500	-2.28683300	3.19153000
C	1.11405100	-3.06750400	1.19963300
H	0.05895500	-3.60171100	-0.61130200

C	2.30231100	-3.56247800	3.69545200
H	2.77351100	-1.47218600	3.74649500
C	1.12172900	-4.37309700	1.74786300
C	1.70176500	-4.61442100	2.96768600
H	2.75785800	-3.76929000	4.66039000
H	0.65668400	-5.17927500	1.18371000
H	1.70179800	-5.61983000	3.38067200
C	-3.06873600	4.46892900	0.98470400
C	-3.69949400	5.24315100	0.00940300
C	-3.40090700	4.70085600	2.32914000
C	-4.64657100	6.20728100	0.34223700
H	-3.46615400	5.07321800	-1.04035800
C	-4.32696900	5.66421400	2.67591900
H	-2.91351600	4.12122100	3.11041400
C	-4.96325800	6.42153100	1.68399700
H	-5.12936300	6.77603100	-0.44632800
H	-4.57855100	5.85696500	3.71574100
C	-3.11858300	1.59258600	1.97647700
C	-2.80568900	0.83826700	3.10925600
C	-4.47496100	1.76127400	1.65287100
C	-3.79347500	0.27257500	3.90871900
H	-1.76228000	0.70510100	3.38964000
C	-5.46663900	1.19672300	2.43020700
H	-4.75084200	2.33265000	0.76910900
C	-5.13488100	0.44975500	3.56782600
H	-3.50644300	-0.29478800	4.78838000
H	-6.51695800	1.31298100	2.17558400
C	5.19743500	-0.20219700	-2.80269400
C	5.52974300	-0.43400200	-4.14711600
C	5.82811700	-0.97648300	-1.82739400
C	6.45585100	-1.39732000	-4.49388700
H	5.04242600	0.14569900	-4.92838800
C	6.77523500	-1.94057600	-2.16021800
H	5.59467900	-0.80663500	-0.77764100
C	7.09205000	-2.15471400	-3.50196600
H	6.70753900	-1.58997800	-5.53370000
H	7.25796100	-2.50938400	-1.37165400
C	5.24725600	2.67408700	-3.79448200
C	4.93439300	3.42851100	-4.92719900
C	6.60362700	2.50523800	-3.47093800
C	5.92220700	3.99417400	-5.72664900
H	3.89098600	3.56179200	-5.20753900
C	7.59533400	3.06975400	-4.24826300
H	6.87948000	1.93375200	-2.58723600
C	7.26360700	3.81684500	-5.38581000
H	5.63519900	4.56162800	-6.60625900
H	8.64565000	2.95337200	-3.99368700
O	-5.86196100	7.32943600	2.12567900
O	-6.17701700	-0.05609900	4.26419600
O	8.30576700	4.32265600	-6.08217600
O	7.99080700	-3.06257200	-3.94363600

C	-6.54985200	8.10366000	1.16222400
H	-7.14447600	7.47135100	0.49030300
H	-7.21797600	8.76335800	1.71757100
H	-5.85827600	8.71187200	0.56532600
C	-5.89101400	-0.82785100	5.41469400
H	-5.35982800	-0.23770200	6.17240200
H	-6.85217800	-1.14780000	5.81918000
H	-5.29336000	-1.71409000	5.16520600
C	8.67863400	-3.83684700	-2.98017700
H	7.98702500	-4.44513200	-2.38339300
H	9.34683500	-4.49647700	-3.53551400
H	9.27317200	-3.20457000	-2.30815000
C	8.01979800	5.09454000	-7.23259300
H	7.42224200	5.98081600	-6.98300300
H	8.98097800	5.41443000	-7.63708800
H	7.48852300	4.50451200	-7.99033400

PC 5b – neutral triplet

(-2723.092185)

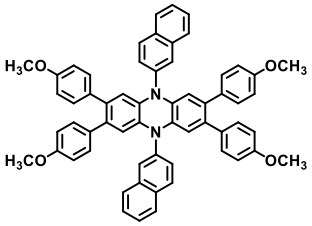

C	-0.09037900	2.45918700	-2.82762800
C	0.11274100	1.23650400	-2.20184200
C	0.78753000	1.11417900	-0.98185100
C	1.27561600	2.29172400	-0.35356900
C	1.06417200	3.52336300	-0.98316000
C	0.38930800	3.64283900	-2.19071700
H	-0.22675000	0.33355600	-2.70264200
H	1.40341200	4.42796300	-0.48525900
N	1.00551000	-0.11579100	-0.38181300
N	1.93489800	2.18988400	0.86131900
C	1.66477800	-0.23674900	0.82886000
C	1.94185300	-1.46555800	1.41622100
C	2.13717200	0.97263300	1.48806700
C	2.61532500	-1.59781500	2.62948500
H	1.69904700	-2.36445900	0.85475300
C	2.73664800	0.86034000	2.73619400
C	2.94131600	-0.36072800	3.37916000
H	2.97186700	1.77797300	3.26989100
C	2.50512100	3.36483500	1.45430200
C	1.73187400	4.17534400	2.24475200
C	3.86647900	3.64982600	1.21273100
C	2.29361500	5.33491400	2.83274200
H	0.68497200	3.92954900	2.41698200
C	4.43208400	4.76548500	1.77458400
H	4.44177900	2.97547200	0.58253200
C	1.53131100	6.20266200	3.65094600
C	3.66800500	5.63406500	2.59426200

H	5.47946400	5.00101200	1.59605700
C	2.10387600	7.31865800	4.20905200
H	0.48336000	5.96732700	3.82799000
C	4.22804400	6.79271300	3.18413800
C	3.46407700	7.61630700	3.97333100
H	1.51034400	7.97918900	4.83602000
H	5.27704000	7.01718300	2.99874000
H	3.90483400	8.50350800	4.42100700
C	0.50459600	-1.30439200	-1.00938400
C	1.24626300	-1.91650300	-1.98656200
C	-0.74103800	-1.82266400	-0.59453000
C	0.76296500	-3.09110500	-2.61139000
H	2.20552800	-1.49601600	-2.28505000
C	-1.22682800	-2.96221100	-1.18377300
H	-1.29300200	-1.30626500	0.18746400
C	1.49403500	-3.75117400	-3.62790900
C	-0.49508400	-3.62418900	-2.20152000
H	-2.18657300	-3.37368500	-0.87731400
C	1.00149300	-4.89030900	-4.21435200
H	2.45308300	-3.33736800	-3.93433300
C	-0.97512000	-4.80047900	-2.82635900
C	-0.24424500	-5.41939200	-3.80993900
H	1.56973500	-5.39062400	-4.99436900
H	-1.93578800	-5.20371600	-2.51074800
H	-0.62292100	-6.32207900	-4.28271900
C	0.15455000	5.00121600	-2.72486100
C	1.18811400	5.93906600	-2.77002200
C	-1.11631400	5.41330400	-3.15800800
C	0.98510000	7.23828000	-3.22954700
H	2.18720300	5.64375400	-2.45321100
C	-1.33590400	6.69931900	-3.61431900
H	-1.94646400	4.71048900	-3.12447400
C	-0.28512000	7.62318900	-3.65650500
H	1.82097400	7.93077300	-3.25582100
H	-2.32210600	7.02116400	-3.94033500
C	-0.74278200	2.46200900	-4.15436500
C	-1.90376700	1.72027100	-4.38146900
C	-0.19652000	3.16335700	-5.24172900
C	-2.51399500	1.67093700	-5.63279200
H	-2.35707000	1.17687900	-3.55381800
C	-0.78742800	3.12321100	-6.49043000
H	0.71498300	3.74109200	-5.10176800
C	-1.95425400	2.37778700	-6.69626400
H	-3.42128800	1.08837200	-5.76088600
H	-0.35865000	3.65828300	-7.33438800
C	3.07355600	-2.92243900	3.03379300
C	4.30980800	-3.12137600	3.68932300
C	2.32120900	-4.07680500	2.75042100
C	4.76086800	-4.38530200	4.01789300
H	4.93630200	-2.26219800	3.91664800
C	2.76139800	-5.35272700	3.08034300

H	1.34505000	-3.97330300	2.27914400
C	3.99197900	-5.51584000	3.72040400
H	5.72241300	-4.52734700	4.50650200
H	2.13221000	-6.20703100	2.84786400
C	3.33610700	-0.35602700	4.78249400
C	2.86862600	-1.31690300	5.69946400
C	4.18297200	0.64882500	5.30256100
C	3.20423200	-1.27965800	7.04830300
H	2.19942300	-2.10083000	5.35340100
C	4.52721800	0.69365100	6.63865800
H	4.60201400	1.39508000	4.62956000
C	4.04030000	-0.27164700	7.52936000
H	2.80173800	-2.03781300	7.71411400
H	5.19149300	1.46517000	7.02164800
O	-0.60028400	8.85626300	-4.12424100
O	-2.45988700	2.40561800	-7.95409200
O	4.44021700	-0.14504800	8.82245700
O	4.51857200	-6.71222600	4.09384900
C	0.43065700	9.82049900	-4.18055900
H	1.24338500	9.50375000	-4.84754900
H	-0.01892500	10.73311700	-4.57493700
H	0.84577000	10.02589900	-3.18492000
C	-3.63443300	1.66213100	-8.20587800
H	-4.47465100	2.01556200	-7.59356500
H	-3.87484700	1.80881900	-9.26001100
H	-3.48186400	0.59106000	-8.01792400
C	3.77152800	-7.87367300	3.80348900
H	3.60701700	-7.98971700	2.72360400
H	4.35636800	-8.72014500	4.16753400
H	2.79770400	-7.86664800	4.31169400
C	3.97332700	-1.10377700	9.74657500
H	4.29988600	-2.11759300	9.47775100
H	4.39983500	-0.83737200	10.71518600
H	2.87752400	-1.09285400	9.82264500

References

[1]Z. Huang, S. Xiang, Q. Zhang, X. Lv, S. Ye, R. Guo, and L. Wang, *J. Mater. Chem. C*, 2018, **6**, 2379.

[2]J. C. Theriot, C. H. Lim, H. Yang, M. D. Ryan, C. B. Musgrave, and G. M. Miyake, *Science*, 2016, **352**, 1082–1086.

[3]B. G. McCarthy, R. M. Pearson, C. Lim, S. M. Sartor, N. H. Damrauer, and G. M. Miyake, *J. Am. Chem. Soc.*, **140**, 15, 5088-5101.

[4]J. P. Cole, C. R. Federico, C. H. Lim and G. M. Miyake, *Macromolecules*, 2019, **52**, 747–754.

[5]H. He, P. Zapol and L. A. Curtiss, *J. Phys. Chem. C*, 2010, **114**, 21474–21481.

[6]J. A. Tossell, *Comput. Theor. Chem.*, 2011, **977**, 123–127.

[7]P. Winget, C. J. Cramer, and D. G. Truhlar, *Theor. Chem. Acc.*, 2004, **112**, 217–227.

[8]Y. Zhao, D. G. Truhlar, *Theor. Chem. Acc.*, 2008, **120**, 215–241.

[9]T. Yanai, D. P. Tew, and N. C. Handy, *Chem. Phys. Lett.*, 2004, **393**, 51–57.

[10]C. H. Lim, M. D. Ryan, B. G. McCarthy, J. C. Theriot, S. M. Sartor, N. H. Damrauer, C. B. Musgrave and G. M. Miyake, *J. Am. Chem. Soc.*, 2017, **139**, 348–355.

[11]M. A. Spackman, *J. Comp. Chem.*, 1996, **17**, 1–18.

APPENDIX 2 – Supporting Information for Chapter 2

MATERIALS AND INSTRUMENTATION

Chemical Purchase, Preparation, and Storage

All chemicals were used as received unless otherwise specified. Diphenylamine, aniline, pyridine, pyrrolidine, allyl bromide, bicyclo[2.2.1]hept-2-ene (norbornene), dicyclopentadiene (DCPD), butylated hydroxytoluene (BHT), phenylmagnesium bromide (PhMgBr), elemental sulfur (S_8), 2-norbornene-5-methanol, and 1,3,5-trimethoxybenzene (TMB) were all purchased from Sigma-Aldrich. Sodium carbonate (Na_2CO_3), magnesium sulfate ($MgSO_4$), sodium sulfate (Na_2SO_4), calcium hydride (CaH), triethylamine (TEA), 1,8-diazabicyclo[5.4.0]undec-7-ene (DBU), 1,4-diazabicyclo[2.2.2]octane (DABCO), and bicyclo[2.2.1]heptan-2-one (norcamphor) were purchased from Oakwood Chemicals. Sodium thiophenolate (PhSNa) was purchased from Acros Organics. Tert-butylamine, dibenzo-18-crown-6, and 1-bromohexane were purchased from TCI Chemicals. Dimethyl-5-norbornene-2,3-dicarboxylate was purchased from Alfa-Aesar.

3Å molecular sieves were purchased from Sigma Aldrich and were dried under vacuum at 350 °C for 15 hours before being brought into a nitrogen filled glovebox for storage (in a Schlenk tube) and use.

Ethyl acetate (EtOAc), hexanes, *N,N*-dimethyl formamide (DMF), diethyl ether, carbon disulfide (CS_2) (reagent grade) were purchased from Fischer Sicentific and used as received unless otherwise specified.

Solvents for polymerizations and depolymerizations: Tetrahydrofuran, benzene, and toluene were obtained from an mBraun MB-SPS-800 solvent purification system, kept under a nitrogen atmosphere, and stored over activated 3Å molecular sieves for 48 hours before use.

Initiators for polymerization and depolymerization: DABCO was sublimed under reduced pressure at 50 °C then brought into a nitrogen filled glovebox for storage. 1,3-di-*t*burylimidazol-2-ylidine (NHC*t*Bu), purchased from TCI America, was used as received. P_4*t*Bu, purchased from Sigma Adrich as a ~0.8 M solution in hexanes, was used as received. The actual concentration was estimated via ^{1}H-NMR using trimethoxy benzene as an internal standard. Benzyl alcohol (BnOH), purchased from Oakwood Chemicals, was degassed using the freeze-pump-thaw technique, distilled under vacuum, transferred to a nitrogen filled glovebox, then stored over 3Å molecular sieves for 48 hours before use. Allyl bromide (AllylBr), 1,8-diazabiyclo(5.4.0)undec-7-ene (DBU), TEA, pyridine, aniline, pyrrolidine were distilled under vacuum, degassed using the freeze-pump-thaw technique, transferred to a Nitrogen filled glovebox, then stored over 3Å molecular sieves (20% by volume) for 48 hours before use.

Solvents for characterization: Deuterated benzene was stirred over CaH for 12 hours, distilled into a flame dried Schlenk flank under vacuum, degassed by freeze-pump-that method (3 cycles) then stored under nitrogen in a nitrogen filled glovebox. Deuterated chloroform was distilled then stored over dried 3Å for 3 days before use. All solvents used for mass analysis and GPC analysis were HPLC grade.

Equipment for Polymerization and Depolymerization

Glass syringes, metal needles, Teflon stir bars, and glass vials were stored in a 140 °C oven for 48 hours then brought directly into the antechamber of the glovebox and placed under reduced pressure to cool before being brought into a nitrogen filled glovebox. Plastic needles, syringes, and caps were all stored in a descant chamber under vacuum for at least 48 hours before use.

Instrumentation for Characterization

Nuclear Magnetic Resonance Spectroscopy

Nuclear magnetic resonance (NMR) spectra were obtained using a Bruker 400 MHz NMR Spectrometer at 298 K. All ^{1}H NMR experiments are reported in parts per million (ppm) and were measured relative to the signals for residual chloroform (δ = 7.26 ppm) in deuterated chloroform. ^{13}C NMR spectra reported in ppm are relative to chloroform (δ = 77.16 ppm) and were obtained with ^{1}H decoupling.

Gel Permeation Chromatography

Molecular weights were determined by Gel Permeation Chromatography (GPC) coupled with multi-angle light scattering (MALS) using an Agilent HPLC fitted with one guard column, three PL-gel 5 μm MIXED-C gel permeation columns, a Wyatt Technology TrEX differential refractometer, and a Wyatt Technology miniDAWN TREOS light scattering detector (MALS).

Thermogravimetric Analysis

Thermogravimetric Analysis (TGA) was performed using a Mettler-Toledo TGA/SDTA851. Samples were heated in platinum pans from ambient temperatures using a heating rate of 10 °C/min under N_2 purge.

Dynamic Scanning Calorimetry

Differential scanning calorimetry (DSC) measurements were performed using a TA Instruments Auto Q20 in N2 atmosphere. All cycles used heating and cooling rates of 10 °C/min.

Ultraviolet-visible (UV-Vis) Spectroscopy

UV-Vis spectroscopy was performed on a Cary 5000 spectrophotometer. DMAc was used as the solvent for all data presented in this work. All samples were analyzed in 1 cm pathlength quartz cuvettes.

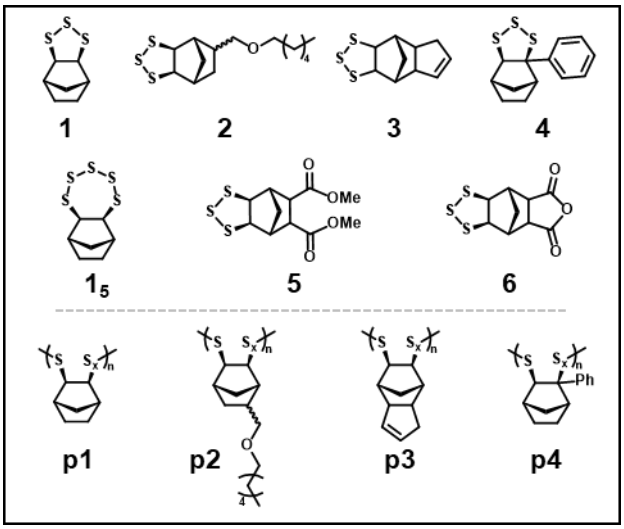

Figure A2.1: Chemical structures of norbornane trithiolane monomers (top) and poly(norbornane trithiolanes) (bottom) discussed in this work.

SYNTHESIS AND CHARACTERIZATION

Monomer Synthesis (procedures, ^{1}H-NMR, ^{13}C-NMR, Mass Spec)

Synthesis of **1** (NS_3)

Norbornene (0.471 g, 5.00 mmol, 1.00 eq.), S_8 (0.480 g, 1.88 mmol, 0.375 eq.), $[Ni(NH_3)_6Cl_2]$ (0.023 g, 0.100 mmol, 2.00 mol%) (we have shown that several other amine additives, can be used to achieve a similar yield in this reaction), and 10 mL DMF were added to a 50 mL round bottom flask equipped with a reflux condenser and heated to 120 °C for 18 hours. Diethyl ether was added to the crude reaction mixture which was then washed with H_2O three times to remove DMF. The organic layer was then dried with Na_2SO_4 and concentrated under reduced pressure. **1**$_5$ was recrystallized as a white solid from the crude reaction mixture in 1:5 EtOAc:hexanes at

30 °C. The remaining reaction mixture was purified by flash column chromatography (15% EtOAc : 85% hexanes) to yield the desired product as a yellow oil (83.2% yield). ^{1}H NMR (400 MHz, $CDCl_3$) δ 3.64 (d, *J* = 1.8 Hz, 2H), 2.47 (p, *J* = 2.1 Hz, 2H), 1.94 (dt, *J* = 10.5, 2.1 Hz, 1H), 1.73 (dqt, *J* = 8.0, 5.1, 2.6 Hz, 2H), 1.27 (qd, *J* = 6.4, 2.6 Hz, 2H), 1.06 (dt, *J* = 10.5, 1.9 Hz, 1H). ^{13}C NMR (101 MHz, $CDCl_3$) δ 69.96, 40.90, 32.45, 27.74.

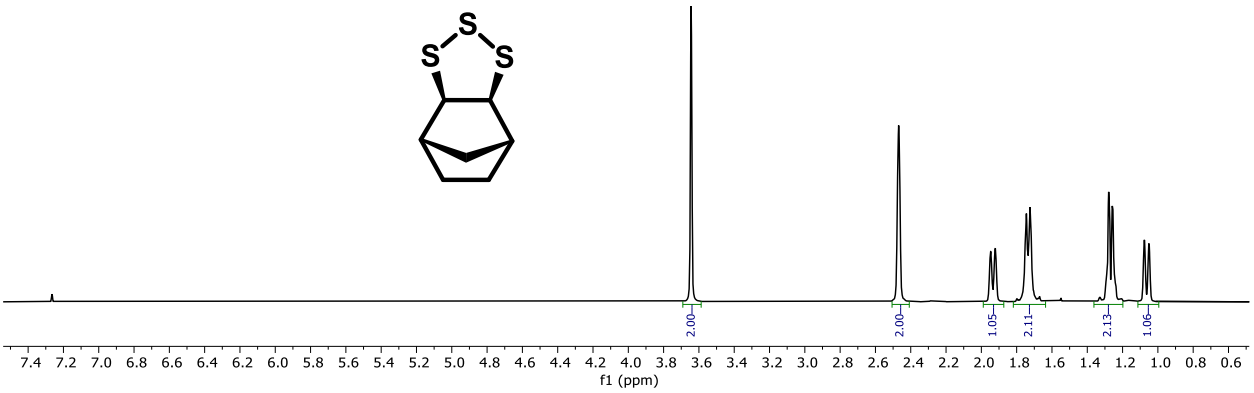

Figure A2.2: ^{1}H NMR of **1** in $CDCl_3$.

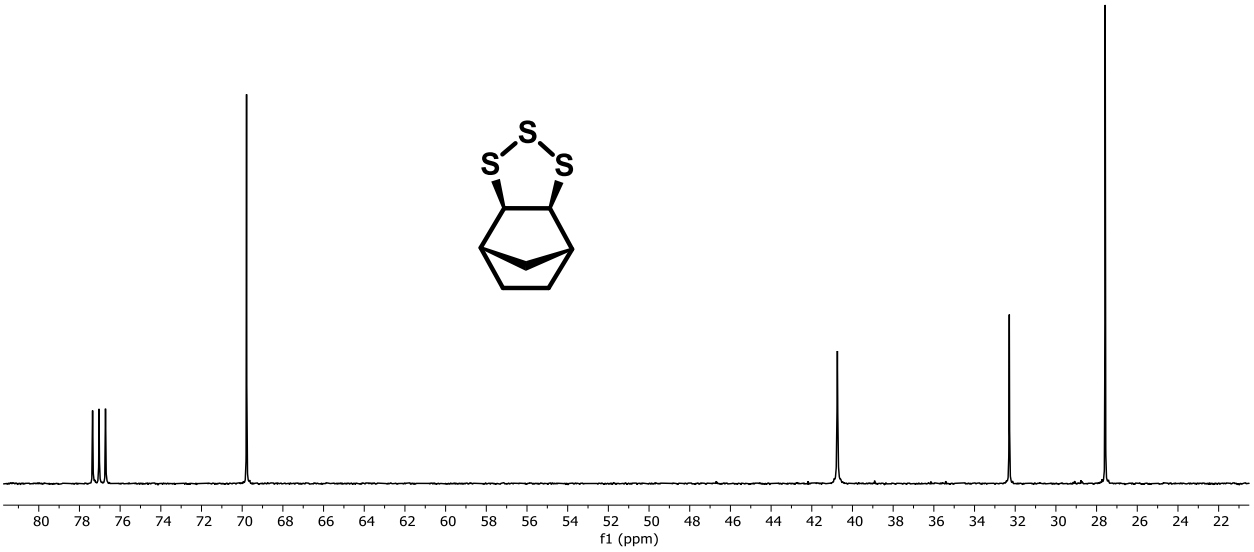

Figure A2.3: ^{13}C NMR of **1** in $CDCl_3$.

Isolation of **1_5**

1_5 can be isolated from **1** by recrystallization in ethyl acetate at -18 ºC.

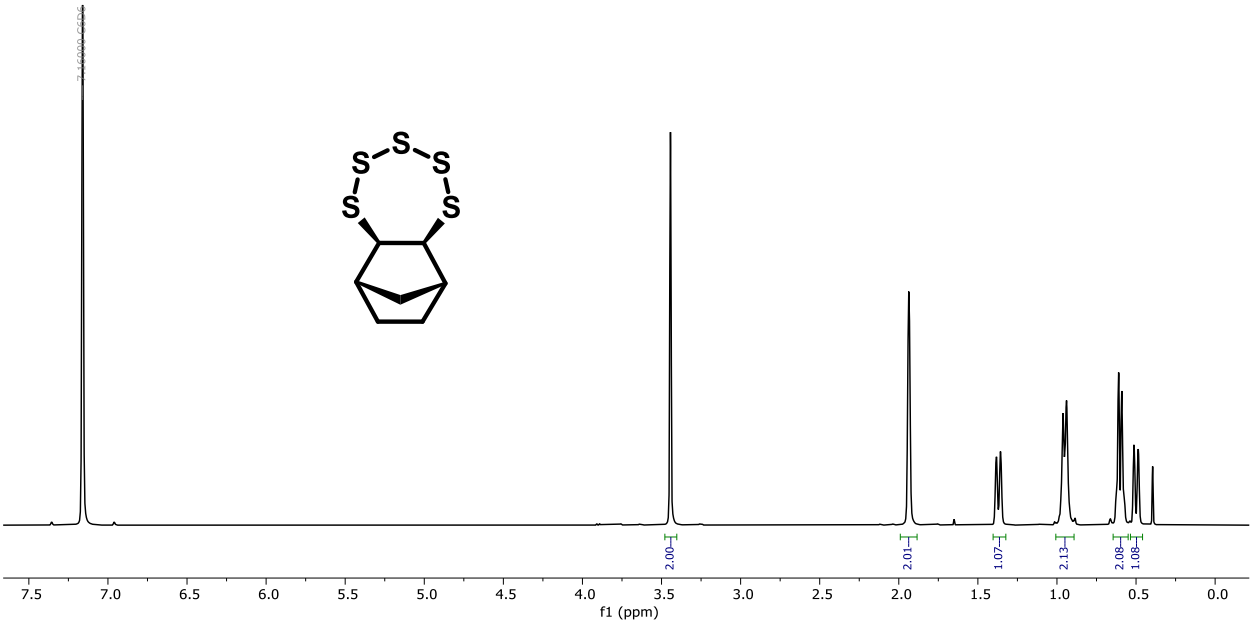

Figure A2.4: ^{1}H NMR of **1_5** in $CDCl_3$.

Synthesis of **2** ($MHENS_3$)

Step 1: Synthesis of NB-MHE

NaH (3.93 g, 164 mmol, 2.85 eq.) was charged to a 250 mL Schlenk flask equipped with a teflon coated magnetic stir bar. 200 mL of anhydrous THF was then added and the reaction flask transferred to a dry ice/acetone bath (-80 °C). Meanwhile 5-norbornene-2-methanol and 1-bromohexane were sparged with N_2 for 20 minutes. 5-norbornene-2-methanol (10.0 g, 80.5 mmol, 1.40 eq.) was then added dropwise to the mixture of NaH in THF and stirred for 12 hours while slowly coming to room temperature. Next, 1-bromohexane (9.49 g, 57.5 mmol, 1.00 eq.) was added dropwise to the reaction mixture which was then heated to 90 °C and refluxed for 48 hours. After 48 hours the reaction was cooled and 200 mL of 1M HCl was added slowly. In a separation funnel the product was extracted by washing the aqueous layer three times with 200 mL of diethyl ether. The organic phase was then washed with a saturated solution of Na_2CO_3 followed by brine and finally dried over $MgSO_4$. The crude reaction mixture was purified by column chromatography (20% EtOAc, 80% Hexanes) to yield the desired product (isolated yield: 73.5%).

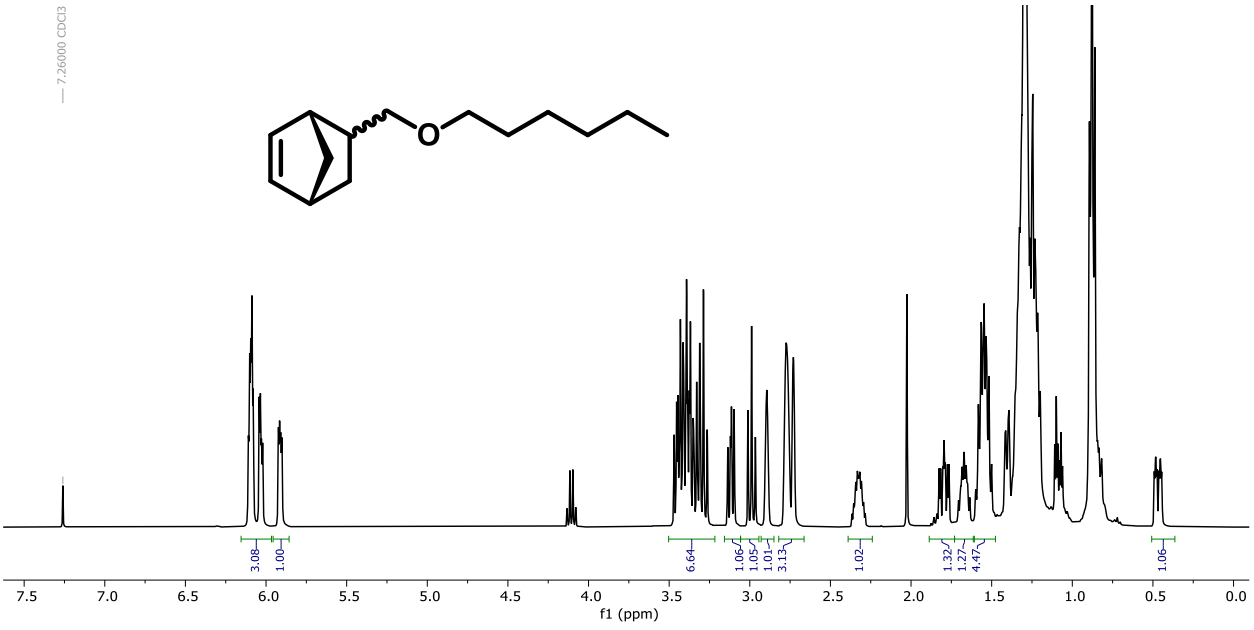

Figure A2.5: ^1H NMR of NB-MHE in $CDCl_3$.

Step 2: Synthesis of **2** ($MHENS_3$)

NB-MHE (5.00 g, 37.8 mmol, 1.00 eq.), S_8 (3.64 g, 14.2 mmol, 0.375 eq.), $Ni(NH_3)_6Cl_2$ (0.175 g, 0.756 mmol, 2.00 mol%), and 70 mL DMF were added to a 100 mL round bottom flask equipped with a reflux condenser and heated to 120 °C for 18 hours. Diethyl ether was added to the crude reaction mixture which was then washed with H_2O three times to remove DMF. The organic layer was then dried with Na_2SO_4 and concentrated under reduced pressure and purified by flash column chromatography hexanes (100%) to yield the desired product as a yellow solid (82.6% isolated yield).

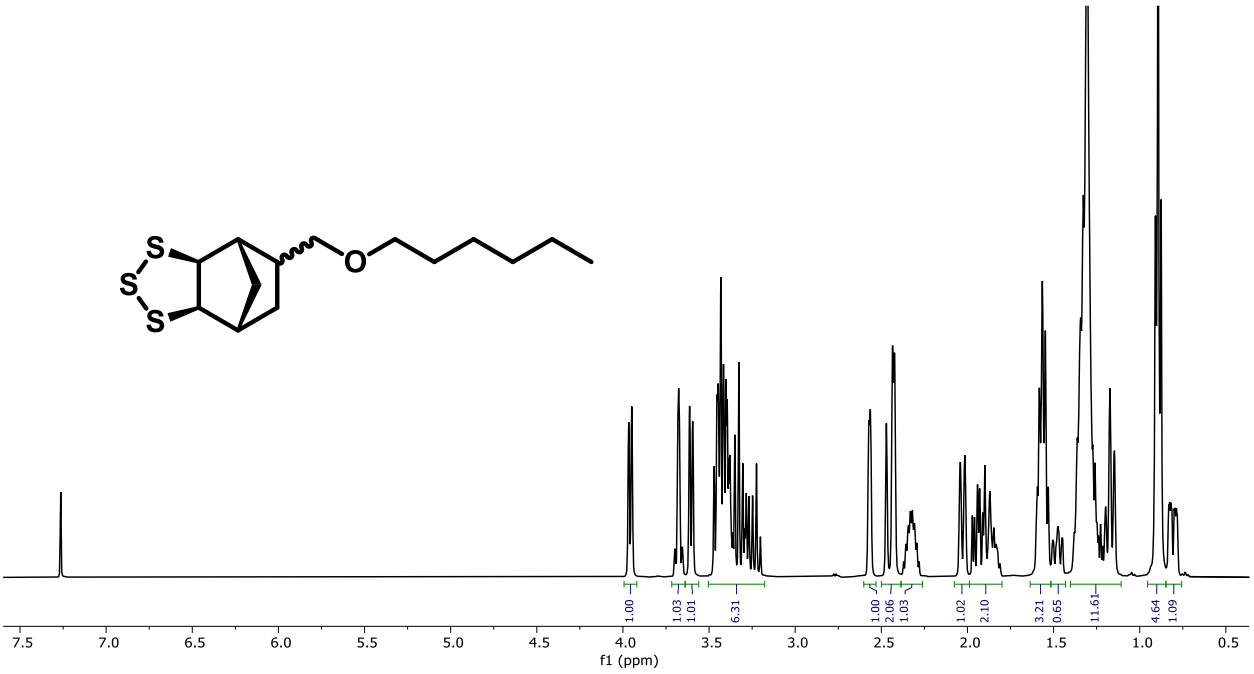

Figure A2.6: ^1H NMR of **2** in $CDCl_3$.

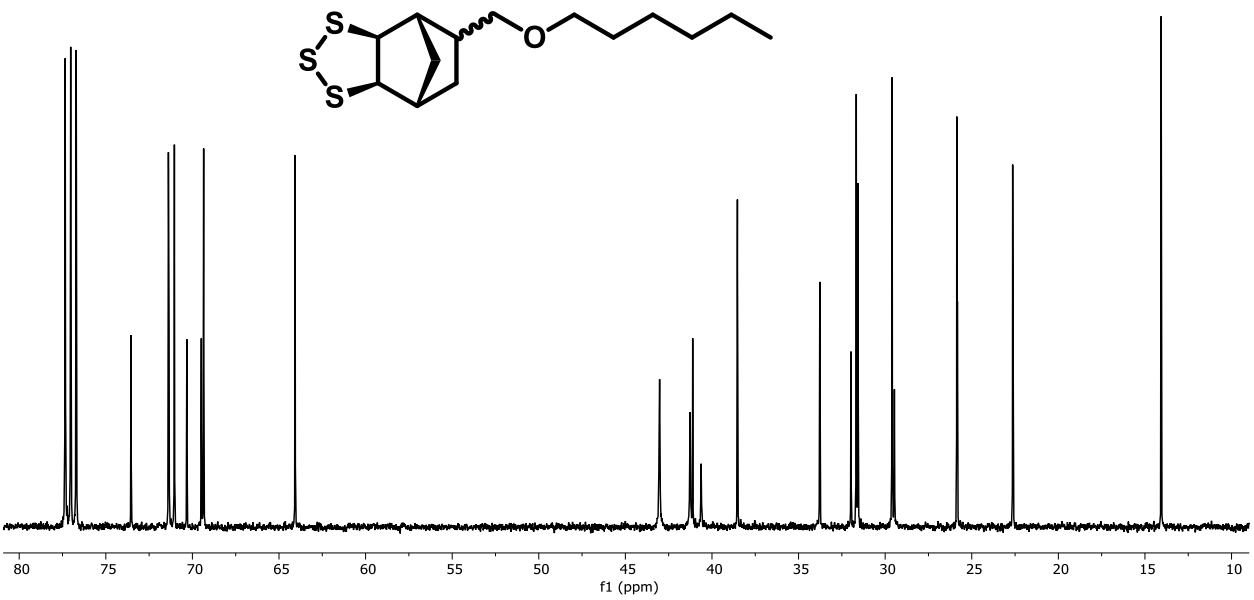

Figure A2.7: ^{13}C NMR of **2** in $CDCl_3$.

Synthesis of **3** ($DCPS_3$)

Dicyclopentadiene (5.00 g, 37.8 mmol, 1.00 eq.), S_8 (3.64 g, 14.2 mmol, 0.375 eq.), $Ni(NH_3)_6Cl_2$ (0.175 g, 0.756 mmol, 2.00 mol%), and 70 mL DMF were added to a 100 mL round bottom flask equipped with a reflux condenser and heated to 120 °C for 18 hours. Diethyl ether was added to the crude reaction mixture which was then washed with H_2O three times to remove DMF. The organic layer was then dried with Na_2SO_4 and concentrated under reduced pressure and purified by flash column chromatography hexanes (100%) to yield the desired product as a yellow solid (82.6% yield).

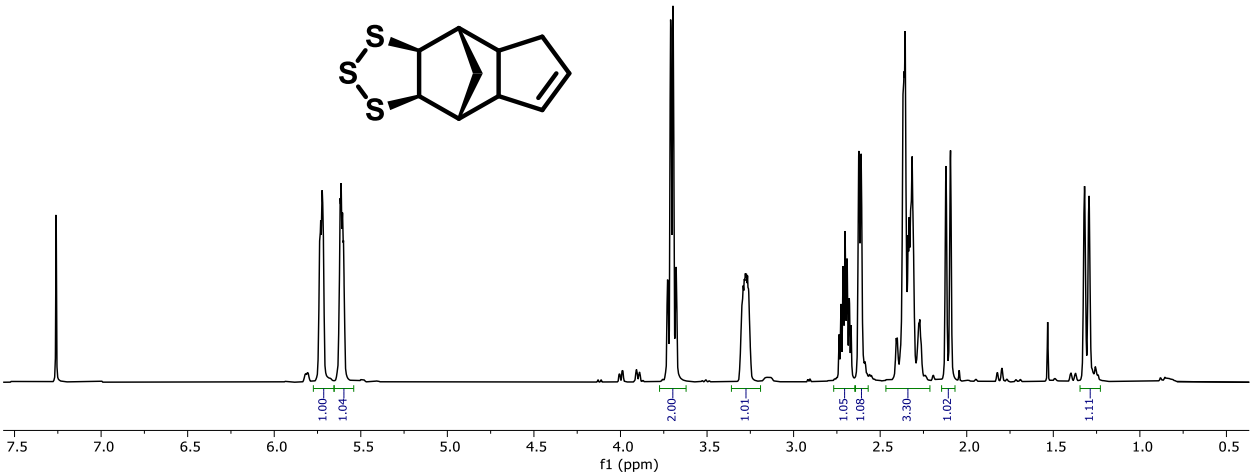

Figure A2.8: ^{1}H NMR of **3** in $CDCl_3$.

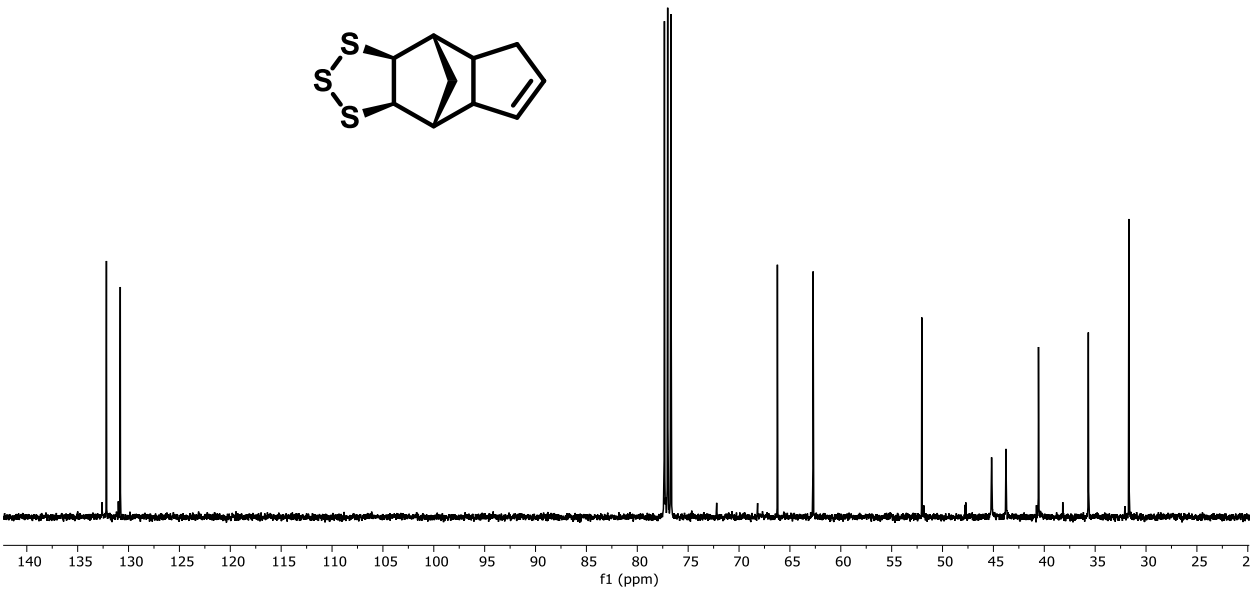

Figure A2.9: ^{13}C NMR of **3** in $CDCl_3$.

Synthesis of **4** ($PhNS_3$)

Steps 1 and 2: Synthesis of 2-phenyl-2-norbornene

Norcamphor (10.00 g, 90.78 mmol) and dry tetrahydrofuran (THF) were added to a dry 500 mL RBF under N_2. Phenylmagnesium bromide (PhMgBr) (34.0 mL, 100 mmol) was added dropwise to the solution and stirred at 0 °C for 30 min. Aqueous 0.10M HCl was added dropwise, solution was concentrated, then extracted with diethyl ether (x2), rinsed with brine solution, and dried over anhydrous sodium sulfate. After drying, the solution was filtered, then concentrated under vacuum to obtain the 2-phenyl-bicyclo[2.2.1]heptan-2-ol intermediate. 2-phenyl-bicyclo[2.2.1]heptan-2-ol (13.011 g, 14.470 mol) was then added to a nitrogen filled 500 mL round bottom flask. Potassium bisulfate (10.349 g, 76 mmol, 1.10 eq) was added to flask and heated to 100 °C for 2 hours. The solution was then extracted with hexanes, rinsed with brine solution, then the organic layer was dried over anhydrous sodium sulfate. After drying, the solution was filtered and concentrated under vacuum. The product was purified by column chromatography (100% hexanes) to yield desired product as clear oil. (65% yield)

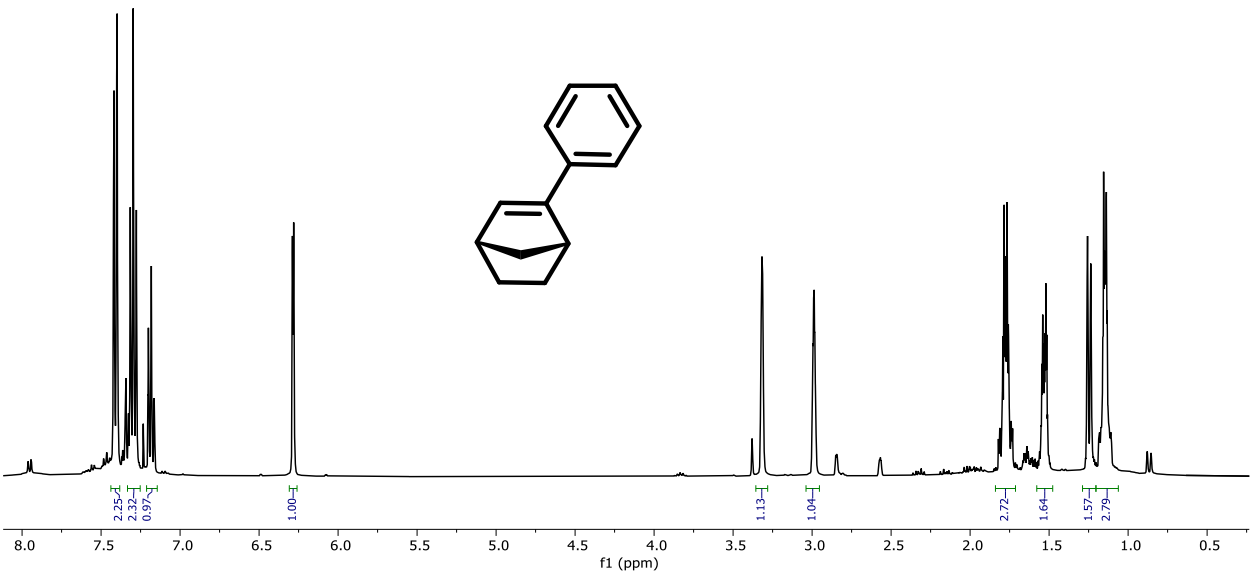

Figure A2.10: ^{1}H NMR of 2-Phenyl-2-Norbornene.

Step 3: Synthesis of **4** ($PhNS_3$)

2-phenyl-2-norbornene (2.00 g, 11.7mmol, 1.00 eq.), sulfur (S_8) (1.13 g, 35.2 mmol, 0.375 eq.), $[Ni(NH_3)_6]Cl_2$ (0.055 g, 0.237 mmol, 0.02 eq.), and 2,6-di-tert-butyl-4-methylphenol (BHT) (0.518 g, 2.35 mmol, 0.2 eq.) and 20 mL DMF were added to a 50 mL round bottom flask equipped with a reflux condenser and heated to 120°C for 18 hours. The crude mixture was passed through a silica plug (5% EtOAc, 95% hexanes) then concentrated. The concentrated crude product was then purified using flash column chromatography (100% hexanes). The product was a yellow solid (57.2% yield). ^{1}H NMR (400 MHz, $CDCl_3$) δ 7.52 – 6.96 (m, 5H), 7.16 (t, *J* = 6.4 Hz, 1H), 3.90 (d, *J* = 2.0 Hz, 1H), 3.15 (dt, *J* = 3.2, 1.5 Hz, 1H), 2.41 (dq, *J* = 10.5, 2.0 Hz, 1H), 2.31 (dq, *J* = 2.8, 1.5 Hz, 1H), 1.68 – 1.56 (m, 1H), 1.60 – 1.50 (m, 1H), 1.39 – 1.26 (m, 1H), 1.22 (dq, *J* = 10.6, 1.7 Hz, 1H), 1.03 – 0.91 (m, 1H). ^{13}C NMR (101 MHz, $CDCl_3$) δ 143.38, 128.09, 126.99, 87.10, 69.43, 34.11, 27.47, 24.55. HRMS (ESI): calculated for M+ $C_{13}H_{14}S_3$ 266.03; measured 266.0258.

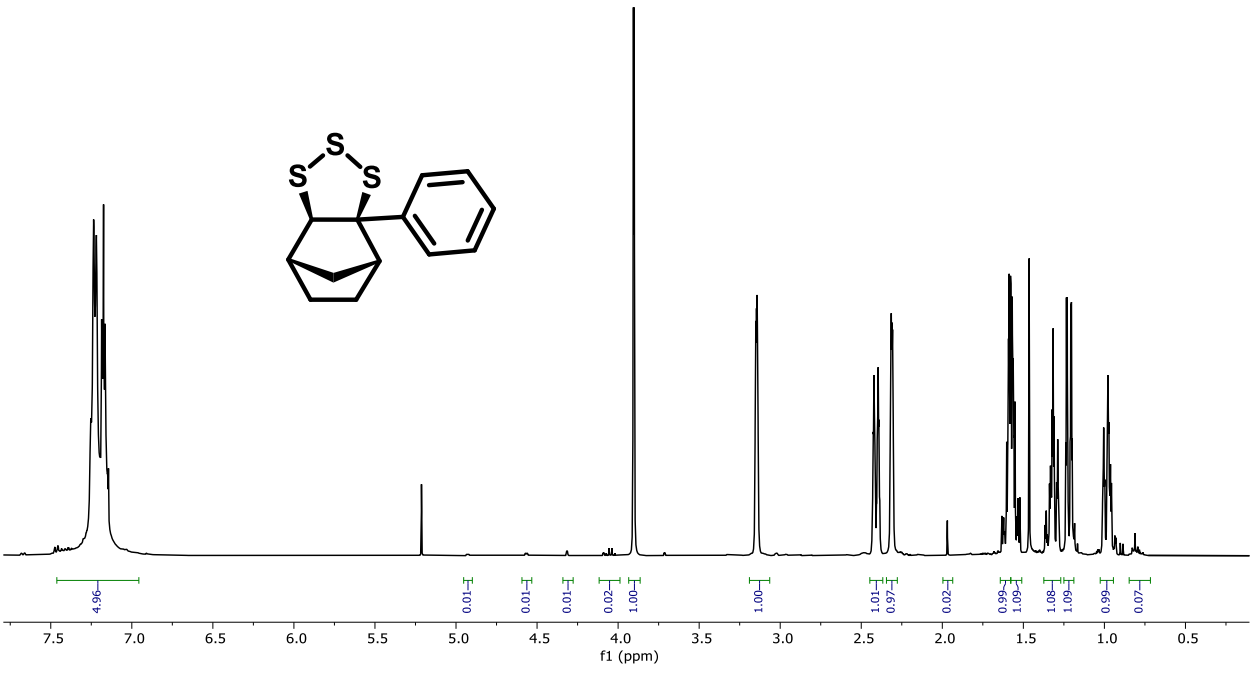

Figure A2.11: ^{1}H NMR of **4** in $CDCl_3$.

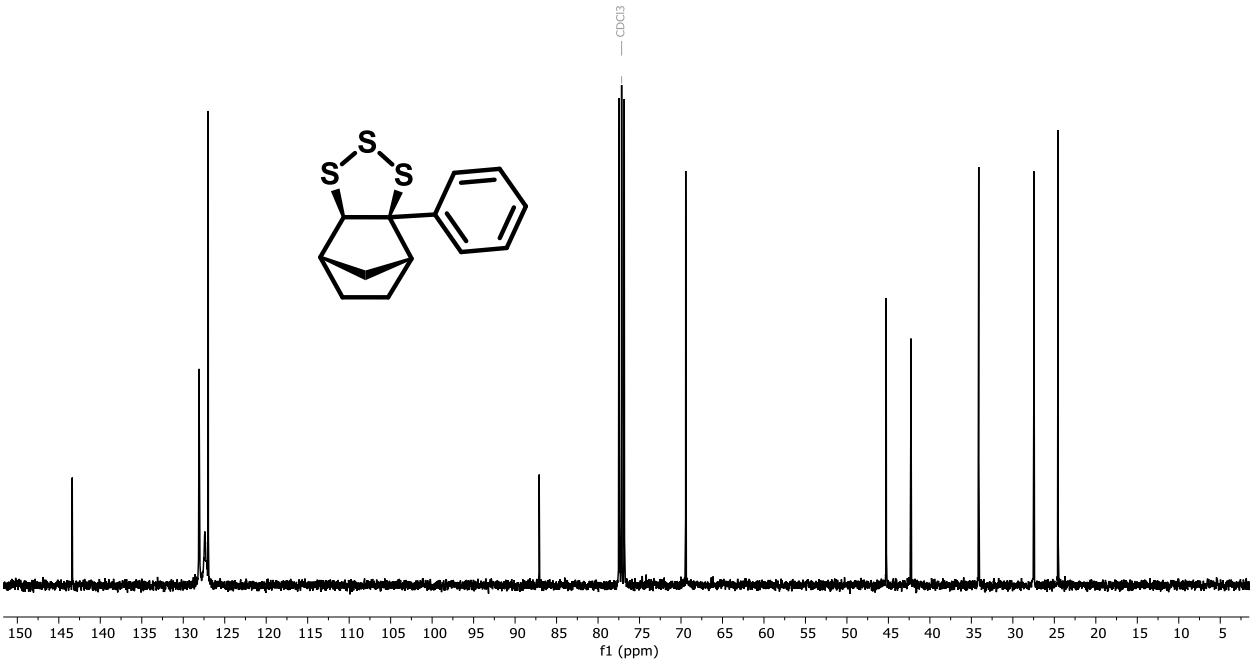

Figure A2.12: ^{13}C NMR of **4** in $CDCl_3$.

Synthesis of **5** (NS_3-diester)

Dimethyl-5-norbornene-2,3-dicarboxylate (1.05g, 5.00 mmol, 1.00 eq.), sulfur, S_8 (0.480 g, 1.88 mmol, 0.375 eq.), $Ni(NH_3)_6Cl_2$ (0.023g, 0.100 mmol, 2.00 mol%) and 10 mL DMF were added to a 50 mL round bottom flask equipped with a reflux condenser and heated to 120°C for 18 hours. The reaction mixture was passed through a silica plug (15% EtOAc : 85% hexanes), concentrated under reduced pressure, and then purified by column chromatography (10% EtOAc : 90% hexanes), yielding the product as a yellow solid. (62.8% yield) ^1H NMR (400 MHz, $CDCl_3$) δ 1.41 (dp, 1H) δ 2.13 (dq, 1H) δ 2.80 (d, 1H) δ 2.85 (m, 1H) δ 2.96 (dd, 1H) δ 3.42 (t, 1H) δ 3.71 (dd, 1H) δ 3.73 (s, 3H) δ 3.76 (s, 3H) δ 3.83 (dd, 1H).

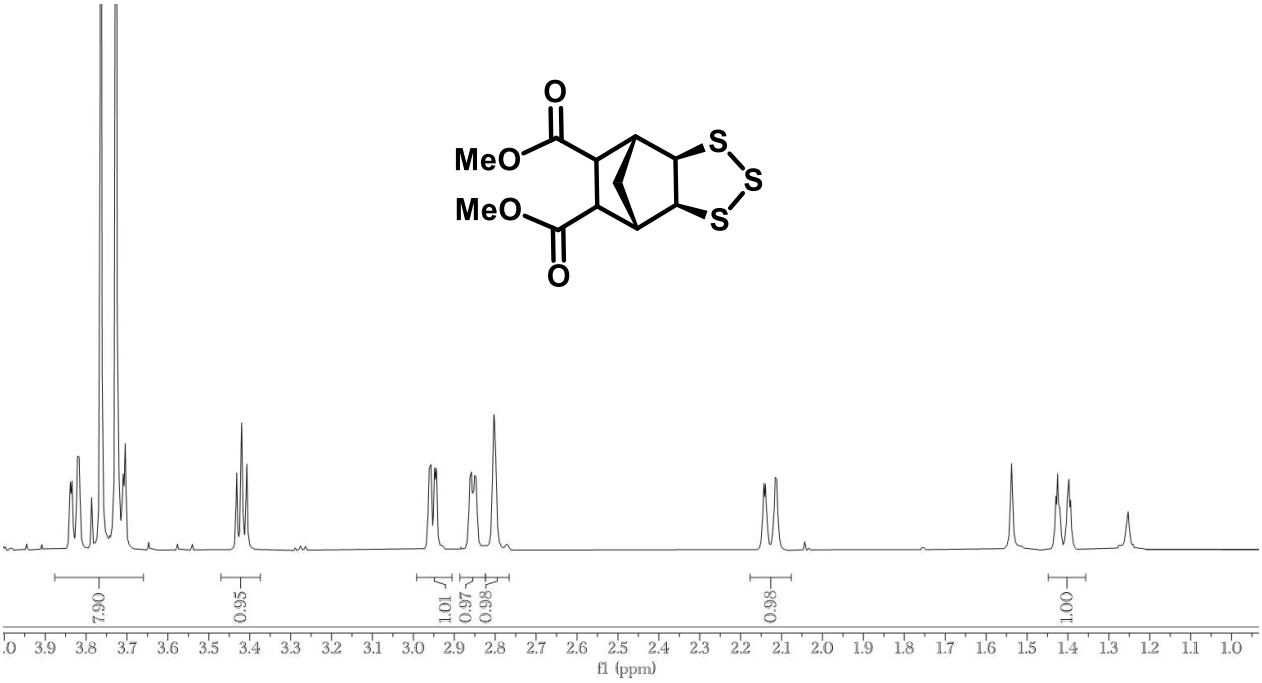

Figure A2.13: ^{1}H NMR of **5** in $CDCl_3$.

Synthesis of **6** (NS_3-anhydride)

Cis-5-Norbornene-endo-2,3-dicarboxylic anhydride (1.05g, 5.00 mmol, 1.00 eq.), sulfur, S_8 (0.480 g, 1.88 mmol, 0.375 eq.), $Ni(NH_3)_6Cl_2$ (0.023g, 0.100 mmol, 2.00 mol%) and 10 mL DMF were added to a 50 mL round bottom flask equipped with a reflux condenser and heated to 120°C for 18 hours. The reaction mixture was then diluted with 50 mL of H_2O, extracted 3x with EtOAc and finally passed through a silica plug (15% EtOAc : 85% hexanes). The recovered mixture was concentrated under reduced pressure and purified by sublimation at 130 °C under vacuum (20 mTorr) yielding the product as a yellow solid (22% yield). ^1H NMR (400 MHz, $CDCl_3$). δ 1.25 (d, 1H), δ 2.27 (d, 1H), δ 3.02 (S, 2H), δ 3.13 (S, 2H), δ 3.81 (S, 2H).

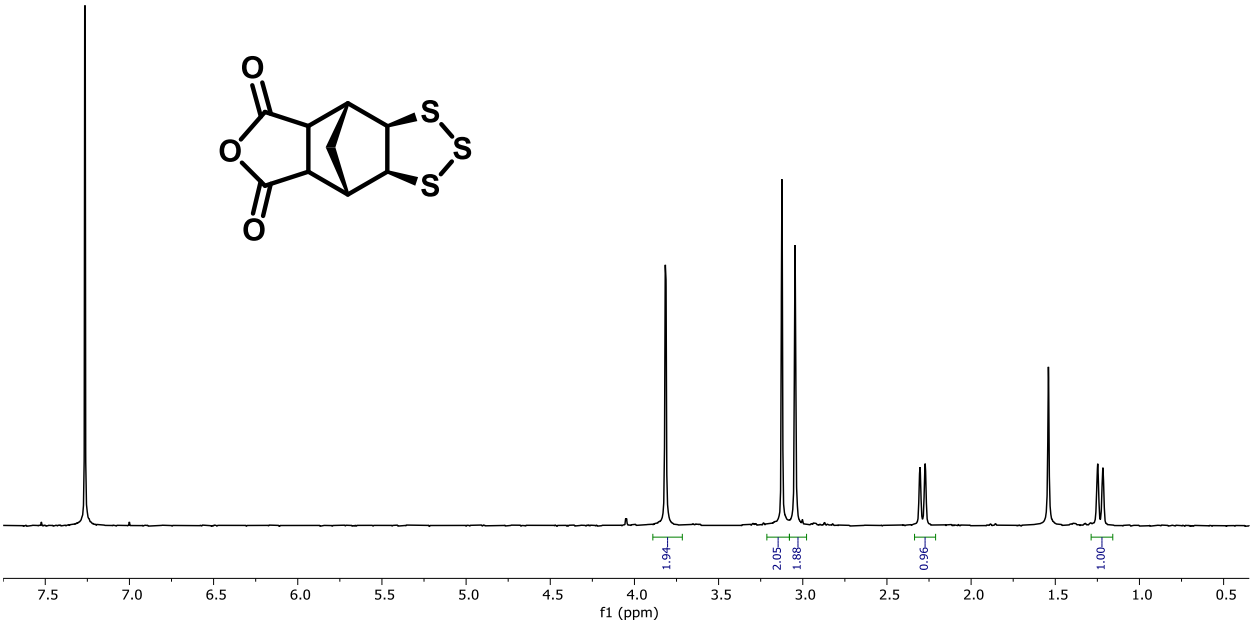

Figure A2.14: ^1H NMR of **6** in $CDCl_3$.

Amine Screening (Table A2.1)

In a 10 mL high pressure reaction tube, norbornene (50.0 mg, 0.531 mmol, 1.00 eq.), S_8 (51.1 mg, 0.199 mmol, 0.375 eq.), amine (0.0106 mmol, 2.00 mol%), and DMF (2.00 mL) were mixed then heated to 120 °C. Time points were taken by taking a 500 uL sample from the reaction mixture, then analyzed by ^{1}H NMR. Trimethoxy benzene was used as an internal standard.

Table A2.1: Impact of amine on conversion of norbornene to **1.**

Entry[a]	Amine	Time (h)	Conv. (%)[c]	1_3 : 1_5[d]
1	none	18	>99	0.65 : 0.35
2a	$[Ni(NH_3)_6]Cl_2$	2	83	0.70 : 0.30
2b	$[Ni(NH_3)_6]Cl_2$	8	>99	0.75 : 0.25
2c	$[Ni(NH_3)_6]Cl_2$	18	>99	0.75 : 0.25
3a	1-naphthylamine	2	47	0.72 : 0.28
3b	1-naphthylamine	8	>99	0.75 : 0.25
3c	1-naphthylamine	18	>99	0.75 : 0.25
4a	aniline	2	49	0.69 : 0.31
4b	aniline	8	>99	0.68 : 0.32
4c	aniline	18	>99	0.77 : 0.23
5a	diphenylamine	2	35	0.73 : 0.27
5b	diphenylamine	8	>99	0.70 : 0.30
5c	diphenylamine	18	>99	0.76 : 0.24
6	DABCO	18	>99	0.78 : 0.22
7a	triethylamine	2	68	0.69 : 0.31
7b	triethylamine	8	>99	0.69 : 0.31
7c	triethylamine	18	>99	0.77 : 0.23
8a	*t*-butylamine	2	28	0.71 : 0.29
8b	*t*-butylamine	8	>99	0.77 : 0.23
8c	*t*-butylamine	18	>99	0.73 : 0.27

Light-driven monomer synthesis (Table A2.2)

In a 2 dram vial equipped with stir bar, norbornene (50.0 mg, 0.531 mmol, 1.00 eq.), S_8 (51.1 mg, 0.199 mmol, 0.375 eq.), 1,4-diazabicyclo[2.2.2]octane (DABCO) (2.00 mg, 0.0106 mmol, 2.00 mol%), and carbon disulfide (CS_2) (2.00 mL) were added. The vials were placed in a dark box equidistant from light source and irradiated for up to 72 hours with a 390 nm Kessil lamp (heat generated from lamp during reaction was monitored and reached between 40 – 50 °C). The reaction mixtures were then dried, redissolved in $CDCl_3$ and conversion of the norbornene derivative was measured.

Table A2.2: Relevant data from synthesis of several monomers using light-driven approaches.

Run	Target Monomer	Amine	Yield (%)
1	**1**	DABCO	40
2	**3**	DABCO	34
3	**4**	DABCO	11
4	**5**	DABCO	40
5	**6**	DABCO	32

Data from TGA of monomers

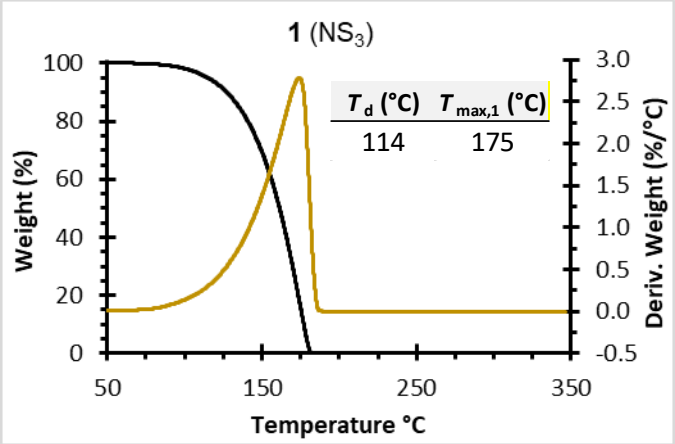

Figure A2.15: Data from TGA of monomer **1**. T_d is assessed at 5% weight loss. T_{max} temperatures are reported for the maxima of the functions of wight%/temperature and represent the temperature at which degradation rate is fastest.

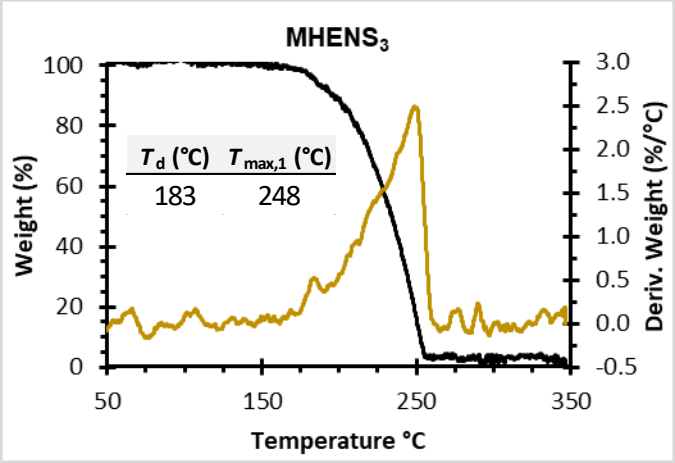

Figure A2.16: Data from TGA of monomer **2**. T_d is assessed at 5% weight loss**.** T_{max} temperatures are reported for the maxima of the functions of wight%/temperature and represent the temperature at which degradation rate is fastest.

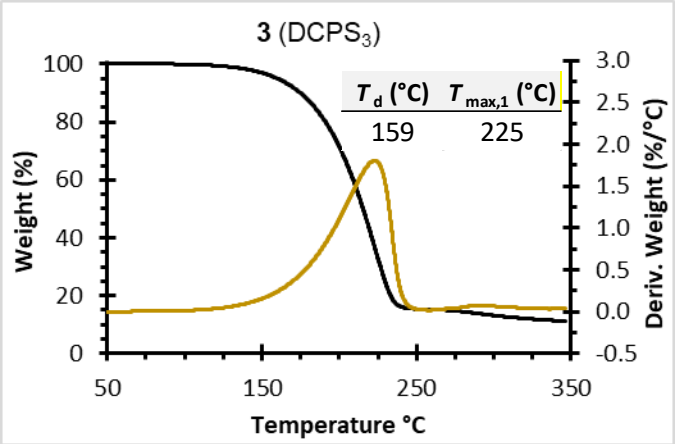

Figure A2.17: Data from TGA of monomer **3**. T_d is assessed at 5% weight loss. T_{max} temperatures are reported for the maxima of the functions of wight%/temperature and represent the temperature at which degradation rate is fastest.

DSC of Monomers

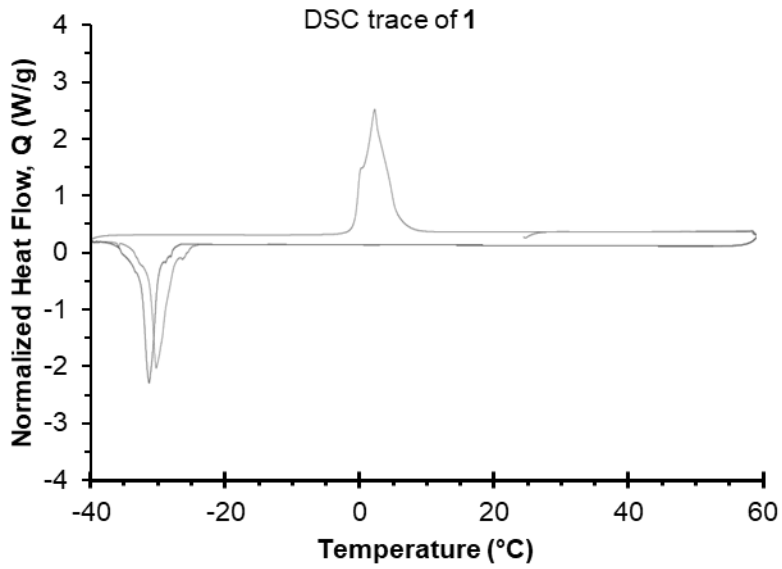

Figure A2.18: DSC trace of pure **1** showing endotherm at 5 °C and exotherm at -30°C.

Polymer Synthesis Methods

Methods for ROP (Supplementary Polymerization Results (Table A2.3 and A2.4))

All work was carried out in a nitrogen filled glovebox in the absence of light. Before use, all polymerization initiators were dissolved in air-free anhydrous solvent to prepare stock solutions. The stock solutions of initiator were allowed to sit over molecular sieves (20% by volume) for three days before use and were stored in the freezer when not in use. Note that stock solutions of BnOH were prepared separately from the bases. Monomer was then weighed into a 1 dram vial equipped with a Teflon coated magnetic stir bar and any additional solvent needed was added. For polymerizations initiated without BnOH, the reaction vial containing the monomer was placed onto a magnetic stir plate and stirred at 600 rpm. The polymerization was then started by directly injecting the initiator solution into the stirring monomer. For polymerizations wherein BnOH was used, a 1:1 mol ratio of the base and BnOH were stirred for 20 minutes then the appropriate volume was directly injected into the stirring monomer. The reactions were quenched by adding a solution of allyl bromide (10 mol eq. relative to mols initiator) in chloroform and were vortexed until completely dissolved. The sample was then dried down and redissolved in $CDCl_3$ so that conversion could be estimated by ^1H NMR. After measuring conversion, the sample was dried down and redissolved in HPLC-grade $CHCl_3$ for molecular weight analysis by GPC-MALS.

Light Driven Polymerizations (Table A2.5)

In a nitrogen filed glovebox in a dark room, monomer (0.200 g) was weighed into a 1 dram vial equipped with a Teflon coated stir bar and anhydrous and air free toluene was added. The reaction vial was capped and covered then set up in front of a 390 nm Kessel lamp. The lamp was turned on and the polymerization allowed to stir for 3 hours before 1 mol eq. of TEMPO was added. The sample was then dried down and redissolved in $CDCl_3$ so that conversion could be estimated by ^1H NMR. After measuring conversion, the sample was dried down and redissolved in HPLC-grade

$CHCl_3$ for molecular weight analysis by GPC-MALS. Next, the sample was recovered and precipitated into cold methanol. The solids were recovered by centrifugation, then redissolved and reprecipitated from $CHCl_3$ into cold methanol two more times before dried under vacuum. A sample of the dried polymers was used for thermal properties analysis by TGA and for making solutions to measure the dn/dc.

Supplementary Polymerization Results

Table A2.3: Relevant data from screening conditions for the polymerization of **1** (NS_3).

Entry	Temp (°C)	$[1]_0$ (mol/L)	Solvent	Initiator (I)	I:NS3	Conv. (%)	M_w (kDa)	M_n (kDa)	$Đ$ (M_w/M_n)	I^* (%)
1	22	5.02	THF	NHC*t*Bu	1:100	43.7	509	283	1.80	2.94
2	22	5.02	THF	DBU	1:100	50.7	38.5	18.5	2.08	52.2
3	22	5.02	Benz	P_4*t*Bu	1:100	51.5	52.3	17.9	2.92	54.6
4	22	5.02	THF	PhSNa	1:100	52.7		20.3	1.66	44.2
5	22	5.02	THF	NHC*t*Bu/BnOH	1:100	45.7	29.7	13.4	2.22	66.0
6	22	5.02	THF	DBU/BnOH	1:100	45.2	42.6	26.3	1.62	33.2
7	22	5.02	Benz	P_4*t*Bu/BnOH	1:100	45.4	25.7	14.7	1.75	59.9
8	22	5.02	THF	PhSNa/BnOH	1:100	44.0		17.8	1.70	51.1
9	22	5.02	THF	BnOH	1:100	--		--	--	--
10	22	2.49	Tol	NHC*t*Bu/BnOH	1:100	7.80	--	--	--	--
11	22	4.02	Tol	NHC*t*Bu/BnOH	1:100	24.5	11.1	8.27	1.34	58.2
12	22	5.02	Tol	NHC*t*Bu/BnOH	1:100	42.5	30.6	17.6	1.74	46.7
13	22	6.00	Tol	NHC*t*Bu/BnOH	1:100	56.7	116	23.2	4.99	47.2
14	22	6.52	Tol	NHC*t*Bu/BnOH	1:100	67.6	242	26.8	9.03	48.6
15	-34	4.02	Tol	NHC*t*Bu/BnOH	1:100	41.5	26.3	15.2	1.73	52.6

16	-34	5.02	Tol	NHC*t*Bu/BnOH	1:100	50.2	116	22.1	5.26	43.9
17	-34	6.00	Tol	NHC*t*Bu/BnOH	1:100	55.2	153	23.9	6.39	44.6
18	22	5.02	Tol	NHC*t*Bu/BnOH	0.5:1:100	41.9		26.3	1.65	30.9
19	22	5.02	Tol	NHC*t*Bu/BnOH	1:100	53.9	71.0	23.6	3.01	44.2
20	22	5.02	Tol	NHC*t*Bu/BnOH	1:500	49.7	155	75.7	2.05	62.7
21	22	5.02	Tol	NHC*t*Bu/BnOH	1:1000	49.1	250	126	1.99	74.4
22	22	6.00	Tol	NHC*t*Bu/BnOH	1:1000	54.3	299	119	2.51	86.9

Table A2.4: Relevant data from monomer scope using ROP conditions.

Run	Monomer	$[M]_0$	Conv. (%)	M_w (kDa)	M_n (kDa)	$Đ$ (M_w/M_n)	I* (%)
1	NS_3	6.00	59.3	296	164	1.81	68.9
2	$DCPS_3$	4.82	60.0	201	135	1.50	68.9
3	$MHENS_3$	3.47	25.0	49.5	29.9	1.65	255
4	$PhNS_3$	4.20	10.0	6.05	3.92	1.54	680

*all polymerizations in Table A2.4 were run on a 200 mg scale for 3h

Table A2.5: Relevant data from monomer scope using photopolymerization conditions.

Run	Monomer	$[M]_0$	Conv. (%)	M_w (kDa)	M_n (kDa)	$Đ$ (M_w/M_n)	T_d (%)
1	NS_3	6.00	46.2	43.1	28.5	1.52	175
2	$DCPS_3$	4.82	47.0	106	69.1	1.54	147
3	$MHENS_3$	3.47	84.0	19.9	16.5	1.21	160
4	$PhNS_3$	4.20	30.0	28.4	12.8	2.21	189

*All polymerizations in Table A2.5 were run on a 200 mg scale for 3h. T_d is assessed at 5% weight loss.

TGA of Polymers

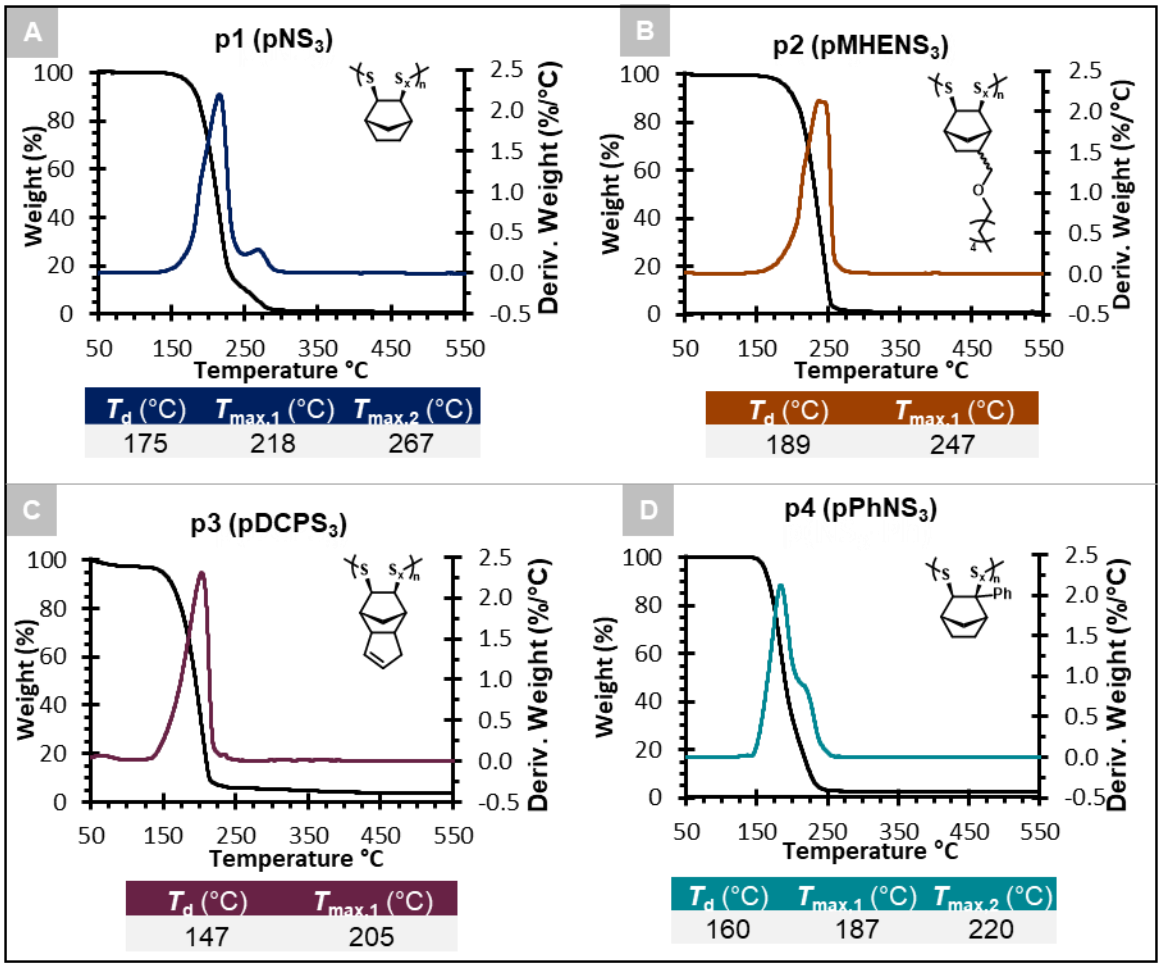

Figure A2.19: Data from thermogravimetric analysis (TGA) of polymer samples synthesized via photopolymerization (see

Table A2.5). T_d is assessed at 5% weight loss. T_{max} temperatures are reported for the maxima of the functions of wight%/temperature and represent the temperature at which degradation rate is fastest.

Depolymerization

Chemical Depolymerization Procedure 1 (Table A2.6, Entries 1-7): A 50 mg/mL stock solution of **p1** (M_n = 29.9 kDa) was prepared in benzene (note that the solution was cloudy due to incomplete solvation) under nitrogen atmosphere Aliquots of 0.5 mL of the stock were distributed to 1-dram

vials. Stock solutions of base were pre-prepared in anhydrous and air free benzene. An aliquot of the base was then added to each depolymerization vial such that the identity of the base and the mol eq. are as shown in Table A2.6 and that the final concentration of **1** if 100% depolymerization was reached would be 0.25 M. After 1 hour, the depolymerization reactions were quenched with 2 mol eq. of benzoic acid (relative to moles of base). After quenching, reaction vessels were dried over air and ^{1}H-NMR spectra were obtained to determine the conversion of **p1** to **1** under the given conditions.

Depolymerization of other poly(norbornane trithiolane) derivatives (Table A2.6, Entries 8-10): Solutions of each poly(norbornane trithiolane) derivative were prepared at 0.0625 M (**p4**: M_n = 3.92 kDa, **p3**: M_n = 135 kDa) and 0.125 M (**p2**: M_n = 29.9 kDa) in 1 dram vials equipped with a Teflon coated magnetic stir bar. An aliquot of a stock solution of NHC*t*Bu (prepared in anhydrous, air free benzene) was then added to each reaction vessel at 0.01 mol eq. (relative to monomer repeat units). After 1 hour, each reaction was quenched with 2 mole equivalence of benzoic acid (relative to mol NHC*t*Bu) and the reaction mixtures were dried under air then the conversion to monomer measured by ^{1}H-NMR in $CDCl_3$.

Table A2.6: Relevant results from chemical depolymerization condition optimization and scope.

Entry	Polymer	Solvent	Base	**[Base]** (mol eq.)	**Depolymerization Conv.** (%)	**Rxn Time** (h)
1	**p1**	Benzene	triethylamine	1	33.4	1
2	**p1**	Benzene	triethylamine	0.01	5.23	1
3	**p1**	Benzene	pyrrolidine	1	>99	1
4	**p1**	Benzene	Pyrrolidine	0.01	13.7	1
5	**p1**	Benzene	DBU	1	>99	1

6	**p1**	Benzene	DBU	0.01	74.0	1
7	**p1**	Benzene	NHC*t*Bu	0.01	>99	1
8	**p2**	Benzene	NHC*t*Bu	0.01	88.0	1
9	**p3**	Benzene	NHC*t*Bu	0.01	87.0	1
10	**p4**	Benzene	NHC*t*Bu	0.01	82.0	1

Procedure for kinetics study (Table A2.7) (A2.20):

A 25 mg/mL pNS_3 (M_n = 156 kDa) stock solution was prepared in benzene under nitrogen. Aliquots of 2.0 mL of polymer stock solution was added into two 1-dram vials equipped with a Teflon coated magnetic stir bar. Next, NHC*t*Bu or DBU was added at 0.01 mol equivalence (relative to total monomer repeat units) while stirring with magnetic stir bar. The reaction volume was adjusted to achieve a final monomer concentration (assuming 100% depolymerization) of 0.0625 M. After 1, 5, 10, 30, and 60 minutes, 0.30 mL of the reaction mixture was removed and combined with 2 mol eq. of benzoic acid (relative to the mol of initiator in the time point). The time points were dried under air and ^{1}H NMR spectra were obtained to determine the conversion of **p1** to **1**. After ^{1}H NMR analysis, the samples were dried down again and redissolved in HPLC grade $CHCl_3$ for molecular weight analysis by GPC-MALS.

Table A2.7: Relevant data from kinetic study on depolymerization of **p1.**

Kinetic study of depolymerization of p1 to 1						
Base		1 min	5 min	10 min	30 min	60 min
DBU	conv.	19.7%	38.6%	48.8%	64.8%	76.3%
	M_n	2.28	1.60	1.44	1.38	1.35
NHC*t*Bu	conv.	92.6%	93.5%	95.2%	98.0%	>99%

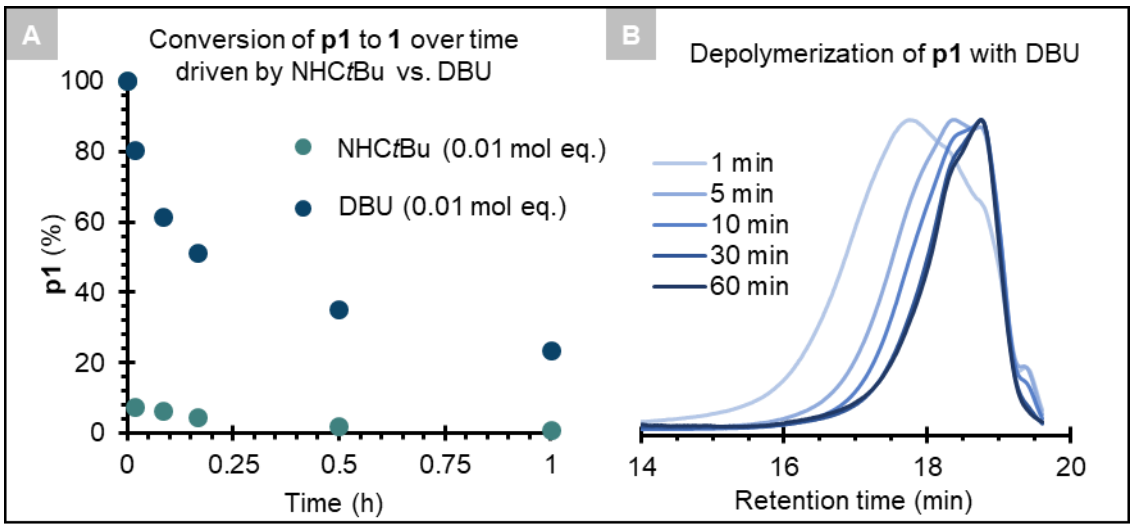

Figure A2.20: (A) Graph showing the change in concentration of **p1** as a function of time when depolymerization is done in the presence of NHC*t*Bu or DBU (Table A2.7). (B) Change in molecular weight of **p1** over time when depolymerization is done in the presence of DBU.

Thermal depolymerization method: A sample of 191.8 mg of **p1** (M_n=156 kDa) was heated a 25 mL Schlenk tube wrapped in heat tape. The Schlenk tube was connected to a Schlenk flask by a distillation head and the system was placed under static vacuum at 100 mTorr. The collection flask was placed in liquid nitrogen and then the heat tape was set to connected to a thermocouple which was set to a temperature of 105 °C. After 24 hours, the system was cooled, heat was removed, and the isolated yield of **1** was assessed by mass and the purity confirmed by ^{1}H-NMR.

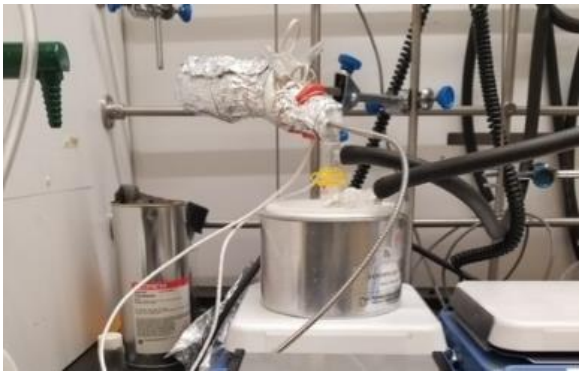

Figure A2.21: Picture of thermal depolymerization setup.